Ph.D. Program in Civil, Chemical and Environmental Engineering

Curriculum in Fluid Dynamics and Environmental Engineering

Department of Civil, Chemical and Environmental Engineering

Polytechnic School, University of Genoa, Italy

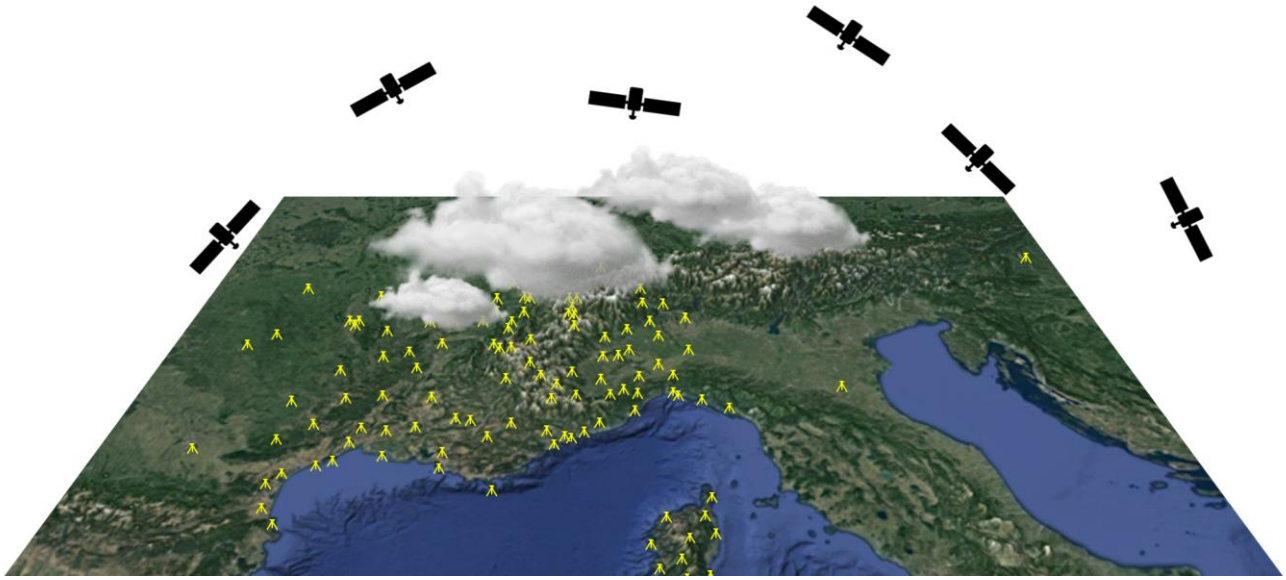

GNSS Contribution to Monitor Severe Rainfalls: an Innovative Procedure for Wide and Orographically Complex Area with existing Infrastructures

Ilaria Ferrando

GNSS Contribution to Monitor Severe Rainfalls:

an Innovative Procedure for Wide and

Orographically Complex Area with Existing Infrastructures

By

Ilaria Ferrando

Dissertation discussed in partial fulfillment of
the requirements for the Degree of

DOCTOR OF PHILOSOPHY

in Fluid Dynamics and Environmental Engineering,
Doctoral Program in Civil, Chemical and Environmental Engineering,
Department of Civil, Chemical and Environmental Engineering, University of Genoa, Italy

March, 2017

Adviser:
Prof. Bianca Federici – Department of Civil, Chemical and Environmental Engineering (DICCA), University of Genoa

External Reviewers:
Prof. Toshitaka Tsuda – Research Institute for Sustainable Humanosphere (RISH), Kyoto University
Prof. Giovanna Venuti – Department of Civil and Environmental Engineering (DICA), Polytechnic of Milan

Examination Committee:
Prof. Alessandro Stocchino – Department of Civil, Chemical and Environmental Engineering (DICCA), University of Genoa
Prof. Marco Colombini – Department of Civil, Chemical and Environmental Engineering (DICCA), University of Genoa
Prof. Ambrogio Manzino – Department of Environment, Land and Infrastructure Engineering (DIATI), Polytechnic of Turin

Ph.D. program in Civil, Chemical and Environmental Engineering

Curriculum in Fluid Dynamics and Environmental Engineering

Cycle XXIX

Cover-design: Giulia Curletto (XXIX cycle) and Margherita Pongiglione (XXVIII cycle)

ABSTRACT

The research activity concerned the development of an innovative methodology to monitor the content of Precipitable Water Vapour (PWV), starting from Zenith Tropospheric Delay (ZTD) estimations obtained from GNSS permanent stations, and Pressure (P) and Temperature (T) observed in meteorological sensors networks. In particular, an automatized procedure, named G4M (GNSS for Meteorology), for preparing and elaborating the data collected from the existing infrastructures and for producing PWV maps will be presented. The G4M procedure has been applied to study two critical events occurred on Genoa city; this analysis led to the definition of a “Heterogeneity Index”, accounting for PWV spatial variability, which has been considered a promising indicator to highlight and locate severe meteorological events in time and space. Additionally, ZTD and PWV time series have been obtained for selected GNSS Permanent Stations in order to identify recognizable patterns in ZTD/PWV that can be related to the occurrence of severe meteorological events.

INDEX

INDEX OF FIGURES

INDEX OF TABLES

INTRODUCTION

The typical application of GNSS[1] (Global Navigation Satellite System) technology is obtaining the coordinates of a receiver by means of spatial triangulation, knowing the satellites orbits and positions. As widely known, the positioning precision determined by GNSS measures is affected by different sources of bias due to structural and non-structural issues: receiver/satellite clock errors, multipath, code/phase range, etc. One of the aspects that mainly influences the position's precision is the crossing of the atmosphere by the electromagnetic GNSS signal, due to ionospheric and tropospheric refraction. The ionospheric bias is frequency dependent and is dominant, but it can be easily eliminated by means of L1 and L2 phase combination for double frequency receivers, i.e. geodetic receivers. The tropospheric bias can't be reduced by means of any combination, hence it has to be taken into account. The tropospheric effect produces a bias in each satellite-receiver observation that can be related with the so called Zenith Total Delay (ZTD), computed in the zenith direction above the GNSS station, by means of an appropriate *mapping function*. On one hand, the estimation of ZTD and its time and space variability could help to enhance the positioning precision and, on the other hand, the monitoring of ZTD could be useful to study and interpret severe meteorological events, as previous studies demonstrate (Bouma and Stoew, 2001; De Pondeca and Zou, 2001; Basili et al., 2003; Bock et al., 2008; Boniface et al., 2009; Bennitt and Jupp, 2012; Crespi et al., 2014; Piccardo and Sguerso, 2007; Sguerso et al., 2013, 2015; Tsuda et al., 2013).
In this context, considering the atmosphere as a biphasic fluid composed by a mix of dry and wet gases, ZTD may be split in its two components, the Zenith Hydrostatic Delay (ZHD) and the Zenith Wet Delay (ZWD). The first one is due to the mix of dry gases in atmosphere, is dominant (it covers about the 90% of the total tropospheric delay) and can be easily modelled, by means of relations involving the atmospheric pressure and depending on the latitude and the elevation of the GNSS station; the latter is due to the water vapour refractivity caused by the dipole moment of water vapour molecules and it can't be easily modelled, therefore it is typically obtained by difference between ZTD and ZHD. ZWD is closely related to the value of Precipitable Water Vapour (PWV). PWV represents the maximum amount of condensable water due to the water vapour contained in an imaginary unitary base column that extends from the GNSS receiver height to the upper limit of the troposphere. This quantity can be considered the upper limit of the precipitable water, if the triggering conditions to make the water vapour condensate are present.

1 The acronym GNSS refers to the satellites' multi-constellations system providing global coverage. The system consists of different satellites' constellations: USA's NAVSTAR GPS (Global Positioning System), Russia's GLONASS (GLObal'naya NAvigatsionnaya Sputnikovaya Sistema), Europe's GALILEO, China's BeiDou (formerly known as COMPASS) and other newer systems, currently under preparation (e.g. Japan's QZSS, Quasi Zenith Satellite System, and India's IRNSS, Indian Regional Navigational Satellite System).

PWV can be estimated starting from ZTD by means of the relations by Bevis et al. (1992 and 1994), involving Pressure (P), Temperature (T) and geographic information about the position of the GNSS receiver (latitude and ellipsoidic height).

In literature, the researches on GNSS meteorology are generally carried out in one dimension, with the investigation of the zenith profile of ZTD and PWV above a GNSS Permanent Stations. Recently, 2D approaches have been introduced thanks to the equipment of small areas with densely distributed GNSS receivers, with P and T sensors from which is possible to monitor the evolution of PWV with high spatial and temporal resolution.

Starting from Bevis' assumptions, a GIS (Geographic Information System) procedure called G4M (GNSS for Meteorology) has been conceived by the Laboratory of Geodesy, Geomatics and GIS to produce 2D PWV maps with high spatial and temporal resolution (1 km and 6 minutes respectively). Differently from literature applications, the input data of the G4M procedure are GNSS, P and T observations not necessarily co-located, coming from existing infrastructures.

On spite of the low density and the different configurations of GNSS, P and T networks, the procedure is capable to produce 2D PWV maps and to detect severe meteorological events, thanks to a simplified physical model, owned by the research group and currently in the preliminary phase of patent application, and an index of the PWV spatial variability as indicator to localize severe meteorological events in time and space. The procedure has been applied on a wide and orographically complex area covering approximately the north-west of Italy and the French-Italian border region, to study two severe meteorological events occurred in Genoa and other meteorological alert cases with reliable results.

Summarising, the aim of the present thesis is to show the results of the GIS procedure and its ability to produce 2D PWV maps on an orographically complex area, in order to understand the role of PWV in severe meteorological events, for both a posteriori and near real-time applications, starting from ZTD, P and T data coming from existing infrastructures.

The thesis is structured as follows: after an introductory chapter on GNSS basics (Chapter 1), the atmosphere's structure, the fundamental equations and the state of the art in the field of GNSS Meteorology are described in Chapter 2. The following Chapter 3 is dedicated to the presentation of data and their structure, the acquisition methods and the ZTD estimations procedure. In Chapter 4, the traditional 1D analysis over the two Genoa's GNSS Permanent Stations (PS) GENO and GENU is illustrated and discussed, while in Chapter 5 the 2D innovative GIS procedure is presented together with the methods to integrate the different sources of data and the analysis of the different techniques for data interpolation, and the codes for the procedure automation. Chapter 6 is dedicated to 2D two-hourly PWV maps realisation for a posteriori applications: the procedure has been applied to the 4th November 2011 and the 9th October 2014 severe meteorological events on Genoa. The PWV maps are compared with the re-analysed P, T and PWV fields, to evaluate the reliability of the GIS procedure. In Chapter 7 the near

real-time monitoring of troposphere is presented, discussing the new settings for obtaining ZTD, P and T data for a short time span (6 minutes), compatible with near-real time application. Additionally, the spatial variability of PWV is taken into account as a promising indicator to highlight remarkable features related to the occurrence of severe meteorological events.

The conclusions and future perspectives are exposed in the final chapter.

1. A GLANCE ON GNSS

The terrestrial positioning technology using the satellites is commonly referred as GPS[2]. Actually, NAVSTAR GPS[3] is just one of the many different satellite systems allowing terrestrial positioning. It was the first installed by USA Department of Defense in 1970s and it is the most widespread. Afterwards, the Russian Federal Government decided to invest in satellite positioning by developing the GLONASS[4] system. In the last years, other countries started to develop their own systems: the European Union presented EGNOS[5] and Galileo, Japan is developing QZSS[6], China is working on BeiDou and India on IRNSS[7]. Due to the increasing number of satellite systems, based on the same positioning concepts, the satellite technology is currently named GNSS[8], referring to the satellites' multi-constellations system providing global coverage.

1.1. GNSS PRINCIPLES

GNSS is used to determine the position of a receiver by means of constellations of multiple artificial satellites, knowing the positions of the satellites, the *ephemerides*. The determination of the receiver position, i.e. latitude, longitude and height, relies on the calculated distance from several satellites. Theoretically, from a purely geometrical point of view, the minimum needed number of satellites is three, to solve the three unknowns system.

Theoretically figuring the range covered by a satellite as a sphere centred in the satellite itself, the position of a point can be represented as the intersection of spheres: the intersection of two spheres forms a closed line and the intersection of three spheres individuates two points, one of them can be easily identified as a point of outer space.

The signals of each satellite allow the user to measure the distance between the receiver and the satellite. This operation is based on two clocks, one on the satellite and one on the receiver, which have totally different time scales: in fact, the receiver’s clocks starts when the receiver is switched on. This effect is

2 Global Positioning System.

3 NAVigation Satellite Timing and Ranging GPS.

4 GLObal'naya Navigatsionnaya Sputnikovaya Sistema.

5 European Geostationary Navigation Overlay System.

6 Quasi-Zenith Satellite System.

7 Indian Regional Navigational Satellite System.

8 Global Navigation Satellite System.

called *synchronisation offset* δt and it has to be estimated. Moreover, as widely known, the satellites are equipped with atomic clocks which can be synchronized to the level of nanosecond, but GNSS receivers are typically equipped with less expensive crystal clocks. The synchronisation between clocks has to be estimated with high precision: a synchronization error of 1 μs could lead to a position error in the order of 300 meters.

The satellite-receiver distance is calculated on the basis of the signals time of travel $\tau_{sat,rec}$, using the speed of light c

$$\rho = c \cdot \tau_{sat,\,rec} \tag{1.1}$$

where ρ is called *pseudo-range* because it is affected by the synchronisation offset.

The introduction of δt leads to a system of four unknowns, which must be solved by mean of four equations. Thus, to overcome the synchronization problem, a fourth satellite is needed.

As a matter of facts, having more than four satellites will not result in a more precise solution, but will just increase the control on the observations, thanks to redundancy.

1.2. GNSS ARCHITECTURE

A GNSS is composed by three main parts, named *segments*:

- space segment
- control segment
- user segment.

To form the *space segment*, each GNSS has its own constellation of satellites, arranged in orbits to provide the desired coverage. The space segment consists of GNSS satellites, orbiting above the Earth's surface in nearly circular orbital planes. There are three main orbit altitudes: low earth orbit (LEO), medium earth orbit (MEO), and geostationary earth orbit (GEO). The relation between orbit altitude and Earth circulation period is fixed: LEO satellites are located under 2000 km of height from Earth' surface and circulate the Earth in the range of 95 to 120 minutes; MEO satellites are located in an altitude range between 5000 and 20000 km and take around 6 hours to circulate the Earth; finally, the altitude of GEO satellites is fixed at about 35000 km, at which the satellites exactly match the Earth rotation speed, allowing the satellite to remain at the same point from the Earth view. The satellites have various identification systems to be recognised.

The *control segment* is responsible for controlling the whole system, including the deployment and maintenance of the system, the tracking of the satellites in their orbits and the clock parameters, the upload of the data message to the satellites. Tracking stations located around the world coordinate the

activities for controlling and monitoring the system using bidirectional communication with GNSS satellites.

Finally, the *user segment* consists of all the users equipped with passive receivers, i.e. GNSS receivers and antenna, able to acquire, decode and record the signals coming from satellites.

A scheme of GNSS segments is depicted in Figure 1.1.

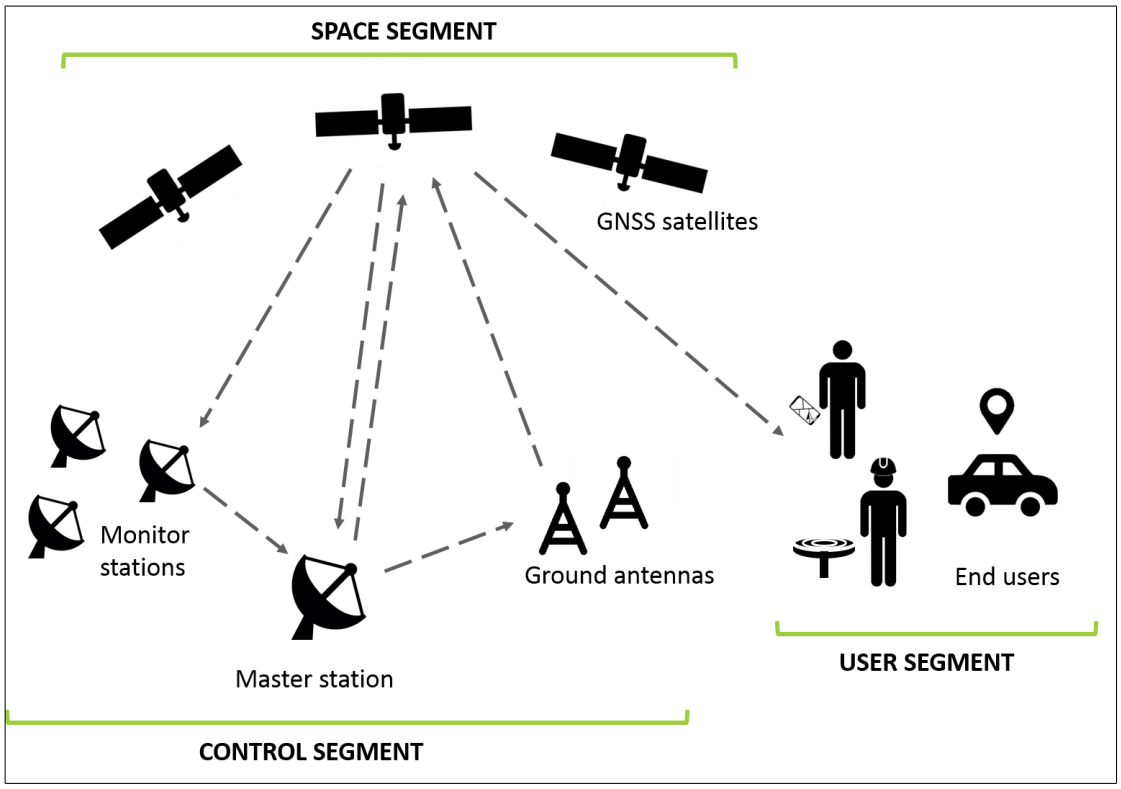

Figure 1.1. GNSS segments.

1.2.1. GPS

The U.S. Department of Defense has started to develop the GPS since 1973 for military purpose. The first satellite was launched in 1977. The NAVSTAR Global Positioning System reached the full military operational capacity in 1995. Then, in 2000, the U.S. Congress made the GPS available for civilians too, thus since that time civilians can access GPS service worldwide free of charge.

The space segment of GPS consists of 24 active MEO satellites, at an altitude of 20200 km, distributed in six equally spaced orbit planes with inclination of 55° on to the Equator. Each satellite circulates the Earth in a period of 12 hours. The constellation allows the visibility of at least four satellites everywhere and in every time with an elevation of more than 15° on the horizon; this is the minimum requirement for retrieving of the position (see section 1.1), but often a higher number of satellites (7 or 8) can be seen. It

is important to underline that the geometrical collocation of the satellites strongly influences the positioning accuracy. The effect of satellites geometry is usually expressed by the DOP[9] index.
The different parameters to quantify the goodness of the geometrical configurations are called PDOP[10], HDOP[11], VDOP[12], TDOP[13] and GDOP[14].
The control segment consists of a network of monitoring stations spread around the world mainly along the Equator, and a master control station located in Colorado Springs (Colorado, USA).
The GPS signal is based on the *fundamental frequency*

$$f_0 = 10.23 \ [\text{MHz}] \tag{1.2}$$

whose stability and accuracy is guaranteed by the atomic clocks on the satellites. The satellites send signals at two-band frequencies, L1 and L2, obtained as multiple of the fundamental frequency, which represents the carrier component.

$$\begin{aligned} f_1 &= 154 \cdot f_0 = 1575.42 \quad [\text{MHz}] \\ f_2 &= 120 \cdot f_0 = 1227.60 \quad [\text{MHz}] \end{aligned} \tag{1.3}$$

The two corresponding wavelengths are:

$$\begin{aligned} \lambda_1 &= \frac{c}{f_1} = 19 \quad [\text{cm}] \\ \lambda_2 &= \frac{c}{f_2} = 24 \quad [\text{cm}] \end{aligned} \tag{1.4}$$

The information content in a GPS signal is introduced modulating two different codes on the carrier wave. These codes are specific for each satellite and are called codes of Pseudo-Random Noise (PRN). The L1 frequency is designed to be modulated with two PNR codes, for civil and military use, while the L2 frequency is modulated just with the military code. There are two types of codes on the carrier signals: Coarse Acquisition (C/A) code and Precise (P) code.

9 Dilution Of Precision.

10 Position DOP. It measures the position accuracy (3D coordinates).

11 Horizontal DOP. It measures the horizontal accuracy (2D coordinates).

12 Vertical DOP. It measures the vertical accuracy (height).

13 Time DOP. It measures the time accuracy (time).

14 Geometric DOP. It measures the overall accuracy (3D coordinates and time).

The C/A code is modulated on the L1 carrier; it is a binary sequence of 1023 bit generated at the frequency of 1.023 MHz, a period of 1 ms and a wavelength of 293.1 m. The C/A code contains the time information on the transmission of the signal according to the satellite atomic clock, and it is also used to identify the satellites, because each satellite has its own C/A code.
The P code is modulated on both the L1 and L2 carriers; it is a more complex binary sequence than C/A, generated at the frequency of 10.23 MHz, a period of 7 days and a wavelength of 29.3 m. The P code contains the time information according to the satellite atomic clock when the signal was transmitted as C/A code, except that it has a ten times higher resolution.
Besides L1 and L2, there is another frequency called L5, at 1176.45 MHz, and exclusively reserved for safety of life transportation and other high performance applications.
The GPS Navigation Message is transmitted in both L1 and L2 frequencies at a very low rate (50 bps). The Navigation Message allows the users to know the satellites positions in real time and it contains the broadcast ephemerides, the predicted model coefficients of the satellite clocks, information about the GPS state system and an approximate model of the ionosphere.
The GPS coordinates are transformed from Cartesian geocentric to Geodetic ones and expressed in the WGS84[15] reference frame. The reference time of GPS is GPS time (GPST), the time scale implemented by the atomic clocks on the GPS ground control segment and the GPS satellites themselves. GPS time started at 0 h UTC on 6th January 1980 and since it is not affected by leap seconds, GPS is now ahead by 17 seconds on UTC.

1.2.2. GLONASS

GLONASS has been developed by Russian Federal Space Agency and Ministry of Defense since 1970. The first GLONASS satellites were launched in 1984; in 1993 the orbital constellation of GLONASS reached 12 satellites. In 1996, GLONASS became fully operational with completed constellation of 24 satellites. Between 1996 and 1998, the number of available satellites decreased due to the financial problems. After 2000, the Russian economy recovered and the restore of GLONASS to full operability, reached in 2011, when the GLONASS constellation reached the number of 24 operating satellites in orbit. GLONASS has been developed mainly for military purpose, but it is now available for civilian usage too.
The GLONASS space segment consists of 24 satellites in three orbital planes with 64°.8 of inclination with respect to the Equator, and divided by 45° in latitude. Among these satellites, 21 are active and the other three are used as spares. This constellation ensures at least five visible satellites at any point in the Earth.

15 World Geodetic System 1984.

The control segment consists of the Ground-based Control Complex (GCS) in Krasnoznamensk and connected with 8 Command Tracking Stations (CTS) distributed across the country.
GLONASS gives two different signals: Standard Precision (SP) and High Precision (HP). Just the SP are available for civil users, and the frequencies of the signals are:

$$\begin{aligned} f_1 &= 1602 + n \cdot 0.5625 \quad [\text{MHz}] \\ f_2 &= 1246 + n \cdot 0.4375 \quad [\text{MHz}] \end{aligned} \tag{1.5}$$

where n is the number of the channel; it means that each satellite transmits on a particular frequency.
The signals are modulated by C/A code and P code; the C/A code is only modulated onto L1, while P code is modulated onto L1 and L2. Besides L1 and L2 carriers, GLONASS satellites transmit signals in L3 carrier frequency (1204.704 MHz). This third frequency increases the reliability and accuracy where developers announced that it will be used especially for safety of life applications.
The navigation message includes information about the satellites orbits, satellites status, correction data, and the almanac data about all satellites within GLONASS constellation. In addition, it includes the correction to GLONASS time relative to UTC and the time difference between GLONASS time and GPST.
GLONASS coordinates are expressed using PZ-90[16] reference frame. The GLONASS reference time is GLONASS time (GLONASST), which is synchronized within 1 ms with UTC time, with a constant offset of three hours.

1.2.3. Galileo

In 2002 the European Union (EU) and European Space Agency (ESA) agreed to introduce their own GNSS, called Galileo, as an autonomous, alternative, competitive but compatible GNSS to GPS and GLONASS. The Galileo system was scheduled to be working in 2012, but nowadays is not still completed (at May 2016, 14 satellites were in orbit). The first experimental Galileo satellites, GIOVE-A and GIOVE-B, were launched in 2005 and 2008; the first Galileo satellite was launched on October 2011.
Space segment of Galileo will include a constellation of 30 satellites, orbiting on three circular MEO planes, at 23600 km of altitude. The inclination of each plane will be 56° with respect to the Equatorial plane. Galileo constellation guarantees that at any point on the Earth, there will be at least 6 satellites in the view.
Ground segment consists of two ground-control centres, located in Oberpfaffenhofen (Germany) and Fucino (Italy), five tracking stations, and several uplink and sensor stations.

16 Parametry Zemli 1990 (Parameters of Earth 1990).

Galileo will provide signals in four frequency ranges 1164-1215 MHz (E5a and E5b), 1260-1300 MHz (E6) and 1559-1591 MHz (E2-L1-E1[17]).
The navigation message contains navigation data, integrity data and other supplementary data, including the needed parameters for the time conversion to UTC and GPST.
Like GPS, Galileo will establish a dedicated terrestrial reference frame, called GTRF[18], which will be an independent realization of the ITRS[19].
Galileo has its own system time, called Galileo System Time (GST), a continuous atomic time scale. The GST start epoch is 0 h UTC on Sunday 22nd August 1999, and since it is not affected by leap seconds, GST is now ahead by 15 seconds on UTC.

1.2.4. BeiDou

BeiDou (also known as BeiDou-2 or COMPASS) is the Chinese navigation system, which is still under construction. The idea of a Chinese satellite system was conceived in 1980s. In 2000-2003 the experimental BeiDou-1 constellation, consisting of 3 satellites, was realised. In 2012 the regional BeiDou navigation system, consisting of 10 satellites, started providing service in Asia-Pacific region; by 2020 it is planned to be fully operative with global coverage.
BeiDou constellation will consist of 35 satellites: 27 MEO satellites, 5 GEO satellites and 3 IGSO[20] satellites, transmitting signals in three frequencies: 1575 MHz (B1), 1191 MHz (B2) and 1268 MHz (B3).
BeiDou reference frame is CGCS2000[21], which is consistent with the ITRS. The BeiDou reference time is BeiDou time (BDT), a continuous navigation time scale, without leap second. The BDS started on 0 h UTC on Sunday 1st January 2006, and it is now ahead by 1 s on UTC.

1.2.5. QZSS

QZSS is the Japanese regional navigation satellite system, currently under development. QZSS covers East Asia and Oceania, centring on Japan, and it is designed to ensure that users are able to receive positioning signals from a high elevation at all times.

17 Sometimes indicated as L1.

18 Galileo Terrestrial Reference Frame.

19 International Terrestrial Reference System.

20 Inclined Geosynchronous Orbit.

21 China Geodetic Coordinate System 2000.

The spatial segment consists of three HEO[22] satellites distributed on three orbital planes, containing a satellite each and composing an angle of 120°. Each satellite is active for 8 hours over Japan and 16 hours in the other areas.
The control segment is composed of a master control station, several tracking control stations, laser ranging stations and monitoring stations. The network of monitoring stations covers East Asia and Oceania region, with stations in Japan and abroad (India, Australia, Thailand and USA).
There are 6 signals planned for the QZSS system.
QZSS uses the JGS[23] reference frame. The QZSS reference time is QZSS time (QZSST), conform to UTC.

1.3. POSITIONING CONCEPTS

GNSS positioning is based on a forward intersection, calculating the distances between satellites and receiver, known the coordinates of the satellites themselves by the ephemerides. There are two different ways of measuring GNSS signals: the code and the phase measures, with the same geometric content, i.e. the satellite-receiver distance, but different observables and precisions. In the following paragraphs, the code and phase observation equations will be presented (1.3.1 and 1.3.2), together with the main sources of bias in positioning (1.3.3).

1.3.1. Code pseudo-ranges

The term code measure indicates the measuring of satellite-receiver distance on the basis of the time of flight ΔT of the electromagnetic wave. This measurement is carried out by means of the correlation between the signal generated by the receiver itself and the signal transmitted by the satellite.
The observable is the temporal shift ΔT that the receiver gives to the generated signal to overlap it with the received one at time t.

$$\Delta T = \left(t^S + \delta^S(t)\right) - \left(t_R + \delta_R(t)\right) \tag{1.6}$$

where t^S is the emission time of the signal, t_R is the receiving time of the signal, $\delta^S(t)$ and $\delta_T(t)$ represent the time offsets for satellite and receiver clocks respectively, which are time dependent quantities representing the range biases. The superscript S indicate quantities related to satellite, the subscript R refers to receiver.

22 High Elliptical Orbit.

23 Japan Geodetic System.

The measure of ΔT is possible by means of the C/A code. The C/A code repeats every millisecond, which corresponds to about 300 km in range. Since the satellites are at a distance of about 20000 km from the Earth, C/A code pseudo-ranges are ambiguous, unless the position of the receiver is known with an accuracy higher than 300 km, the length-scale of the code. This makes the ambiguity resolved during the initial phase of acquisition by introducing approximate coordinates of the receiver (Lachapelle, 1991).
The observation equation for code measures is given by

$$L_R^S = c \cdot \Delta T = c \cdot \left(t^S - t_R\right) + c \cdot \left(\delta^S(t) - \delta_R(t)\right) = \rho_R^S + c \cdot \left(\delta^S(t) - \delta_R(t)\right) \tag{1.7}$$

where c is the speed of light, and ρ_R^S is the straight satellite-receiver distance, which is equal to

$$\rho_R^S = \sqrt{\left(x^S - x_R\right)^2 + \left(y^S - y_R\right)^2 + \left(z^S - z_R\right)^2} \tag{1.8}$$

The term $\left(\delta^S(t) - \delta_R(t)\right)$ is often referred to as *global time unknown*.

1.3.2. Phase pseudo-ranges

The term phase measures indicates the measuring of satellite-receiver distance on the basis of the phase deviation of the frequency generated inside the receiver from the frequency transmitted by the satellite.
The two signals will be shifted by a quantity corresponding to the satellite-receiver distance. Due to the periodic nature of the carrier phase, the receiver can't recognise the number N of initial integer cycles between satellite and receiver signals. For this reason, the term N, called *integer ambiguity*, has to be added to the code pseudo-range equation (1.7) as unknown.
From the initial time t_0, in which the receiver is switched on, to a generic time t, the receiver can measure the integer variation of cycles ΔN between t_0 and t; thus, at time t, N will be expressed as:

$$N = N_0 + \Delta N \tag{1.9}$$

where N_0 is known as *initial ambiguity*.
The observation equation becomes:

$$\phi_R^S(t) = \frac{1}{\lambda} \cdot \rho_R^S(t) + \frac{c}{\lambda} \cdot \left(\delta^S(t) - \delta_R(t)\right) + N_R^S(t) \tag{1.10}$$

where ϕ_R^S is the phase pseudo-range, λ is the wave length, ρ_R^S is the straight satellite-receiver distance, $\delta^S(t)$ and $\delta_T(t)$ represent the time offsets for satellite and receiver clocks respectively and N_R^S is an additional unknown for each visible satellite.
Remembering that the relation between speed of light, the wave length and the frequency is expressed by

$$c = \frac{\lambda}{T} = \lambda \cdot f \tag{1.11}$$

it turns out that

$$f = \frac{c}{\lambda} \tag{1.12}$$

Thus equation (1.10) can be written as

$$\phi_R^S(t) = \frac{1}{\lambda} \cdot \rho_R^S(t) + f \cdot \left(\delta^S(t) - \delta_R(t)\right) + N_R^S(t) \tag{1.13}$$

The number of unknowns is four, i.e. receiver coordinates and the global time unknown, plus one additional unknown for every visible satellite.

The problem is not solvable just by means of adding new satellites because each additional satellite carries one additional unknown. A so called *initialization phase* is needed to determine N_0 for every visible satellite. This initialization phase has also to be carried out every time a loss of signal is experienced during the survey, e.g. tunnels, obstructions, dense vegetation.

1.3.3. Main sources of bias

The distances between the satellites and the receivers are computed estimating the so called flight time multiplied by the speed of light.

The flight time is mainly influenced by the synchronization between satellites and receiver time scales, but other effects have to be taken into account: ionospheric and tropospheric delays, multipath and several hardware errors, summarized in Table 1.1, together with the corresponding order of magnitude.

Bias source	**Range**
Satellite orbit	2 m
Satellite clock	2 m
Ionospheric delay	2 – 10 m in zenith direction
Tropospheric delay	2.3 – 2.5 m in zenith direction
Multipath[24]	Code: 0.5 – 1 m Phase: 0.5 – 1 cm
Receiver noise	Code: 0.25 – 0.5 m Phase: 1 – 2 mm

Table 1.1. Main sources of bias (Misra and Enge, 2011)

24 Highly dependent on environment.

Figure 1.2 represents a graphical scheme of the main sources of bias.

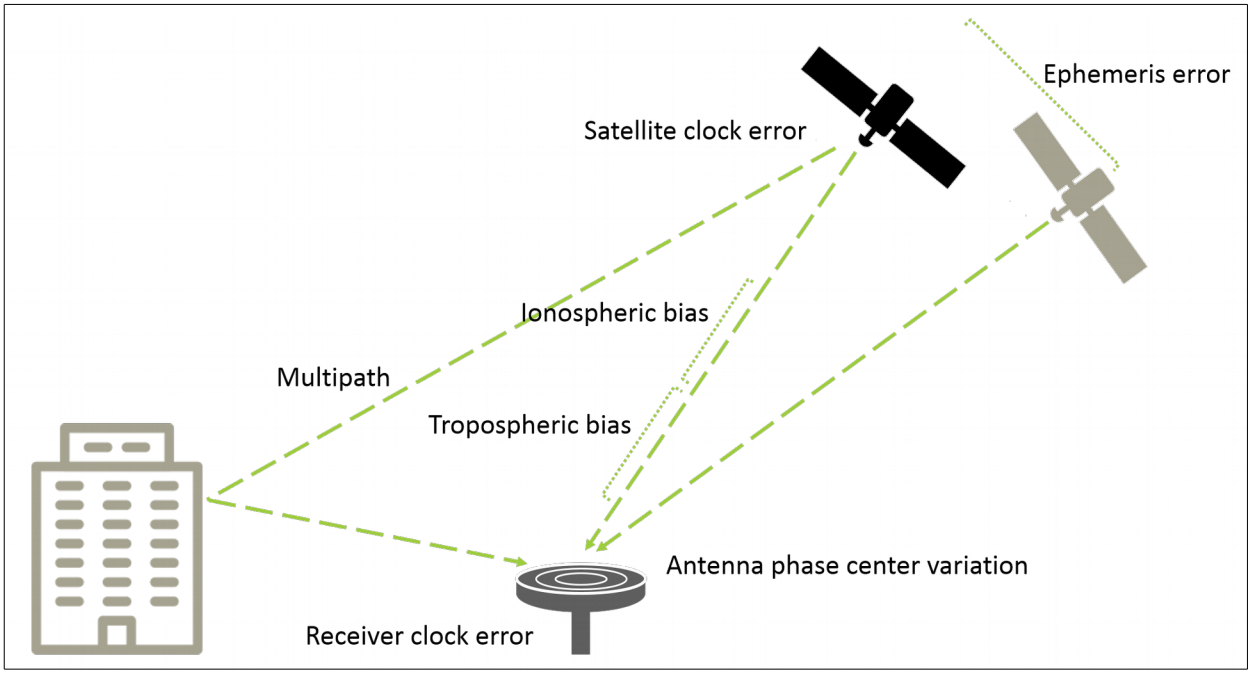

Figure 1.2. Main sources of bias in GNSS signals' transmission.

Briefly, the different sources of bias are described in the following.

- Ionospheric bias: the Ionosphere a layer of the atmosphere. It is a dispersive layer medium. During the crossing of the Ionosphere, GNSS signal is dispersed by the free electrons that are present in the layer. The effect of Ionosphere is very variable from day to day and within the same day due to the physical interactions with solar conditions. The ionospheric effect is more significant for lower the satellites on the horizon. The ionospheric effect can be modelled with an ionospheric model to eliminate the error by using a linear combination of dual frequencies (L1 and L2). For more details, see 2.2, page 26.
- Tropospheric bias: The troposphere is the lowest atmospheric layer. It is not a dispersive layer: in Troposphere, the transmission of the GNSS signal is frequency independent for frequencies higher than 15 GHZ, including GNSS signal frequencies. Tropospheric models are present to estimate the tropospheric delay, depending on temperature, pressure, and humidity. The tropospheric bias will be extensively treated the next chapter. For more details, see 2.2 and 2.3, from page 26.
- Orbital error: the satellites are positioned in precise orbits, but deviations from the orbits could occur due to gravitation forces. To overcome the orbit errors, the satellites positions are monitored and controlled regularly and the corrected data are included in the ephemerides data, which are broadcast within the navigation message.
- Satellite clock error: the satellite clock bias, drift and drift-rate are explicitly determined by the master station of the control segment, which monitors the behaviour of the satellites clocks and broadcast these parameters in the navigation message.

- Multipath: the multipath is caused by the reflection of satellite signal on objects (buildings, trees, etc...). The reflected signal takes more time to reach the receiver than the direct signal, this producing multiple signals from the same satellite (at least one direct and one indirect signal).
- Satellites geometry: the satellites geometry is one of the major factors that affect the position accuracy. When the satellites are spread, the area of overlap of the signals is small, thus the uncertainty area is relatively small; vice versa, when the satellites are allocated close to each other, the area of overlap of the signals is larger (see Figure 1.3). The effect of satellites geometry is usually expressed by the GDOP.

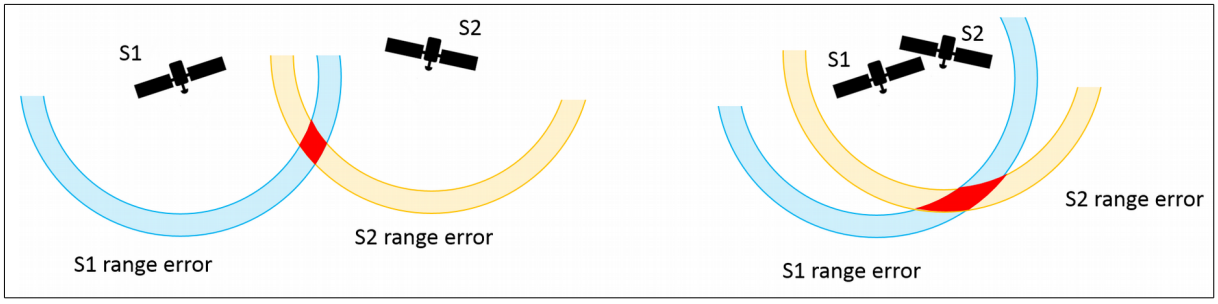

Figure 1.3. Overlapping signals' areas for spread and close satellites.
(On the left and on the right respectively).

1.3.4. Relative positioning

Due to the previously introduced biases, the autonomous point positioning, i.e. *absolute positioning*, can provide accuracy in the order of several meters. To achieve a better positioning precision and to overcome the presence of these errors, several positioning techniques have been developed, typically named *relative GPS*.

Taking into account the main over-mentioned biases, the equation (1.10) can be written as

$$\phi_R^S(t) = \frac{1}{\lambda} \cdot \rho_R^S(t) + f \cdot \left(\delta^S(t) - \delta_R(t)\right) + N_R^S(t) + I_R^S(t) + T_R^S(t) + E_R^S(t) \tag{1.14}$$

where $I_R^S(t)$ is the ionospheric bias, $T_R^S(t)$ is the tropospheric bias and $E_R^S(t)$ is the ephemerides bias.

Considering two generic receivers A and B, simultaneously observing the same satellite j, the observation equation (1.14), could be written as:

$$\begin{aligned} \phi_A^j(t) - f^j \cdot \delta^j(t) &= \frac{1}{\lambda} \cdot \rho_A^j(t) + N_A^j(t) - f^j \cdot \delta_A(t) + I_A^j(t) + T_A^j(t) + E_A^j(t) \\ \phi_B^j(t) - f^j \cdot \delta^j(t) &= \frac{1}{\lambda} \cdot \rho_B^j(t) + N_B^j(t) - f^j \cdot \delta_B(t) + I_B^j(t) + T_B^j(t) + E_B^j(t) \end{aligned} \tag{1.15}$$

The difference between the two equations in (1.15) is

$$\phi_B^j(t) - \phi_A^j(t) = \frac{1}{\lambda} \cdot \left(\rho_B^j(t) - \rho_A^j(t)\right) + N_B^j(t) - N_A^j(t) - f^j \cdot \left(\delta_B(t) - \delta_A(t)\right) + \\ + I_B^j(t) - I_A^j(t) + T_B^j(t) - T_A^j(t) + E_B^j(t) - E_A^j(t) \tag{1.16}$$

This process is called *single differences* (SD). It is important to note that the single differences lead to the elimination of the terms $f^j \cdot \delta^j(t)$, which are related to the non-synchronization of the satellite's clock and are common to the two equations in the hypothesis that the two receivers are observing the same satellite j. While the term depending on the satellite clock bias is eliminated by means of single differences, equation (1.16) is still sensitive to both receivers clock errors (δ_A and δ_B are still present in the equation). Introducing the following notations:

$$\begin{aligned} \phi_{AB}^j(t) &= \phi_B^j(t) - \phi_A^j(t) \\ \rho_{AB}^j(t) &= \rho_B^j(t) - \rho_A^j(t) \\ N_{AB}^j &= N_B^j - N_A^j \\ \delta_{AB}^j(t) &= \delta_B^j(t) - \delta_A^j(t) \end{aligned} \tag{1.17}$$

(1.16) turns into

$$\phi_{AB}^j(t) = \frac{1}{\lambda} \cdot \rho_{AB}^j(t) + N_{AB}^j - f^j \cdot \delta_{AB}^j(t) + \Delta I_{AB}^j(t) + \Delta T_{AB}^j(t) + \Delta E_{AB}^j(t) \tag{1.18}$$

Considering two generic receivers A and B, simultaneously observing the same two satellites i and j, it is possible to write two single differences equations, one for each satellite:

$$\begin{aligned} \phi_{AB}^i(t) &= \frac{1}{\lambda} \cdot \rho_{AB}^i(t) + N_{AB}^i - f^i \cdot \delta_{AB}^i(t) + \Delta I_{AB}^i(t) + \Delta T_{AB}^i(t) + \Delta E_{AB}^i(t) \\ \phi_{AB}^j(t) &= \frac{1}{\lambda} \cdot \rho_{AB}^j(t) + N_{AB}^j - f^j \cdot \delta_{AB}^j(t) + \Delta I_{AB}^j(t) + \Delta T_{AB}^j(t) + \Delta E_{AB}^j(t) \end{aligned} \tag{1.19}$$

Assuming that the two signal frequencies are equal[25], the difference between the two equations in (1.19) is

$$\phi_{AB}^j(t) - \phi_{AB}^i(t) = \frac{1}{\lambda} \cdot \left(\rho_{AB}^j(t) - \rho_{AB}^i(t)\right) + N_{AB}^j - N_{AB}^i + \nabla\Delta I_{AB}^{ij}(t) + \nabla\Delta T_{AB}^{ij}(t) + \nabla\Delta E_{AB}^{ij}(t) \tag{1.20}$$

25 This assumption is true for all GNSS constellation apart from GLONASS: for this constellation, each satellite transmits the signal in a specific frequency (see (1.5), page 10).

The symbols $\nabla\Delta$ indicate the double differences operated on the ionospheric, tropospheric and ephemerides biases. This process is called *double differences* (DD). It is important to note that the double differences lead to the elimination of the terms $f^j \cdot \delta^j_{AB}(t)$, which are related to the receivers' clock bias and are common to the two equations in the hypothesis that the two signal frequencies are the same.
Introducing the notations:

$$\begin{aligned} \phi^{ij}_{AB}(t) &= \phi^j_{AB}(t) - \phi^i_{AB}(t) \\ \rho^{ij}_{AB}(t) &= \rho^j_{AB}(t) - \rho^i_{AB}(t) \\ N^{ij}_{AB} &= N^j_{AB} - N^i_{AB} \end{aligned} \tag{1.21}$$

(1.20) turns into

$$\phi^{ij}_{AB}(t) = \frac{1}{\lambda} \cdot \rho^{ij}_{AB}(t) + N^{ij}_{AB} + \nabla\Delta I^{ij}_{AB}(t) + \nabla\Delta T^{ij}_{AB}(t) + \nabla\Delta E^{ij}_{AB}(t) \tag{1.22}$$

To remove the time independent ambiguities, two double differences referring to two different epochs could be used, obtaining the *triple differences* (Remondi, 1984).
Considering two epochs t_1 and t_2, it is possible to write two double differences equations, one for each epoch

$$\begin{aligned} \phi^{ij}_{AB}(t_1) &= \frac{1}{\lambda} \cdot \rho^{ij}_{AB}(t_1) + N^{ij}_{AB} + \nabla\Delta I^{ij}_{AB}(t_1) + \nabla\Delta T^{ij}_{AB}(t_1) + \nabla\Delta E^{ij}_{AB}(t_1) \\ \phi^{ij}_{AB}(t_2) &= \frac{1}{\lambda} \cdot \rho^{ij}_{AB}(t_2) + N^{ij}_{AB} + \nabla\Delta I^{ij}_{AB}(t_2) + \nabla\Delta T^{ij}_{AB}(t_2) + \nabla\Delta E^{ij}_{AB}(t_2) \end{aligned} \tag{1.23}$$

Ignoring[26] the ionospheric, tropospheric and ephemerides biases, the difference between the two equations in (1.23) is

$$\phi^{ij}_{AB}(t_2) - \phi^{ij}_{AB}(t_1) = \frac{1}{\lambda} \cdot \left(\rho^{ij}_{AB}(t_2) - \rho^{ij}_{AB}(t_1)\right) \tag{1.24}$$

It is important to note that the triple differences lead to the elimination of the terms N^{ij}_{AB}, which is related to the unknown phase ambiguities.

26 For baselines not exceeding 10-15 km, it is always possible to consider the space correlated ionospheric, tropospheric and ephemerides residuals equal to zero, assuming that the biases are equivalent.
For single and double differences expressions, the ionospheric, tropospheric and ephemerides biases have been reported for completeness; in order not to weight the writing too much, they have been ignored for triple differences.

The triple differences is often considered a pre-processing technique to obtain good quality approximate positions for the double differences solution, thanks to the linear combination, which let to remove the ambiguity.

2. THE REMOTE SENSING OF ATMOSPHERE: GNSS METEOROLOGY

There are different techniques to measure the atmospheric parameters such as temperature, humidity, pressure and water vapour content: from surface observations on the ground to weather balloons, from meteorological radar to satellite images. Figure 2.1 depicts a variety of instruments to monitor the atmosphere's parameters, some of which are capable to measure the vertical and horizontal distribution of water vapour; the most common radiosonde and Water Vapour Radiometers (WVR).

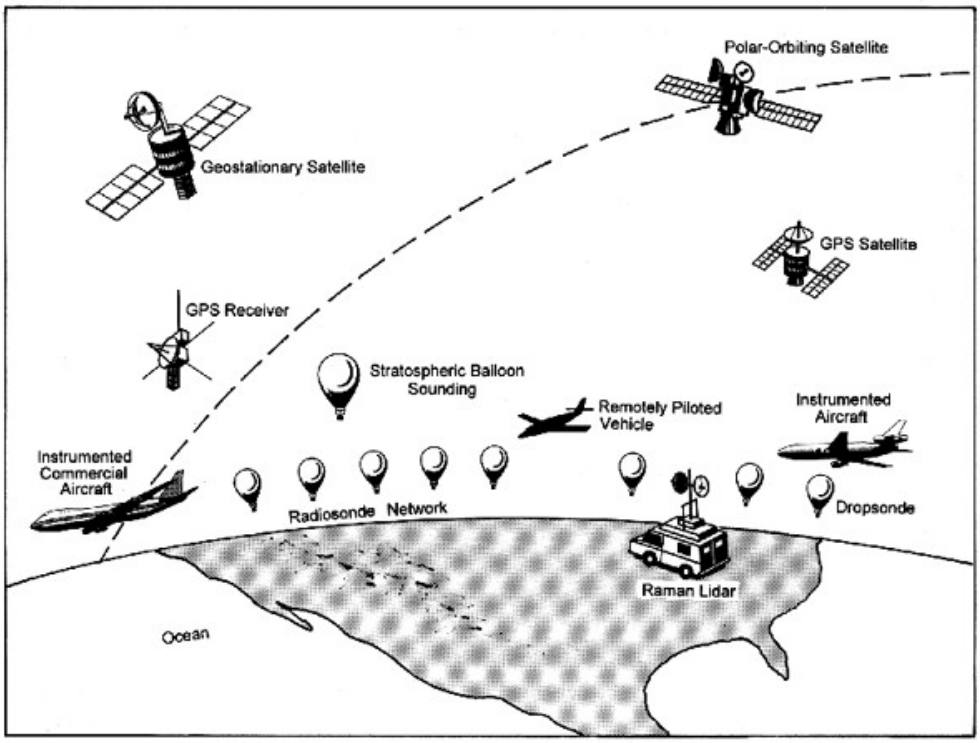

Figure 2.1. Different techniques to monitor the atmospheric parameters.

A radiosonde is a balloon-borne instrument typically equipped with pressure, temperature and humidity gauges, a GPS receiver and a parachute (see Figure 2.2). The radiosonde is used to retrieve the vertical profile of the atmosphere along its path. This instrument provides a good vertical resolution but it is an expensive technique, available for a restricted number of launches (the standard is twice a day) in a limited number of stations; this leads to consider the radiosonde measurements inadequate to resolve the temporal and spatial variability of water vapour, which has finer spatial and temporal scales than the ones available using this technique.

Figure 2.2. A radiosonde lifted by a balloon filled with helium.

Regarding the Water Vapour Radiometers, there are two main categories of instruments: the upward and the downward looking.

The upward-looking WVR is a ground-based instrument that measures the microwave radiation produced by atmospheric water vapour and can estimate the Integrated Water Vapour (IWV) and the Integrated Liquid Water (ILW) content along a given line of sight.

Figure 2.3 reports the two WVRs mounted on the roof of A17 building of Helmoltz Centre, GFZ[27] in Albert Einstein Science Park at Telegraph Hill (Telegrafenberg), Potsdam.

Figure 2.3. Two WVRs mounted in Albert Einstein Science Park at Telegrafenberg, Postsdam.

The downward-looking WVR is a space-based instrument that measures the absorption lines in the radiation from the hot background provided by the Earth; the determination of IWV is complicated by the not uniform temperature of land and by the presence of clouds.

27 Deutsches GeoForschungsZentrum, German Research Centre for Geosciences.

Ground-based units can provide a good temporal coverage but they are lacking in spatial coverage, whereas space-based WVR have the opposite characteristics.

In this context, among the different existing technique, the observation of GNSS (Global Navigation Satellite System) signals can provide a useful contribution for remote sensing the atmosphere, with particular interest to investigate meteorological severe events. As will be discussed in the following sections, the amount of water vapour present in the atmosphere can be estimated as an output of GNSS Permanent Stations (PSs) network compensation, starting from observations on the delay of the electromagnetic signal transmission. This results extremely useful in adding a new independent technique to monitor the atmosphere; it can be used both for comparison with other techniques, to evaluate the reliability of the obtained results, and for improving the observation network, adding a new source of data.

Among the over-mentioned techniques, VLBI (Very Long Baseline Interferometry) has to be cited.

Figure 2.4. Noto VLBI Telescope, belonging to the European VLBI Network (EVN).
Photo credits: Istituto di Radioastronomia - INAF

Similarly to GNSS, VLBI is a technique that exploits signals transmission delay. It is mainly used to determine the reference frames for stars[28] and for Earth[29], and to predict the orientation of the Earth[30]; as a collateral application, VLBI can be employed in remote sensing the atmosphere, in order to derive the amount of water vapour. This is a highly reliable technique (Niell et al. 2001), but has a very low spatial resolution: there are less than 150 telescopes world-wide, mostly located in Northern hemisphere and not

28 Celestial Reference Frame (CFR).

29 Terrestrial Reference Frame (TFR).

30 Earth Orientation Parameters (EOP).

operating continuously, also for the high operations expenses. Figure 2.4 represents the VLBI telescope located in Noto (Italy), belonging to the European VLBI Network.

2.1. THE STRUCTURE OF EARTH'S ATMOSPHERE

The atmosphere is the layer of gases surrounding the Earth. From a chemical point of view, the atmosphere of Earth is mostly composed of Nitrogen (N_2, 78%), Oxygen (O_2, 20%), Argon (Ar, 1%), water vapour (H_2O, variable in the range 0-5%) and other gases (CO_2, N_2O, O_3, …) in lower percentage. Nitrogen, Oxygen and Argon are called *permanent gases*, because their chemical composition and percentage are constant, whereas the other gases are called *variable gases*, due to their not constant presence in atmosphere. Additionally, the atmosphere contains aerosols, suspended particles derived from sea and land, i.e. salt, dust and volcanic hash. On spite of their small concentrations and amounts, they have some important functions; in fact they are responsible of clouds formation, as they act as condensation nuclei, and of scattering the solar radiation.

Among the variable gases, water vapour is the most variable among the major constituents of the atmosphere, thanks to atmospheric circulation: the horizontal distribution, intimately linked with the temperature, is variable from less than 0.01% in Arctic areas up to 5% in warm and tropical locations, and the vertical distribution of water vapour is concentrated in the lowest 2 km from the Earth's ground, rapidly decreasing with height. The distribution of water vapour is intrinsically coupled with the distribution of clouds and rainfall. The water vapour has also the unique characteristic of being the only gas in the atmosphere with phase transitions. The water vapour phase transition is the main cause of large latent heat releasing, which is the primary source of atmospheric energy for thunderstorms and hurricanes, and plays a critical role in the vertical stability of the atmosphere.

In addition, water vapour is a greenhouse gas and it is responsible of the absorption of the radiation coming from Earth, this maintaining a temperature suitable for life on Earth.

For these reasons, water vapour plays a key role in atmospheric processes on a wide range of temporal and spatial scales.

The atmosphere is typically described as a set of concentric layers surrounding the Earth, with different chemical and physical properties. The vertical structure of the atmosphere can be described on the basis of different criteria, depending on the characteristics of the different layers: the temperature, the chemical composition and the electric properties.

Following the temperature criterion, which is the most common one, the atmosphere can be divided into five layers, in each of which the temperature has a typical behaviour, decreasing or increasing with height. The different layers are separated by *pauses* where the temperature experiments inversion. From the Earth's surface to the open space the atmospheric layers are: the Troposphere (it extends from the ground up to about 12 km), the Stratosphere (separated from the Troposphere by the Tropopause, it

extends from the top of the Troposphere to about 50-55 km), the Mesosphere (separated from the Stratosphere by the Stratopause, it extends from the top of the Stratosphere to about 80-85 km), the Thermosphere (separated from the Mesosphere by the Mesopause, it extends from the top of the Mesosphere to the Thermopause, located at an altitude range of 500-1000 km from Earth surface and highly variable due to solar activity), and the Exosphere (separated from Thermosphere by the Thermopause, it extends from the top of Thermosphere to about 10000 km).

A scheme of the different layers and the temperature lapse rate is represented in Figure.

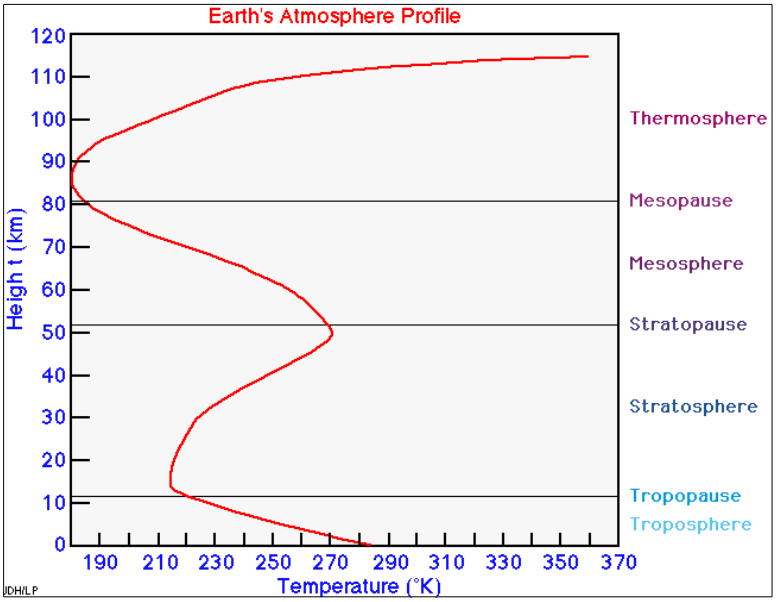

Figure 2.5. The atmosphere's layers and temperature lapse rate.

As Figure 2.5 shows, in the Troposphere and in the Mesosphere the temperature decreases with height, while in the Stratosphere and in the Thermosphere the temperature increases with height. The temperature profile clearly shows the inversion of the temperature in the pauses between two layers.

Focusing on the Troposphere, it is the most interesting layer for GNSS signal transmission because it is the zone of active weather, where all the clouds types and meteorological precipitations, i.e. rain, snow, hail, develop. The Troposphere contains about 75% of the mass of the atmosphere (and 50% of the total mass of the atmosphere resides in the first 6 km from the ground), and nearly all atmospheric water vapour or moisture.

In parallel to the temperature based definition, another important atmospheric layers classification is the electric properties based, where the Ionosphere is defined as the region within the upper atmosphere (from about 80 km up to 600 km of height) where large concentrations of ions and free electrons are present. The density of ions and electrons is highly variable, depending on the intensity of solar radiation, the geographic position, the seasonality and the period of the day. The Ionosphere has practical importance because, among other functions, it influences radio propagation.

In Figure 2.6, the Ionosphere is represented with the five layers of the temperature-based definition.

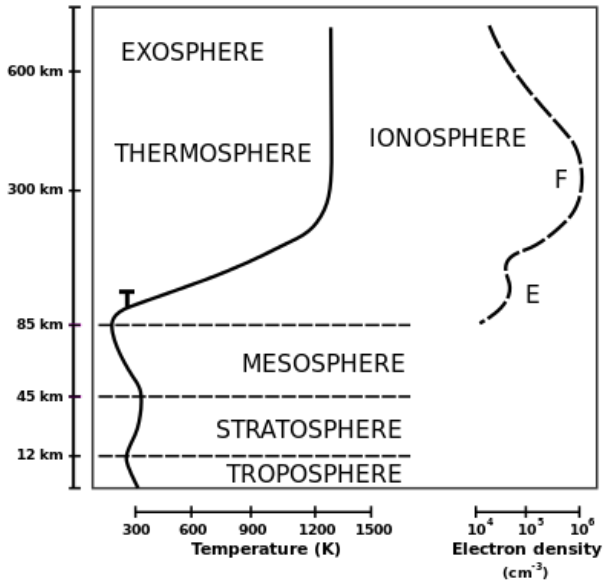

Figure 2.6. The Ionosphere and the five layers of temperature based classification.

Following the electric properties based definition, the first three layers of atmosphere (Troposphere, Stratosphere and Mesosphere) are often referred to as neutral atmosphere, because they consist of non-ionized (neutral) gases, in contrast with the Ionosphere. Figure 2.6 also shows the absence of free electrons in these three layers.

In the following paragraph, the importance of both Troposphere and Ionosphere in GNSS signals transmission will be discussed.

2.2. EFFECTS OF ATMOSPHERE ON GNSS SIGNAL'S TRANSMISSION

GNSS has originally been designed for navigational purposes, to determine the position, expressed by the coordinates (φ, λ, h)[31], of the receiver by means of pseudo-range or phase measures. Both these approaches are affected by biases, primarily produced by the Earth's atmosphere, that has the effect of increasing the real distance between satellite and receiver, and by structural and non-structural causes: receiver/satellite clock errors, multipath, code/phase range, etc.

The basic GNSS carrier phase observable can be written as follows

$$\phi_R^S(t) = \frac{1}{\lambda} \cdot \rho_R^S(t) + f \cdot \left(\delta^S(t) - \delta_R(t)\right) + N_R^S(t) + I_R^S(t) + T_R^S(t) + E_R^S(t) + MP(t) + \varepsilon \qquad (2.1)$$

31 (φ, λ, h) stands for (Latitude, Longitude, Ellipsoidic height).

where λ is the wavelength of carrier phase, ρ_R^S is the satellite-receiver distance in vacuum (obtained by satellite and receiver coordinates), $f = \frac{c}{\lambda}$ is the frequency of the signal (expressed as ratio between the speed of light and the wave length), δ^S and δ_R are the satellite and receiver clock errors, N_R^S is the unknown initial phase ambiguity, I_R^S is the ionospheric (slant) delay, T_R^S is the tropospheric (slant) delay, E_R^S is the ephemerides bias, MP is the multipath error, and ε contains all the remaining un-modelled errors.

Most of the terms of (2.1) can be neglected by means of appropriate precautions during the installation of the instrumentation and expedients when the system is operative. For example, ρ_R^S estimation can be improved by means of accurately known satellites and receiver positions, δ^S and δ_R can be eliminated using the double differences strategy[32] (or can be estimated in Precise Point Positioning, PPP), N_R^S needs to be resolved in the initialization phase, I_R^S can be eliminated using the *iono-free* combination[33], the multipath effect can be mitigated choosing the position of the antenna far from reflecting objects, installing special antenna (chocke-ring antenna), masking low elevation signals or by means of techniques and models specifically designed to recognise the reflected signals and discard them.

The presence of atmosphere instead of vacuum affects the electromagnetic signals' transmission in two different ways: it makes the satellite-receiver path curved and it slows down the electromagnetic waves. This effect is commonly known as *refraction error* or *atmospheric bias* and descends from Fermat's law[34] for signal propagation.

The evaluation of the transmission delay can enhance the positioning precision and, at the same time, can help to monitor the atmosphere and to interpret severe meteorological events.

The employment of GNSS to monitor the atmosphere results in GNSS Meteorology, this term meaning the field of science that uses ground-based GNSS receivers to remote sensing the atmosphere, with particular attention to its lower part. GNSS Meteorology produces an important improvement in making the observations network denser, thanks to the global coverage and the addition of new source of data; additionally, GNSS measurements can be performed under every meteorological condition, this leading to the possibility of continuous atmosphere monitoring with reliable results, even during meteorological events.

As previously mentioned, the atmosphere produces a delay due to the refraction along the path from satellite to the receiver (Askne and Nordius 1987; Solheim et al. 1999). GNSS signals are delayed by

32 See double differences, page 18.

33 See Appendix (I.b, page 153) for further details.

34 “Light travels between two points along the path that requires the least time, as compared to other nearby paths”.

water vapour, dry air, hydrometeors and other particulates which can be found in the atmosphere (Neill, 1996; Solheim et al., 1997). This delay can be expressed in terms of an increase of path length, given by

$$\Delta L = \int_L n(s)\, ds - \rho \tag{2.2}$$

where n(s) is the refractive index, depending of the position s along the path L, and ρ is the length of the straight path, i.e. the length of the path if the signal travelled in vacuum instead of in the atmosphere. Equally,

$$\Delta L = \int_L (n(s) - 1)\, ds + (S - \rho) \tag{2.3}$$

where S is the total length of the path along L.

Referring to the two effects produced by the atmosphere in electromagnetic signal's transmission, the term (n(s) – 1) represents the slowing of signal in propagating in the atmosphere instead of vacuum, and (S – ρ) is relative to the bending, depending on the elevation angle of the satellites over the horizon. The bending term can be neglected for elevation angles greater than 15° using cut-off angles of the same magnitude, thus ΔL depends on the slowing term only.

Commonly, the atmospheric refraction is expressed as a function of refractivity N

$$N = 10^6 \cdot (n - 1) \tag{2.4}$$

where n is the index of refraction, thus (2.3) turns in

$$\Delta L = 10^{-6} \cdot \int_L N\, ds \tag{2.5}$$

where N refers to Troposphere or Ionosphere depending on the considered layer and it is function of temperature, pressure and water vapour pressure (Smith and Wientraub, 1953; Thayer, 1974).

The Ionosphere is a dispersive layer, thus its effect depends on the frequency of the electromagnetic signal: to higher signal's frequency corresponds a lower ionospheric effect. In particular, frequencies lower than 30 MHz are reflected, whereas higher frequencies can cross the Ionosphere, but they suffer dispersion. The phase velocities of carrier waves increase, whereas the group velocities of modulations decrease. The magnitude of these velocities variations are similar, but their effects differ in the sign. The

group delay is proportional to the Total Electron Content[35] (TEC) along the satellite-receiver path and inversely proportional to the square root of the carrier frequency[36].

Vice versa, the Troposphere can be considered a non-dispersive layer for frequencies lower than 15 GHz, including radio waves, thus the Troposphere's refraction is frequency independent and it is only due to temperature, pressure and relative humidity.

Both Ionosphere and Troposphere have to be taken into account when remote sensing the atmosphere, due to the different biases they introduce in GNSS positioning, the ionospheric and the tropospheric bias, respectively.

The ionospheric bias is dominant but can be easily modelled and eliminated by means of proper L1 and L2 phase combinations (*iono-free model*) transmitted by GNSS satellites and using the dispersion relations for Ionosphere (Spilker, 1980; Brunner and Gu, 1991). This is the reason why GNSS satellites transmit the signal on two carrier frequencies: L1 at 1.57542 GHz (wavelength: 190 mm) and L2 at 1.22760 GHz (wavelength: 244 mm). Conversely, the tropospheric bias can't be reduced by means of any combination because of the not-dispersive behaviour of the Troposphere, hence the residual bias is attributable to the tropospheric bias.

2.3. TROPOSPHERIC DELAY ESTIMATION

As previously stated, the tropospheric refraction induces a delay on GNSS signals that affects the real satellite-receiver distance.

The atmosphere is a mixture of dry gases and water vapour, which is the only constituent with a dipole moment to contribute to atmosphere's refractivity. It is common to treat the dipole component of water vapour refractivity separately from non-dipole components in the atmosphere because it is about 20 times larger. The two components are commonly referred to as the *wet* and *hydrostatic delays*; both of them assume smaller values along the zenith direction and increase with the inverse of the elevation angle's sine.

The hydrostatic component is dominant and contributes for about the 90% on the total effect, its order of magnitude is about 2.3 meters in the zenith direction. The wet component is variable from few centimeters up to about 35 centimeters; on spite of the smaller effect, it represents the main source of bias

35 The Total Electron Content (TEC) is highly variable in time and space. Since it is strongly dependent from the solar radiation flux, the TEC increases during the day and decreases during the night, when the ionizing effect of solar energy is lower and the free electrons recombine with ions. A wide number of atmospheric phenomena have an impact on TEC: sunspot cycle, sun's rotation, Travelling Ionospheric Disturbances (TID), ionospheric scintillation, Earth's magnetic field, seasonality and location.

36 See Appendix (I.a, page 151) for further details.

for its larger variability and more difficult predictability with respect to theoretical models and meteorological measurements from surface (Resch, 1984; Tralli et al., 1988).

Geodesists use to obtain the hydrostatic delay from surface measurements and attempt to deduce the wet delay. The wet delay can be measured by Water Vapour Radiometer (WVR) observations (Resch, 1984; Ware et al., 1986; Elgered et al., 1991), with the complications due to the low spatial coverage previously outlined.

Traditionally, the techniques to estimate hydrostatic and wet delays are focused on correcting the GNSS signals to improve the positioning precision. Starting from high-precisely known positions, i.e. GNSS Permanent Stations' positions, it is possible to "invert" the positioning problem and use GNSS measurements to study the atmosphere, the water vapour distribution and the spatio-temporal variation of hydrostatic and wet delays. In this context, a GNSS-based approach has been developed to determine the Zenith Hydrostatic and Wet Delays (Tralli et al., 1988; Herring et al., 1990); the delay along an arbitrary path consists of the zenith delay multiplied by a *mapping function*, which is used to relate the zenith delay and the elevation angle (Davis et al., 1985).

The delay on the satellite-receiver line-of-sight (also known as Slant Total Delay, STD) can be mapped in the zenith direction to retrieve the Zenith Total Delay (ZTD).

ZTD can be expressed as the sum of its two components, the Zenith Hydrostatic Delay (ZHD) and the Zenith Wet Delay (ZWD):

$$ZTD = ZHD + ZWD \tag{2.6}$$

ZTD can be estimated using scientific software for every GNSS receiver to obtain the correction to be applied to the delay computed in a defined time span (generally, two hours or lower) with a tropospheric model adopted in standard atmosphere conditions.

The total delay D of a GNSS signal with a certain elevation angle θ is given by

$$D = ZTD \cdot m(\theta) \tag{2.7}$$

where $m(\theta)$ is the mapping function, typically independent from azimuthal direction and only depending on the elevation angle, since the simplification of azimuthal symmetry is widely introduced.

Figure 2.7 shows an example of how the mapping function works in transforming the Slant Total Delays (STD) from many satellites to one single Zenith Total Delay (ZTD), referred to the single GNSS station.

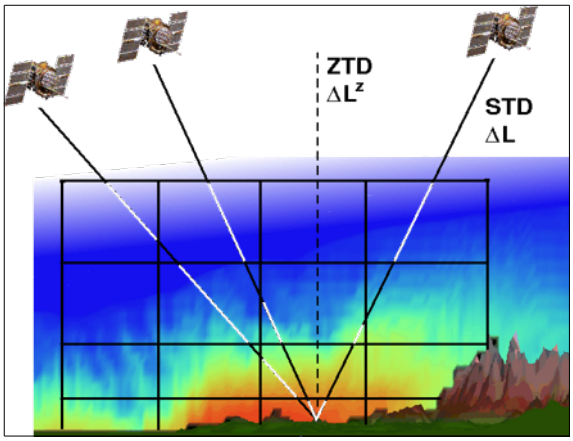

Figure 2.7. Example of mapping function to transform multiple STD in one ZTD.

Since the tropospheric effect is frequency independent and can't be eliminated by means of phase combinations, a modelling depending on other parameters, such as temperature, pressure and relative humidity is required.

Having surface pressure measurements, Saastamoinen (1972) showed that ZTD can be split into the Zenith Hydrostatic Delay, which depends only on atmospheric pressure, and the Zenith Wet Delay. It is possible to model the Zenith Hydrostatic Delay with reliable accuracy (in the order of few millimeters), as long as the accuracy of pressure measurement is higher than 0.3 mbar.

Elgered et al. (1991) proposed the following relation

$$\mathrm{ZHD} = \frac{(2.2779 \pm 0.0024) \cdot P_s}{f(\varphi, H)} \tag{2.8}$$

where ZHD is measured in mm, P_s is the total surface level pressure (in mbar) and $f(\varphi, H)$ is a function accounting for the gravitational acceleration variation depending on the latitude φ and the height H on the ellipsoid (measured in km).

$$f(\varphi, H) = 1 - 0.00266 \cdot \cos(2\varphi) - 0.00028 \cdot H \tag{2.9}$$

Davis et al. (1985) suggested

$$\mathrm{ZWD} = 10^{-6} \cdot \left(k_2' \cdot \int \left(\frac{P_v}{T} \right) dz + k_3 \cdot \int \left(\frac{P_v}{T^2} \right) dz \right) \tag{2.10}$$

to obtain ZWD (in mm), where P_v is the partial pressure of water vapour (in millibar), T is the atmospheric temperature (in Kelvin) and

$$\begin{aligned} k_2' &= (17 \pm 10) \quad \left[\frac{K}{mbar}\right] \\ k_3 &= (3.776 \pm 0.03) \cdot 10^5 \quad \left[\frac{K^2}{mbar}\right] \end{aligned} \tag{2.11}$$

The expression provided in equation (2.10) can be evaluated having P_v and T profiles provided by radiosonde, but with the already discussed problem of low availability of data (see page 21). Indeed, the predictability of the ZWD by means of models and surface measurements is much lower than the ZHD one. For this reason, for GNSS Meteorology applications, ZWD is typically obtained by difference between ZTD and ZHD.

Once the two components of ZTD have been obtained, it is possible to express the total delay D of GNSS signal as

$$D = ZHD \cdot m_h(\theta) + ZWD \cdot m_w(\theta) \tag{2.12}$$

where $m_h(\theta)$ and $m_w(\theta)$ represent the hydrostatic and the wet mapping function respectively, both depending on the elevation angle θ. Many relations have been proposed for the hydrostatic and wet mapping functions (Chao, 1972; Black and Eisner, 1984; Lanyi, 1984; Davis et al., 1985), varying the number of meteorological parameters involved, i.e pressure, temperature, humidity.

The possibility of representing the two contributes separately is a great advantage due to the different entity and spatio-temporal variability. Again, this permits to obtain ZWD by subtraction between ZTD and ZHD.

2.4. PRECIPITABLE WATER VAPOUR ESTIMATION

As previously outlined, the tropospheric Zenith Total Delay (ZTD) quantified in the GNSS data analysis is closely related to the value of Integrated Water Vapour (IWV) above each GPS station. IWV is defined as the quantity of atmospheric water vapour overlying the GNSS station, expressed as the vertically integrated mass of water vapour per unit area; thus IWV unity of measure is kg/m^2.

Once the Zenith Wet Delay has been calculated from ZTD, it is possible to estimate the Precipitable Water Vapour (PWV), defined as the maximum amount of condensable water due to water vapour contained in the unitary base column that extends from the receiver's height the limit of troposphere.

PWV is related to IWV by the following relation

$$PWV = \frac{IWV}{\rho} \tag{2.13}$$

where ρ is the density of liquid water. From equation (2.13), it's clear that PWV is expressed in meters, referring to the height of the equivalent column of water above the GNSS station.

PWV can be obtained using the relation proposed by Bevis et al. (1992)

$$PWV = \Pi \cdot ZWD \tag{2.14}$$

Π is a function of the physical parameters and the weighted mean temperature of the atmosphere T_m, representing the average temperature of atmosphere weighted by the pressure of water vapour, and depending on surface temperature, Troposphere's temperature profile and vertical distribution of water vapour.

The proposed relation for Π is

$$\frac{1}{\Pi} = 10^{-6} \cdot \left(k_2' + \frac{k_3}{T_m} \right) \cdot R_v \cdot \rho \tag{2.15}$$

where R_v is the specific gas constant for water vapour, k_2' and k_3 have already been defined in (2.11) and ρ is the density of water.

$$R_v = 461.70 \quad \left[\frac{J}{kg \cdot K} \right] \tag{2.16}$$

Davis et al. (1985) defined the weighted mean T_m as

$$T_m = \frac{\int \left(\frac{P_v}{T} dz \right)}{\int \left(\frac{P_v}{T^2} dz \right)} \tag{2.17}$$

As already stated, it's difficult to estimate the partial pressure of vapour P_v and the temperature T, thus an approximate expression for the weighted mean temperature T_m has been found. This can be done in several ways, for example by means of statistical analysis of radiosonde profiles, using operational meteorological models, or by means of surface temperature observations.

The analysis of 8718 radiosonde profiles over 2 years on United States sites' (latitude range: 27°-65°; height range: 0-1.6 km) led the following linear regression (Bevis et al., 1992)

$$T_m = 70.2 + 0.72 \cdot T_s \tag{2.18}$$

where T_s is the surface temperature. The approximation in (2.18) introduces an error lower than 4% in PWV estimation as long as the temperature T_s is measured with an accuracy of 0.5 K or better.

The previous equations, with particular reference to (2.14), represent the basic equations of GNSS Meteorology and demonstrate the possibility of retrieve the Precipitable Water Vapour spatio-temporal distribution in the atmosphere by means of GNSS observations, which makes possible the monitoring of

PWV by employing a network of continuously operating stations, both for a posteriori and near real-time applications.

2.5. APPLICATIONS IN GNSS METEOROLOGY: THE STATE OF THE ART

As already mentioned, especially designed, dense GPS/GNSS networks have been set up and used for remote sensing the horizontal and vertical distribution of water vapour in the atmosphere, with particular reference to its lower layer, i.e. the Troposphere. In this context, three different approaches have been conducted: the investigation of the vertical PWV column over a single station (Rocken et al., 1997), the exploitation of existing national GNSS networks with mean spacing of about 20 km (Seko et al., 2007; Inoue and Inoue, 2007), and the implementation of especially designed dense and hyper-dense GNSS networks, eventually formed by both dual-frequency and single-frequency receivers (Zhang et al., 2008; Realini et al. 2012; Sato et al., 2013; Tsuda et al., 2013; Oigawa et al., 2015). All the mentioned studies aim to monitor the water vapour content in space and time, in order to support weather forecast and to interpret, and eventually predict, severe meteorological events.
The final purpose of all the studies is to improve the knowledge of the water vapour distribution, which still remains one of the most poorly characterized meteorological parameter.

2.5.1. Vertical water vapour sensing over a GPS/GNSS station

Rocken et al. (1997) proposed to remote sense the water vapour column over a GPS Permanent Stations (PSs) network in near real-time (within 30 minutes of GPS data collection), in order to introduce it in weather forecasting. As the authors stated, the needed data are GPS observations and real-time high-accuracy orbits available. The used GPS network is located in the centre of USA and extends from the Mississippi gulf coast to Yellowstone; the large extension of the network (more than 1500 km) allows to retrieve the vertical of water vapour data without needing additional global GPS stations (Rocken et al., 1993). The network is formed by 16 stations: 15 of them are operated by Forecast System Laboratory (FSL) of NOAA[37], most of them co-located with radar sites (used as comparison) and equipped with meteorological parameters gauges; the last station is operated by University of Utah, and it is used to monitor the geodetic deformation. All the GPS stations are equipped with dual frequency receivers. The authors decided to compare the GPS-derived water vapour columns with the ones sensed by radiosonde and radiometer, to verify the reliability of the obtained results. To do this, radiosondes are released in 5 stations (Vici, Purcell, Haskell, Hillsborough and Lamont) and the data are available twice a day or more frequently, depending on the considered station[38], whereas radiometers operate continuously in the same

37 National Oceanic and Atmospheric Administration (http://www.noaa.gov/).

38 Vici, Purcell, Haskell and Hillsborough provide data twice a day.

sites and provide data every 5 minutes. Real-time GPS data have been retrieved every hour and Bernese 4.0 software has been used to estimate the water vapour column, fixing the stations' coordinates and knowing the satellites' orbits (the predicted satellites orbits computed by the University of Berne are used). The Zenith Hydrostatic Delay is modelled using surface pressure measurements and Niell's mapping function (Niell, 1996), and the Zenith Wet Delay is estimated every 30 minutes and then converted to zenith column water vapour using the relations proposed by Bevis et al. (1992) and summarised in sections 2.3 and 2.4. The near real-time GPS-sensed columns have been obtained for each station of the network every 30 minutes and interpolated to cover the entire study area at the radiosonde release times. The quality of the water vapour columns is evaluated by comparison with the water vapour columns obtained using post-processed GPS data, radiosondes profiles and water vapour radiometers measurements. This comparison showed good agreement with radiosonde and water vapour radiometer and with post-processed GPS-derived columns in 4 month of data.

This application showed the reliability of the obtained data and the procedure to remote sense the water vapour in near real-time. This lead to the possibility of including the GPS-sensed water vapour in operational numerical weather models, in addition to the already mentioned advantages of the technique: accuracy, all-weather operating, high temporal resolution and complementarity with the other observation systems (radiosondes, water vapour radiometers, environmental satellites, …). Finally, this study proves that it is possible to exploit existing networks not specifically designed for meteorological purposes to get interesting and reliable results in water vapour monitoring, provided that the GPS stations are equipped with meteorological sensors, or they are located in proximity of them.

This aspect will be deepened in Chapters 3 and 5, where the innovative GIS procedure to monitor PWV and the needed input data will be presented.

2.5.2. The use of existing GNSS networks for meteorological purposes

The study of atmospheric moisture, its distribution in space and its evolution in time are highly developed in Japan. In particular, the moisture variations associated with moist convection have been carried out analysing PWV derived by the nationwide GNSS network called GEONET[39], introduced in Shoji et al. (2000) and Shoji et al. (2004). Since 1993, GSI[40] started to build a GNSS permanent observation network. Nowadays GSI operates a GNSS network that covers Japan with more than 1300 stations at an average distance of about 20-30 km between two neighbouring stations. Each site is equipped with GNSS dual-frequency receiver, antenna (covered with radome), communication device and backup battery. The main purpose of the network is the monitoring of crustal deformation, but in the near future, the GNSS network will be established for survey and positioning applications also (Imakiire and Nakahori, 2001).

39 GNSS Earth Observation Network System (http://datahouse1.gsi.go.jp/terras/terras_english.html).

40 Geospatial Information Authority of Japan (http://www.gsi.go.jp).

The data observed by all stations are sent and analysed once a day at the central station, settled in Tsukuba, to determine the coordinates of each station. Therefore, the product of final solution is the three-dimensional position of every station in the network for the considered day. Those results are reported to committees responsible to evaluate seismic and volcanic hazard. Some interesting results were achieved in hazard mitigation in different volcanic eruptions and earthquakes: Usu Volcano eruption in Hokkaido (March 2000) and Oyama volcano eruption and earthquake swarm around Kodzu and Niijima Island (June 2000). In those occasions, significant crustal deformations have been observed and analysed.

As already stated, besides the mentioned monitoring activities, which are helpful to study geodynamics and earthquake engineering, GEONET network has a high potential as meteorological sensor (Shoji, 2009), and it has been used for meteorological applications (Seko et al., 2007; Inoue and Inoue, 2007).

Since 2009, MRI[41] of JMA[42] has been using the GEONET derived PWV for operational mesoscale analyses, after the MRI itself deeply tested the possibility to introduce it in NWP[43] (Nakamura et al., 2004; Koizumi and Sato, 2004; Seko et al., 2004a).

Seko et al. (2007) used data from AMeDAS[44] of JMA, GEONET derived PWV, conventional and doppler radar observations and data resulting from numerical simulation by JMANHM[45] to investigate the evolution and the structure of the convective systems that caused the Nerima heavy rainfall, which took place in the Tokyo metropolitan area on 21 July 1999.

Following the TAPS[46] project, observations coming from different equipment, such as Doppler radars and GEONET GPS observations, were employed to describe the structure and evolution of the heavy rainfall.

Previous studies (Seko, 1998; Kanda et al., 2000) investigated the relation between GPS derived PWV and rainfalls over the Kanto Plain, highlighting that an increasing in PWV value precedes rainfall. The combination of the different techniques allowed to observe and study the Nerima thunderstorm, even if the intense rainfall was very localized. This pointed out that the GPS derived PWV alone would not be able to describe the meteorological phenomenon in its complexity, due to the sparse inter-distance between GEONET stations (about 20-30 km), not compatible with the high resolution requested to localize heavy rainfall, which often have very rapid evolution in time and space.

Inoue and Inoue (2007) studied the characteristic features of water vapour fields and tried to relate them to thunderstorms, also using PWV derived from GPS observations coming from GEONET network.

41 Meteorological Research Institute (http://www.mri-jma.go.jp/).

42 Japan Meteorological Agency (http://www.jma.go.jp).

43 Numerical Weather Prediction.

44 Automated Meteorological Data Acquisition System.

45 Japan Meteorological Agency Non-Hydrostatic Model.

46 Tsukuba Area Precipitation Experiment.

Before Inoue and Inoue's study, focusing on Japan's Kanto district during 2001-2005, the water vapour variation associated with convective activities was studied, but only in a limited region (Iwasaki and Miki, 2002) or for one thunderstorm event (Seko et al., 2004). For this reason, the characteristics of water vapour field seemed not been sufficiently clarified. To investigate the characteristics of water vapour field the 5 minutes PWV data were used and compared with the one-hourly accumulated Cloud to Ground (CG) stroke number[47] and one-hourly accumulated rainfall of Radar-AMeDAS, to discover the relationship between the time variation of PWV and that of the convective activity associated with a thunderstorm. What emerges from Inoue and Inoue's study is that GPS-derived PWV appears to reflect the local variations associated with a thunderstorm and could be a prior-signal for thunderstorm occurrence, even if it has not enough resolution to discuss the individual convective cloud, due to the low resolution of GEONET network.

2.5.3. Dense and hyper-dense GNSS networks for meteorological purposes

As already outlined in section 2.5.2, the studies by Inoue and Inoue (2007) and Seko et al. (2007) highlighted that the horizontal resolution of Japan's GEONET network is not high enough to describe the extremely fine structure of the water vapour field associated with a convective cell, because the horizontal scale of convection is in the order of few km. This inspired a new field of GNSS Meteorology: the design and installation of dense and hyper-dense GNSS networks, especially dedicated to meteorological purposes.

In this context, several studies have to be cited: Zhang et al. (2008) for the design of dense mixed single-frequency and double-frequency network, and Realini et al. (2012), Sato et al. (2013), Tsuda et al. (2013), Oigawa et al. (2015) for the implementation of a hyper-dense GNSS network and its exploitation for monitoring water vapour.

Zhang et al. (2008) implemented a mixed single-frequency and double-frequency ground-based GPS water vapour monitoring network in order to support operational weather forecasting in the metropolitan area of Beijing (China). The inter-distance between the GPS stations is about 5-10 km; this can provide an accurate retrieval of single-frequency GPS observations, once the ionospheric delay bias has been corrected with an ionospheric model. The network is formed by 8 single-frequency receivers and 38 dual-frequency receivers. The mixed network has been set up in a way that it can meet the requirements of monitoring the atmospheric water vapour evolution with high resolution, focusing on a region particularly prone to severe meteorological events. The network is equipped with surface meteorological instrumentation, to measure temperature, pressure and relative humidity for every GPS station of the network, a remote transfer and control system, a processing and analysis system for GPS data (mainly devoted to ionospheric bias correction, PWV retrieval, multipath effect correction), a WEB-GIS system

47 The CG stroke number shows the total number of cloud-to-ground (CG) lightings.

for delivering operational products, and a data assimilation system for NWP. The network provides PWV every 30 minutes for every station in the network and 3D tomography charts every 15 minutes. The predisposition of such network highly improved the understanding of storm evolution: the investigation of the severe meteorological event occurred in the flood season of 2004 indicated that precipitation is associated with a sharp increase of PWV followed by a sharp decline. Moreover, the prediction of the timing, location, and intensity of heavy rainfall events are significantly improved thanks to the assimilation of the ground-based GPS precipitable water vapour data.

Realini et al. (2012) and Sato et al. (2013) installed 17 dual-frequency GNSS stations network, specifically designed for high resolution PWV retrieval. The network has a horizontal spacing of 1-2 km, it covers an area of about 10 × 6 km^2 and it is located near Uji Campus of Kyoto University (Japan). The network is surrounded by 5 GEONET GNSS stations. All the 17 receivers are identical and observe GPS, GLONASS and QZSS[48] at 1 Hz. The network is equipped with surface pressure and temperature gauges, which are needed for ZWD and PWV retrieval. GNSS and meteorological observations are automatically synchronised, and the data are sent every 5 minutes to the central processor. This lets near real-time monitoring of PWV and allows to improve the horizontal resolution of PWV maps, useful for the implementation of an early warning system for now-casting severe local events.

The network was used for several different scientific applications. A first test was carried out by Realini et al. (2012) to characterise the temporal and spatial variability of PWV at local scale. The GNSS-derived PWV, detected by high rate (5 and 30 seconds) PPP[49], has been validated by comparison with radiosonde and microwave radiometers measurements. Finally, the PWV estimated with the Uji Campus' GNSS network is interpolated to obtain 2D PWV maps over the study area.

Sato et al. (2013) deepened the analysis already conducted by Realini et al. (2012) and more rigorously validated the coherence between GNSS-derived and radiosonde/radiometers PWV by selecting single GNSS slant delays passing near the radiosonde or radiometers direction. They also improved the PWV horizontal resolution by means of employing only high-elevation satellites, with the final purpose to take advantage of QZSS for applications in the near future.

Tsuda et al. (2013) tested the accuracy of GNSS derived PWV adding the comparison with Raman Lidar[50] to the previously mentioned radiosonde and radiometers techniques. They also studied the temporal and spatial fluctuations of water vapour on the local scale of few km, showing that the PWV fluctuations are a significant signal and they are not related to GNSS measurements noise. The authors also proposed to

48 Quasi-Zenith Satellite System.

49 Precise Point Positioning.

50 The Raman Lidar is an active, ground-based laser remote-sensing instrument that measures vertical profiles of water vapour, mixing ratio and several cloud- and aerosol-related observables. Differently from radar, which exploits microwave radiation, the Raman Lidar uses the pulses of laser radiation to remote sense the atmosphere.

extend the monitoring system in order to cover the entire urban area with high resolution, introducing several hundreds of receivers. Thus, they suggested to use single-frequency receivers in order to maintain the costs as low as possible. Of course, the employment of single-frequency receivers needs the introduction of an ionospheric bias model, because the ionospheric delay could not be estimated with a single frequency signal. The authors themselves developed an ionospheric model to be applied to the single-frequency receivers, starting from the observations of the near double-frequency receivers.

Concluding, Oigawa et al. (2015) exploited the Uji Campus' GNSS network focusing on the heavy rainfall event of 13-14 August 2012 around Uji. They mainly focused on the correlation of PWV fluctuations and the occurrence of heavy rain, in effort to find remarkable features that precede severe rainfalls. They employed the JMANHM model to simulate the precipitation intensity, and they compared the meteorological radar observations of rain and the GNSS derived PWV.

3. DATA INFRASTRUCTURES AND DATABASE

As previously outlined, the GNSS Meteorology applications that have 2D PWV maps as final product mainly exploit existing national GNSS networks or specifically designed dense GNSS networks (sections 2.5.2 and 2.5.3).

An element of innovation in this field has been introduced by Andrea Walpersdorf[51], who proposed to use existing regional, national and international GNSS Permanent Stations (PSs) for the retrieval of ZTD, to be used in climatological applications and studies (Sguerso et al. 2013).

Exploiting this network and existing Pressure (P) and Temperature (T) observations, coming from NOAA, PWV can be estimated. The particularity of this networks configuration, differently from the previously mentioned GNSS Meteorology applications, is that the input GNSS observations, P and T data are not necessarily co-located. Another novelty of the proposed method is the introduction of a simplified physical model, owned by the research group and currently in the preliminary phase of patent application, which permits to overcome the low density and the sparseness of the networks and the different networks configurations and distribution (Sguerso et al. 2014).

In the following section 3.1, the GNSS PSs network will be presented. Sections 3.2 and 3.3 are dedicated to the description of the ZTD estimation and validation procedures, respectively. Once the ZTD estimations have been obtained and validated, the ZTD DataBase (DB) described in section 3.4 has been created. Finally, in section 3.5 the Pressure and Temperature data needed for obtain PWV will be presented.

3.1. GNSS PERMANENT STATION NETWORK

The Global Navigation Satellite System (GNSS) data from 181 Permanent Stations (PSs), belonging to different International, National and Regional networks covering the French-Italian neighbouring area, have been used to estimate a set of homogeneous tropospheric parameters (ZTD, horizontal North-South and East-West tropospheric gradients) through common elaboration techniques and procedures. The elaboration of GNSS data has been firstly conducted from January 1998 to May 2012 to create a database of ZTD and gradients[52] (Sguerso et al., 2013); under the supervision of Andrea Walpersdorf, I contributed to a recent update, concluded on February 2016, made the data available until the end of December 2015, this producing a set of two-hourly ZTD estimates and couples of N-S and E-W gradients over 18 years.

51 Insitut des Sciences de la Terre (ISTerre), Université Grenoble Alpes, Grenoble (France).

52 ftp://renag.unice.fr/products/GPS_climatology_Sguerso_Labbouz_Walpersdorf/

The GAMIT/GLOBK software ver. 10.4 and 10.6[53] (Herring et al., 2010 and 2015), developed at the Department of Earth, Atmospheric and Planetary Sciences, MIT[54], was employed to elaborate the GNSS data.

The 181 identified PSs belong to different types of existing networks: global (IGS[55] Tracking Network and EUREF[56] Permanent Network), trans-national (GAIN[57]), national (France: RENAG[58] and RGP[59]; Switzerland: AGNES[60]; Italy: GEODAF[61] and RING[62]), and the networks of Italian regions Piemonte[63,64] and Liguria[65].

The total extent of the GNSS network is depicted in Figure 3.1.

53 GAMIT/GLOBK ver. 10.4 was used for the first elaboration (January 1998 - May 2012), whereas the newer ver. 10.6 was employed for the update (June 2012 - December 2015).

54 Massachusetts Institute of Technology.

55 International GNSS Service (http://www.igs.org/).

56 EUropean REference Frame (http://epncb.oma.be/).

57 Geodetic Alpine Integrated Network (http://www.alpine-space.org).

58 RÉseau NAtional GNSS permanent (http://webrenag.unice.fr).

59 Réseau GNSS Permanent (http://rgp.ign.fr).

60 Automated GNSS NEtwork for Switzerland (www.swisstopo.admin.ch).

61 GEOdetic Data Archiving Facility (http://geodaf.mt.asi.it).

62 Rete Integrata Nazionale GPS (http://ring.gm.ingv.it).

63 http://www.spingnss.it

64 http://webgis.arpa.piemonte.it

65 http://www.gnssliguria.it

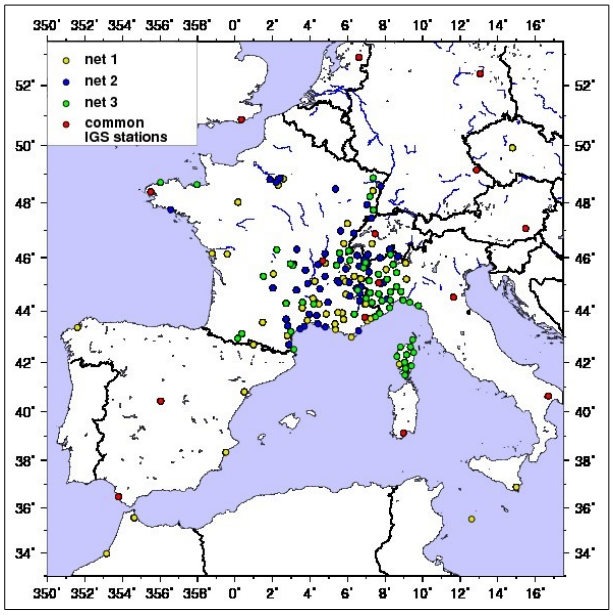

Figure 3.1. The total extension of GNSS network.

Due to computational limits of GAMIT/GLOBK software, the 181 Permanent Stations network has been split in three sub-networks according to decreasing station age (net1, net2 and net3, respectively), to obtain network geometries that are as stable as possible in time. net1 includes the oldest Permanent Stations, which started to be operative from January 1998 to June 2004; net2 includes the PS started before June 2008; lastly, net3 includes the youngest PS, started later than July 2008. Among the 181 PS, 50 stations provide more than 10 years of data, and 57 stations between 5 and 10 years of data. The 74 remaining stations have less than 5 years of available data.

A common set of 15 stations was included in each sub-network in order to achieve a stable reference frame for the entire time span. Within these 15 stations, 13 belong to IGS and 2 to EUREF networks.

To estimate the total amount of ZTD and not only the relative value between the different stations, several IGS stations at large distances (more than 1500 km, according to Tregoning et al., 1998) from the local network were included in each analysis. The IGS and EUREF stations were included in the analysis to ensure a stable reference frame between sub-networks and to de-correlate the vertical positions and the tropospheric delays, thanks to their long baselines.

Figure 3.2 represents a zoom on the French-Italian neighbouring area, where the PS are denser, with a mean spacing of about 40 km between neighbouring PS.

In Figure 3.2, the subdivision of the network is highlighted: net1, net2 and net3 are represented with yellow, blue and green dots respectively, whereas the 15 common PS are represented with red dots.

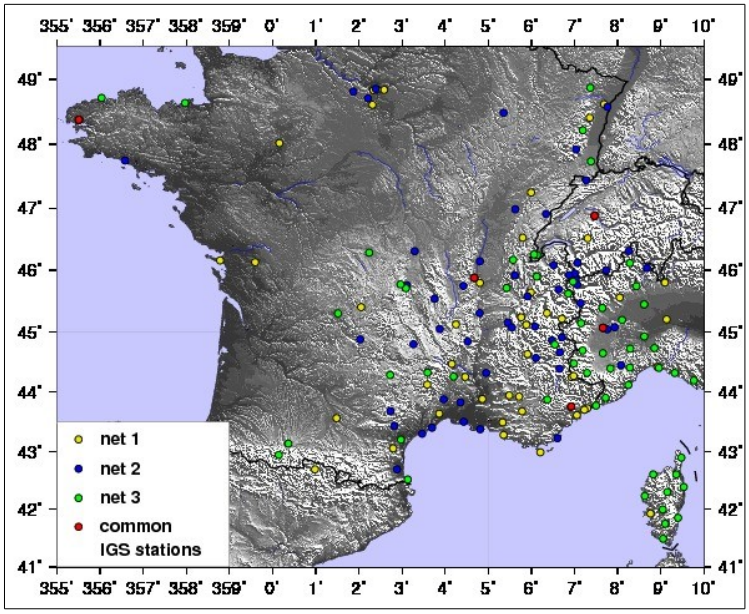

Figure 3.2. Zoom on the denser zone, covering the French-Italian border region.
The common PS are represented with red dots; net1, net2 and net3 are represented with yellow, blue and green dots.

The entire list of Permanent Stations, with stations coordinates (latitude, longitude and elevation), and corresponding sub-network are reported in the Appendix (see II, page 155).
The elaboration criteria and procedures will be explained in the following section 3.2.3.

3.2. ZTD ESTIMATIONS

The present section is dedicated to the description of the methodology and criteria to estimate ZTD for the network introduced in section 3.1. After a presentation on the software used for the elaboration (section 3.2.1), the criteria and procedures to compute ZTD and gradients will be discussed (section 3.2.2 and 3.2.3).

3.2.1. GAMIT/GLOBK software

The software used to compute the ZTD estimations is GAMIT/GLOBK.
GAMIT/GLOBK is a GPS analysis package developed at MIT[66]. The software is designed for estimating the station coordinates and velocities, the representations of post-seismic deformation, the atmospheric delays, the satellite orbits, and the Earth orientation parameters. Two different versions of the software, ver. 10.4 and 10.6, where used in the elaboration process. Ver. 10.4 was used to elaborate the data and obtain ZTD estimations from January 1998 to April 2012, forming the ZTD database; then, in 2015, the new version 10.6 was released and it was used to elaborate the data from may 2012 to December 2015, forming the update of the ZTD database.

66 Massachusetts Institute of Technology.

GAMIT/GLOBK runs under any UNIX operating system.

GAMIT consists of several sub-programs to prepare the data for processing (*makexp* and *makex*) and the batch control files (*fixdrv*), to generate reference orbit and rotation values for the satellites (*arc*, *yawtab*), to interpolate the values of atmospheric and to load models (*grdtab*), to compute the residual observations and the partial derivatives (*model*), to detect outliers (*autcln*), and to perform a least squares analysis (*solve*).

The previously mentioned modules can be run individually or together in a batch file, contained in the *sh_gamit* script.

sh_gamit simply searches for raw or RINEX data and invokes the GAMIT programs to produce constrained and loose estimates of coordinates, sky plots, atmospheric delays, and other outputs.

3.2.2. Setup phase

The data preparation phase consists in assembling the metadata from station log files, setting up the control files and collecting the non-IGS data.

A project[67] directory, containing two sub-directories named *rinex* and *tables,* has to be created. In this specific case, the directory architecture is outlined in Figure 3.3

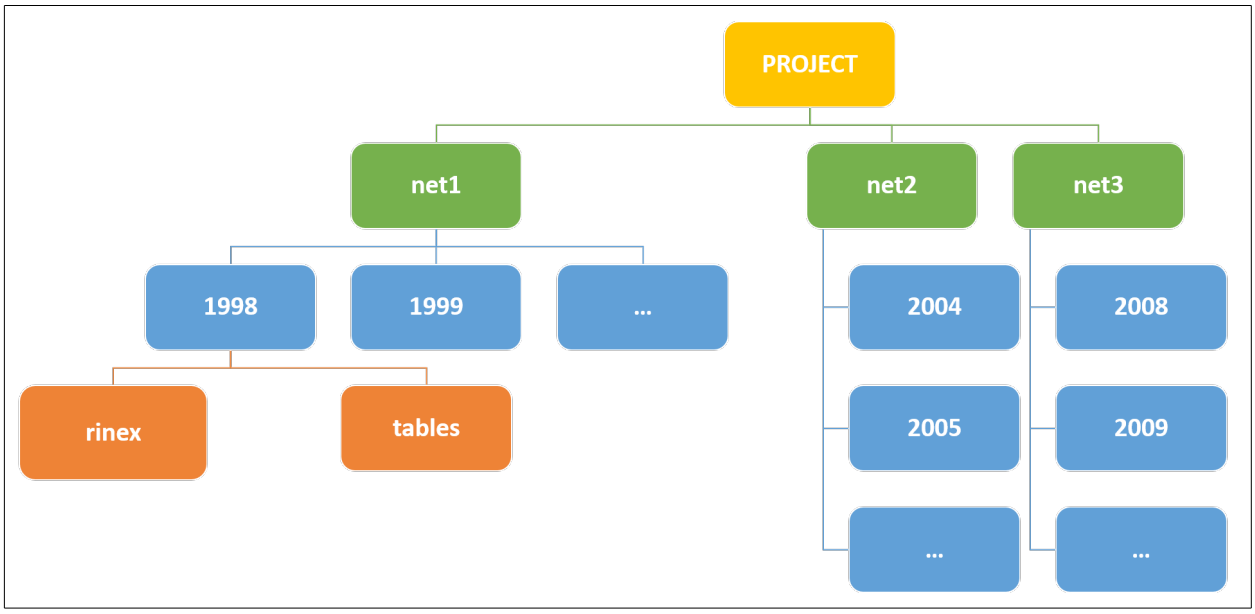

Figure 3.3. Project directories architecture.

where the main folder (*PROJECT*) contains one sub-directory for every sub-network. Each sub-network directory contains a sub-directory for every each year included in the elaboration. Finally, each year

67 In case the project develops in many years, it is suggested to create in the project directory as many subdirectories as the years to include in the project, each of them containing the rinex and tables folders.

directory contains the rinex and tables directories, which should be created manually, whereas other directories will be automatically created and populated during the elaboration.

The rinex directory contains the local RINEX[68] files, manually copied there from local folders, and the RINEX files automatically downloaded from publicly available archives during the processing.

The RINEX format for GPS data provides the current IGS standard for the distribution of phase and pseudorange data (o file), the navigation message (n file) file recorded by a receiver, and a less used file for meteorological data (m file).

A RINEX file is typically named nnnndddf.yyt (e.g. GENO2250.16o) where:

- nnnn is the 4-character station name designator, e.g. GENO for IGS's Genoa Permanent Station
- ddd is the day of the year of first record, e.g. 225 for 12th August 2016
- f is the file sequence number/character. For daily RINEX files f equals zero; for hourly RINEX files f equals a letter (from a to x) depending on the hour, e.g. a for first the hour (from 00 to 01), b for the second hour (from 01 to 02), …, x for the 24th hour (from 23 to 24)
- yy is the two digits indicating the year, e.g.16 for 2016
- t indicates the type of file:
  - o: observation file
  - d: observation file, Hatanaka[69] compressed
  - n: GPS navigation message file
  - m: meteorological data file
  - g: GLONASS navigation message file
  - l: Galileo navigation message file
  - p: mixed GNSS navigation message file
  - h: SBAS Payload navigation message file
  - b: SBAS broadcast data file
  - c: clock file
  - s: summary file (used by IGS, it is not a standard format).

A sample of RINEX file GENO2250.16d, referred to GENO Permanent Station for 12th Augustr 2016 can be found in the Appendix (see VI, page 180).

68 Receiver INdependent Exchange.

69 In order to additionally reduce the size of observation files, Yuki Hatanaka developed a special compression scheme that takes advantage of the structure of the RINEX observation data by forming higher-order differences in time between observations of the same type and satellite. This compressed file is an ASCII file that is subsequently compressed again using the standard compression programs.

The following control and data files have to be copied (from ~/gg/tables) in the /tables directory:

- process.defaults: contains the specifications of the computation environment and the processing directory structure, the sources for data and orbit files, the session parameters (start time and sampling interval), and the instructions for archiving the results;
- sites.defaults: contains the list of stations to be used and how the station metadata are to be handled;
- station.info: contains the site metadata (e.g. receiver and antenna type, height of instrument, start and stop times of occupation) as a function of time for each station. These information are typically stored in the station log sheet[70]. Any change in the instrumentation has to be recorded in this file, and it should be kept updated;
- coordinate files: the .apr file contains the a priori Cartesian coordinates (position and velocity) of stations; lfile. can contain either Cartesian position and velocity or spherical position. The lfile. is updated after each processed day if the adjustments exceed a specified value;
- sestbl. and sittbl.: sestbl. controls experiment observations and models; sittbl. controls a priori constraints on sites;
- autcln.cmd: controls for cleaning the data in program autcln.

A sample of the files listed above is available in Appendix (see VIII, page 190 and followings).

Once the control files have appropriately been edited, *sh_setup* should be used to check the links to the global files appropriate for the year, especially the *grid* files (otl.grid, atl.grid, map.grid, met.grid from ~/gg/tables), and sh_rx2apr should be launched to prepare and verify the a priori file (.apr).
Then the processing can start from within the experiment directory by using the *sh_gamit* command, followed by at least the 4-character code for the project, and the year and the range of days to process.
The basic *sh_gamit* command is:

```
sh_gamit -expt [expt-name] -s [yr] [start-doy] [stop-doy] > out.log
```

where `-expt` indicates the name of the project and `-s` the year followed by starting doy and ending doy of the processing. For example, to process 4th December 2009:

```
sh_gamit -expt net1 -d 2009 338 > log308.log
```

The `log308.log` file will contain a summary of the processing, indicating the number of stations used, the standard deviation of the phase residuals for the two best and two worst stations, the number of ambiguities resolved, and a list of any large adjustments to station coordinates. These statistics are useful for evaluating the GAMIT output for further possible reprocessing.

70 A sample of site log sheet is reported in Appendix (see VII, page 182).

3.2.3. Elaboration settings, procedure and automation

As already stated in the previous section, the GNSS Permanent Station network was elaborated with GAMIT/GLOBK to produce a database of two-hourly ZTD estimations and couples of N-S and E-W gradients estimated 7 times a day. The NS (North-South) and EW (East-west) gradients are the difference between the slant delay calculated at 10° elevation toward the North (East) and toward the South (West), following the GAMIT manual definition.

The ZTDs and the gradients are calculated for each station, simultaneously with a daily positioning solution for 24 hours sessions.

The following settings were implemented for the ZTD estimations (see Sguerso et al., 2013, and 2015 for deeper details):

- the troposphere was modelled using the empirical Global Mapping Function (GMF) (Boehm et al., 2006), that accounts for the seasonal effects unchanged for each year. The GMF was chosen for its homogeneity over climatological time spans. Moreover, GMF has the peculiarity of being independent from weather models, differently from other widely used mapping functions, e.g. VMF1 (Boehm et al., 2004; Boehm et al., 2006a), which is constrained by 6 hourly ECMWF[71] analysis results;
- the a priori information on pressure and temperature of each PS were computed using the Global Pressure and Temperature (GPT) model (Boehm et al., 2007)[72];
- the absolute antenna phase centre was modelled with IGS_08 model (Schmid et al., 2007);
- the ocean loading FES2004 (Lyard et al., 2006) and atmospheric loading (according to Tregoning and van Dam, 2005) have also been taken into account;
- the IGS final orbits were re-adjusted during the analysis and coherent Earth orientation parameters were used;
- the a priori coordinates used for the PS came from ITRF2008 (Altamimi et al., 2011), when available. The ITRF2008 a priori coordinates were extracted from the daily position using the corresponding ITRF2008 velocity and were kept loosely constrained (Brenot et al., 2006) to ensure a consistent tropospheric parameter estimation (0.5 m on the initial estimate, 0.03 $m/hr^{1/2}$ for the variability of ZTDs, for the offset and for the variability of horizontal gradients, respectively);
- the elevation cut-off was kept fixed to the conservative value of 10 degree, to avoid variations in ZTD and vertical position. However, an elevation dependent down-weighting was introduced in the elaboration.

71 European Centre for Medium-range Weather Forecasts.

72 Since 2013, GMF and GPT have been replaced by a new mapping function and pressure and temperature model, the GPT2 model (Lagler et al., 2013). The differences in tropospheric parameter evaluation due to the choice of the tropospheric model have been analysed for the PSs network (Sguerso et al., 2015), and are briefly reported in the following.

For further specification on the chosen parameters, refer to the sestbl. file, reported in Appendix (see VIII.f, page 200).

Once these settings have been chosen, it is possible to start the elaboration procedure to produce the ZTD and gradient estimations. The procedure consists of two consecutive phases: the local RINEX data download, followed by the operative GAMIT elaboration.
The first step is downloading the RINEX files for those PSs which do not have publicly available ftp, by means of the following command, to be launched in the rinex directory:

```
sh_get_rinex -archive [arch-name] -yr [year] -doy [start doy] -nday [days] -sites [site]
```

where `-archive` is the name of the archive where to search for RINEX data, `-yr` is the year, `-doy` is the first doy to download in the chosen year, `-nday` is the number of consecutive doys to be downloaded, and `-sites` is the name of the site.
Since the `-nday` specification is not always working, a bash script was written to automatically download local RINEX file. It should be run inside the rinex folder. The code can be found in Appendix (see IX.a, page 208).
Then, the `sh_gamit` command can be run in the year folder as follows:

```
sh_gamit -orbit [orbit] -expt [name] -eops [eop] -d [year doy]
```

where `-orbit` specifies the type of orbit to use (IGS final orbits were used in the elaboration), `-expt` is the name of the experiment, as reported in sites.defaults file (in this case, the experiment name is net1, net2 or net3 according to the network to be elaborated), `-expt` specifies the Earth orientation parameters to be used (the USNO[73]), and `-d` indicates the year and the initial and final doy to be processed. Additionally, the string `> testdoy.out` was added to produce a text file with the summary of elaboration. For example, the command

```
sh_gamit -orbit IGSF -expt net2 -eops usno -d 2012 276 > test276.out
```

processes the 2nd October 2012 for net2, using IGS final orbits and USNO Earth orientation parameters, and produces the test276.out output file.
In order to better control the process, to be able to individuate and solve any problem that may occur, and to speed up the elaboration, enabling the automatic processing of several groups of days in parallel, a simple bash script, named *prepare_gamit*, was used. The script, originally written by Laurent Labbouz and slightly modified, automatically creates several text files, each of them containing about 30 lines of sh_gamit command, corresponding to likewise days to be processed. The text files can run in parallel, this

73 United States Naval Observatory.

allowing to save processing time. The bash script and the output file can be found in Appendix (see IX.b and IX.c, page 208 and followings).

The elaboration produces a directory for each processed doy and a set of automatically generated and populated folders (e.g. archive, control, ionex, …). The daily solution is found in the corresponding doy folder. Concerning the ZTDs and gradients, they can be extracted from the GAMIT O-file, a file called o + expt name + a. + doy (e.g. onet3a.090 is the file relative to 30th March for net3) which can be found in each doy directory. This file contains the error correlation matrix, the coordinates adjustment, the ZTDs and gradients (both ambiguity free solution and ambiguity fixed solution).

The ZTDs and horizontal gradients were estimated for 24 hours sessions and were extracted from the ambiguity free solution. The ambiguity free solution was chosen in order not to introduce biases in the ZTDs, which are correlated with the vertical positioning (Santerre, 1991; Walpersdorf et al., 2007).

To extract the ZTD and gradient estimations from the solution file, a bash script (*extract_atm*), originally written by Laurent Labbouz and slightly modified, was used. Starting from a file listing the PS to extract the data for, the script is intended to extract ZTDs, N-S and E-W gradients from GAMIT O-file simply using the *grep* Unix command on specified lines, exploiting the regular formatting of O-file itself. *extract_atm* produces three files as outputs: an .az file containing the ZTD estimations, and two files, .ns and .ew, containing the gradients. The *extract_atm* bash script and a sample of the three output files can be found in appendix (see IX.d, IX.e, IX.f, IX.g, page 209 and followings).

All the previously introduced bash scripts result extremely useful in the perspective of realising a ZTDs and gradients DataBase, where a large amount of data has to be processed. They have firstly been tested and then widely applied during the DB realisation (see section 3.4, for further details on the DB).

3.3. ZTD VALIDATION

In the future perspective to analyse several severe weather events from 1998 to present, a homogeneous set of tropospheric parameters is needed. Therefore the tropospheric parameters have to be obtained through common elaboration techniques and procedures.

First of all, the position of the PSs must be stable in time, to be able to interpret any tendency in the estimated troposphere parameters. The majority of long term GNSS PSs undergo modifications, documented in the stations log sheets when concerning antenna and receiver, whereas the modifications in the surrounding environment are generally not monitored and not modelled. Sguerso et al. (2015) performed the quality check of the position time series of the PSs network presented in section 3.1, focusing on the vertical component, to distinguish residual offsets related to an equipment change from offsets due to undocumented modifications or to undocumented measurement failures. The result is the attribution of a quality index to PSs (1 for good quality stations, 2 for medium quality stations to be used under specific conditions, and 3 for low quality stations).

Apart from test on the stability in time of PSs positions, the ZTD estimations have been validated by means of two strategies: the first one is an intra-net comparison of ZTDs from the 13 IGS and the 2 EUREF stations, based on results from the three sub-networks in which these stations were included; the latter is a comparison with IGS's official ZTD estimations[74]. Both of them result extremely useful to check the coherence of tropospheric parameters evaluated in different networks and to understand how much the network in which a PS station is included can influence the determination of the troposphere parameters.

The intra-net and IGS comparisons will be presented in sections 3.3.2 and 3.3.3 respectively.

Finally, the mapping function and P/T model used in the elaboration are aspects to take into account in the validation process in order to assess the quality of the tropospheric parameters. The influence of mapping function and P/T model will be summarised in section 3.3.4.

Section 3.3.1 is dedicated to the description of two Fortran codes (*read_GAMIT_ZTD.f90* and *read_IGS_ZTD.f90*) used to automatically formatting the GAMIT and IGS ZTD estimations, filling in the hour(s) and day(s) gaps in case of lack of data and maintaining the two-hourly step between consecutive data. A third Fortran code (*compare_GAMIT_IGS_ZTD.f90*), used to automatically compare the GAMIT and IGS ZTD estimations, will be presented too.

All these Fortran codes have been applied in the validation process.

3.3.1. Automatic read-write codes

In the following sections, the three Fortran codes used for automatically formatting and comparing the ZTD estimations from GAMIT processing and from IGS are described.

read_GAMIT_ZTD.f90 Fortran code

The *read_GAMIT_ZTD.f90* Fortran code is intended to read the output of the *extract_atm* bash script, containing the GAMIT ZTD estimations, and to produce an output file formatted in "IGS format", containing four columns: doy, hour, rms and ZTD. Additionally the code is able to fill in the gaps in case of lack of data and to maintain the two-hourly step between consecutive data.

The code is designed to produce 11 observations (from 00 to 22 UTC) per day in the chosen time span.

Briefly, the code works as follows:

- defines the number of days for each month of the year;
- opens the ancillary file *input_GAMIT.txt* and reads the name of the stations for which to extract the ZTDs, the year, the starting month and day, the ending month and day;
- performs a test on leap year and converts the starting and ending dates in doys (the present and the following instructions are iterated for all the PS included in *input_GAMIT.txt*);

74 The IGS official public solution is publicly available on ftp://cddis.gsfc.nasa.gov/pub/gps /products/troposphere/.

- creates the blank output file, named NAME_netX.year, where NAME is the PS name, read from *input_GAMIT.txt* file, and X is the number of subnetwork to which the PS belongs;
- counts the lines of the input file containing the ZTD, named NAME.year.netX.az, and reads the data;
- converts the date read in the NAME.year.netX.az in doy, and performs a test to verify that the read date is included in the doys interval defined in *input_GAMIT.txt* file;
- performs a test to skip the first 0 UTC time in each day in the NAME.year.netX.az file
- writes on the created blank output file the doy, hour, rms and ZTD (both in mm), filling in any possible gap in the data with the "99999" code (see page 65 for the possible gaps description).
  Again, as in the Pressure and Temperature formatting code (see section 3.5.2, page 65), the criterion whereby the hour(s) and/or day(s) gaps are found is the comparison between the actual read hour and day, and the last hour and day written: if the difference between the two hours is more than 2, a gap is detected and filled with "99999" code.

The output file is a set of column containing station doy, hour, rms and ZTD.
The ancillary input file, the code and a sample of output file can be found in Appendix (see X.a, page 213 and followings).

read_IGS_ZTD.f90 Fortran code

The *read_IGS_ZTD.f90* Fortran code is intended to read the official IGS ZTDs, estimated every 5 minutes, and to produce an output file containing four columns: doy, hour, rms and ZTD. Additionally the code is able to fill in the gaps in case of lack of data and to maintain the two-hourly step between consecutive data.
The code is designed to produce 11 observations (from 00 to 22 UTC) per day in the chosen time span.
Briefly, the code works as follows:

- defines a two-hourly time resolution, so that the resulting output ZTD values is the extraction of two-hourly ZTD estimations from 5-minutes estimations;
- opens the ancillary file *input_IGS.txt* and reads the name of the stations for which to extract the ZTDs, the year, the initial and starting doy (the present and the following instructions are iterated for every PS included in *input_IGS.txt)*;
- creates the blank output file, named name_IGS.year, where name is the PS name, read from *input_IGS.txt* file;
- separates the year following the decimal notation (thousands, hundreds, tens and units) and transforms the components in character format to be used for the definition of input file, following the IGS ZTD DataBase architecture (a main directory corresponding to year containing a sub-directory for each day of year. Every doy directory contains the ZTD estimations for all the IGS PS). An analogous operation is made on the doys (from the initial to the final);
- defines the output file, named name_IGS.year;

- opens the input file containing the ZTD, named name.doy0.YYzpd, counts its lines, skips the headers and reads the data from it
- writes on the created blank output file the doy, hour, rms and ZTD (both in mm), extracting the two-hourly data and filling in any possible gap in the data with the "99999" code. In this case, only hour(s) gaps are possible, because of the IGS DB architecture, which ensures the continuity of doys. Again, the criterion whereby the hour(s) gaps are found is the comparison between the actual read hour and the last hour written: if the difference is more than 2, a gap is detected and filled with "99999" code.

The output file is a set of column containing doy, hour, rms and ZTD.

The ancillary input file, a sample of IGS ZTD estimation file, the code and a sample of output file can be found in Appendix (see X.b, page 219 and followings).

compare_GAMIT_IGS_ZTD.f90 Fortran code

The *compare_GAMIT_IGS_ZTD.f90* Fortran code is intended to read two-hourly ZTD estimations from the two output files of the previously described Fortran codes (*read_GAMIT_ZTD.f90* and *read_IGS_ZTD.f90*) and compare the data, in order to validate the GAMIT ZTD estimations. It produces an output file containing five columns: doy, hour, GAMIT ZTD, IGS ZTD and difference. Thanks to the continuity of two-hourly data, achieved with the previous passages, the gap filling is not needed at this stage.

Briefly, the code works as follows:

- opens the ancillary *cfr.txt* file and reads the PS names to be compared (upper-case letters for GAMIT and lower-case letters for IGS, respectively) and the year;
- defines and opens the output file;
- opens the corresponding files and checks that the files are not empty;
- computes the difference between GAMIT and IGS ZTD estimations. If one of the ZTD estimations is 99999, the resulting difference will be 99999.

The ancillary input file, the code and a sample of output file can be found in Appendix (see X.c, page 225 and followings).

3.3.2. Intra-net comparison

The 15 PSs common to the three networks[75], belonging to IGS and EUREF networks, have been used to fix a common reference frame. They have also been used to verify the internal consistency between the three networks calculations.

Sguerso et al. (2015) performed the inter-comparison as a test over an interval of 2 days, on 3rd and 4th November 2011. The results are shown in Table 3.1.

75 BRST, CAGL, GRAS, GRAZ, HERS, MATE, MEDI, POTS, SFER, SJDV, TORI, VILL, WSRT, WTZR, ZIMM.

Intra-net comparison (3rd and 4th November 2011)		
	With outliers	Without outliers
Average difference [mm]	net1-net2 = -1 net1-net3 = 0 net2-net3 = 1	net1-net2 = -1 net1-net3 = 0 net2-net3 = 1
Standard deviation [mm]	net1-net2 = 2 net1-net3 = 3 net2-net3 = 2	net1-net2 = 1.7 net1-net3 = 2.2 net2-net3 = 2
Maximum and minimum differences [mm]	net1-net2 = (-12;19) net1-net3 = (-15;20) net2-net3 = (-14;6)	net1-net2 = (-7;3) net1-net3 = (-6;6) net2-net3 = (-5;6)

Table 3.1. Comparison of ZTDs for the common 15 PS for 3rd and 4th November 2011.

ZTD biases of 1 mm are observed for the three sub-networks; the standard deviations values are almost identical, too. This means that the ZTD estimates are coherent between the three sub-networks, with differences within the typical errors of 3-5 mm. The maximum and minimum values of the differences for the considered 15 PSs in the specified time span are also reported: excluding the values outside the tolerance interval (average ± 3σ), which can be interpreted as outliers, the maximum and minimum values reduce substantially. Removing the outliers, the average difference remains the same as in the case of presence of outliers, whereas the standard deviations decrease.

This kind of approach can be extended to longer time span thanks to the previously mentioned Fortran codes intended to automatically formatting and comparing the data. For example, Table 3.2 reports the average differences and standard deviation values for the entire 2011, for the same PSs.

Intra-net comparison (2011)		
	With outliers	Without outliers
Average difference [mm]	net1-net2 = 0.4 net1-net3 = 1.4 net2-net3 = 0.9	net1-net2 = 0.4 net1-net3 = 1.4 net2-net3 = 0.9
Standard deviation [mm]	net1-net2 = 1.8 net1-net3 = 2.0 net2-net3 = 1.9	net1-net2 = 1.6 net1-net3 = 1.7 net2-net3 = 1.6
Maximum and minimum differences [mm]	net1-net2 = (-48;26) net1-net3 = (-67;56) net2-net3 = (-70;55)	net1-net2 = (-6;8) net1-net3 = (-5;8) net2-net3 = (-6;7)

Table 3.2. Comparison of ZTDs for the common 15 PS for 2011.

Again, the average difference values are the same considering or excluding the outliers, and the standard deviations slightly decrease removing the outliers. The maximum and the minimum value of differences reduce substantially if the outliers are removed.

Almost the same average differences and slightly smaller standard deviations can be noticed if compared with the ones referred to 3rd and 4th November 2011 (see Table 3.1). Maximum and minimum differences appear higher with outliers; removing them, a smaller interval is obtained if compared with the ones referred to 3rd and 4th November 2011. This can be due to the different length of the statistical sample or to the criticality of the two chosen day from the meteorological point of view, so that high variation in ZTD values can be expected.

Table 3.3 reports some statistics on ZTD intra-net comparison outliers; in particular, the average number and the maximum number of outliers in the three comparisons are useful to check the quality of elaboration. These statistics have been carried out both for the 3rd and 4th November 2011 and for the entire year 2011.

The average number of outliers is almost the same in the three comparisons, with slightly better results for net1-net2; the same behaviour is confirmed in the maximum number of outliers, which is much higher for net1-net3 and net2-net3 with respect to net1-net2. The PS with the maximum number of outliers are reported in Table 3.3.

	Intra-net comparison outliers	
	3rd and 4th November 2011	2011
Total number of data	24	4380
Average number of outliers	net1-net2 = 0 net1-net3 = 0 net2-net3 = 0	net1-net2 = 58 net1-net3 = 69 net2-net3 = 66
Maximum number of outliers	net1-net2 = 1 (HERS, WTZR) net1-net3 = 1 (SJDV, WTZR) net2-net3 = 1 (HERS)	net1-net2 = 82 (SFER) net1-net3 = 182 (TORI) net2-net3 = 175 (TORI)
Average percentage of outliers	net1-net2 = 0.6% net1-net3 = 0.6% net2-net3 = 0.3%	net1-net2 = 1.4% net1-net3 = 1.6% net2-net3 = 1.6%
Maximum percentage of outliers	net1-net2 = 4.4% net1-net3 = 4.4% net2-net3 = 4.3%	net1-net2 = 1.9% net1-net3 = 4.5% net2-net3 = 4.3%

Table 3.3. Statistics on ZTD intra-net comparison outliers.

3.3.3. Comparison with IGS's official ZTD estimations

The comparison with IGS's official troposphere product[76] is needed to validate the ZTD estimations.
This comparison has been done over year 2002 for 16 PSs[77]; the value of ZTD were extracted from net1 elaboration. Again, the Fortran codes described in section 3.3.1 were employed to make the process of formatting and comparing as automatic as possible.
Globally, the comparison shows total differences with a mean bias of -3.6 mm and a standard deviation of 4.5 mm. The persistent bias could be related to the different network configurations (a regional local network is compared to the IGS global network), to the lack of constrain in any a priori position in the regional network elaboration, and to possible differences in the troposphere models used in the two solutions. Additionally, the different time spans at which the two ZTD estimations are carried out (5 minutes for IGS solutions and 2 hours for GAMIT solutions) should be taken into account.
Nevertheless, the observed constant bias does not diminish the capacity of investigating the evolution of ZTD in time.
Table 3.4 reports the GAMIT-IGS ZTDs comparison results for all the considered PSs.
Table 3.5 contains the overal statistics for the 16 PSs, both considering and removing the outliers.
Table 3.6 reports some statistics on the outliers of GAMIT-IGS ZTD comparison for year 2002 on the 16 PSs included in the comparison.

GAMIT-IGS ZTD comparison				
	Mean [mm]	rms [mm]	Max [mm]	Min [mm]
AJAC	-2.8	4.6	47.6	-25.8
CAGL	-3.5	4.7	33.1	-24.2
EBRE	-3.9	4.8	28.5	-30.3
GOPE	-6.1	3.9	19.9	-25.8
GRAZ	-3.3	3.5	21.6	-19.5
HERS	-3.1	4.1	38.6	-31.7
MATE	-5.1	5.4	36.7	-42.0
MEDI	-4.6	4.4	29.8	-29.3
NOT1	-3.7	5.5	38.9	-34.5

76 Available at ftp://cddis.gsfc.nasa.gov/pub/gps /products/troposphere/zpd.

77 AJAC, CAGL, EBRE, GOPE, GRAZ, HERS, MATE, MEDI, NOT1, POTS, RABT, SFER, VILL, WSRT, WTZR, ZIMM.

POTS	-2.8	3.8	15.2	-35.1
RABT	-6.5	5.9	18.9	-39.4
SFER	-4.3	5.1	31.7	-28.6
VILL	-3.3	4.7	45.5	-25.7
WSRT	0.4	4.0	41.3	-18.1
WTZR	-2.3	3.5	19.7	-21.5
ZIMM	-2.9	3.9	31.5	-30.2
Mean values	-3.6	4.5	31.2	-28.9
Extreme values	(-6.1;0.4)	(3.5;5.9)	(15.2;47.6)	(-42.0;-18.1)

Table 3.4. GAMIT-IGS ZTD comparison for the 16 PSs.

GAMIT-IGS comparison (2002)		
	With outliers	Without outliers
Average difference [mm]	GAMIT-IGS = -3.6	GAMIT-IGS = 0.4
Standard deviation [mm]	GAMIT-IGS = 4.5	GAMIT-IGS = 1.6
Maximum and minimum differences [mm]	GAMIT-IGS = (-42;47.6)	GAMIT-IGS = (-6;8)

Table 3.5. Comparison between GAMIT and IGS ZTD estimations.

Total number of data	4380
Average number of outliers	GAMIT-IGS = 61
Maximum number of outliers	GAMIT-IGS = 97 (EBRE)
Average percentage of outliers	GAMIT-IGS = 1.6%
Maximum percentage of outliers	GAMIT-IGS = 2.3% (EBRE)

Table 3.6. Statistics on ZTD GAMIT-IGS comparison outliers.

EBRE PS, which is the one with the maximum amount of outliers, is taken as example to show how the tolerance interval is influenced by the presence of outliers. On top of Figure 3.4, the ZTD differences (blue dots) and the tolerance interval (red lines) between GAMIT and IGS ZTD estimations before the outliers removal are shown, whereas the bottom part shows the results after the outliers have been

removed. Removing the outliers, the absence of values outside the tolerance interval and the slightly smaller tolerance interval can be appreciated in the bottom part of Figure 3.4.

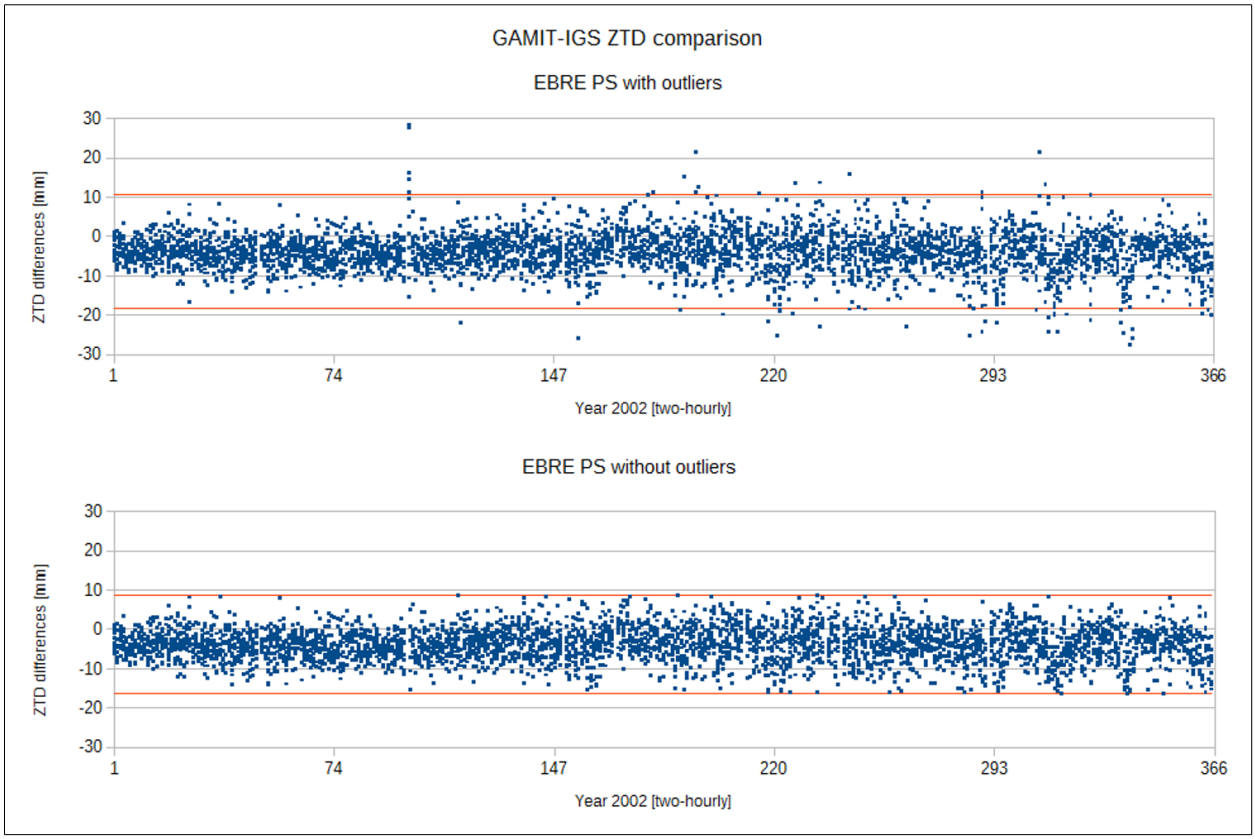

Figure 3.4. EBRE PS GAMIT-IGS ZTD comparison.
The ZTD differences are depicted as blued dots, the tolerance interval is represented by red lines.

3.3.4. Mapping function influence on ZTD estimations

The chosen mapping function and model for a priori pressure and temperature, GMF (Boehm et a., 2006) and GPT (Boehm et al., 2007) models respectively, have the characteristic of remaining the same throughout time.

As previously mentioned, the network has been elaborated to create a ZTD database for 18 years, from 1998 to 2015. In 2013, a new climatological model combining both mapping function and pressure and temperature values has been published, the GPT2 model, proposed by Lagler et al. (2013). It is constraint by a longer series of ECMWF meteorological analyses with higher spatial resolution than GMF/GPT. It also includes a semi-annual cycle, not described in the GMF/GPT.

To evaluate and quantify the impact of the new tropospheric model, Sguerso et al. (2015) re-analysed the entire year 2000 for net1, calculating the average ZTD and the standard deviation for five PSs (BRST, FCLZ, GENO, GRAS and SJDV), depicted in Figure 3.5, using GMF+GPT models and GPT2 model.

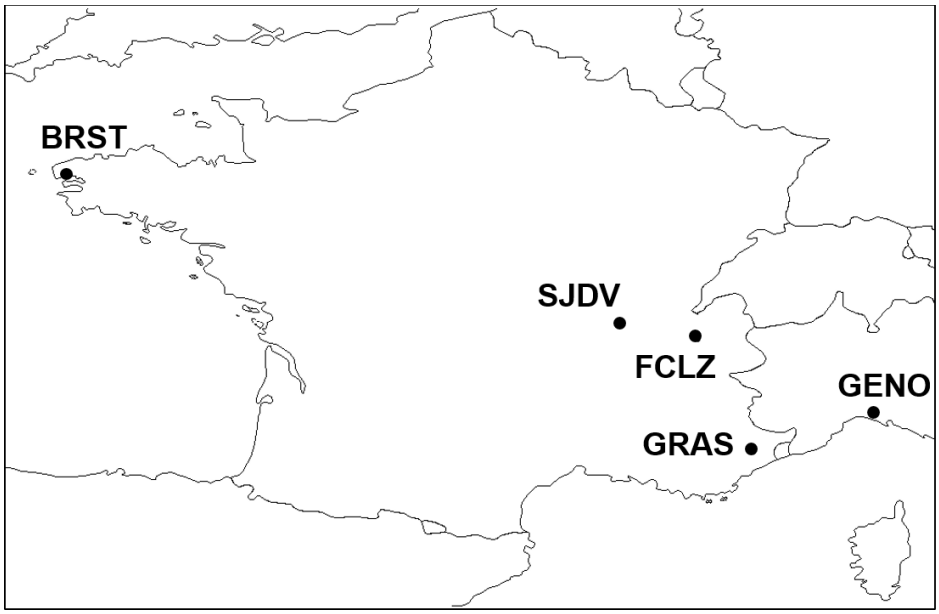

Figure 3.5. Locations of PSs used for GMF/GPT and GPT2 comparison.

The results of the comparison are summarised in Table 3.7.

	GMF/GPT		GPT2		Differences GMF/GPT - GPT2	
Station	Mean ZTD [m]	rms [mm]	Mean ZTD [m]	rms [mm]	ZTD [mm]	rms [mm]
BRST	2.4266	45.2	2.4267	45.3	-0.1	-0.1
FCLZ	2.0492	34.7	2.0494	34.7	-0.2	0
GENO	2.4026	49.4	2.4028	49.2	-0.2	-0.2
GRAS	2.0523	36.5	2.0520	36.6	0.3	-0.1
SJDV	2.3157	41.1	2.3155	41.2	0,2	-0,1

Table 3.7. Average ZTD and rms over year 2000, calculated with GMF and GPT, and with GPT2.

Differences of 0.2 mm or less in ZTD and in standard deviation can be noticed in Table 3.7, indicating that the change in mapping function does not introduce any bias in ZTD estimation. Moreover, the annual ZTD variability, responsible for most of the standard deviation, does not seem to have a significantly different amplitude.

The results summarised in Table 3.7, are depicted in Figure 3.6, where the differences of ZTD estimates for the 5 PS over year 2000 are represented. ZTD differences of 2 mm with an apparent semi-annual signature can be appreciated, as expected from the evolution of GPT2.

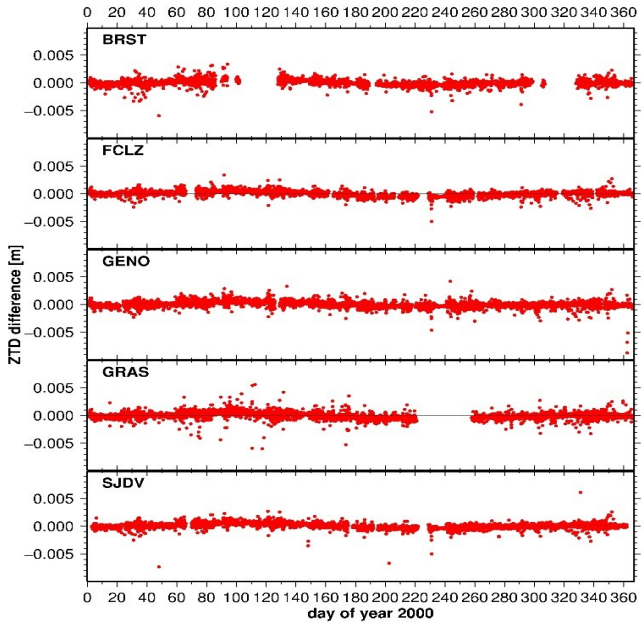

Figure 3.6. Differences in ZTD evaluation with GMF/GPT and GPT2.
(Sguerso et al., 2015)

To conclude, some differences in tropospheric parameter evaluation can clearly be noted depending on the choice of the mapping function, but no significant long term bias is noticeable, confirming that the GMF/GPT models were appropriate for tropospheric parameter estimations.

3.4. ZTD DATABASE

After performing the tests described in the previous section, ZTD estimations and gradients have been computed for 18 years, from 1998 to 2015.

The two-hourly ZTD estimations and three-hourly tropospheric gradients for the 181 PSs belonging to the trans-national network have been included in a DataBase (DB), hereafter called RENAG DB (ftp://renag.unice.fr//products/GPS_climatology_Sguerso_Labbouz_Walpersdorf).

The database is structured as follows:

- DATA_ASCII directory: it contains three sub-directories (net1, net2, net3), one for each sub-network, filled with a number of directories equal to the number of PSs in the corresponding sub-network. The PS directory includes:
  - gradient file (NAME_netX_GRD_year_v1.0.dat): each gradient file corresponds to an entire year of data. Each file has a header reporting PS name (first line), latitude, longitude and elevation

(second and third lines) and columns names (fourth line); then the following lines report the tropospheric gradients estimations, structured in 11 columns:

- doy_1998 and doy (columns 1 and 2): the doy_1998 column contains the doy computed from 1st January 1998, whereas the doy columns contains the doy computed from the first day of the considered year;
- year, month, day, hours, minutes (columns 3-7);
- err_NS, grad_NS (columns 8-9): the err_NS column contains the rms values for the NS gradients and the grad_NS column contains the NS gradient values;
- err_EW, grad_EW (columns 10-11): the err_EW column contains the rms values for the EW gradients and the grad_EW column contains the EW gradient values.

- ZTD file (NAME_netX_ZTD_year_v1.0.dat): each ZTD file corresponds to an entire year of data. Each file has a header reporting PS name (first line), latitude, longitude and elevation (second and third lines) and columns names (fourth line); then the following lines report the tropospheric gradients estimations, structured in 9 columns:
  - doy_1998 and doy (columns 1 and 2): the doy_1998 column contains the doy computed from 1st January 1998, whereas the doy columns contains the doy computed from the first day of the considered year;
  - year, month, day, hours, minutes (columns 3-7);
  - RMS_err, ZTD (columns 8-9): the RMS_err column contains the rms values for the ZTD estimations and the ZTD column contains the ZTD estimations.

  In the ASCII files there is no flag for missing data, hence the time-step between two consecutive data is not constant. A sample of ZTD and gradient files in ASCII format can be found in Appendix (see XI, page 229and followings).

- DATA_NETCDF directory: the same data reported in DATA_ASCII folder are here reported in netCDF format. There are two netCDF files for each network: one containing the gradients and one containing the ZTDs. Contrary to the ASCII files, the netCDF files contain a missing value flag, thus the time-step is constant (2 hours for the ZTD and 24/7 hours for the gradients).
- info_stations directory: this folder contains the following 6 files:
  - st_coord file: the file is structured with three columns reporting the PSs coordinates (latitude, longitude and elevation);
  - st_names file: the file is structured with a single column reporting the PSs names;
  - st_net1, st_net2, st_net3 files: each file is structured with a single column reporting the names of the PSs included in the considered sub-network;
  - station.info file: contains the site metadata (see station.info, page 47).

- readme.txt file: it contains motivations and general informations about the dataset;
- GPS_repro.tar.gz: it contains all the previously mentioned folders and files in a compressed folder.

All the previously mentioned information are already available for years from 1998 to 2012; the data will be soon made available until 2015. All the data contained in the RENAG DB are ready and available for ZTD/gradient trend estimation and conversion from ZTD to PWV using Pressure and Temperature observations.

The ZTD and gradients values are given in meters, whereas the rms errors are expressed in millimeters.

3.5. PRESSURE AND TEMPERATURE DATA

Pressure (P) and Temperature (T) observations are necessary to derive PWV from ZTD. Following the criterion of exploiting existing infrastructures, it was chosen to use P and T observations coming from NOAA. P and T data, together with other atmospheric, oceanic, and geophysical data, are available through CDO[78] service, which provides free access to NCEI[79] archive (formerly NCDC[80]) of global historical weather and climate data.

Among the different sources of data available, e.g. ground-based stations, satellite, radar, weather balloons, NWP outputs, the interest is here focused on land-based observations. This data are collected from instruments spread all over the Earth. The observed atmospheric variables include temperature, dew point, relative humidity, precipitation, wind speed and direction, visibility, atmospheric pressure, and types of weather occurrences such as hail, fog, and thunder. Data are available on sub-hourly, hourly, daily, monthly, annual, and multi-year time-scales.

A selected number of NOAA stations located in the French-Italian border region and falling in the area where the PS network is denser has been chosen. P and T stations are not always co-located, because not all the stations measure both P and T or because occasional lack of P or T data. These are the reasons why the density of the networks are not the same, also depending on the analysed case study. A deepening on the resolution of the networks and their spatial analysis will be carried out in section 5.3.

A representation of the complete P and T networks is given in Figure 3.7, where P stations are reported in the upper part, and T stations in the lower part of the figure. The scale-bar (in meters) refers to the ASTER GDEM[81], used as background.

78 Climate Data Online (https://www.ncdc.noaa.gov/cdo-web/).

79 National Centers for Environmental Information (https://www.ncei.noaa.gov/).

80 National Climatic Data Center.

81 ASTER Global Digital Elevation Model (https://asterweb.jpl.nasa.gov/gdem.asp).

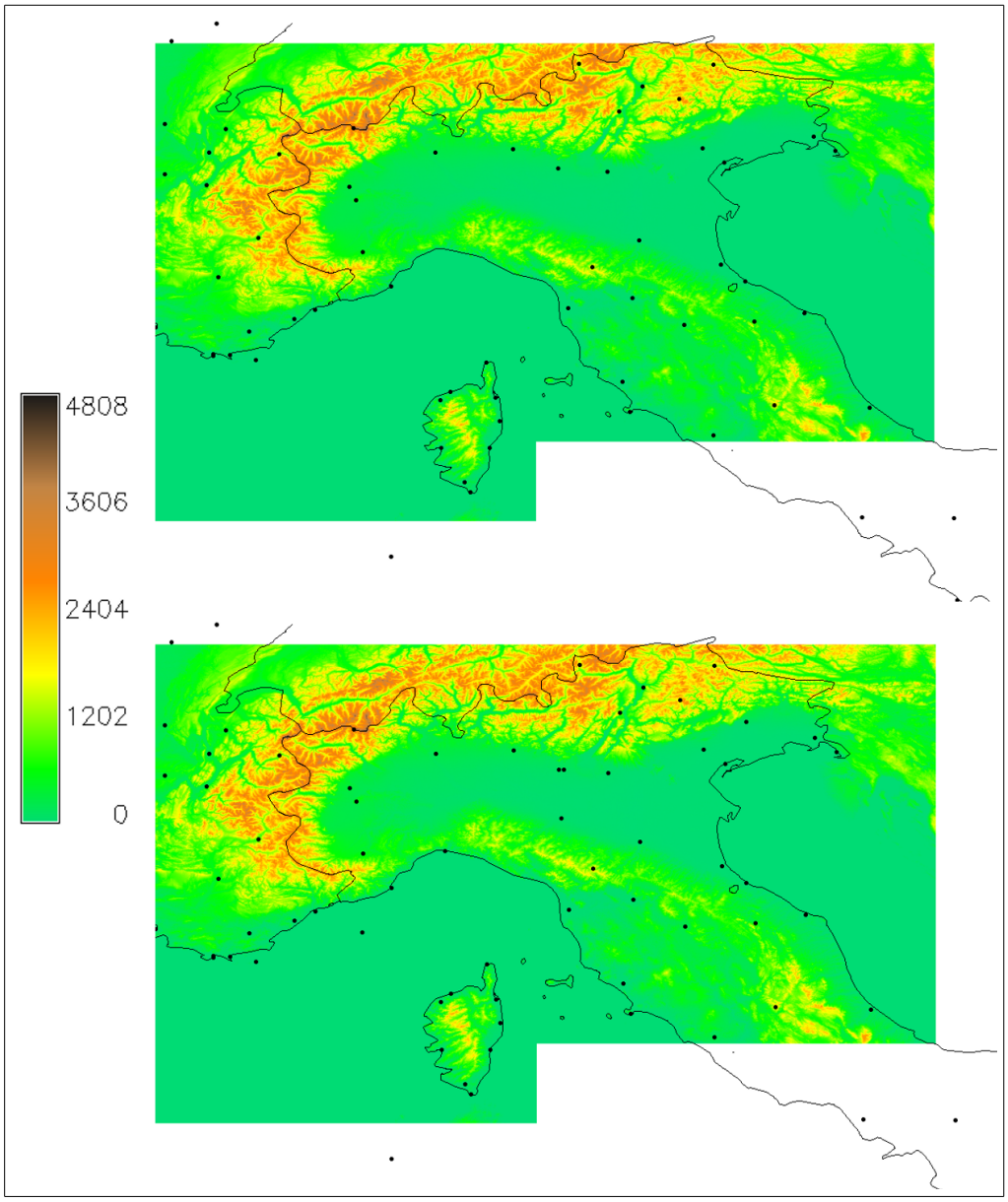

Figure 3.7. P (top) and T (bottom) stations, extracted from NOAA.

A list containing the location, coordinates (latitude, longitude and elevation) and measured observable (P, T or both) is reported in Appendix (see III, page 160).

3.5.1. Data access

Pressure and Temperature data, together with other atmospheric observables (wind speed and direction, cloud coverage, sky visibility, precipitation, …) can be accessed and downloaded from NCEI's climate and weather datasets[82].

82 https://www.ncdc.noaa.gov/data-access

The *Quick Links*[83] provides access to NCEI's dataset and products. Among the different resources, the *Integrated Surface Data, Hourly, Global*[84] provides digital dataset of detailed hourly (and sub-hourly, depending on the station) observational climate data for thousands of locations worldwide. Via the ISD/CDO link, it is possible to access to data selection with simplified or advanced options. The simplified options allow an easy selection of data for a single station or multiple stations, for user-selected time period, providing precipitation, temperature, dew point, winds, visibility, cloud cover, pressure, and present weather (if available for the chosen stations); the advanced options allow to select the observables of interest. Both options require to indicate the geographic area[85] where retrieve the data, the stations to include in the request and the period of interest.

The outputs are 4 files:

- doc.txt: text file containing Surface Data Hourly Global format documentation, to interpret the data
- dat.txt: text file containing the observed data
- stn.txt: text file containing information on the stations (stations names, IDs, coordinates, ...)
- inv.txt: inventory file, providing information on the request (number of data for every station in the request, on the basis of data type).

Among the different files, the doc.txt, dat.txt and stn.txt files are the most important because they contain the description of data, the data and the station information respectively.

The doc.txt file is a list explaining the different columns of the dat.txt file and the numeric symbols used to quantify the various observables in an abbreviated format (see IV.a, page 162).

Briefly, the dat.txt file can be described as a set of formatted columns containing (see IV.b, page 170 for a sample of dat.txt file):

- columns 1-2: station information (station code in the Air Force catalogue and NCDC number)
- column 3: time of observation (year, month, day, hour and minute)
- columns 4-6: wind data (direction, speed and gust)
- columns 7-12: sky coverage (cloud ceiling, sky cover, low, middle and high cloud types, visibility)
- columns 13-21: present weather (manually observed and automatically observed, four columns each for different kinds of weather observed) and past weather
- columns 22-23 and 27-28: temperature (observed temperature and dewpoint; maximum and minimum temperature)
- columns 24-26: pressure: (sea level pressure, altimeter setting, surface pressure)

83 https://www.ncdc.noaa.gov/data-access/quick-links

84 https://www.ncdc.noaa.gov/data-access/quick-links#dsi-3505

85 The data can be retrieved for worldwide, a geographic region (Continent or Ocean), a specific country, or selecting the range of stations to be included in the request.

- columns 29-32: precipitation (in the preceding 1 hour, 6 hours, 24 hours, and usually 12 hours)
- column 33: snow (snow depth).

Finally, the stn.txt file is a formatted set of columns containing (see IV.c, page 173 for a sample):

- columns 1-5: station information (station code in the Air Force catalogue, NCDC number, station name, country, state)
- columns 6-9: station coordinates (latitude, longitude and elevation).

3.5.2. P and T data formatting

In order to use the P and T data for the GIS procedure to produce two-hourly PWV maps, the data have to be prepared in a way that two single files (one for P and one for T data) can contain both the information related to the stations (name and coordinates) and the desired data, assuring the continuity of data in the considered time span. The continuity of data is a key issue because it is necessary for combining Pressure, Temperature and ZTD data to derive PWV. Since the data could be not continue and present gaps of hours and/or days of observations, for example due to maintenance or malfunction of the station, an automatic read-write Fortran[86] code was written. The code, called *read_NOAA.f90*, is intended to create a file containing both station information and P or T data; it is able to fill in the gaps in case of lack of data and to maintain the two-hourly step between consecutive data.

The code is designed to produce 11 observations (from 00 to 22 UTC[87]) per day in the chosen time span.

Briefly, the code works as follows:

- creates two blank files, one for Pressure and one for Temperature data respectively;
- opens the stn.txt file and reads all stations' ID, name, country and coordinates;
- opens the dat.txt files and reads all station ID, date, and all the data present in the file, and converts the temperature from Fahrenheit to Kelvin;
- converts the date in separate columns (year, month, day, hour and minute) and performs some adjustments, rounding the minutes different from zero[88];
- writes on the created blank files the station ID and name (retrieved in dat.txt file), the coordinates (retrieved in stn.txt file) and two-hourly Pressure or Temperature data (retrieved in dat.txt file), filling in any possible gap in the data with the “99999” code.

  The possible gaps are relative to:

86 http://www.fortran.com/

87 Universal Time Coordinated.

88 In some locations, the observations are carried out every 30 minutes, at 20 and 50 minutes of every hour, or in minutes different from 0. In order not to have too many stations rejected due to low number of data, the observations within 20 minutes on the hour are considered as observed in the hour.

- single or multiple gaps of hours in a day (e.g. data missing from 14 to 18 UTC of the considered day);
- single or multiple gaps over two days (e.g. data missing from 20 UTC of day 1 to 04 UTC of day 2);
- single or multiple gaps of hour in the initial hours of the initial day (e.g. data missing from 00 to 04 UTC of the initial day);
- single or multiple gaps of hour in the final hours of the final day (e.g. data missing from 18 to 22 UTC of the final day);
- single or multiple gaps of days;
- combinations of the gaps mentioned above.

The criterion whereby the hour(s) and/or day(s) gaps are found is the comparison between the actual read hour and day, and the last hour and day written: if the difference between the two hours is more than 2, a gap is detected and filled with "99999" code.

The output file is a set of column containing station ID, station name, latitude, longitude, elevation, followed by several columns (11 per day in the considered time span) containing one Pressure or Temperature observation each. A so formatted file can be easily imported in a GIS software as a vector file for the following elaboration.

The code and a sample of output file can be found in Appendix (see V.a and V.b, page 174 and followings).

4. PWV 1D ANALYSIS

Starting from the two-hourly ZTD estimations, it is possible to perform the transformation from ZTD to PWV introducing Pressure and Temperature observations taken in the same site of the PS, in case that the PS is equipped with P and T sensors, or near the PS. The availability of long time series of ZTD estimations allows to obtain PWV time series, to be used for the interpretation of PWV trends and severe events.

The present chapter is structured as follows: section 4.1 is dedicated to a short summary of the relations used to obtain PWV from ZTD, P and T observations, and to the presentation of the case studies analysed; in section 4.2 PWV variance propagation is approached, to present the different components and their errors in order to compute the PWV error; these results have been used to perform the sensitivity analysis in section 4.3; ZTD and PWV time series are reported in section 4.4; finally, section 4.5 is dedicated to the analysis of ZTD and PWV time series with the purpose to find an indicator for highlighting the occurrence of severe meteorological events.

4.1. FROM ZTD TO PWV

As already discussed in sections 2.3 and 2.4, it is possible to use Pressure (P) measurements and PS coordinates (latitude and elevation) to split ZTD in its two components: the hydrostatic (ZHD) and the wet (ZWD) ones. Finally, introducing Temperature (T) observations, PWV is derived from ZWD.

A summary of the needed equations to pass from ZTD to PWV is reported in (4.1).

$$
\begin{aligned}
&ZTD = ZHD + ZWD \;\rightarrow\; \text{estimation} \\
&ZHD = \frac{\left(2.2779 \pm 0.024\right) \cdot P_S}{\left(1 - 0.00266 \cdot \cos\left(2 \cdot \varphi\right) - 0.00028 \cdot H\right)} \\
&ZWD = ZTD - ZHD \\
&PWV = ZWD \cdot \Pi \\
&\frac{1}{\Pi} = 10^{-6} \cdot \left(k_2' + \frac{k_3}{T_m}\right) \cdot R_v \cdot \rho
\end{aligned}
\tag{4.1}
$$

As shown in (4.1) and already mentioned in section 2.4, the relations employed to obtain PWV from ZTD estimations involve Pressure (through P_S, representing P at PSs height) and Temperature (through T_m, representing the weighted mean temperature T at PSs height), and other informations on PS position (latitude φ and elevation H).

In the following, an application on ZTD and PWV time series analysis for the city of Genoa (Italy) is shown, to study the possibility of interpret severe meteorological events using the time series.
The city of Genoa is located on Ligurian sea on the North-Western part of Italy (see Figure 4.1).

Figure 4.1. Localization of Genoa city.

Genoa has been chosen as example because it has been recently and historically hit by intense meteorological events (e.g. 4th November 2011 and 9th October 2014), which will be described and analysed in the following chapters (see Chapter 6, page 107 and followings).

4.1.1. Genoa's PS

Two PSs are present in Genoa: GENO[89] and GENU[90].
GENO is an IGS PS and it is located on the roof of Istituto Idrografico della Marina building, whereas GENU is one of the six PSs belonging to the Regione Liguria positioning service[91], and it is located on the roof of Department of Civil, Chemical and Environmental Engineering (DICCA) of the University of Genoa.
As Figure 4.2 shows, the two PSs are about 5 km apart.
In Figure 4.3, the monument of the two PSs is depicted: GENO on the left and GENU on the right side.
Finally, Table 4.1 summarises GENO and GENU PSs coordinates in WGS84 reference frame.

89 https://igscb.jpl.nasa.gov/network/site/geno.html

90 www.gnssliguria.it/pdf/GENU.pdf

91 Servizio di Posizionamento GNSS, Rete Regionale Ligure (www.gnssliguria.it).

Figure 4.2. GENO and GENU PSs.
© OpenStreetMap contributors

Figure 4.3. GENO (on the left) and GENU (on the right) PSs monuments.
Photo credits: IGS and Servizio di Posizionamento GNSS, Rete Regionale Ligure.

	GENO	GENU
Latitude [°]	44.4190	44.4030
Longitude [°]	8.9211	8.9593
Elevation [m]	110.018	81.864

Table 4.1. GENO and GENU PSs coordinates (WGS84).

The data provided by these PSs, i.e. 30 seconds daily RINEX files, have been used to produce two-hourly ZTD estimations time series from 1998 to 2015 and from 2009 to 2015 for GENO and GENU, respectively.

The ZTD time series will be analysed in the following section 4.4.1, and they will be used in combination with P and T data to obtain PWV time series, discussed in section 4.4.2.

4.1.2. Genoa's P and T meteorological stations

GENO and GENU PSs are not equipped with Pressure and Temperature sensors, thus P and T data, needed to retrieve PWV from ZTD, have been extracted from two University of Genoa's Meteorological Stations (MSs) near the PSs: the Meteorology Observatory of University of Genoa[92] (hereafter DISTAV MS) and the Villa Cambiaso[93] (hereafter DICCA MS) meteorological stations.

Figure 4.4 shows the positions of the two meteorological stations, also with respect to GENO and GENU PSs. Table 4.2 summarises DISTAV and DICCA MSs coordinates in WGS84 reference frame.

Figure 4.4. DISTAV and DICCA Meteo Stations.
© OpenStreetMap contributors.

92 Osservatorio Meteorologico dell'Università di Genova, DISTAV – Dipartimento di Scienze della Terra, dell'Ambiente e della Vita (www.distav.unige.it/rsni/meteo_sito/main.htm).

93 Stazione Meteo Villa Cambiaso, DICCA – Dipartimento di Ingegneria Civile, Chimica e Ambientale (www.dicca.unige.it/meteo).

	DISTAV MS	DICCA MS
Latitude [°]	44.4152	44.4000
Longitude [°]	8.9267	8.9667
Elevation [m]	58.3	40

Table 4.2. DISTAV and DICCA MSs coordinates (WGS84).

DISTAV Meteo Station

DISTAV MS provides data since 1993, when a Siap SM3820 automatic meteorological station was installed near the historical Osservatorio Meteorologico di Genova, which is operative since 1832. The sensed data are the fundamental atmospheric parameters: barometric pressure, temperature, humidity, wind velocity and direction, solar radiation and precipitation.

The data before 1st January 2002 are recorded in printed format, whereas later the data are also available in digital format.

The data made available from DISTAV MS provider, from January 2002 to December 2015, are: mean, maximum and minimum temperature and barometric pressure at MS height (58.3 m above mean sea level). The time step is hourly. An example of DISTAV MS data can be found in Appendix, together with the Fortran code used to sample from hourly to two-hourly even data and to fill the eventual gaps between data, and the output of the Fortran code (see XII, page 234 and followings).

DICCA Meteo Station

DICCA MS provides data in digital format since 1989 with half hour time step, available on DICCA MS website[94], where also daily, monthly, annual and multi-year data are available, in graphical and table formats. The MS is equipped with a CAE SP-102 station which senses the following data: atmospheric pressure, temperature, humidity, wind velocity and direction, solar radiation and precipitation.

The data found in the annual files are: temperature, humidity, pressure, solar radiation, wind velocity and rain. All the data are referred to MS height (40 m above mean sea level).

An example of DICCAMS data can be found in Appendix, together with the Fortran code used to sample from half-hourly to two-hourly even data and to fill the eventual gaps between data, and the output of the Fortran code (see XIII, page 240 and followings).

4.2. PWV VARIANCE PROPAGATION

The PWV variance propagation has been performed to understand the role of each component and its uncertainty, expressed by the rms (σ), and to evaluate the final rms of PWV.

94 www.dicca.unige.it/meteo/text_files/dati

4.2.1. Variance propagation theory

Having a casual variable (y) depending on another one (x)

$$y = f(x) \tag{4.2}$$

if a linear transformation is applied

$$y = a \cdot x + b \tag{4.3}$$

where a and b are constant coefficients, the average of y experiences the same transformation

$$\mu_y = \frac{1}{N} \cdot \sum_{i=1}^{N} y_i = \frac{1}{N} \cdot \sum_{i=1}^{N} (a \cdot x_i + b) = \frac{a}{N} \cdot \sum_{i=1}^{N} x_i + b = a \cdot \mu_x + b \tag{4.4}$$

The variance of y turns into

$$\begin{aligned} \sigma_y = \frac{1}{N} \cdot \sum_{i=1}^{N} (y_i - \mu_y)^2 = \frac{1}{N} \sum_{i=1}^{N} \left(a \cdot x_i + b - (a \cdot \mu_x + b)\right)^2 = \frac{1}{N} \sum_{i=1}^{N} \left(a \cdot (x_i - \mu_x)\right)^2 = \\ = \frac{1}{N} \sum_{i=1}^{N} a^2 \cdot (x_i - \mu_x)^2 = \frac{a^2}{N} \cdot \sum_{i=1}^{N} (x_i - \mu_x)^2 = a^2 \cdot \sigma_x \end{aligned} \tag{4.5}$$

From (4.5), it's clear that the variance is not influenced by the coefficient b.
Equation (4.3) can be extended to

$$y = a_1 \cdot x_1 + a_2 \cdot x_2 + ... + a_n \cdot x_b + b \tag{4.6}$$

if multiple independent variables (x_i) concurring to form the dependent variable y, where a_i and b are constant coefficients.
Exploiting the linearity of the average shown in (4.4)

$$\mu_y = a_1 \cdot \mu_{x1} + a_2 \cdot \mu_{x2} + ... + a_n \cdot \mu_{xn} + b \tag{4.7}$$

Using (4.5), the variance of y can be expressed as

$$\begin{aligned} \sigma_y^2 = a_1^2 \cdot \sigma_{x1}^2 + a_2^2 \cdot \sigma_{x2}^2 + ... + a_n^2 \cdot \sigma_{xn}^2 + 2 \cdot a_1 \cdot a_2 \cdot \sigma_{x1x2} + \\ + 2 \cdot a_1 \cdot a_3 \cdot \sigma_{x1x3} + ... + 2 \cdot a_1 \cdot a_n \cdot \sigma_{x1xn} + 2 \cdot a_2 \cdot a_3 \cdot \sigma_{x2x3} + ... + 2 \cdot a_{n-1} \cdot a_n \cdot \sigma_{xn-1xn} \end{aligned} \tag{4.8}$$

where the terms σ_{ij} are called covariances and can be neglected if the variables x_i are uncorrelated.
The previous relations are valid for linear transformations. In case of non-linear transformation, if the transformation can be linearised, i.e. the depending variable y can be approximated as

$$y = f(x) \sim f(\mu_x) + f'(\mu_x) \cdot (x - \mu_x) \tag{4.9}$$

thus

$$\mu_y \sim f(\mu_x) \tag{4.10}$$

and

$$\sigma_y \sim \left(f'(\mu_x)\right)^2 \cdot \sigma_x^2 \tag{4.11}$$

If multiple independent variables (x_i) concurring to form the dependent variable y

$$y = f(x_1, x_2, \ldots, x_n) = f(\underline{x}) \tag{4.12}$$

and the non-linear transformation can be linearised as follows

$$f(x_1, x_2, \ldots, x_n) \sim f(\mu_{x1}, \mu_{x2}, \ldots, \mu_{xn}) + \left(\frac{\partial f}{\partial x_1}\right)\Big|_{\underline{\mu x}} \cdot (x_1 - \mu_{x1}) + \ldots + \left(\frac{\partial f}{\partial x_n}\right)\Big|_{\underline{\mu x}} \cdot (x_n - \mu_{xn}) \tag{4.13}$$

hence

$$y = f(\underline{x}) \sim f(\underline{\mu}_{\underline{x}}) + J(\underline{\mu}_{\underline{x}}) \cdot (\underline{x} - \underline{\mu}_{\underline{x}}) \tag{4.14}$$

thus

$$\mu_y = g(\underline{\mu}_{\underline{x}})\Big|_{\underline{\mu x}} \tag{4.15}$$

and

$$\begin{aligned} \sigma_y = \left(\frac{\partial f}{\partial x_1}\right)^2\Big|_{\underline{\mu x}} \cdot \sigma_{x1}^2 + \ldots + \left(\frac{\partial f}{\partial x_n}\right)^2\Big|_{\underline{\mu x}} \cdot \sigma_{xn}^2 + 2 \cdot \left(\frac{\partial f}{\partial x_1}\right) \cdot \left(\frac{\partial f}{\partial x_2}\right)\Big|_{\underline{\mu x}} \cdot \sigma_{x1\,x2} + \ldots + \\ + 2 \cdot \left(\frac{\partial f}{\partial x_{n-1}}\right) \cdot \left(\frac{\partial f}{\partial x_n}\right)\Big|_{\underline{\mu x}} \cdot \sigma_{x\,n-1\,xn} \end{aligned} \tag{4.16}$$

Equation (4.16) will be used in the next section to compute PWV variance propagation.

4.2.2. Application of variance propagation on PWV

Remembering equation (2.14), PWV can be expressed as

$$PWV = ZWD \cdot \Pi \tag{4.17}$$

thus, equation (4.16) gives

$$\sigma^2_{PWV} = \left(\frac{\partial PWV}{\partial ZWD}\right)^2 \cdot \sigma^2_{ZWD} + \left(\frac{\partial PWV}{\partial \Pi}\right)^2 \cdot \sigma^2_{\Pi} \tag{4.18}$$

As already mentioned, ZWD is typically obtained by difference between ZTD and ZHD; so that, using equation (4.8), the variance of ZWD is given by

$$\sigma^2_{ZWD} = \sigma^2_{ZTD} + \sigma^2_{ZHD} \tag{4.19}$$

Bevis et al. (1992) suggest a value of ZTD rms equal to 3 mm.
Equation (2.8) (Elgered et al., 1991) suggests that ZHD is a function of Pressure, latitude and PS height, thus

$$\sigma^2_{ZHD} = \left(\frac{\partial ZHD}{\partial P}\right)^2 \cdot \sigma^2_P + \left(\frac{\partial ZHD}{\partial \varphi}\right)^2 \cdot \sigma^2_\varphi + \left(\frac{\partial ZHD}{\partial z}\right)^2 \cdot \sigma^2_z \tag{4.20}$$

Supposing a latitude of 45° and a height of 1000 m known with high precision ($\sigma_\varphi = \sigma_z = 0$)

$$\frac{\partial ZHD}{\partial P} = 2.227 \cdot 10^{-3}\ m/mbar \tag{4.21}$$

For PSs equipped with barometer, Bevis et al. (1992) suggest a rms of 0.5 hPa; a precautionary value of 1 hPa is assumed in the present case, considering that PSs and meteorological stations are not co-located. For this reason, thanks to the previous assumptions ($\varphi = 45°$, $z = 1000$ m, $\sigma_\varphi = \sigma_z = 0$)

$$\sigma^2_{ZHD} = \left(\frac{\partial ZHD}{\partial P}\right)^2 \cdot \sigma^2_P = 5.185 \cdot 10^{-6}\ m^2 \tag{4.22}$$

and

$$\sigma_{ZHD} = 2.277 \cdot 10^{-3}\ m = 2.277\ mm \tag{4.23}$$

Using (4.19), the suggested value for σ_{ZTD} and the value retrieved in (4.23), it turns out

$$\sigma^2_{ZWD} = \sigma^2_{ZTD} + \sigma^2_{ZHD} = 14.185\ mm^2 \tag{4.24}$$

and

$$\sigma_{ZWD} = 3.77\ mm \tag{4.25}$$

Concerning σ^2_Π, Π is a function of the density of water ρ, the gas constant R, the two constants mentioned in (2.11) and the weighted average temperature T_m. Supposing that ρ and R are known with high precision ($\sigma_\rho = \sigma_R = 0$), it turns out

$$\sigma_{\Pi}^2 = \left(\frac{\partial \Pi}{\partial k'_2}\right)^2 \cdot \sigma_{k'2}^2 + \left(\frac{\partial \Pi}{\partial k_3}\right)^2 \cdot \sigma_{k3}^2 + \left(\frac{\partial \Pi}{\partial T_m}\right)^2 \cdot \sigma_{Tm}^2 \tag{4.26}$$

Developing the three derivatives in (4.26) and assuming the following values in (2.11) for k'_2, k_3 and the relative σ, and evaluating T_m and the relative σ^2 as

$$\left.\begin{array}{c} T_m = 70.2 + 0.72 \cdot T \\ \sigma_T = 1 \ \ K \end{array}\right\} \rightarrow \ \sigma_{Tm}^2 = 0.518 \ \ K^2 \tag{4.27}$$

it turns out that

$$\begin{gathered} \sigma_{\Pi}^2 = \left(\frac{\partial \Pi}{\partial k'_2}\right)^2 \cdot \sigma_{k'2}^2 + \left(\frac{\partial \Pi}{\partial k_3}\right)^2 \cdot \sigma_{k3}^2 + \left(\frac{\partial \Pi}{\partial T_m}\right)^2 \cdot \sigma_{Tm}^2 = \\ = \left(1.330 \cdot 10^{-8}\right) \cdot 10^2 + \left(1.708 \cdot 10^{-13}\right) \cdot \left(3 \cdot 10^3\right)^2 + \left(3.128 \cdot 10^{-7}\right) \cdot 0.518 = 2.983 \cdot 10^{-6} \end{gathered} \tag{4.28}$$

and

$$\sigma_{\Pi} = 1.727 \cdot 10^{-3} \tag{4.29}$$

Assuming $T_m = 279$ K as suggested in Bevis et al. (1992), the typical values for k'_2, k_3

$$\Pi = 0.518 \tag{4.30}$$

Introducing a conservative value of 250 mm for ZWD, it follows

$$\begin{gathered} \sigma_{PWV}^2 = \left(\frac{\partial PWV}{\partial ZWD}\right)^2 \cdot \sigma_{ZWD}^2 + \left(\frac{\partial PWV}{\partial \Pi}\right)^2 \cdot \sigma_{\Pi}^2 = \\ = \left(\left(0.518\right)^2 \cdot \left(3.776 \cdot 10^{-3}\right)^2\right) + \left(\left(250 \cdot 10^{-3}\right)^2 \cdot \left(1.727 \cdot 10^{-3}\right)^2\right) = 5.423 \cdot 10^{-7} \ \ m^2 \end{gathered} \tag{4.31}$$

and

$$\sigma_{PWV} = 7.346 \cdot 10^{-4} \ \ m \ \rightarrow \ \sigma_{PWV} = 0.736 \ \ mm \tag{4.32}$$

4.3. PWV SENSITIVITY ANALYSIS

For evaluating how much PWV is sensitive to the variation of the different parameters involved, a sensitivity analysis has been carried out using a MATLAB code, originally written by Daniele Passoni, who I wish to thank. The code is intended to produce two graphs representing the variation of PWV and σ_{PWV} varying one of the parameters. The code consists of one main program (SIGMA_PWV_sensitivity.m) and five functions, one for each variable parameter.

As already mentioned in section 4.2.2, remembering equation (4.18) and using the definition of σ^2_{ZWD} and σ^2_{Π} reported in (4.19) and (4.26) respectively, it turns out that

$$\sigma^2_{PWV} = \left(\frac{\partial PWV}{\partial ZWD}\right)^2 \cdot \sigma^2_{ZWD} + \left(\frac{\partial PWV}{\partial \Pi}\right)^2 \cdot \sigma^2_{\Pi} =$$
$$= \left(\frac{\partial PWV}{\partial ZWD}\right)^2 \cdot \left(\sigma^2_{ZTD} + \sigma^2_{ZHD}\right) + \left(\frac{\partial PWV}{\partial \Pi}\right)^2 \cdot \left(\left(\frac{\partial \Pi}{\partial k'_2}\right)^2 \cdot \sigma^2_{k'2} + \left(\frac{\partial \Pi}{\partial k_3}\right)^2 \cdot \sigma^2_{k3} + \left(\frac{\partial \Pi}{\partial T_m}\right)^2 \cdot \sigma^2_{Tm}\right) \quad (4.33)$$

Remembering from equation (4.20) that ZHD is function of P, latitude and elevation, and supposing latitude and elevation known with high accuracy ($\sigma_\varphi = \sigma_Z = 0$), the main parameters influencing PWV are: ZTD, P, k_2', k_3 and T_m, where

$$T_m = 70.2 + 0.72 \cdot T \quad (4.34)$$

and, consequently

$$\sigma^2_{Tm} = (0.72)^2 \cdot \sigma^2_T \rightarrow \sigma_{Tm} = 0.72 \cdot \sigma_T \quad (4.35)$$

Table 4.3 reports the default parameters values and σ, deriving from literature; they can be changed in the main program.

Variable	Default value		Default σ value	
k'_2	17	K/mbar	10	K/mbar
k_3	$3.776 \cdot 10^5$	K^2/mbar	$0.03 \cdot 10^5$	K^2/mbar
T_m	281.27	K	0.72	K
P	1013.25	mbar	1	mbar
ZTD	2.5	m	0.003	m

Table 4.3. Default values for variables and σ.

The code is structured as follows:

- definition of the five variables, their σ and tolerance intervals (variable-3·σ; variable+3·σ);
- discretisation of the tolerance interval in seven points, to compute the corresponding PWV in the following values: variable±3·σ, variable±2·σ, variable±σ and variable default value;
- definition of which parameter should vary in its confidence interval. Depending on the choice, the corresponding function computes the variance-covariance matrix, PWV varying the chosen parameter, the partial derivatives and the PWV variance propagation;
- generation of the two diagrams, representing the variation of PWV and σ_{PWV}.

The MATLAB code can be found in Appendix (see X, page X).

Table 4.4 reports PWV and σ_{PWV} sensitivity to the variation of the different parameters inside their tolerance intervals; the same results are shown in graphical way in Figures 4.5 and 4.6, where the variable parameter is indicated in the title of each figure.

The following results are computed assuming the default values for the variables and the corresponding σ (as reported in Table 4.3), $\varphi = 45°$ and $z = 1000$ m.

Variable	Confidence interval	PWV [m]			σ_{PWV} [m]		
		Min	Max	Difference	Min	Max	Difference
k'_2	(0;27)	0.0310	0.0315	0.0005	$6.85 \cdot 10^{-4}$	$6.98 \cdot 10^{-4}$	$0.13 \cdot 10^{-4}$
k_3	$(3.68;3.87) \cdot 10^5$	0.0305	0.0320	0.0015	$6.86 \cdot 10^{-4}$	$7.13 \cdot 10^{-4}$	$0.27 \cdot 10^{-4}$
T_m	(279.1;283.4)	0.0310	0.0315	0.0025	$6.86 \cdot 10^{-4}$	$6.98 \cdot 10^{-4}$	$0.12 \cdot 10^{-4}$
P	(1010;1016)	0.0305	0.0322	0.0017	$6.85 \cdot 10^{-4}$	$6.97 \cdot 10^{-4}$	$0.12 \cdot 10^{-4}$
ZTD	(2.491;2.500)	0.0297	0.0327	0.003	$6.84 \cdot 10^{-4}$	$7.00 \cdot 10^{-4}$	$0.16 \cdot 10^{-4}$

Table 4.4. PWV and σ_{PWV} sensitivity.

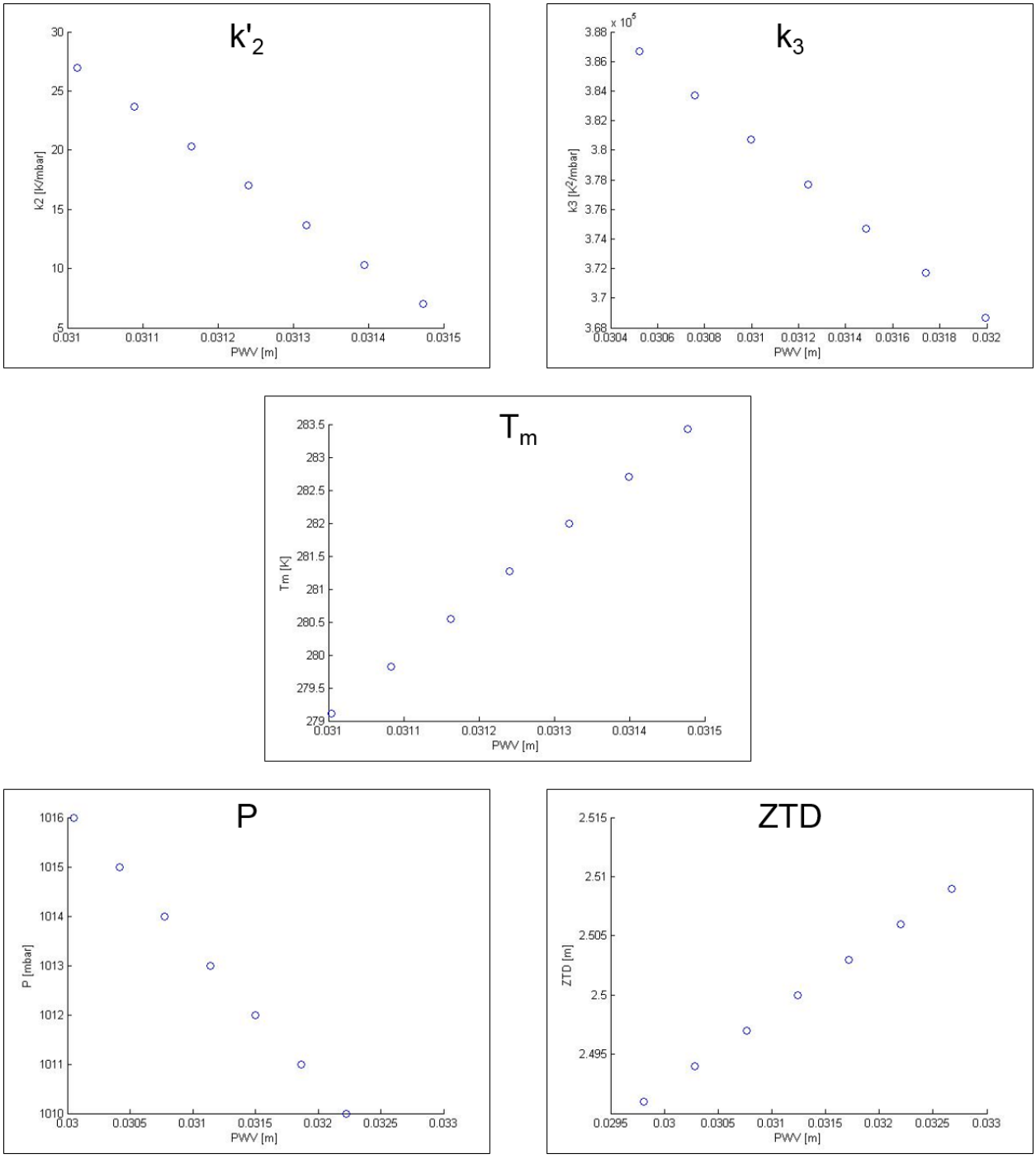

Figure 4.5. PWV variability according to the chosen parameter.
Courtesy of Daniele Passoni.

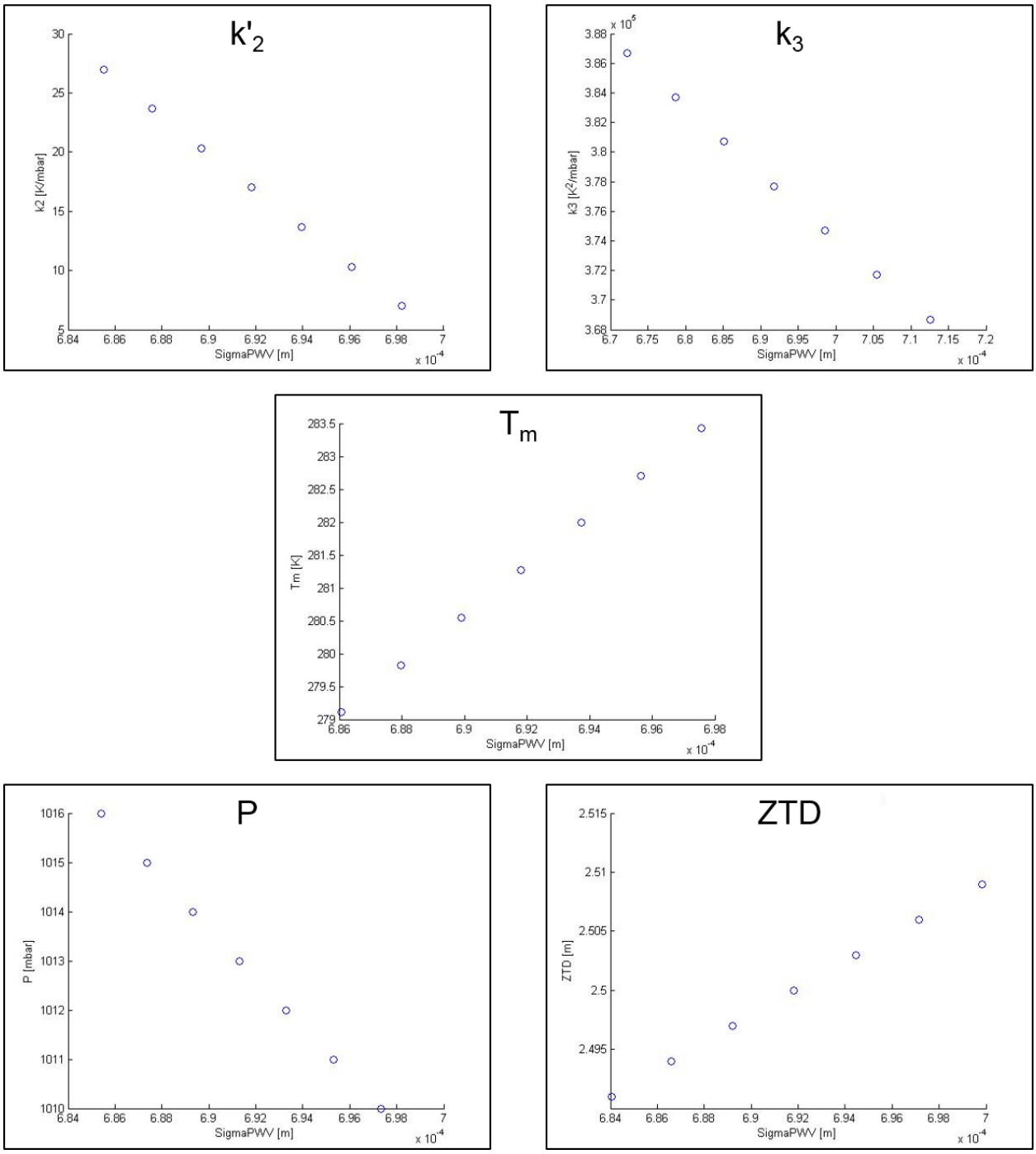

Figure 4.6. σ_{PWV} variability according to the chosen parameter.
Courtesy of Daniele Passoni.

As can be noticed examining Table 4.4 and Figures 4.5 and 4.6, PWV and σ_{PWV} variations are quite limited if the five variables variations are limited inside the corresponding tolerance intervals. What emerges from Table 4.4 is that the parameters which influence the most the PWV values are T_m and ZTD. In fact, a variation of about 4 K in T_m produces a corresponding variation of PWV of about 3 mm; the same variation of PWV can be appreciated if ZTD varies of about 9 mm.

4.4. ZTD AND PWV TIME SERIES

ZTD and PWV time series have been obtained for GENO and GENU PSs in order to study long term ZTD trends (Sguerso et al., 2015) and to identify recognizable patterns in ZTD/PWV that can be related to the occurrence of severe meteorological events. The following sections are dedicated to ZTD (section 4.4.1) and PWV (section 4.4.2) time series analysis, respectively.

4.4.1. ZTD time series

Sguerso et al. (2015) used the homogeneous ZTD time series to establish the long term trends, which should be related to the amount of water vapour above each station. These trends could help characterizing regional climatologies, being water vapour a key variable in climate.

By calculating the ZTD trend over successively increasing time spans for three ancient PSs (BRST, GRAS and SJDV), with data available since the beginning of 1998, they obtained the degree of convergence of ZTD trend to its final value and the uncertainty of the evaluation over the analysed time span (1998-2012). ZTD trends converge to values in the order of 0.5 mm/yr for the three considered PSs, showing that the long term ZTD estimation could provide new constraints on water vapour climatology.

A second approach, to identify ZTD patterns related to intense precipitation events has been carried out, using the entire set of data, until 2015 for GENO and GENU PSs. Indeed, the annual two-hourly ZTD time series allow to compute a *climatological average* of ZTD, by averaging the corresponding two-hourly estimations of each year over the all years of measurements, as Figure 4.7 shows. The black vertical dashed lines indicates two different ZTDs, estimated in different moments of the year, and averaged for all the years available. Thus the climatological average is just composed by ZTD estimations averaged at the same time and the same day of different year. This simple operation has been carried out for both GENO and GENU PSs using the two-hourly ZTD estimations obtained with GAMIT elaboration. Once the climatological average has been retrieved, it can be compared with the ZTD evolution of individual years, in order to identify specific behaviours related to heavy rain events as a contribute to a decision support system for meteorological alerts. An early warning system could be set up thanks to this strategy, simply comparing real time estimates of tropospheric parameters with their long term climatology.

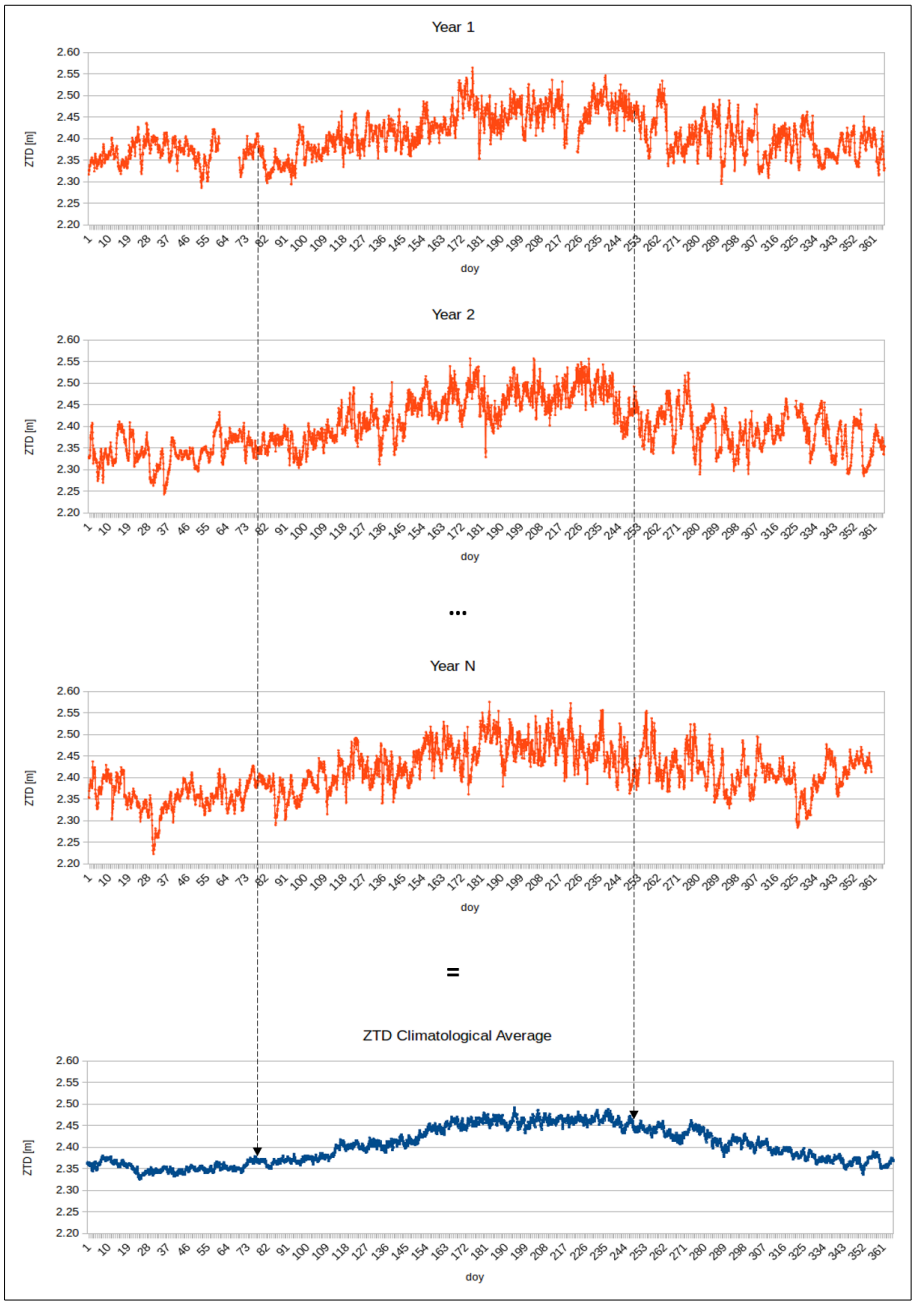

Figure 4.7. Climatological average computation.

This approach is used in the following examples, to study the ZTD evolution during the intense rain event of Genoa on 4th November 2011.

First of all, the climatological averages for GENO and GENU PSs have been compared to the ZTD evolution over year 2011, as Figure 4.8 shows, where GENO is depicted on the top and GENU on the bottom. For both PSs, the blue dots represent the ZTD climatological average and the red dots the year 2011 ZTD.

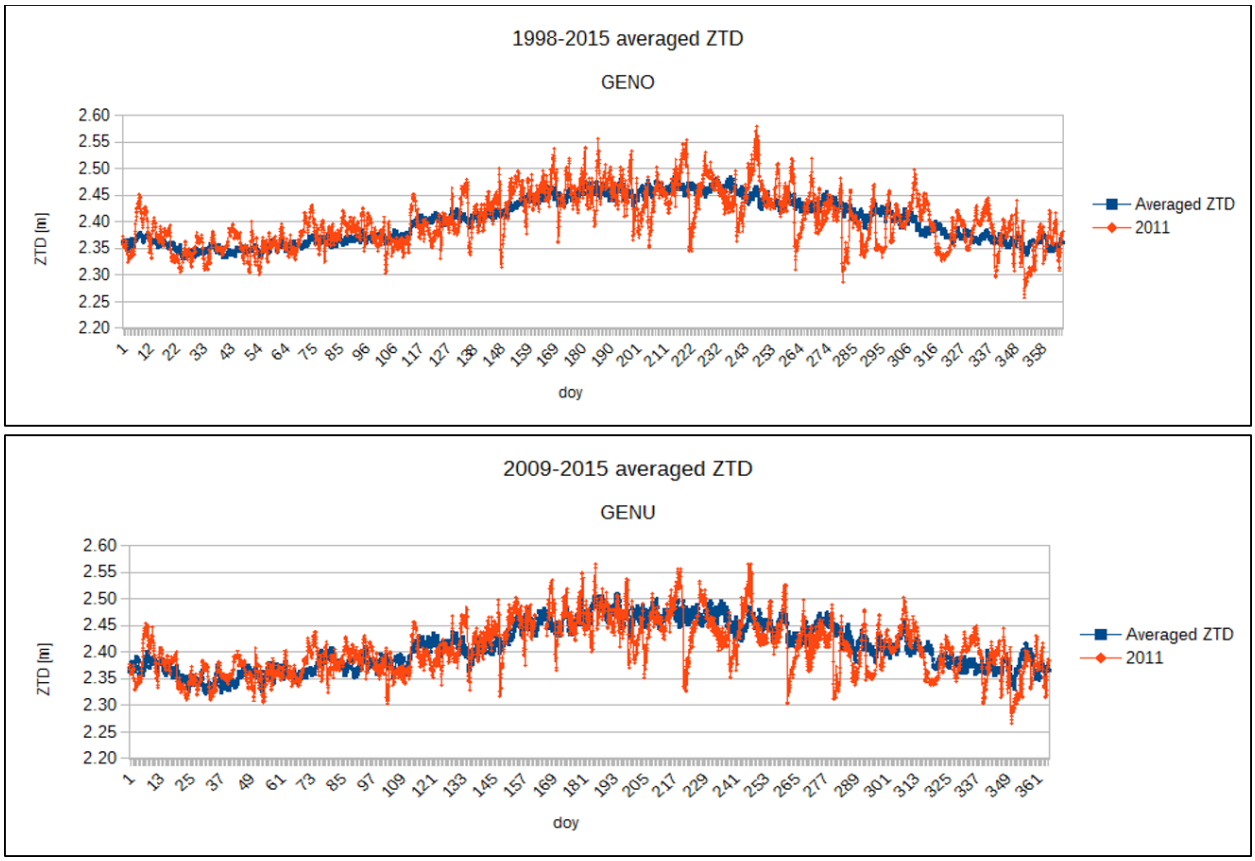

Figure 4.8. GENO and GENU ZTD climatological average (blue) and ZTD evolution in 2011 (red).

The climatological average has been computed since 1998 for GENO and since 2009 for GENU. The different time spans for which the ZTD estimations have been computed could justify the slightly different behaviours of the two climatological averages, as Figure 4.9 depicts.

The green circles in Figure 4.9 represent evident differences in the two ZTD climatological averages.

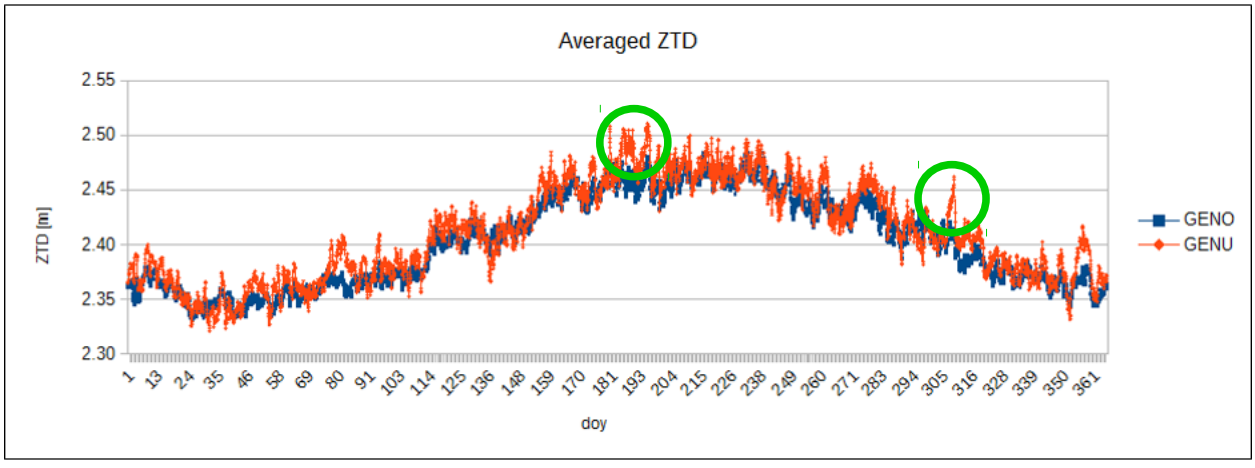

Figure 4.9. Averaged ZTD time series for GENO (blue) and GENU (red) PSs.

On the contrary, Figure 4.10 depicts the year 2011 ZTD time series, which result almost identical. This demonstrates that the two PSs, which are few km apart, inspect the same portion of Troposphere.

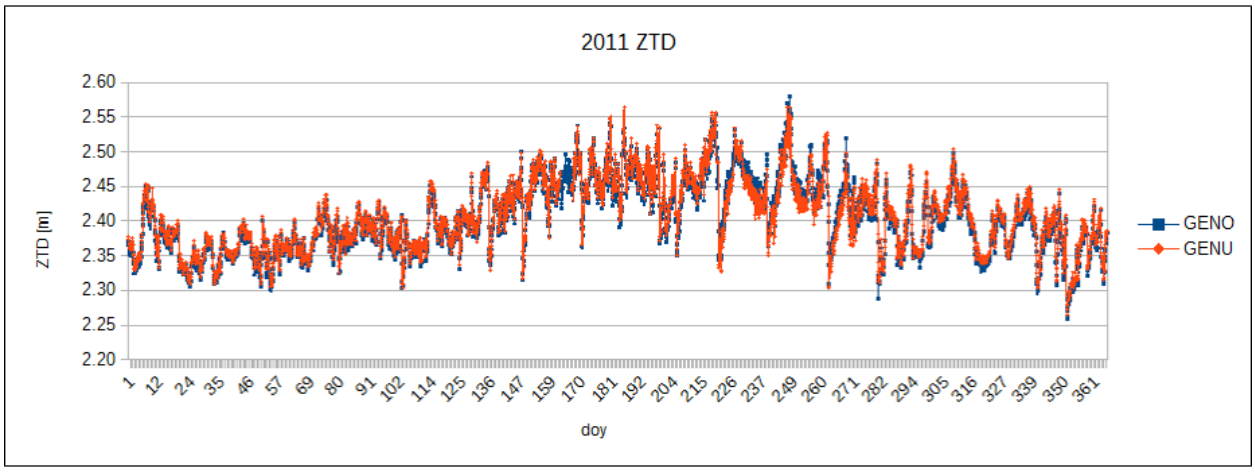

Figure 4.10. 2011 ZTD time series for GENO (blue) and GENU (red).

Focusing on 4th November 2011 rain event and taking GENO PS as example, Figure 4.11 represents the average ZTD time series and the 2011 ZTD time series, together with the error bars (black lines), showing the root mean square differences of the individual years with respect to the climatological average.

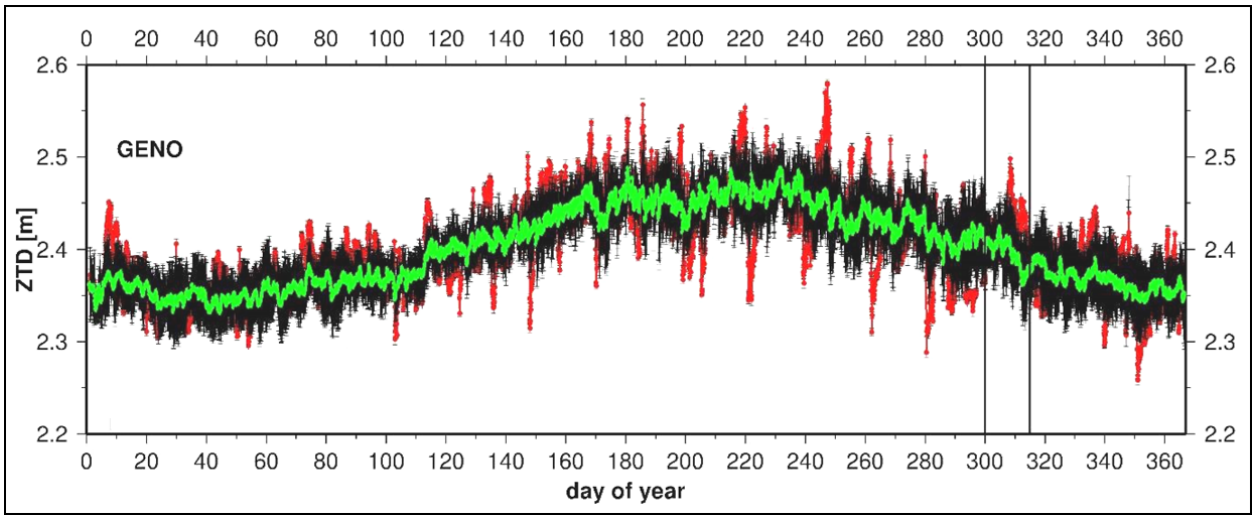

Figure 4.11. Climatological average (green), 2011 ZTD (red) and error bars.
The vertical lines highlight the study interval (3rd-4th November 2011).

Several episodes of 2011 ZTD are significantly higher than the value of climatological average. Among them, the Genoa storm of 4th November 2011, which is highlighted by the black vertical bars. A zoom on Genoa event is depicted in Figure 4.12. The vertical bars underline the 4-hour interval with most of the rainfall. Figure 4.12 represents a zoom on the Genoa storm most intense rain interval and shows that ZTD in correspondence of GENO PS was significantly higher than the climatological average for about 30 hours, starting about 12 hours before the maximum of rainfall on 4th November (doy 308).

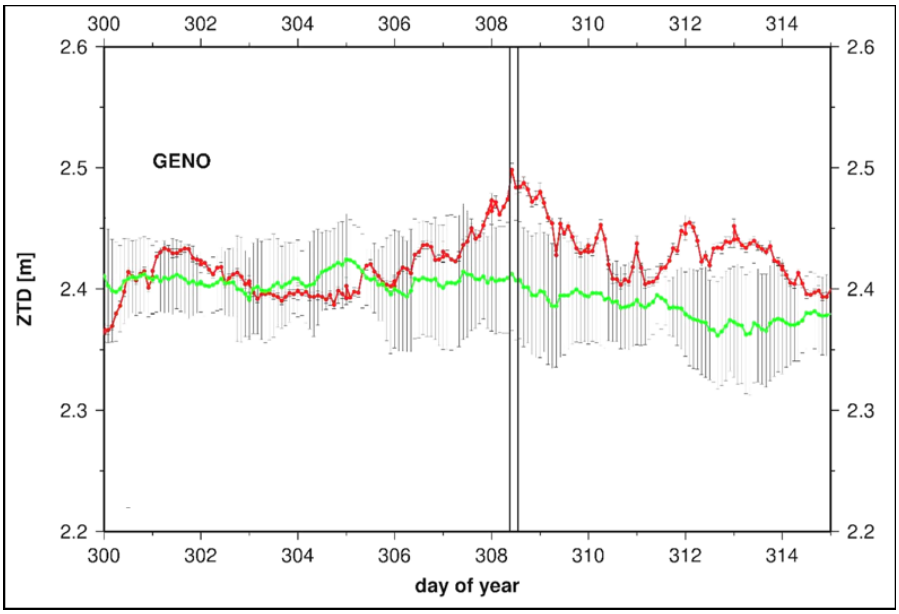

Figure 4.12. Zoom of ZTD time series during 4th November 2011 Genoa storm.
The vertical lines indicate the 4-hour interval with most of the rainfall.

Thanks to the 18 years DB of tropospheric parameters, a dedicated work could be done to study the detailed evolution of ZTD in time and space and to relate it to intense rain events, with the goal of identifying characteristic patterns preceding heavy rainfalls.

4.4.2. PWV time series

Once verified that there is coherence between high values of ZTD and severe meteorological events, the same approach of time series analysis was extended to PWV, to obtain a closer link to potential rain. For this purpose, the 18 years DB of two-hourly ZTD estimations for GENO and GENU PSs and the two-hourly extraction of meteorological observations (retrieved as described in section 4.1.2) have been used to produce the PWV time series from 2002 to 2015 for GENO and from 2009 to 2015 for GENU. Again, the PWV climatological averages have been computed, by averaging the two-hourly values estimated at the same time of the year, as already enounced in 4.4.2 (see Figure 4.7 for graphical explanation).
The PWV climatological averages and the individual 2011 PWV time series for GENO and GENU are represented in Figure 4.13.

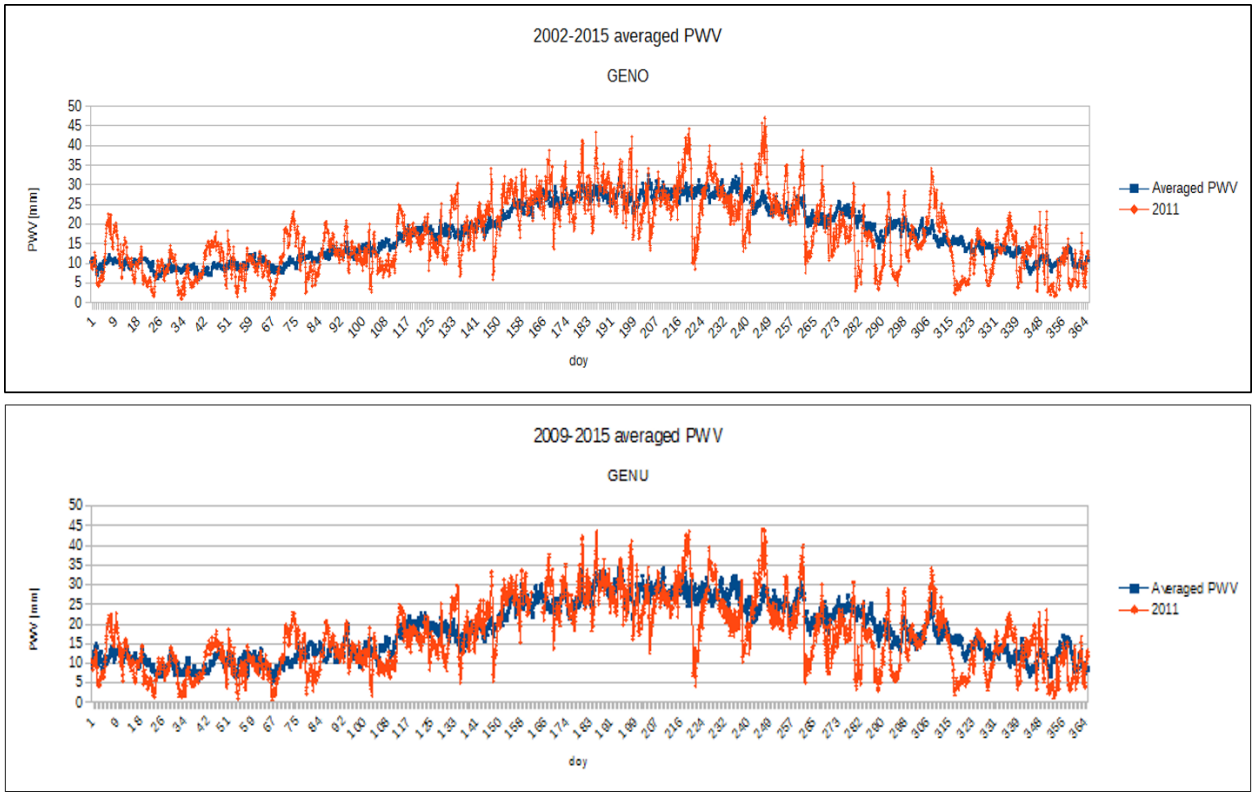

Figure 4.13. GENO and GENU PWV climatological average (blue) and ZTD evolution in 2011 (red).

As in the case of ZTD time series, the climatological averages are affected by the different time spans in which data are available, thus they present some differences.

The year 2011 PWV time series for the two PSs have been compared, as shown in Figure 4.14, where GENO and GENU 2011 PWV time series are represented with blue and red dots, respectively.

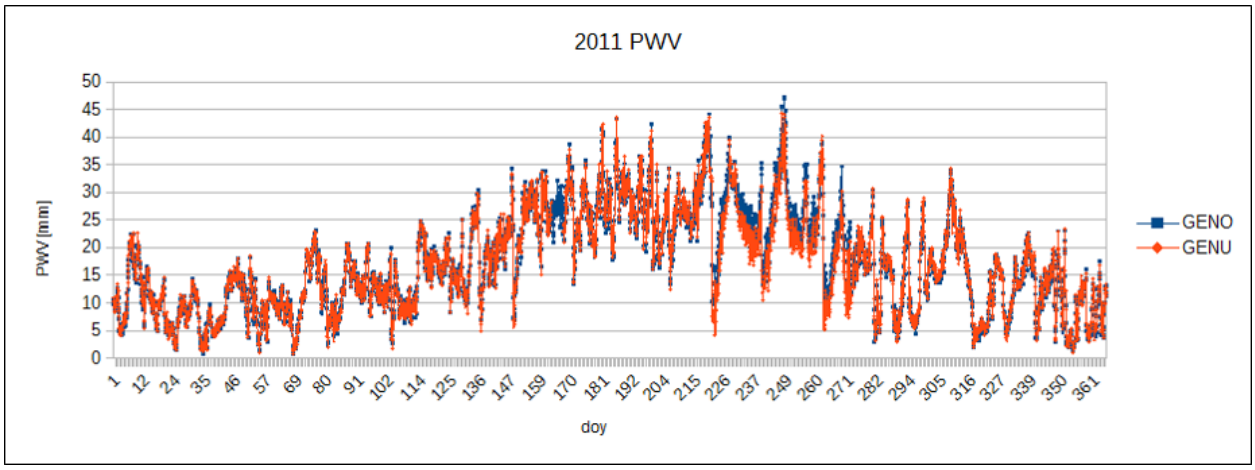

Figure 4.14. 2011 PWV time series for GENO (blue) and GENU (red).

Again, as in the case of ZTD, the two time series are almost identical due to the vicinity of the PSs. For this reason, the further analysis will be focused on GENO, which has the longer time series. The same

results obtained for the comparison of PWV time series in 2011 have been achieved for the other years since 2009, demonstrating the high correlation of the PWV values.

Focusing on 4th November 2011 rain event, Figure 4.15 represents the average PWV time series (in blue) and the 2011 PWV time series (in red), together with the error bars (light grey lines), showing the root mean square differences of the individual years with respect to the climatological average.

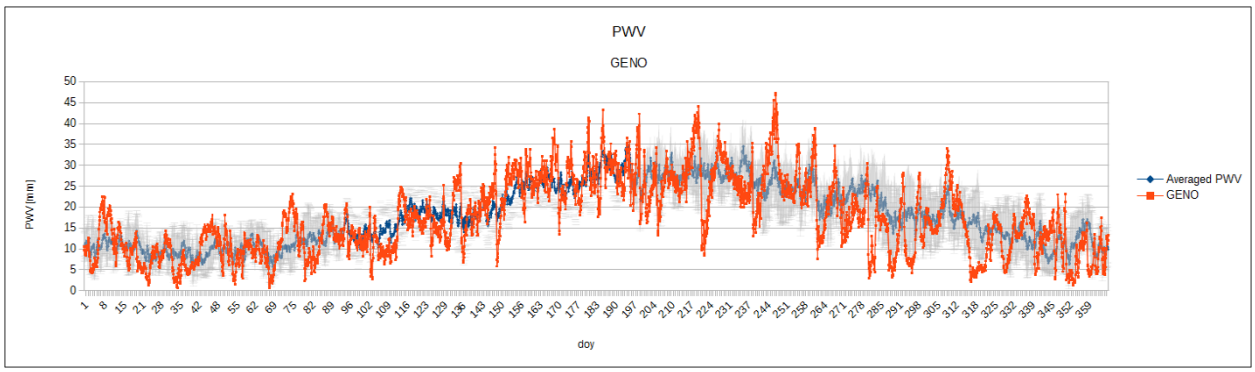

Figure 4.15. Climatological average (blue), 2011 PWV (red) and error bars.

A deeper analysis of PWV time series with the aim of identifying an indicator of potential precipitation is reported in the following section.

4.5. LOOKING FOR AN INDICATOR FOR POTENTIAL RAINFALL

The analysis of individual year PWV time series with respect to the PWV climatological average can be useful in order to recognise characteristic patterns indicating severe rainfalls.

As Figure 4.15 reports, there are several episodes of 2011 PWV which overcome the value of climatological average. Among them, the Genoa storm of 4th November 2011. A zoom on shorter time span, from doy 225 (13rd August) to doy 333 (29th November), is represented in Figure 4.16.

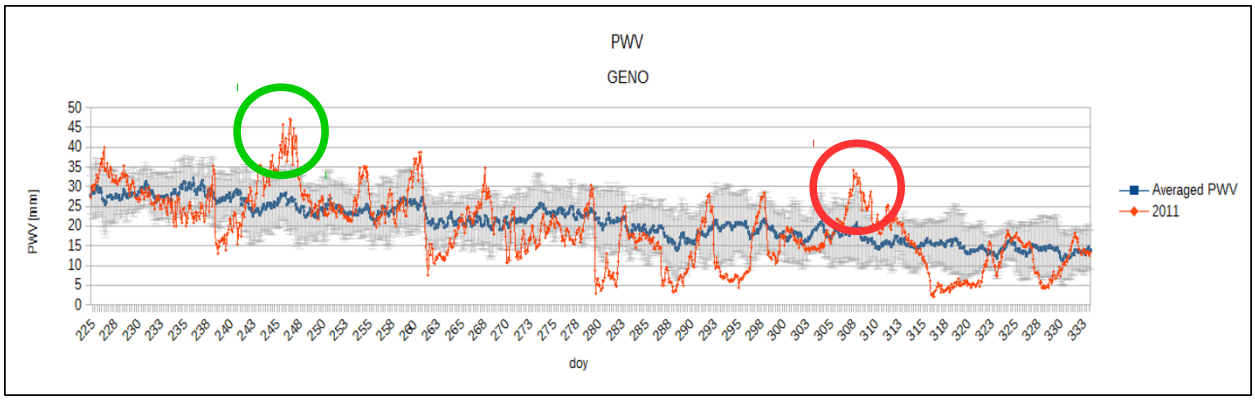

Figure 4.16. Zoom of PWV time series.

The two events in the circles, referring to 4th September 2011 (green circle) and 4th November 2011 (red circle), are taken as example of the overcoming of the threshold represented by the error bars.

The study of the PWV patterns and of the amount of rain resulted extremely useful in detecting remarkable features related to severe events. In both cases, the PWV values were significantly higher than the climatological average and the error bars, but the total amounts of rain were substantially different.
Figure 4.17 depicts the cumulative rain of 4th September (top) and 4th November (bottom) on Genoa.

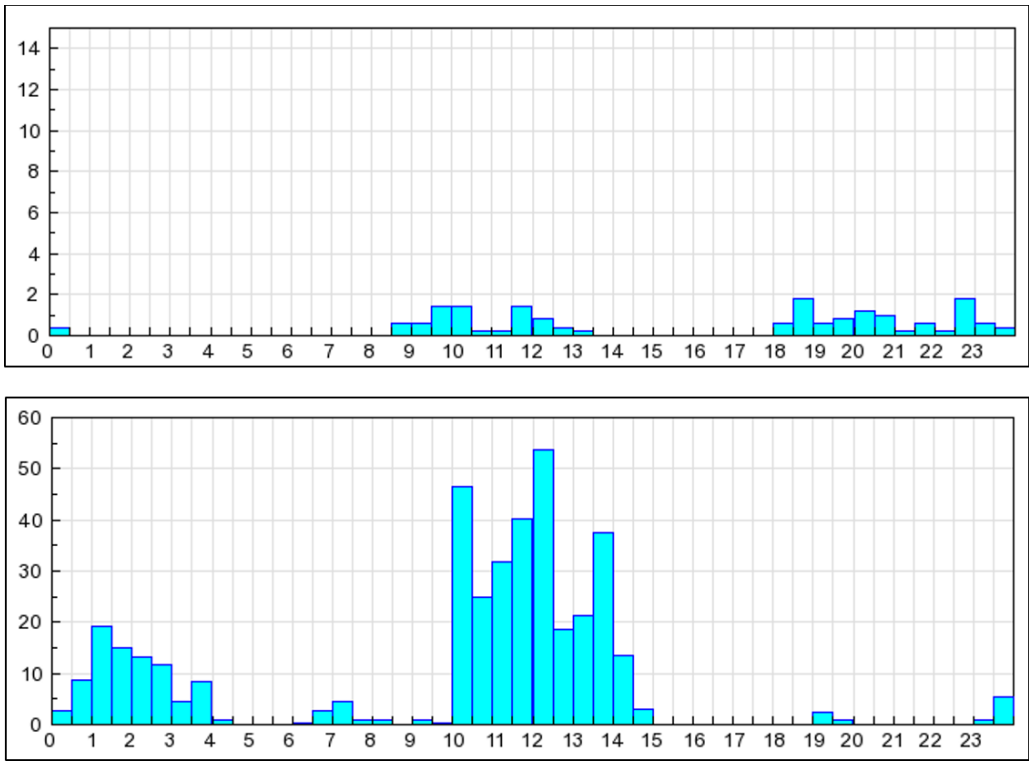

Figure 4.17. Cumulative rain of 4th September (top) and 4th November (bottom) 2011 on Genoa.

Comparing the total amount of rain, in the first case (4th September) the amount of rain was very limited and not likely to produce a meteorological alert, whereas in the second case (4th November) the amount of rain was considerably higher.
Omitting considerations on the triggering conditions, which are more related to an atmospheric physics study, the presented approach, based on the overcoming of a threshold (the value of σ), is considered not exhaustive for individuating the occurrence of severe events.
The 1D approach is still considered valid to characterize the pattern of PWV because there is coherence between GNSS methodology results and weather alerts. Additionally, the whole GNSS methodology is independent from weather forecasting models; thus, it can represent a new source of available data, to be use to deepen the knowledge of meteorological phenomena and their evolution in time and space.
Even so, this strategy could be applied to other test cases in order to improve the method and identify other eventual indicators.
To pursue this goal, a 2D methodology has been conceived, to monitor the evolution of PWV in time and space and to characterize severe meteorological events. The procedure will be presented in Chapter 5.

5. PWV 2D PROCEDURE

This Chapter is dedicated to the description of the GIS (Geographic Information System) procedure, called G4M (GNSS for Meteorology), intended to produce 2D PWV maps for wide and orographically complex area, with input data measured from existing infrastructures.
After a short introduction on GIS and on the GIS software exploited to produce PWV maps (section 5.1), the 2D procedure for the integration of Pressure, Temperature and ZTD data in the GIS working environment will be addressed (section 5.2). In section 5.3, the different interpolation techniques will be presented. The indicator introduced to localise severe meteorological events in time and space will be presented in section 5.4. Finally, the strategies and procedures for the automation of the G4M procedure will be discusses in section 5.5.

5.1. GIS WORKING ENVIRONMENT

After a short presentation on GIS (Geographic Information System), the GRASS GIS software used for performing 2D PWV maps' elaboration is described together with the main characteristics of the GIS working environment. Hence, a focus on the GIS working settings are summarized.

5.1.1. What is a GIS?

A GIS is Geographic Information System composed by procedures and numerical methods, human resources and data which allow to collect, elaborate, visualise and update spatially distributed geographical information. These operations are fundamental in the planning, management and control of the territory.
A GIS is based on the interaction of two informatics tools: the CAD[95], to draw geographic entities, and the relational DBMS[96], to archive and manage the data. The interaction between the CAD and the DB allows to establish a connection between different sources of data, on the basis of a common geographic reference, with the aim of creating new information starting from the available data. For this reason, the GIS does not give just a geometric representation of objects, but combines the graphical aspect with the topological information, providing mutual spatial relations between the different elements and data.
A GIS processes geo-referenced data, with the coordinates of an object stored in a geographic or cartographic coordinates system (latitude, longitude or East, North, and eventually the elevation component).

95 Computer Aided Design.

96 DataBase Management System.

The digital cartographic data can be organized following two different models of representation: *vector* and *raster* data.

The vector data are made of elements such as points, lines and polygons, coded and stored on the basis of significant elements; thus the points are identified by their coordinates, the lines and the polygons are identified by nodes or vertexes coordinates. Every element is associated to a record inside the database, containing the attributes of the represented object.

The raster data are stored creating a matrix of cells; every cell, called *pixel* (contraction of the words "picture element"), is associated with one single information, related to what the raster represents. For example, if the raster is a Digital Terrain Model, the pixels contain the height of the terrain; if the raster is a picture, the pixels contain the colorimetric information; if the raster is a concentration map, the pixels contain the value of concentration.

Both raster and vectorial data have original precisions, which should be taken in account when working in a GIS environment:

- the raster precision is related to the dimension of the pixel, called *resolution* and expressed in the same unit of the reference system in which the raster is framed (typically degrees or meters); the smaller is the pixel, the higher is the number of cells and the better is the resolution; the resolution has to be strictly related to the original precision of the data.
- the vector precision is related to the so called *drawing error*[97] or *cartographic plotting error*[98], which is estimated to be 0.2 mm (corresponding to the minimum width of a pen used to draw the map) at the scale of the map.

In numerical cartography the concept of scale has decayed, because it is possible to visualise and plot a map with the desired enlargement, being the different object stored by means of their coordinates. The scale has been substituted by the concept of nominal scale, defined as the scale in which the map has the same characteristics of the traditional map, both for metric and informative contents. Hence, nominal scale and drawing error are closely related to each other.

5.1.2. The GIS software GRASS

For the realisation of 2D PWV maps, the free and open source GRASS[99,100] GIS ver 6.4. software (GRASS Development Team, 2015) was chosen, for its high processing capacity, the possibility of

97 See Maling, 1989 and Imhof, 2007

98 See Adler, 1995

99 Geographic Resources Analysis Support System.

100 https://grass.osgeo.org

creating ad-hoc automatic procedures for the specific problem, and also for scientific and ethical implications of the free software.

GRASS GIS (hereinafter GRASS) is released under GNU GPLv3[101]. GRASS has been originally developed in 1982 as a project of USA-CERL[102], a branch of the U.S. Army Corp of Engineers, which published the last release (GRASS ver. 4.1) in 1992. Since 1997, the GRASS project has been carried out by the GRASS Research Group of Baylor University (Texas, USA). In 1999, the GRASS Development Team was born and took in charge the GRASS project, with the aim of managing the update and the development of the software.

Nowadays, GRASS fulfils all the features of GIS software, thus it is typically employed in visualization of geo-cartographic data, geospatial data analysis and management, maps production and spatial modelling.

In GRASS, the storage of data follows the hierarchic structure of the *file system*. All the data are stored in a main directory, downloaded together with the software and called *grassdata*, where the user can create various sub-directories, called *locations*, each of which contains the spatial data of a specific geographic region, expressed in the same reference system. The locations are divided into various working directories, called *mapsets*, containing homogeneous maps (e.g. all the maps are referred to the same project). The basic structure of data is depicted in Figure 5.1

101 General Public License version 3 (http://www.gnu.org/licenses/gpl.html)

102 U.S. Army Construction Engineering Research Laboratories

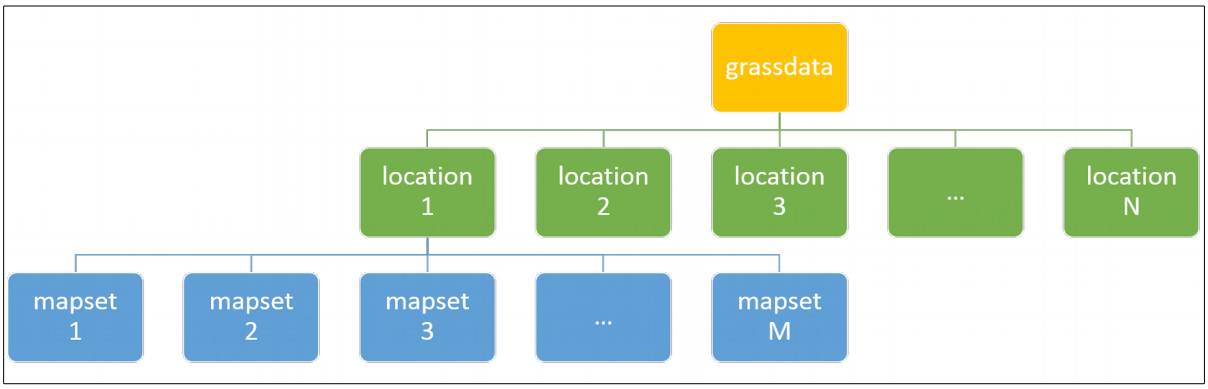

Figure 5.1. Representation of GRASS data structure.

The different locations are expression of likewise reference systems, thus every set of mapsets inside a location has the same reference system.

To create a new location it is necessary to know some fundamental parameters:

- the reference system and the cartographic projection (if present);
- the limits of the area;
- the resolution.

The concept of *computational region* is used to indicate the working area, both from the limits and the resolution point of view.

Among the previously mentioned parameters, the reference system has to be defined during the creation of the location and it is unique for the location, while the limits and the resolution can be defined once the location has been created. Furthermore, many computational regions, usually associated with different limits and resolutions, can co-exist in the same location.

Typically, the reference system is defined by the EPSG[103,104] code, a conventional code that uniquely identifies a coordinate reference system and geographic projection and contains the parameters[105] for defining the transition to the geocentric global reference system WGS84.

The computational region is strictly related to the extension of the data and to the original and desired resolution of the output of the analysis; both these settings can vary during the elaboration phase according to user's requirements (e.g. a computational region for describing the main framework is typically wide and with a coarse resolution; whereas, if a focus on a specific region is needed, the corresponding region will be defined with more restricted limits and higher resolution).

Concerning the resolution, it must be set when working with rasters, while it may not be set when working with vectors. It is also important to underline that the chosen resolution has to be compatible

103 European Petroleum Survey Group.

104 http://www.epsg.org

105 The necessary parameters should be 7 (three translations, three rotations and one scale factor), but they could be less.

with the original precisions of the data involved in the analysis: a resolution equal or lower (i.e. coarser) than the initial precision is typically chosen. It should be noted that choosing a higher resolution would not increase the informative content (which depends on the original resolution). In fact, imagine to have a 5 m resolution raster: if a resolution of 1 meter is set, each (5 × 5) meters cell would be split in 25 sub-cells of (1 × 1) meters, obviously containing the same information of the original (5 × 5) meters cell. In this case, the effect of setting a higher resolution is a fake improved resolution, which would just slow down the computational speed. For this reason, it is suggested to choose the highest resolution found in the data to be processed as upper limit for resolution.
The limits of the areas and the resolutions chosen for the realisation of PWV maps, together with the motivation of the choices and a spatial analysis, will be presented in sections 5.2 and 5.3.

5.2. THE 2D PROCEDURE

A GIS procedure was implemented to produce 2D PWV maps and to analyse its spatial-temporal evolution, integrating ZTD, Pressure and Temperature data coming from existing infrastructures, hence not necessary co-located. The following section describes the procedure and working settings used to analyse two intense meteorological events occurred on Genoa with different spatial resolution and extension.
Through observations coming from GNSS Permanent Stations and measurements of Pressure and Temperature at the ground, it is possible to estimate PWV applying the equations proposed by Bevis et al. (1992), and here summarized:

$$\mathrm{ZHD} = \frac{(2.2779 \pm 0.0024)\cdot \mathrm{P}}{1 - 0.00266\cdot\cos(2\cdot\phi) - 0.00028\cdot \mathrm{H}} \quad [\mathrm{m}] \tag{5.1}$$

where P is the Pressure (in mbar), ϕ is the latitude and H is the ellipsoidic height (in km). As known:

$$\mathrm{ZWD} = \mathrm{ZTD} - \mathrm{ZHD} \tag{5.2}$$

and PWV, closely related to ZWD, is obtained from:

$$\mathrm{PWV} = \Pi\cdot\mathrm{ZWD} \tag{5.3}$$

where

$$\Pi = \frac{10^6}{R_v\cdot\rho}\cdot\left(k'_2 + \frac{k_3}{T_m}\right)^{-1} \tag{5.4}$$

The terms appearing in equation (5.4) are respectively

$$
\begin{aligned}
R_v &= 461.70 \quad \left[\frac{J}{kg \cdot K}\right] \\
\rho &= 1000 \quad \left[\frac{kg}{m^3}\right] \\
k'_2 &= 17 \pm 10 \quad \left[\frac{K}{mbar}\right] \\
k_3 &= (3.776 \pm 0.03) \cdot 10^5 \quad \left[\frac{K^2}{mbar}\right] \\
T_m &= \frac{\int \frac{P_v}{T}}{\int \frac{P_v}{T^2}} \simeq 70.2 + 0.72 \cdot T_s \quad [K]
\end{aligned}
\tag{5.5}
$$

Such equations are applicable to a local site where a meteorological ground station is measuring nearby a GNSS Permanent Station, allowing an estimation of PWV on such site, hence the analysis of its local temporal variation.

But the main outcome of the present research is the production of 2D PWV maps, and the analysis of its spatial-temporal evolution, using data observed by existing infrastructures, hence not necessary co-located. The lack of availability of meteorological observations in correspondence of most of the GNSS PS prevents the assess of PWV for the station points and consequently the creation of spatial PWV maps.

On the other hand, a GIS environment easily allows to implement Bevis' equations in two dimension, to produce 2D PWV maps, starting from spatial distribution of ZTD, P and T, in addition to a Digital Terrain Model, by algebra map calculator. But the main difficulty arises from the production of representative input maps from sparse points, especially over a wide and orographically complex area.

A procedure to produce 2D PWV maps on a wide and orographically complex area using existing infrastructures was defined by the Laboratory of Geodesy, Geomatics and GIS at the University of Genoa, as shown in Figure 5.2.

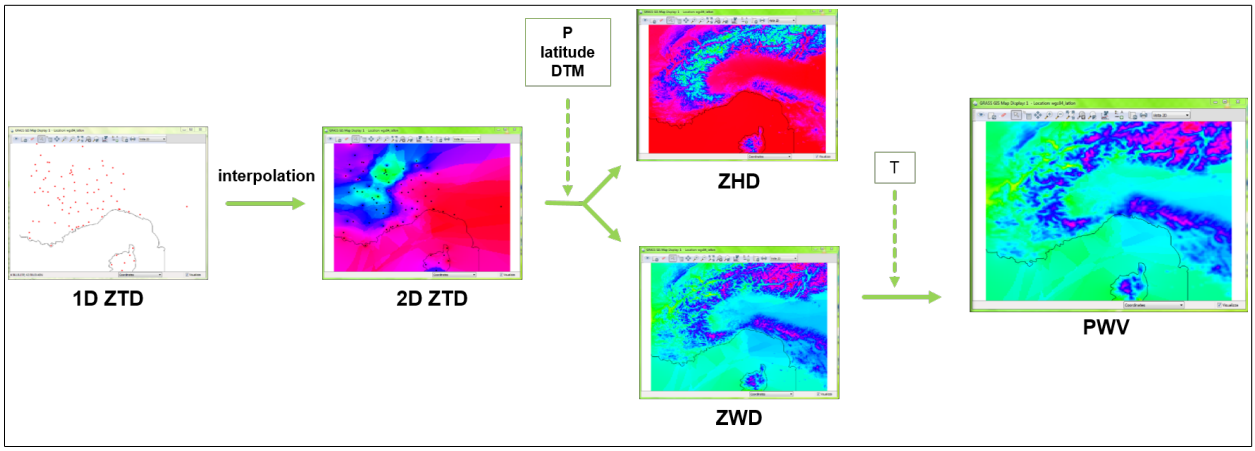

Figure 5.2. A scheme of the procedure.

ZTD map is simply derived by a proper 2D interpolation of ZTD estimated over a Permanent Stations network. But, to analyse the space-time evolution of ZTD, hence consequently of PWV, a ΔZTD temporal variations has to be performed (consequently producing a ΔPWV), measured with respect to a reference "calm" instant, thus reducing the orographic effects on ZTD (Li et al., 2006).

Pressure and Temperature 2D maps are generated applying a simplified model of the atmospheric behaviour, developed by the research group (a closed model of which the research group is owner), to the local sparse data of existing infrastructures (Sguerso et al., 2014; Ferrando et al., 2016).

Such three maps, integrated with latitude and elevation raster maps, allows to produce realistic 2D PWV maps.

To better analyse the evolution in time of ZTD and PWV, the difference of such values relative to a certain time were differentiated with respect to a "calm" time, i.e. an instant characterized by low values of ZTD and PWV.

Pressure and Temperature 2D maps could also be obtained from meteorological models for forecasts. But the procedure was set up to be totally independent from weather models. In this way, the results could be useful as starting conditions for existing meteorological models or as comparison with them, to better understand the meteorological phenomena.

The GIS environment was used to produce 2D PWV maps following the procedure previously illustrated.

The procedure was applied to the neighbouring French-Italian area, from the following input data.

ZTD data come from 181 GNSS/GPS Permanent Stations (PSs) belonging to international, national and regional networks covering the neighbouring French-Italian area (section 3.1). ZTD data have been processed through common elaboration techniques and procedures using GPS signal over 14 years, from January 1998 to May 2012, to estimate a set of two-hourly tropospheric parameters (Sguerso et al., 2013 and 2015), and recently the DataBase has been upgraded until 2015 (as previously described in sections 3.2 and 3.4).

Pressure and Temperature data are a selected number of NOAA meteorological stations (www.noaa.gov) covering approximately the north-western part of Italy and the French-Italian border region (as previously described in section 3.5).

To describe the terrain elevation, the Global Digital Elevation Model (GDEM) of ASTER space project (joint product of METI, the Ministry of Economy, Trade and Industry of Japan, and NASA, the National Aeronautics and Space Administration; http://asterweb.jpl.nasa.gov/gdem.asp) was used. Its original resolution is 1" of arc, corresponding to about 30 m, but during the present procedure it was degraded as illustrated in the following.

To analysed the statistical behaviour of the observed data, the variogram of ΔZTD (the ZTD difference in time) was computed, in R environment (2008). It allowed to quantify the spatial variability of ZTD data in the French-Italian neighbouring area, so to verify the correctness of the grid size of the interpolation

maps (6', about 10 km). Figure 5.3 depicts the empirical points and the variogram model of ZTD data relative to 03/11/2011 04 UT with respect to 03/11/2011 02 UT.

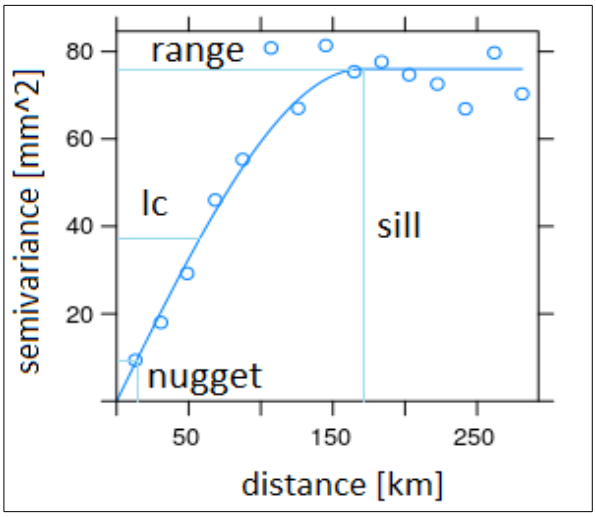

Figure 5.3. Variogram of ΔZTD for 04 UTC with respect to 02 UTC on 3rd November 2011.

The variogram model that best fit the empirical data is a spherical function. The sill, range and empirical nugget parameters that characterize the variogram are respectively 76 mm^2, 170 km and 10 mm^2. The square root of the empirical nugget corresponds to the standard deviation of the signal noise, equal around to 3 mm. The correlation length (indicated in Figure 5.3 as l_c) can be estimated to about 50-60 km, while the mean distance between PSs is around 40-60 km. So similar magnitudes indicate an appropriate density for the considered GNSS network, but represent the upper limit of the sampling. The procedure was mainly applied to two intense meteorological events occurred on Genoa with different spatial resolution and extension, as will be discussed in the following dedicated sections (see 6.1 and 6.2).

5.3. DATA INTERPOLATION

Whatever point density is, to represent a surface or a field through a Digital Model, a discretization is always present. When the surface model has to be investigated on different points or with different spacing, data has to be carried out through mathematical estimate algorithms, i.e. interpolating methods. In general, it's hard to know a priori which interpolator will give better results, because it depends on the distribution and density of the observed data, and on the shape to reproduce.

In general, an interpolation algorithm can be based on a deterministic or stochastic model. In the first case the link between neighbouring points is defined by an explicit law whose parameters are evaluated according to physical criteria; in the second case the same link is expressed through statistical parameters (covariance). In addition an interpolator can be classified as global or local, respectively whether all data or only the nearest ones are used to create the model. The global models are useful to identify the general

trend of the data; however, local methods usually follow local fluctuations of the surface (Davis, 1975; Moritz, 1978; Benciolini, 1992).

In the present research the main and most widespread algorithms (e.g. Petrie and Kennie, 1987; Mitas and Mitasova, 1999), either local and deterministic and global and stocastic, were analysed: Triangulated Irregular Network derived by Delaunay triangulation, Inverse Distance squared Weighting, and Regularized Spline with Tension, hereinafter referred to as TIN, IDW and RST respectively, are deterministic models, and were analysed in GRASS; kriging algorithm is a stochastic method, and was analysed interfacing GRASS with the software R ("gstat" package). In particular simple, ordinary and universal kriging were tested.

The theory behind the most widespread interpolation algorithm is here briefly illustrated, without pretending to be exhaustive, but just to give a hint to help the reader who have never heard about them. Moreover, notes on the specific commands used and on their parameters that has to be set, were briefly outlined. For more details, refers to Neteler and Mitasova (2008), GRASS and R manual.

The choice of the most appropriate interpolation technique to create ZTD, P and T maps in a quick and automatic way for the future near-real time production of PWV maps, in order to support the monitoring of intense meteorological events, is a key issue for the present research.

The main difficulties are obviously due to the sparse distribution of P, T and ZTD data, combined with high resolution of the final map and wide computational region. Moreover the interpolator should be automatically adjustable to different network configurations that can occur in time (for lack of data in some stations at certain times, for example), crucial features for near real-time applications.

Note that, in the reconstruction of a field by interpolation of sparse data, either the spatial distribution of points sampled and the morphological characteristics of the field play an important role. Moreover the quality of the field resulting from the interpolation in general depends both on the quality of individual observation data and on the quality of the interpolation. In fact, data may be affected by errors (either random, gross or systematic). The quality of the interpolation depends on the errors introduced as a result of the interpolation algorithm, but also on the setting of interpolation parameters, especially when surface and dataset are not optimal (rough field and sparse data). The precision of the collected data has to be evaluated so not to ask to the interpolation method a quality too high compared to data quality.

5.3.1. Triangulated Irregular Network (TIN)

Interpolation based on a Triangulated Irregular Network (TIN) uses a triangular tessellation of the original point data to derive a bivariate function for each triangle, which is then used to estimate the values at unsampled locations, i.e. in grid nodes. Linear interpolation uses planar facets fitted to each triangle, while non-linear blended functions (e.g. polynomials) use additional continuity conditions on derivatives to ensure smooth connection of triangles.

Due to their locality (only the three vertices of the triangle are used for interpolation) this method is computationally fast and very good at preserving sudden changes in morphology, with an easy incorporation of discontinuities and structural features. Moreover, it is an exact interpolator.
The most common triangulation algorithm is the Delaunay one, defined so that no point of the dataset can be found inside the circum-hypersphere of any simplex, i.e. the circle circumscribing the triangle in 2-D. It corresponds to the dual graph of the Voronoi tessellation, i.e. the decomposition of the domain into Thiessen polygons defined so that they contains the set of all points closer to the centre of each polygon.
In this study, *r.surf.nnbathy* was used: it is a script interfacing GRASS with the external *nnbathy* utility, which uses a natural neighbour interpolation library called *NN* by P. Sakov, which again relies on J.R. Shewchuk's *Triangle* software for the underlying Delaunay triangulation. Such script, downloadable from GRASS AddOns, may be added to the default commands available in GRASS.
Three algorithm options are implemented in *r.surf.nnbathy*: the linear triangulation, the Watson's algorithm for Sibson interpolation (Sibson, 1981), and the Belikov and Semenov's algorithm for non-Sibsonian interpolation (Belikov et al., 1997). The last two options work similar to IDW, hence they were not applied in the present research; instead, the first algorithm option was used, creating a rough surface that goes exactly through all the input points, connecting them linearly, and then resampling the TIN surface on grid node. No parameters has to be set.
Note that the efficiency of data conversion from TIN to grid is scale dependent, with a negative relationship between output grid and the level of information retained. The use of very fine grid resolutions is computationally demanding and beyond a critical scale may offer little improvement in the representation of the surface.

5.3.2. Inverse Distance Weighting

In Inverse Distance Weighting (IDW) interpolation, data are weighted such that the influence of one point relative to another declines with distance between them. The weight assigned to data points are fractions, and the sum of all the weights is equal to 1.0. Weighting is assigned to data using a weighting power that controls how the weighting factors drop off as distance from a grid node increases. The greater the weighting power, the less effect points far from the grid node have during interpolation. As the power increases, the grid node value approaches the value of the nearest point. For a smaller power, the weights are more evenly distributed among the neighbouring data points (Isaaks and Srivastava, 1989).
The equation used for Inverse Distance to a Power is:

$$z_j = \frac{\sum_{i=1}^{n} \frac{z_i}{d_{ij}^{\beta}}}{\sum_{i=1}^{n} \frac{1}{d_{ij}^{\beta}}} \tag{5.6}$$

where: z_j is the interpolated value for grid node j, z_i are the neighbouring points, d_{ij} is the distance between the grid node j and the neighbouring point i, n is the number of points to use for the interpolation, and β is the weighting power. The resulting surface depends on the weighting power β and on the parameter n.

In the command *v.surf.idw,* present in GRASS (v. 7.0), both the weighting power β and the parameter n may be choosen (Neteler and Mitasova, 2008). Declercq (1996) analysed the effect of n on interpolated surface from high data density, and recommended $n \leq 8$ for "smooth" surfaces and $n \geq 16$ for abruptly changing surfaces. Note that the larger the value of n, the smoother the interpolated surface.

In literature, IDW interpolation is suggested if data density is higher than the density of the resulting grid points and homogeneously distributed, due to its simplicity and computational speed. If data density is low and their spatial distribution is isotropic, a typical artefact of IDW are circular areas around data points, what it's called the "bull's eyes"' pattern.

5.3.3. Regularised Spline with Tension

The term "spline" comes from the spline gadget used by shipbuilders to draw smooth shapes. The important characteristic of spline functions is that they are piecewise polynomial functions: different polynomials may be used in different parts of a domain. A significant advantage of this approach is that it can follow a large, complex curve by using low degree polynomials (Ahlberg et al., 1967; Greville, 1969; Weston, 2002). The simplicity of representation and the ease with which a complex spline's shape may be computed makes spline a popular representation for curves, predominantly in computer graphics (Bartels et al., 1987) but also for other kinds of interpolations as terrain modelling (Brovelli et al, 2001).

Different types of spline exist, depending on the polynomial degree. A function S is called a spline of degree k if all the following conditions are satisfied:

- the domain of S is an interval [a,b];
- S, S', ... $S^{(k-1)}$ are continuous functions on [a,b];
- there are knots t_i such that $a = t_0 < t_1 < \ldots < t_{i-1} < t_i = b$ and such that S is a polynomial of degree at most k on each subinterval $[t, t_{i+1}]$.

The assumption that the interpolation function should be as smooth as possible is mathematically expressed by the condition that the sum of the deviation from the measured points has to be minimum (when the information derived from the observed points are redundant with respect to the polynomial unknown quantities):

$$\sum_{i=1}^{n} |z_i - F(r_i)|^2 \cdot w_i = \text{minimum} \qquad (5.7)$$

where z_i is the observed value measured at discrete point r_i and w_i is a positive weight. F(r) is the spline function, that may assume different expression; for example, in GRASS the bivariate Regularized Spline with Tension (RST) method is used through the command *v.surf.rst* (Mitasova and Mitas, 1993; Neteler and Mitasova, 2008).

RST method uses functions taking into account the sum of all derivatives up to infinity with rapidly decreasing weights, so that the resulting surface has regular derivatives of all order. Moreover, a tension parameter appears, hence the surface can be tuned from an "elastic membrane" to a "thin steel plate". High tension "increases the distances" between points, so reduces the range of impact of each point. Surface with too high tension (e.g. 100) behaves like a membrane with peak or pit in each given point and everywhere else the surface goes rapidly to trend. Low tension "decreases the distances" between points, hence the points influence each other over longer range. Surface with too low tension (e.g. 10) behaves like a stiff plate hard to bend, hence a very smooth surface. The default tension value in *v.surf.rst* is equal to 40.

Besides tension, the principal parameters that has to be defined are smoothing, the anisotropy angle θ and the anisotropy scaling factor scalex.

Smoothing allows the surface to deviate from the data points in its effort to minimize its energy. Its default value is 0.1, hence an approximation is allowed. If smoothing is set to zero, the interpolation function passes exactly through the observed data.

The effect of tension and smoothing on the spline is reported in Figure 5.4.

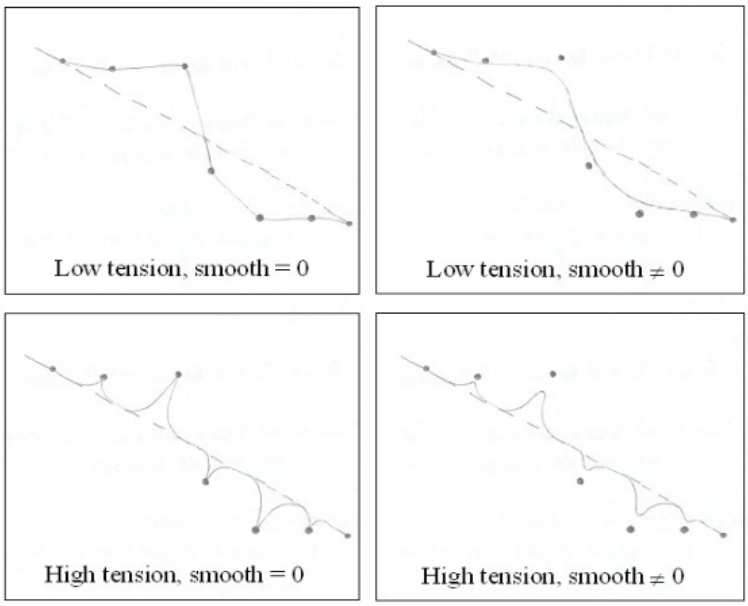

Figure 5.4. Effects of tension and smoothing on splines.

θ and scalex define orientation and ratio of the perpendicular axes put on the longest/shortest side of the data feature, respectively. Theta is measured in degrees from East, counter-clockwise. Scalex is a ratio of axes sizes. Setting scalex in the range 0-1, results in a pattern prolonged in the direction defined by theta, and vice-versa. Scalex value give the idea of the anisotropy strength. Didactic examples of the effects of different values assigned to RST parameters on a river elevation model are reported in Federici and Sguerso (2004).

Predictive error of surface approximation for given parameters may be computed using the -c flag in the command, through a cross-validation procedure. The CV procedure is based on removing one input data point at a time, performing the approximation for the location of the removed point using the remaining data points and calculating the difference between the actual and approximated value for the removed data point. The procedure is repeated until every data point has been, in turn, removed. This form of CV is also known as the "leave-one-out" or "jack-knife" method (Hofierka et al., 2002).

5.3.4. Kriging

Kriging is a geostatistical interpolation method, based on the assumption that the land surface represents the “signal” that has to be analysed. It takes into account spatial correlation between observed data, and aim to minimise the residual variance of the grid (Matheron, 1963; Krige, 1984).

Kriging is based on the assumption of data stationarity, i.e. the expected difference between two points separated by horizontal distance h is zero, and the variance of the difference depends on h and not on the point.

An important component of the kriging method is the variogram, also called structure function, that represents the spatial correlation between data (Barzaghi and Sansò, 1983). The variogram γ(h) is defined as:

$$\gamma(h) = 0.5 \cdot \mathrm{Var}[z(r + h) - z(r)] \tag{5.8}$$

where z(r) is the given data and the vector h contains the distance between two data. If stationary condition of the stochastic process can be assumed, the variogram is so related to the spatial covariance

$$\gamma(h) = C(0) - C(h) \tag{5.9}$$

where C(0) is the covariance value at zero distance, i.e. the variance of the process; for distance values that tends to infinity, C(h) tends to zero, so γ(h) tends to C(0).

Variogram parameters that have to be estimated are: sill C(0); nugget, i.e. the estimation of the spatially uncorrelated residual noise; range, i.e. the distance at which the correlation decreases considerably.

In presence of data anisotropy, the anisotropy direction of the spatial correlation between data can be taken into account fixing the direction of the vector h, with a tolerance angle; hence a directional variogram may be calculated (see also Eriksson and Siska, 2000).

Then it's necessary to fit the experimental variogram with a theoretical one chose from the available models like spherical, exponential, Gaussian, Bessel, etc. These variogram models have to satisfy the strong condition to be negative defined; the parameters of such functions are then optimized for the best fit.

Finally, kriging interpolation is a set of linear regression routines which minimize the estimation variance, weighting data in function of distance h by variogram model.

There are many kind of kriging methods, the most common are simple, ordinary and universal (Wackernagel, 2003). They differ each other for the statistical behaviour of original data. In particular, simple and universal kriging needs to know respectively the average and the trend of the original data, while ordinary assumes a constant but unknown data average.

In the present work, kriging was analysed interfacing GRASS with the software R ("gstat" package).

Details on kriging implemented in R software may be found in Pebesma (2004).

5.3.5. ZTD, P and T interpolations

In order to produce 2D PWV maps, the starting point is the interpolation of ZTD, P and T data in order to transform them from punctual to areal (2D) information. The choice of the most appropriate interpolation technique, according to the spatial distribution of data and the resolution of the final map, was performed comparing their local and global behavoiur.

A first case study has been the event of Genoa on 4th November 2011 (Sguerso et al., 2014). Inverse Distance Weighted (IDW), Regularized Spline with Tension (RST) and Kriging interpolation techniques were compared with low resolution. It results a substantially identical behaviour of the examined interpolation techniques, both for GNSS data and environmental parameters. Considering the greater simplicity and the lower computational effort of IDW with respect to the other techniques, IDW6 has been chosen as interpolator for this case study.

A second case study is relative to 9th October 2014 severe event in Genoa. Differently from the previous analysed case study, higher resolution is used to monitor the localized pattern of the meteorological event. In this case, IDW, RST and Triangulated Irregular Network (TIN) interpolation techniques were compared. TIN was deemed to be the best interpolation technique for the specific application.

In both cases, P and T 2D maps were generated applying a simplified physical model developed and owned by the research group.

The issues related to data interpolation will be discusses in sections 6.1.1, 6.1.2 and 6.1.3 and 6.2.1, also thanks to the comparison with meteorological re-analysis which allows to evaluate both the performance of the simplified physical model in reproducing Pressure and Temperature fields, and of the entire procedure in representing severe meteorological events.

5.4. AN INDICATOR FOR SEVERE RAINFALLS: THE HETEROGENEITY INDEX (HI)

The previously described G4M procedure is capable to produce PWV and ΔPWV maps for monitoring the content of PWV in atmosphere, even during severe meteorological events.

In the context of studying remarkable features in PWV evolution, which can locate and potentially precede severe meteorological events, and to better relate the PWV content to the occurrence of rain, the spatial variability of PWV has been analysed.

The overcoming of a threshold of PWV is not a sufficient parameter to detect remarkable features related to the occurrence of intense rainfalls, as already shown in the 1D analysis of PWV (see section 4.4.2). The same conclusion can be reached looking at a 2D ΔPWV map (as in Figure 5.5 relative to the 4th November 2011 severe event on Genoa), where, on the sole basis of PWV value, it is not possible to locate if a severe meteorological event could occur on A or B or both or none of them. Thus, the PWV and ΔPWV maps were considered not sufficient to localise in time and space severe meteorological events.

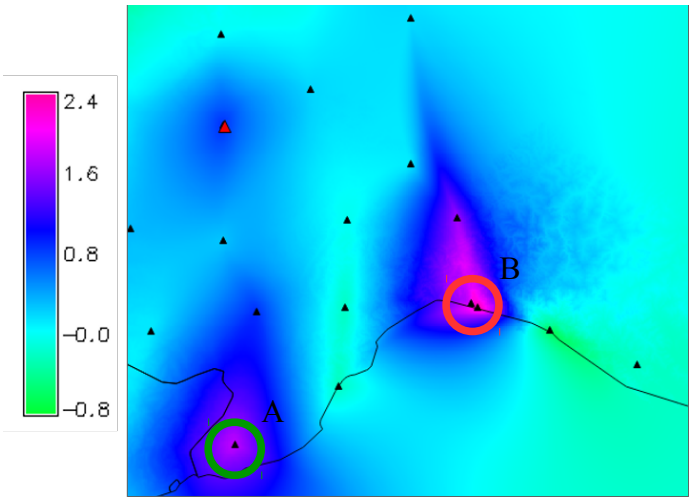

Figure 5.5. Where a severe meteorological event could occur?

Thanks to the suggestion of Prof. T. Tsuda, an index accounting the spatial variability of PWV, hereafter called Heterogeneity Index (HI), has been conceived. The index is obtained by re-sampling the ΔPWV maps to a coarser grid (1 km in the following application) with the value of the standard deviation, using the GRASS module *r.resamp.stats*. Thus, the HI maps represent the value of ΔPWV standard deviation.

As a test case to show the reliability of HI, the 4th November 2011 severe event on Genoa has been considered. Differently by the ΔPWV map (e.g. Figure 5.5), the location and timing of severe rainfall is detected in the HI map, as Figure 5.6 shows. High values of HI are present on B, where the event occurred, and not on A, characterized by high values of ΔPWV, or somewhere else. Moreover HI seems to be related to rain peaks, as will be discussed in section 7.2, where the application of HI will be shown.

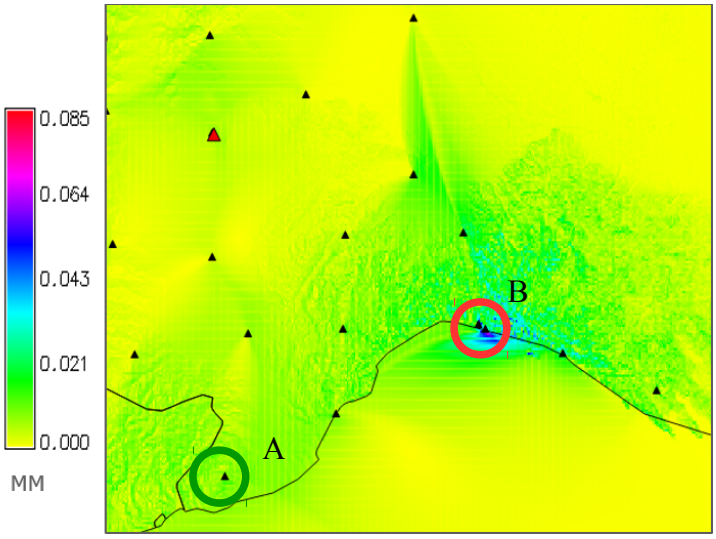

Figure 5.6. HI highlights Genoa (B), where the event occurred.

5.5. PROCEDURE AUTOMATION

The GIS procedure called G4M (GNSS for Meteorology) has been conceived by the Laboratory of Geodesy, Geomatics and GIS to produce 2D PWV maps with high spatial and temporal resolution, for a posteriori and near real-time monitoring of severe meteorological events, in order to support decisions for now-casting and for an early warning system.

Here the strategies and procedures for automatise the G4M procedure are described.

In order to allow the realisation of several PWV and ΔPWV maps, a simple Fortran code has been conceived, to produce a bash script to be launched in GRASS GIS environment. The code requests as input data:

- a raster DTM covering the chosen computational region;
- a raster representing the latitude of the chosen computational region;
- Pressure, Temperature and GNSS data in vector format, already treated with the previously mentioned Fortran code, to ensure the continuity of data.

It is also needed that the computational regions and the resolutions have already been chosen and set. The code can produce two-hourly maps (for a posteriori monitoring) or 6 minutes maps (for near real-time monitoring).

The Fortran code simply works as follows:

- asks the starting day and hour, and the ending day and hour;
- performs some checks on the input dates, accounting the possibility of a change in month between them (if the ending day is smaller than starting day);
- creates a blank file, which will contain the commands for GRASS script;
- writes on the blank file the commands to set the regions and the "general" maps, to pass from ZTD to PWV (latitude, DTM and ZHD denominator);
- implements the simplified physical model for P and T interpolation;
- writes the commands to perform P and T data interpolation using the chosen method (TIN as default), producing a map for every time in the chosen period. The code fills with the "null value", i.e. 99999, the eventual missing data;
- writes the commands to compute T_m and Π for every time in the chosen period;
- writes the commands to perform ZTD interpolation using the chosen method (TIN as default), producing a map for every time in the chosen period. The code fills with the "null value", i.e. 99999, the eventual missing data;
- writes the commands to obtain ZHD combining ZTD and P maps, then computes ZWD and finally PWV, using Bevis' relations;
- asks the time and day to be used as reference to differentiate in time and obtain the ΔPWV maps;
- writes the commands to compute ΔPWV maps for the entire period;

- asks the final resolution at which compute the HI maps, writes the commands to perform the reclassification and obtain HI.

The procedure is under the preliminary phase of patenting, for this reason the code is not available at the time of this writing (December 2016).

6. PWV A POSTERIORI ANALYSIS

In this section, two severe meteorological events occurred in Genoa (Italy) on 4th November 2011 and 9th October 2014 will be analysed respectively in sections 6.1 and 6.2, using the previously introduced procedure. A major issue concerns the interpolation of ZTD, P and T, to identify the most appropriate interpolation technique to create PWV maps in a quick and automatic way, suitable for near-real time application too, in order to support the monitoring of intense meteorological events. The main difficulties are due to the sparse distribution of P, T and ZTD data and the different networks configurations, combined with high resolution and wide computational region. The issues related to data interpolation will be discusses in sections 6.1.1 and 6.2.1, also thanks to the comparison with meteorological re-analysis which allows to evaluate both the performance of the simplified physical model in reproducing Pressure and Temperature fields, and of the entire procedure in representing severe meteorological events. Additionally, some considerations and discussion on the procedure's results will be reported in sections 6.1.4 and 6.2.2.

6.1. 4TH NOVEMBER 2011 EVENT

In the morning of 4th November 2011, a stationary and self-healing storm developed over the city of Genoa causing a very large amount of rain with intensities up to 175 mm/hour nearby the city (http://www.nimbus.it/eventi/2011/111105AlluvioneGenova.htm). In some areas of Genoa, out of the almost 400 mm fallen in the entire day, about 300 mm fell in the four hours between 09 UTC and 13 UTC. This severe meteorological event led to a flooding of the Bisagno River and of its tributary Fereggiano, causing the death of six persons and a large amount of damage, as shown in Figure 6.1.

Figure 6.1. Some of the damages of 4th November 2011 severe event.

6.1.1. Data interpolation

In order to produce 2D PWV maps, the starting point is the interpolation of ZTD, P and T data in order to transform them from punctual to areal (2D) information. The area under exam covers approximately the north-western part of Italy, with particular interest on Genoa and Liguria Region. The computational region was discretized with a resolution of 6' (about 10 km) in WGS84 datum (Sguerso et al., 2014).

The existing infrastructure used for obtaining PWV 2D maps is composed by:

- 117 ZTD data, extracted from the RENAG DB, with a mean spacing of 40 km in the French-Italian border region;
- 27 NOAA meteorological stations, used to extract Pressure (P) and Temperature (T) data (7 and 20 stations respectively), with a mean spacing of 200 and 150 km.

Figure 6.2 a, b and c depict the distribution of the GNSS PSs, Pressure and Temperature networks respectively.

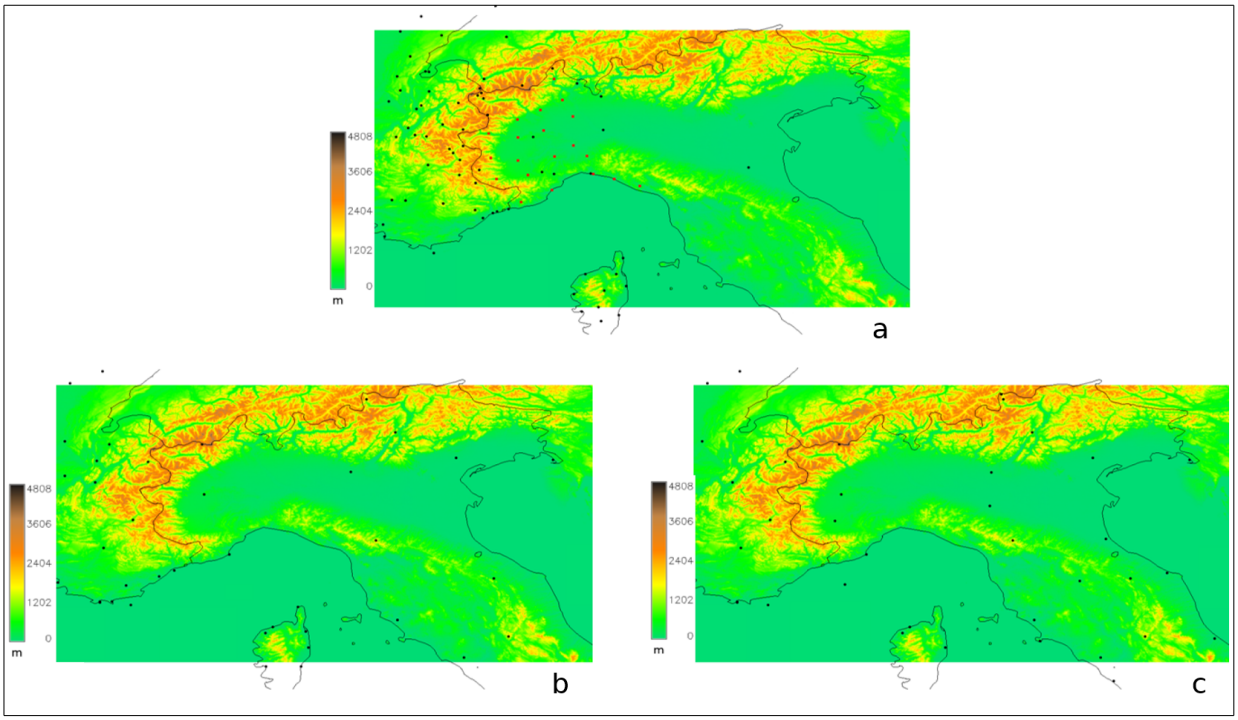

Figure 6.2. Distribution of GNSS (a), Pressure (b) and Temperature (c) stations in the study area.

Due to the different networks configurations, the most appropriate interpolation technique was investigated. The interpolator should be fast and also automatically adjustable to different network configurations that can occur in time (for lack of data in some stations at certain times, for example), crucial features for near real-time applications.

ΔZTD between 04 UTC and 02 UTC of 3rd November 2011 has been interpolated via Universal Kriging (Krig), Regular Spline with Tension (RST) and Inverse Distance Weighted (IDW). In particular, three

different tests have been performed with IDW technique using 3, 6 and 12 nearest points, indicated as IDW3, IDW6 and IDW12 respectively.

In order to define which interpolation technique could be the most representative of the observables, 12 PSs of the 117 (called "verification" points) have not been used for the interpolation itself but to verify the results. Hence, interpolation of the remaining 105 stations was performed. Two different comparisons were carried out: along a transept to analyse the altimetric difference between all of them, and a 2D difference map between IDW6 interpolation and the other methods to analyse the global planimetric behaviour in the study area.

Figure 6.3 depicts the trace of the transept (on the left side) and the values of ΔZTD along it, from South/West to North/East (on the right side), produced applying the interpolation techniques. The results of the interpolations are quite similar, apart from IDW3 which has a trend in steps. Excluding IDW3, the maximum differences between interpolated and true values of ΔZTD are generally less than 4 mm, which is comparable to the standard deviation noise.

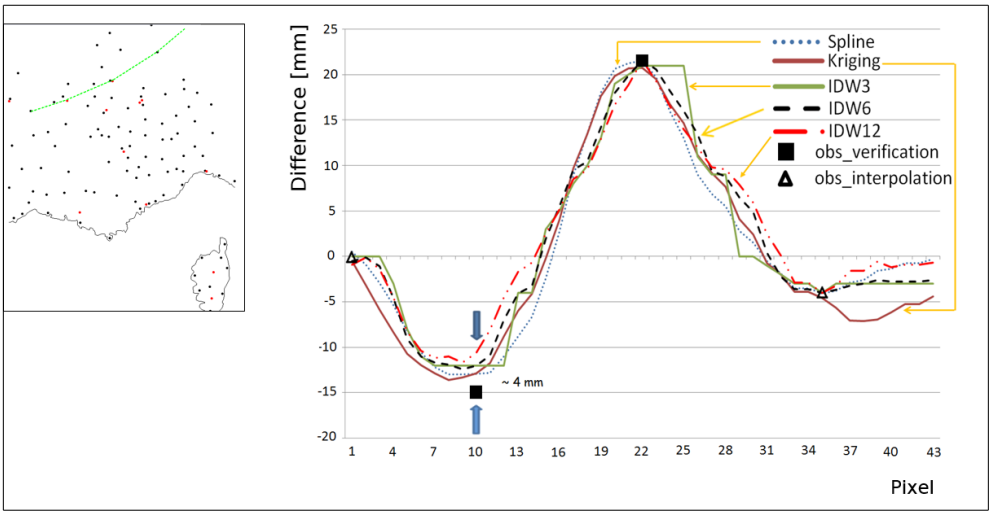

Figure 6.3. Transept position (left) and ΔZTD values from different interpolation techniques (right). The "verification" PSs are the red dots on the left and the squares on the right graph.

Figure 6.4a depicts the 2D interpolation surface of ΔZTD between 03/11/2011 04 UTC and 03/11/2011 02 UTC using IDW6, while Figure 6.4b-e represent, for the same parameters, the differences of the various interpolation techniques in respect to IDW6. The interpolated maps seem quite similar. Mean m and standard deviation std of the entire differences maps are about -0.1 mm and 1.3-1.5 mm respectively for IDW interpolations, while for RST and Kriging mean and std are a little bit higher (-0.2÷0.5 mm and 2.3 mm respectively) due to the different behaviour in the edge region. In Table 6.1 the mean and standard deviation calculated on the 12 "verification" points are reported. The values are very similar for every interpolation method, with slightly better results for Kriging, RST and IDW6. In particular, the differences between interpolated surface values and the true values of the "verification" PSs are always within the mean ± 3σ.

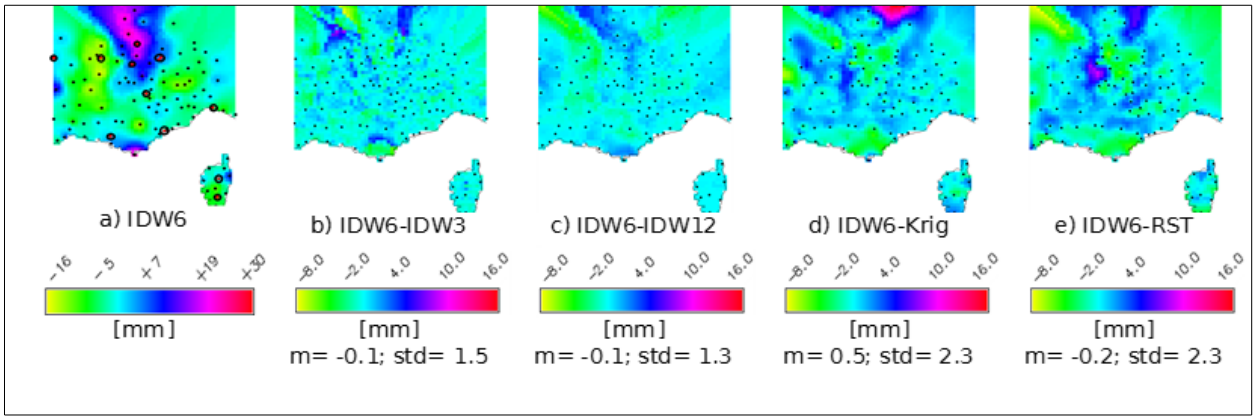

Figure 6.4. ΔZTD created by IDW6 and difference maps with the other interpolation techniques. Mean (m) and standard deviation (std) of the difference maps are reported. The red dots on the first map on the left represent the "verification" points.

Interpolated surface and true values differences for the 12 "test" PSs					
[mm]	Krig	RST	IDW3	IDW6	IDW12
Average difference	-0.7	-0.6	-0.6	-0.7	-0.6
Min and max differences	-11;+3	-11;+4	-15;+3	-14;+3	-14;+4
Standard deviation	4	4	6	5	5

Table 6.1. Comparison between different interpolation methods and true values at 12 test PSs.

Considering the substantially identical behaviour of the examined interpolation techniques, the greater simplicity and the lower computational effort of IDW with respect to Kriging and RST, IDW6 has been chosen as interpolator for this case study.

Finally, a qualitative comparison was carried out applying IDW6 to the "regional" GNSS network and just to the 20 IGS PSs located inside the computational area. The ΔZTD maps are related to 04/11/2011 10 UTC, which represents the moment of most intense rain, in respect to 03/11/2011 02 UTC. Figure 6.5 depicts a zoom of the entire computational area, containing only 4 of the 20 IGS PSs. Comparing Figure 6.5a and Figure 6.5b, it is evident that just the small number of IGS sites is not sufficient to derive the ΔZTD pattern with the desired resolution. Hence a dense GNSS PSs network is needed to produce reliable results.

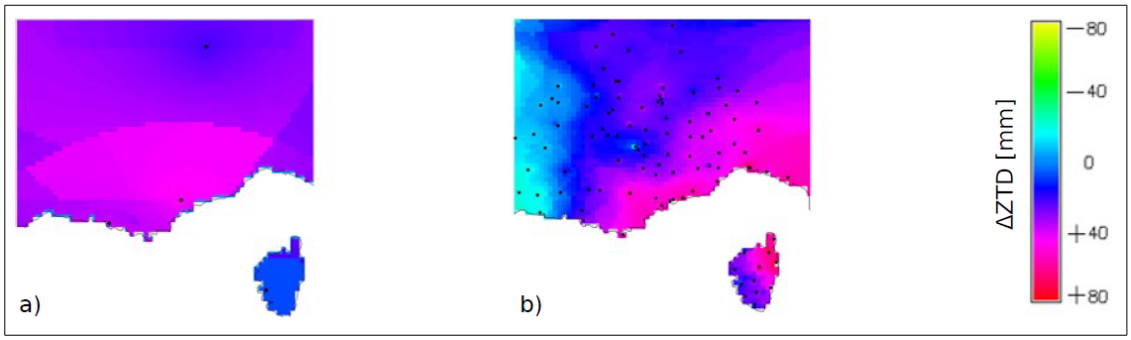

Figure 6.5. ΔZTD between 2011/11/04 10 UTC and 2011/11/03 02 UTC.
ΔZTD is computed by means of 20 IGS PSs (a) and the "regional" GNSS network (b).

An analogous approach was applied to the interpolation of Pressure and Temperature data, giving rather similar results.

6.1.2. Comparison with re-analysis

In this section, to check the adequacy of the adopted simplified physical model to reproduce P and T fields, the interpolated P and T maps and the deriving PWV maps were compared with the ones coming from the so called "meteorological re-analysis".

All the following maps are referred to 4th November 2011 10 UTC, corresponding to the moment of the most intense rain.

To perform the comparison between interpolated fields and re-analysed P and T fields, 53 Pressure and 58 Temperature NOAA meteorological stations were used to obtain P and T fields, together with the simplified physical model. Figure 6.6 shows the spatial distribution of P (circles) and T (crosses) stations, covering approximately north-west of Italy and the French-Italian border region, with a mean spacing of 150 km. Among the total number of meteorological stations, four of them, called "checkpoints" and displayed in Figure 6.6 as small triangles, were excluded from interpolation and used to verify the accordance between interpolated and re-analysed fields.

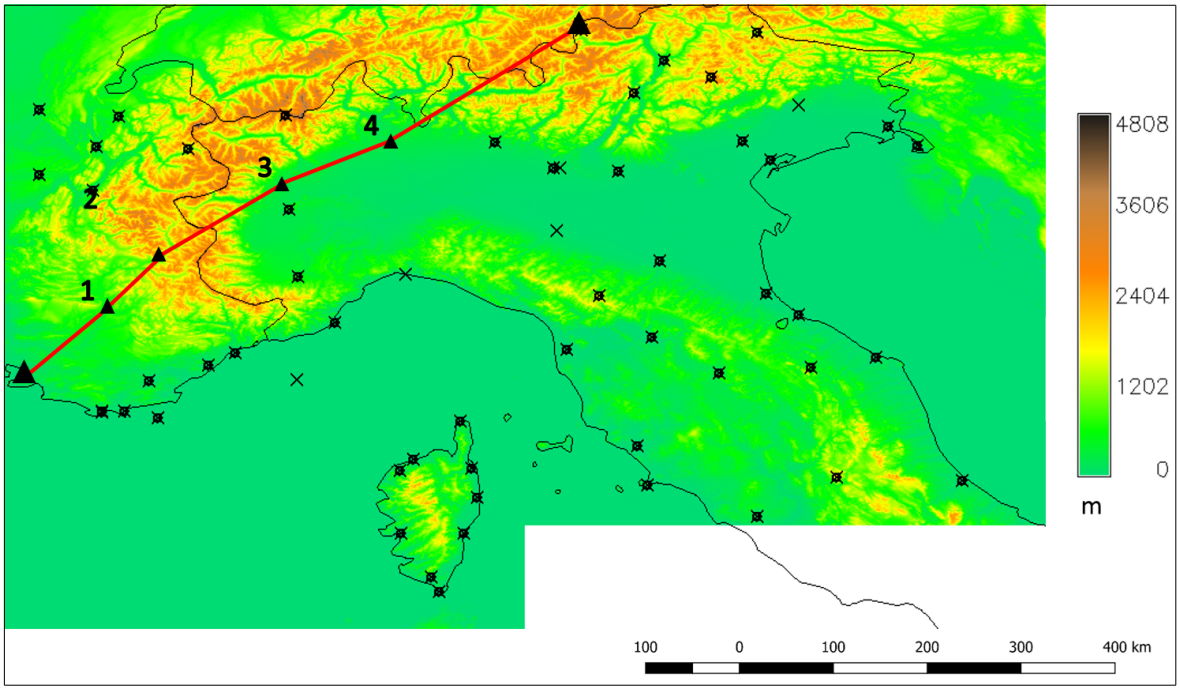

Figure 6.6. Distribution of P (circles) and T (crosses) stations.
The transept crossing the checkpoints (small triangles) is displayed in red.

The interpolation was carried out at a resolution of about 3.5 km, accordingly to the one used for re-analysis. The 2D maps were obtained by Inverse Distance Weighted (IDW), Regularized Spline with Tension (RST) and Triangulated Irregular Network (TIN) techniques using the free and open-source GIS software GRASS. The obtained maps for P and T are shown in Figure 6.7, on top and bottom respectively.

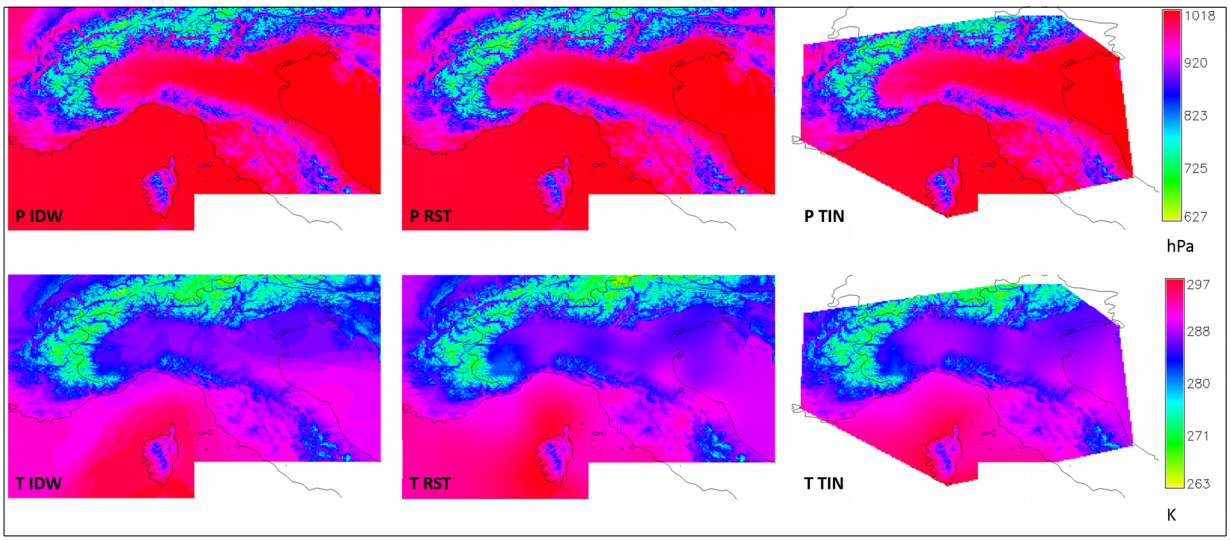

Figure 6.7. P (top) and T (bottom) fields obtained using IDW, RST and TIN interpolation techniques.

Two different comparisons were carried out for the interpolated maps: along the transept to locally check the adherence with the re-analysis and observed data, and 2D differences maps between the re-analysis and the interpolated fields to evaluate the global behaviour in the study area.

The transept passes across some meteorological stations (the checkpoints). Figure 6.8 shows the values along the transept of P and T respectively, for IDW (blue line), RST (red line), TIN (yellow line), re-analysis (green line) and NOAA observed data (black triangles).

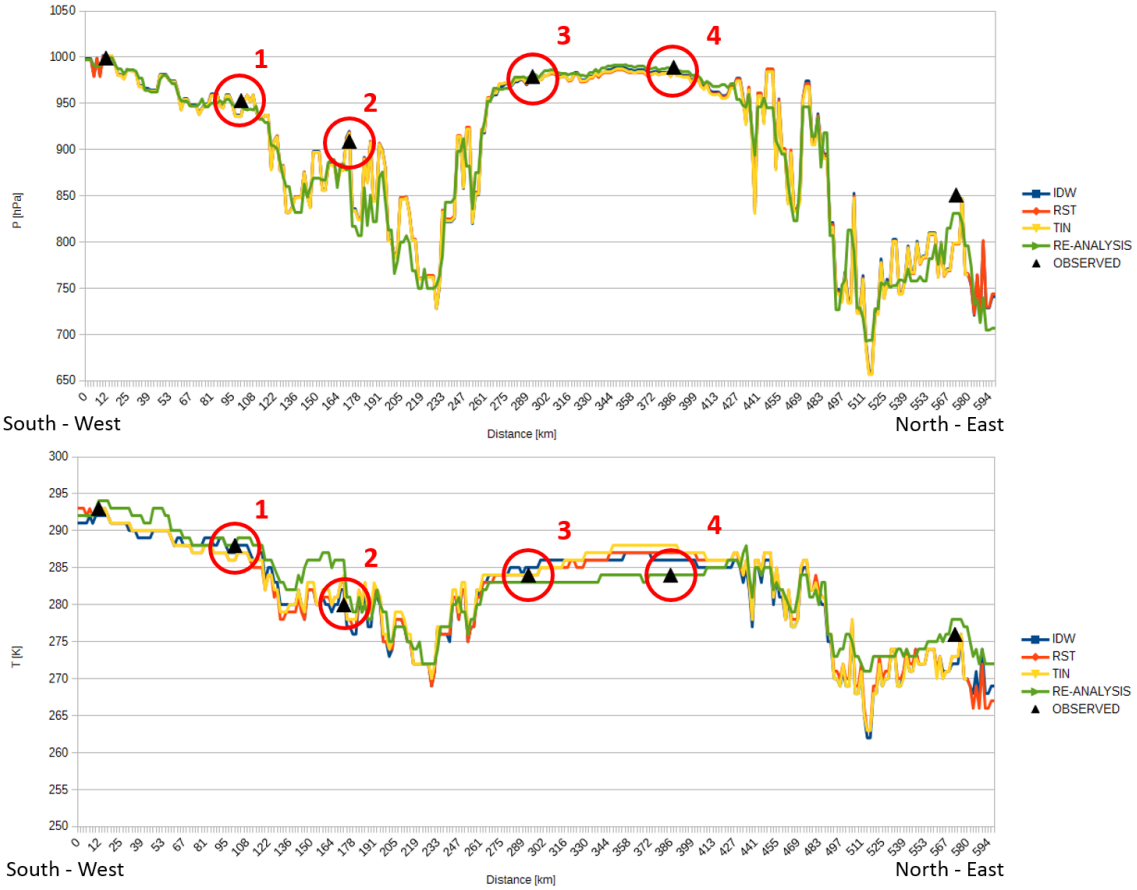

Figure 6.8. P (top) and T (bottom) values along the transept.

The interpolated maps seem quite similar along the transept. The accordance between re-analysis, observed data and interpolated fields is good, in the checkpoints too, showing that it is possible to obtain P and T fields even from sparse data. The major differences occur in high altitude areas, probably due to the generalization of the adopted model. P seems to be more complying to re-analysis and observed data than T. Focusing on the checkpoints, the maximum difference between re-analysis and interpolated fields are around 40 hPa in checkpoint 2 for all the applied techniques, and 4 K for checkpoint 4 for TIN.

It should be noted that on checkpoint 2 there is a disagreement between re-analysis and P observed data, this is maybe the cause of the previously mentioned high differences. Finally, high differences can be noticed on the edge regions, due to the different behaviours of the interpolation techniques.

Concerning the 2D comparison, the difference maps have been obtained subtracting the interpolated maps to the re-analysed fields, both for P and T.

As shown in Figure 6.9, the higher differences are mainly located in high altitude areas (Alps and Apennines), both for P (top of Figure 6.9) and T (bottom of Figure 6.9), where a strong orographic effect

can be appreciated, probably due to the difficulty of the simplified model to fit rapid elevation changes. Conversely, in fat lands (the Po Valley, for example), along the coast and on the sea, the simplified model is capable to well represent the surface level P and T behaviours. Again, some differences can be found also in the edge regions, confirming what previously noted along the transept.

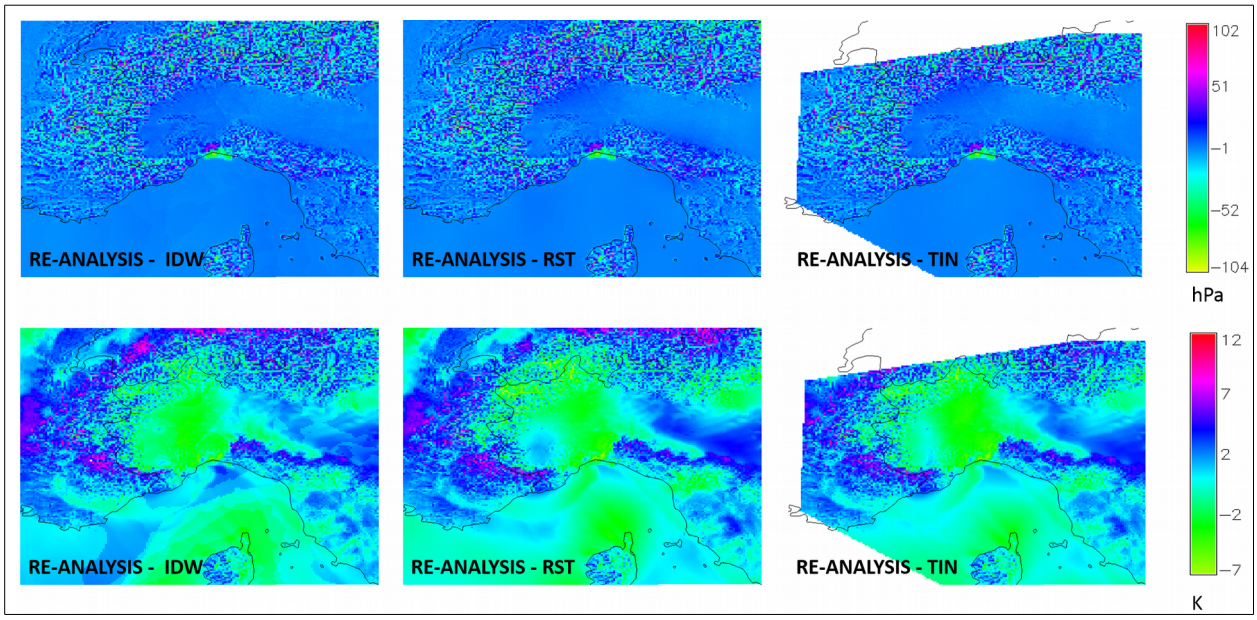

Figure 6.9. P (top) and T (bottom) differences with re-analysis.

Especially in T maps, differences due to the patterns of interpolators can be seen. These differences are in the order of few K, thus they are not considered influential in the description of the field. Differently, as shown in the left part of Figure 6.10, not negligible differences (max=66 hPa; min=-85 hPa) are present in P field around Genoa. This could be caused by the generalization of the simplified model, not capable to describe local strong variations and to the absence of P data in the area.

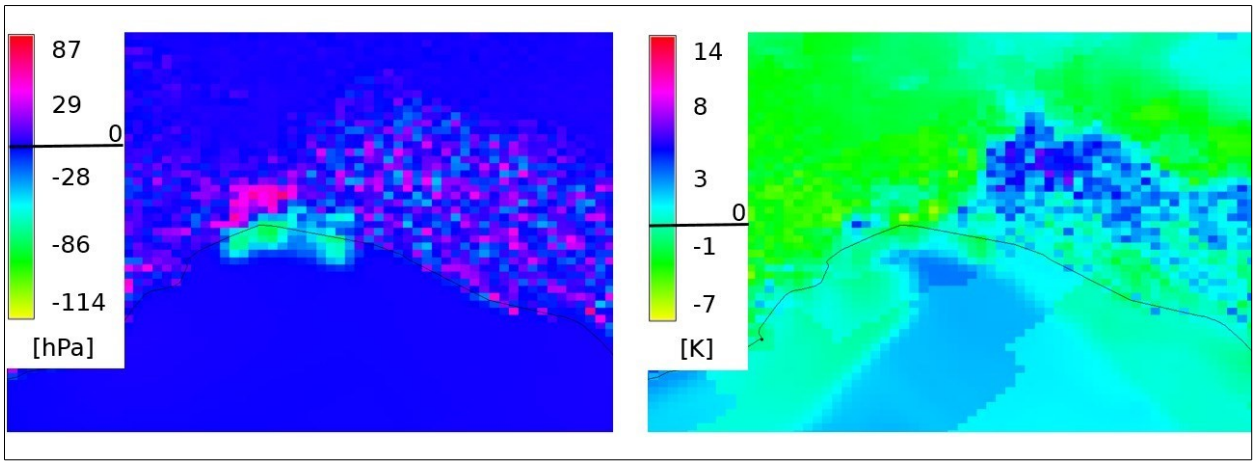

Figure 6.10. P (left) and T (right) differences with respect to re-analysis on Genoa.

Some statistics (mean, standard deviation, minimum and maximum values) of the difference maps are reported in Table 6.2 for the entire study area and for the Genoa study area.

Re-analysis and interpolated P and T maps differences					
		Mean	Rms	Max	Min
Entire study area	P [hPa]	-5	17	87	-114
	T [K]	2	7	14	-7
Around Genoa	P [hPa]	5	25	66	-85
	T [K]	1	4	3	-7

Table 6.2. Statistics of re-analysis and interpolated P and T differences maps.

What emerges from Figure 6.10 and Table 6.2 is that the simplified model seems not able to reproduce localized effects of weather fronts, which can be well modelled by re-analysis.

In order to evaluate the sensitivity of PWV to such differences in P and T maps, the previously described procedure was applied for the 4th November 2011 event at 10 UT, with P and T values coming from re-analysis.

In Figure 6.11, the comparison between PWV maps obtained using P and T fields coming from re-analysis and the simplified physical model are shown.

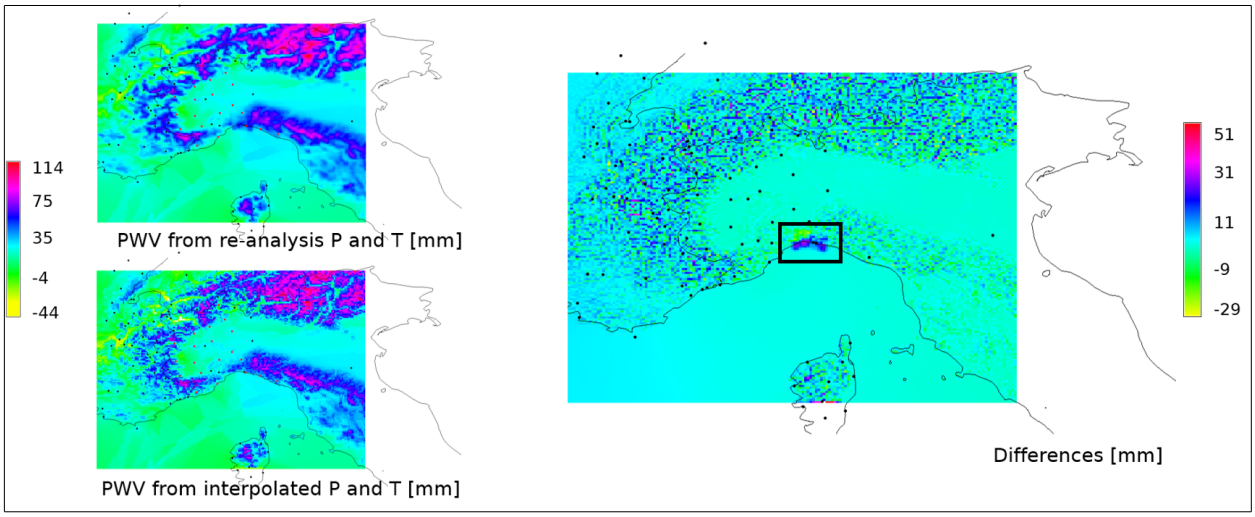

Figure 6.11. Comparison between PWV from re-analysed P and T and from interpolated P and T. The black rectangle underlines the study area on Genoa depicted in Figure 6.12.

A zoom of PWV differences map on Genoa study area is reported in Figure 6.12. In Table 6.3, some statistics of PWV differences for the entire region and around Genoa are reported.

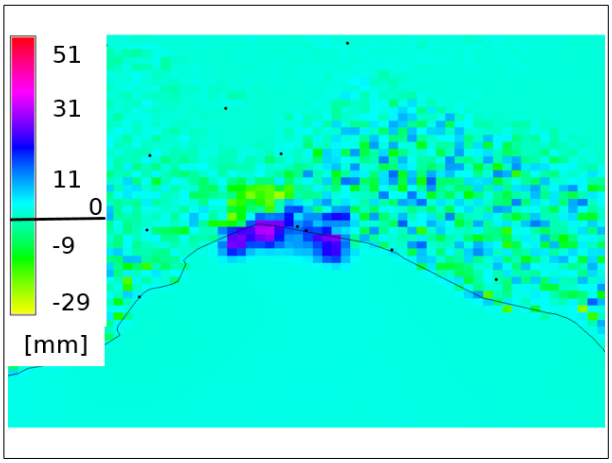

Figure 6.12. PWV differences map around Genoa.

PWV differences using re-analysis and interpolated P and T				
PWV differences [mm]	Mean	Rms	Max	Min
Entire study area	2	6	51	-29
Around Genoa	3	5	36	-17

Table 6.3. Statistics of PWV differences using re-analysis and interpolated P and T.

As previously noted, the larger differences are located in high altitudes, but not negligible differences appear on Genoa too, reflecting a similar behaviour to P and T differences discussed before.

To make the PWV differences map more readable, a reclassification was performed, as shown in Figure 6.13, where yellow and red pixels represent values outside the range of tolerance [-2σ,2σ]: yellow if less than -2σ and red if more than 2σ.

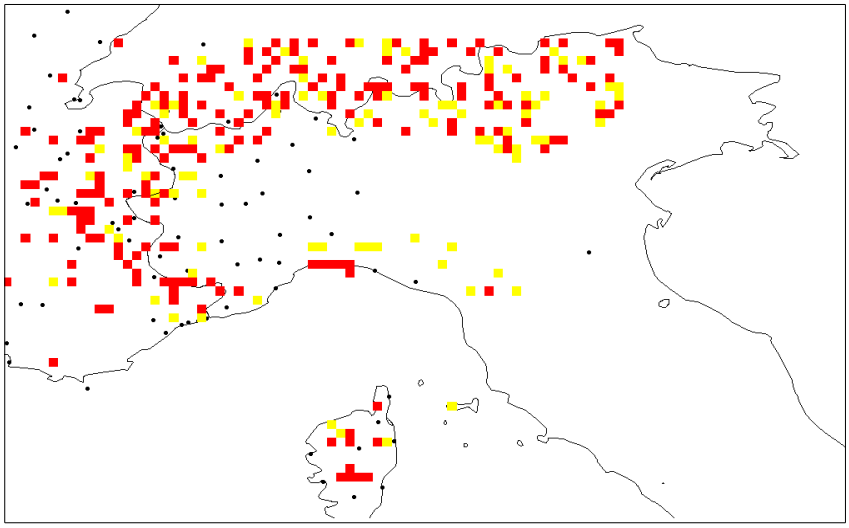

Figure 6.13. PWV differences map after the reclassification.

Again, the main effects seem to be related to orography.

The discrepancy between the re-analysis and simplified physical model P and T fields, also noticeable on PWV difference maps, may be due to an extreme generalization of the simplified model, but also to insufficient number of meteorological stations used to interpolate P and T fields.

In order to evaluate the evolution in time of such differences, PWV maps were realised using P and T coming from both re-analysis and simplified physical model and then queried on GENO PS from 3rd November 02 UTC to 5th November 00 UTC.

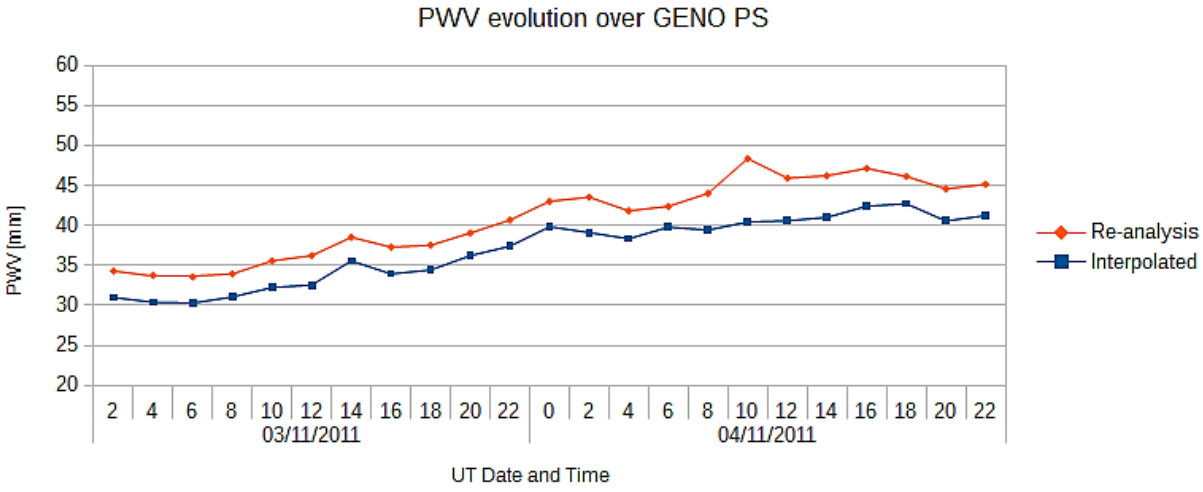

Figure 6.14. PWV evolution over GENO PS.

Looking at Figure 6.14, it is evident that the mean difference between the two curves is approximately stable at about 4 mm, with a single peak of 10 mm. The shift between the two curves, that could be imputable to the already mentioned orographic effects, doesn't interfere with the analysis of PWV evolution in time and its trend (Ferrando et al., 2016), which is important in order to correlate it with the occurrence of rain; thus the procedure is considered reliable for severe meteorological events monitoring.

6.1.3. Geostatistical interpolation

Data of P and T shows a strong correlation with elevation data as shown in Figure 6.15.

For such reason the regression kriging (RK) (Hengl et al., 2007) should be a good interpolation technique as it is able to use elevation data as base data for interpolate values of temperature and pressure. The global digital elevation model ASTER GDEM has been used as raster layer providing the auxiliary variable in order to Kriging of the regression residuals.

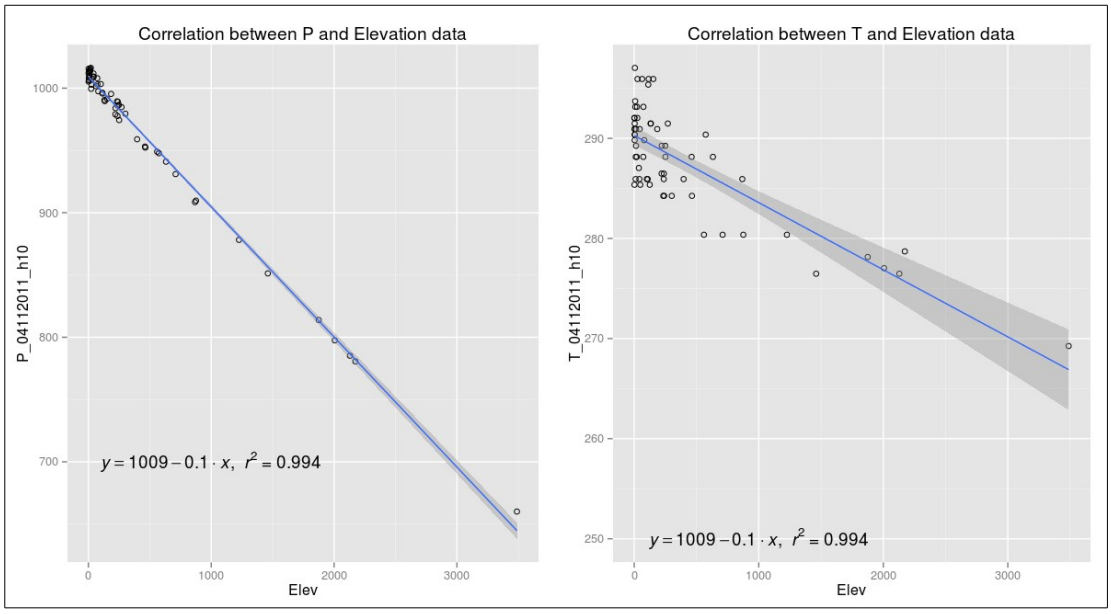

Figure 6.15. Correlation between P and T values versus elevation data.

The goodness of the regression kriging analysis could be observed in Figure 6.16: on the left, the bubble of the cross validation procedure, using 5 k-folds, of IDW is depicted; on the right the same bubble plot of RK interpolation. It turns out how the IDW have a range of errors much more wide then RK, also the location of residuals error is not similar in both cases. IDW shows biggest error in alpine region and in Apennines region whereas RK shows the biggest residual error only in Alpine region.

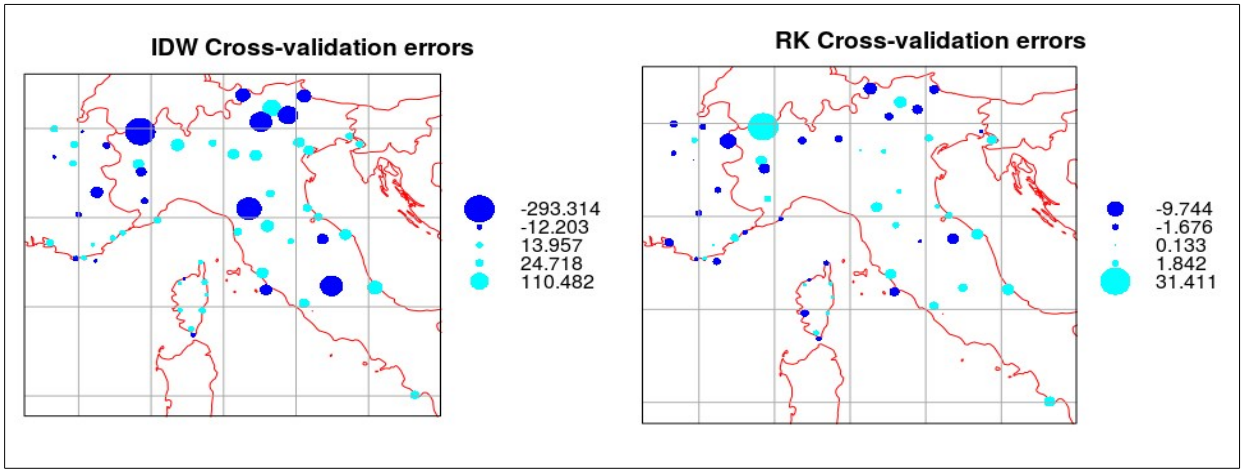

Figure 6.16. Bubble plots comparing IDW (left) and RK (right).

The RK interpolation has been implemented into R statistical software (R Core Team, 2016) using the packages gstat ant intamap, command library related to Spatial and Spatio-Temporal Geostatistical Modelling and to Procedures for Automated Interpolation (Pebesma, 2004; Pebesma et al., 2010). In particular a R code, written by Pierluigi De Rosa, has been produced to run all the procedure automatically. The code is able to load the P and T data, execute the variogram analysis of the dependent

variables on auxiliary variables (elevation from ASTER GDEM) and compute the interpolated raster for P and T and relative map of kriging errors.

6.1.4. Discussion

Considering the substantially identical behaviour of the examined interpolation techniques, both for GNSS data and environmental parameters, the greater simplicity and the lower computational effort of IDW with respect to the other techniques, IDW6 has been chosen as interpolator for this case study.

The two-hourly PVW maps have been obtained thanks to the previously described procedure, from 02 UTC of 3rd November 2011 to 00 UTC of 5th November 2011. The ΔPWV maps have been computed in order to remove the orographic effect with respect to 02 UTC of 3rd November 2011, defined as "calm" moment, used as starting time for differentiation. The ΔPWV maps are depicted in Figure 6.17. It's clear that the amount of water vapour increases in time over the study area, with a peak at 10 UTC on Genoa (red circle in Figure 6.17), corresponding to the time of the heaviest rainfall. The quantity of water vapour remains higher than the one of 3rd November 2011 02 UTC for the entire analysed time span on Genoa, as the pink/red colour indicates. Additionally, the ΔPWV maps show the evolution of the meteorological phenomenon, moving from west to east.

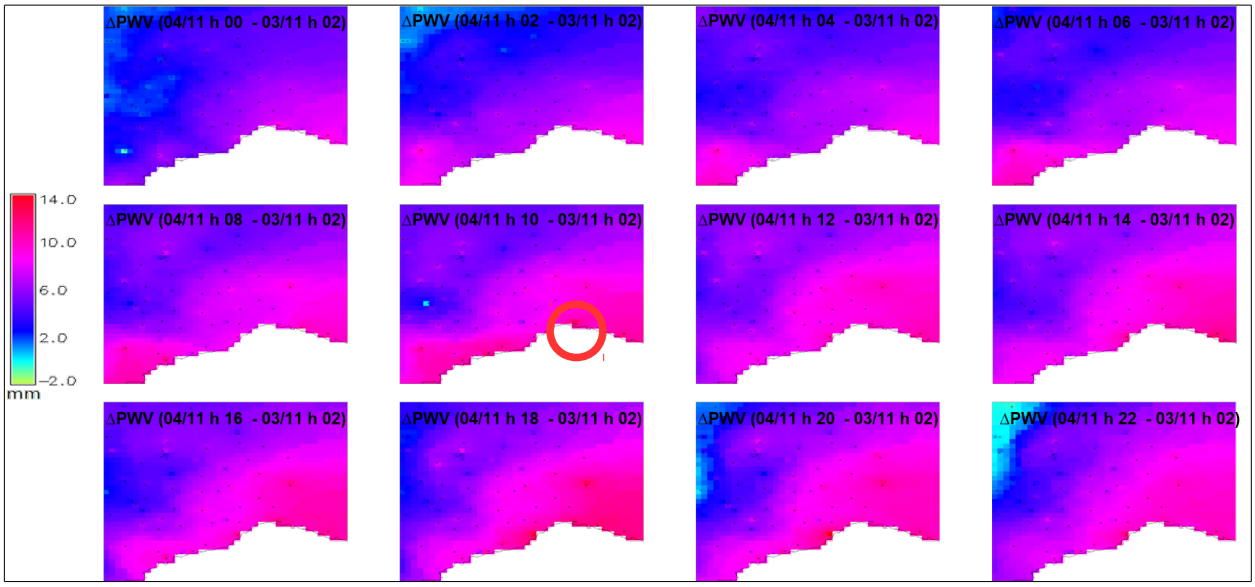

Figure 6.17. ΔPWV maps from 03/11/2011 04 UTC to 05/11/2011 00 UTC.

Figure 6.18 reports the ΔPWV map referred to 10 UTC of 4th November 2011, highlighting the high value of PWV on Genoa.

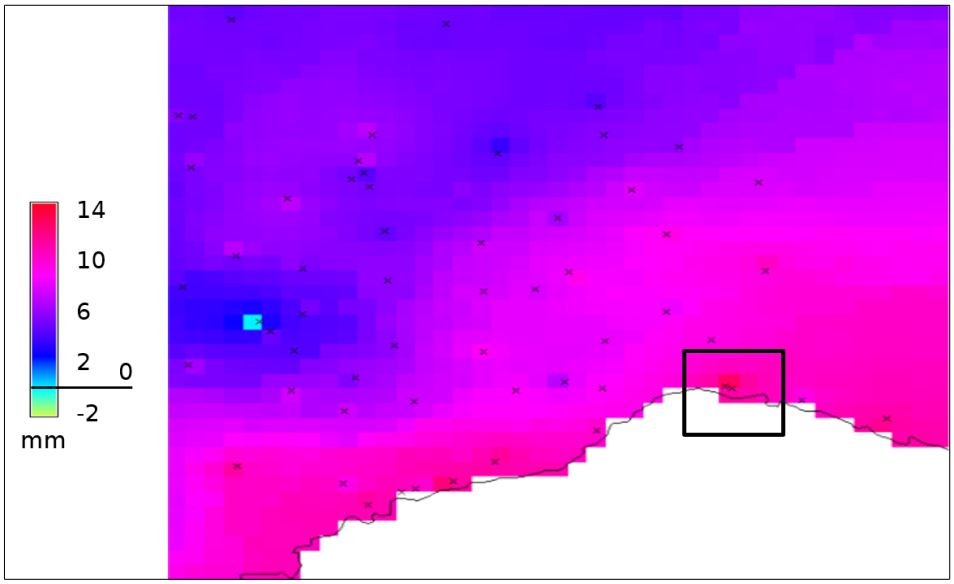

Figure 6.18. ΔPWV map of 4th November 2011 10 UTC on Genoa (black rectangle).

As already described, thanks to the ΔPWV maps, representing the time differentiation of PWV maps, it is possible to interpret the meteorological phenomenon and its evolution in time. The evolution of PWV in time could be an important information to relate the content of water vapour in atmosphere with rain, in order to interpret severe meteorological events. In the ΔPWV map of 4th November 2011 10 UTC, corresponding to the time of most intense rainfall, a red spot on Genoa is evident (see Figure 6.18), that indicates the very high amount of water vapour with respect to 3rd November 2011 02 UTC. The PWV value can be useful to predict the maximum amount of rain that can precipitate if the triggering conditions are present.

Supposing that the rain drops fall with a velocity of 9 m/s from an altitude of 3000 m (typical altitudes of condensation level), it turns out that the rain drops take 666 s to reach the ground, supposed at 0 m of altitude. Supposing that PWV remains almost constant for one hour (3600 s), using the already computed time to reach the ground, the factor k is found as

$$k = \frac{3600}{666} = 5.4 \tag{6.1}$$

k represents the multiplying factor to relate PWV values to the maximum amount of potential rain. Thus, the retrieved value of 42 mm of PWV for 10 UTC of 4th November 2011 can be turned into about 230 mm/h of potential rain.

6.2. 9TH OCTOBER 2014 EVENT

A self-healing V-shaped thunderstorm, induced by the convergence between the northern cold currents and the southern humid currents, hit the city of Genoa in the night between 9th and 10th October 2014,

leading to rain intensity up to 395 mm in 24 hours and to the flooding of 5 streams, and causing the death of one person and huge damages (www.nimbus.it/eventi/2014/141020AlluvioniCentroNord.htm).

Figure 6.19. Some of the damages of 9th October 2014 severe event.
Courtesy of "Secolo XIX".

6.2.1. Data interpolation

To monitor a different phenomena on a similar area, the intense event occurred in Genoa on the 9th October 2014 has been considered. Differently from the previously investigated phenomenon, a higher resolution is used (8", corresponding to about 250 m) to monitor the localized pattern of the meteorological event.

The existing infrastructure used for obtaining PWV 2D maps is composed by:

- 25 PSs of Liguria and Piemonte networks, with a mean spacing of 30-40 km, connected to external IGS PSs (represented as blue and red dots respectively in Figure 6.20);
- 38 Pressure and 36 Temperature NOAA meteorological stations, with mean spacing of about 100 km (represented as red crosses and blue circles respectively in Figure 6.21).

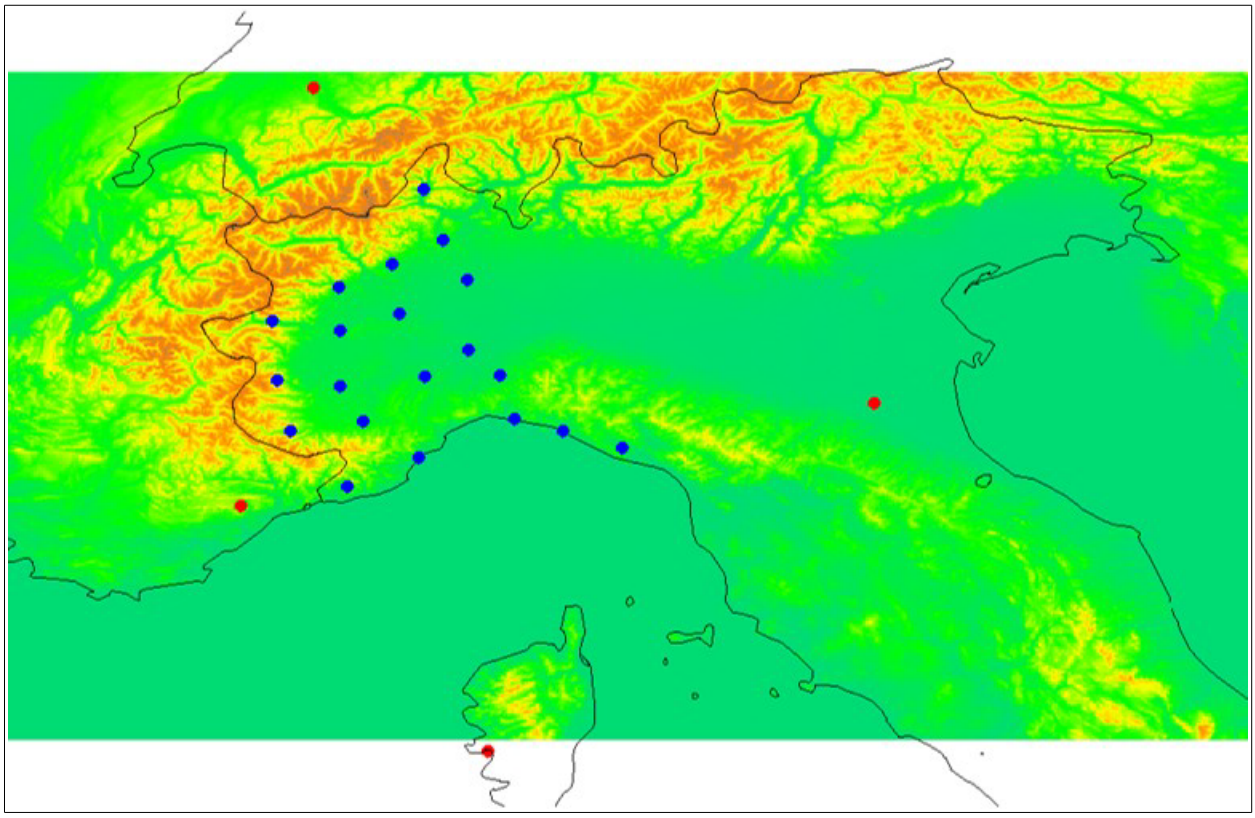

Figure 6.20. Spatial distribution of GNSS PSs.
Red dots represent IGS PSs, blue dots represent Liguria and Piemonte regional networks PSs.

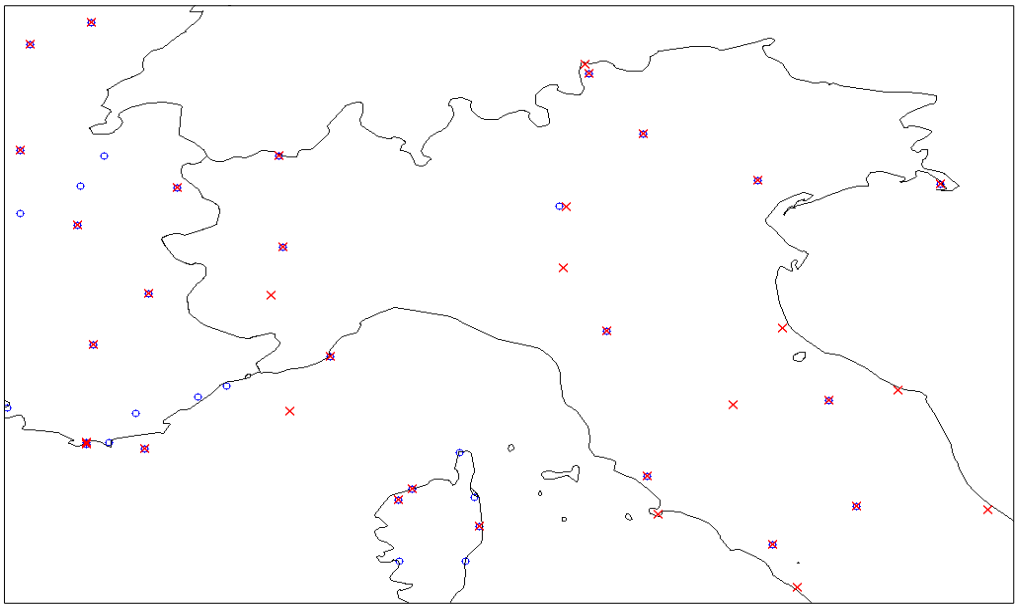

Figure 6.21. Spatial distribution of P (red crosses) and T (blue circles).

The new settings for the GNSS and environmental data networks caused problems to IDW technique, which produced fictitious structures totally unfitting for representing the surface of PWV, as Figure 6.22 shows.

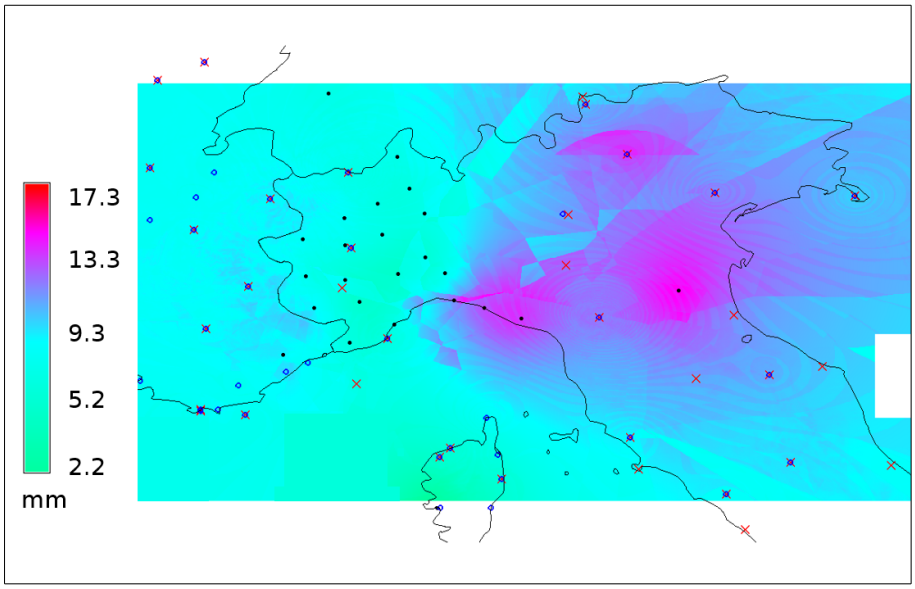

Figure 6.22. ΔPWV map showing the tessellation produced by IDW technique.

Hence, a new comparison of interpolation techniques was performed, applying firstly Regularized spline with Tension (RST) and then Triangulated Irregular Network (TIN).

RST carries out an improvement with respect to IDW technique, but it requires a fine calibration phase. The tension parameter can vary in time according to the number of stations involved in the interpolation. In fact, Pressure (P), Temperature (T) and GNSS stations could be not always recording data during the time span analysed. The smoothing parameter value was set very close to zero in order to make the spline passing through the sampled points, in respect of the standard deviation of the estimated parameter (Sguerso et al., 2014) but, in some points, the tolerance was not respected. Additionally, RST showed sometimes local “bumps and holes” and the orographic effect (Figure 6.23). For these reasons, RST seems not really suitable for this application.

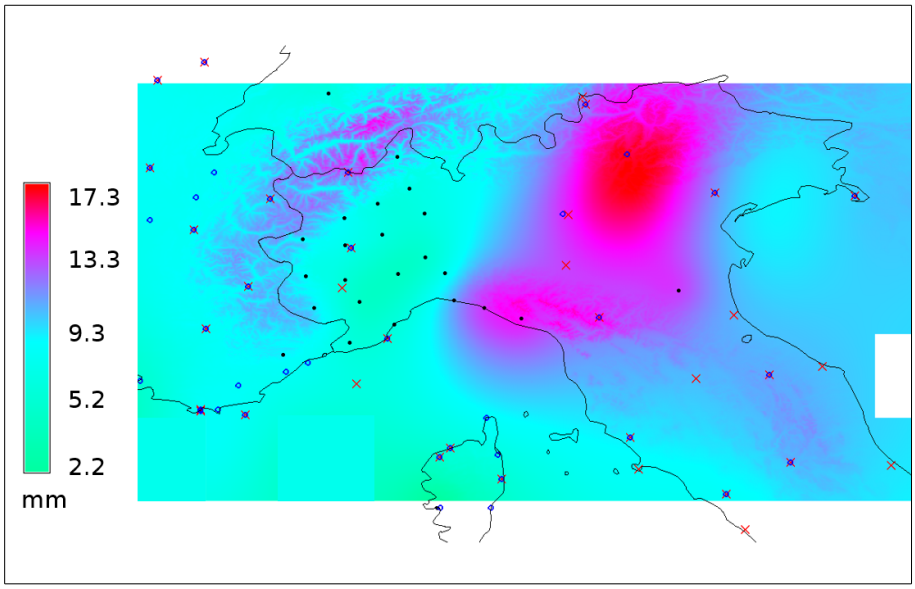

Figure 6.23. ΔPWV map showing the orographic and "bumps and holes" effects produced by RST.

The Triangulated Irregular Network (TIN) method, available as GRASS GIS addon by means of *r.surf.nnbathy* module, was applied. It allows to create a surface as a network of triangles, starting from irregularly distributed nodes, without setting any input parameter. TIN is a very fast method: it is possible to generate an 8" resolution map of a wide area, with a computing time of few seconds. However, the results are available only inside a convex polygon which includes the known data (Figure 6.24), differently from IDW and RST techniques that interpolate data in the entire computational region. Nevertheless, in the present analysis, the ΔPWV map is significant in the area limited to Liguria and Piemonte, where the GNSS network is denser.

TIN was deemed to be the best interpolation technique for the specific application.

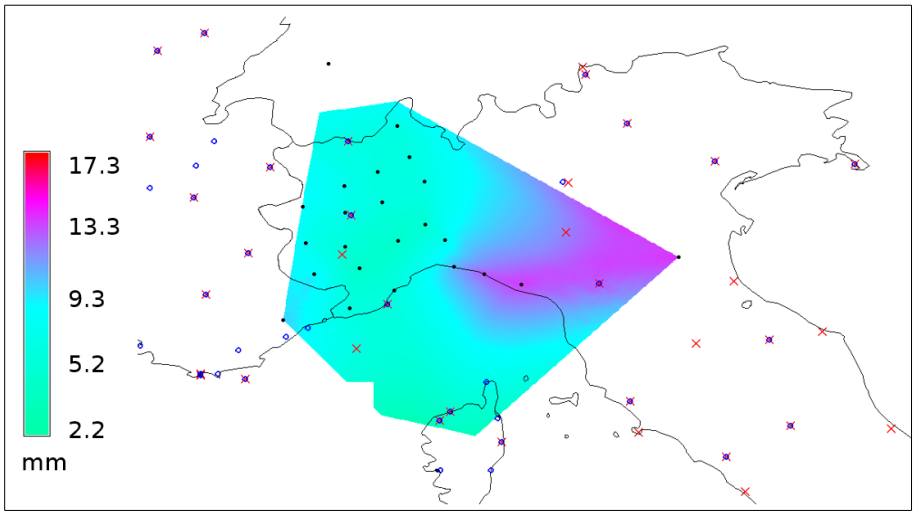

Figure 6.24. ΔPWV map obtained by means of TIN interpolation.

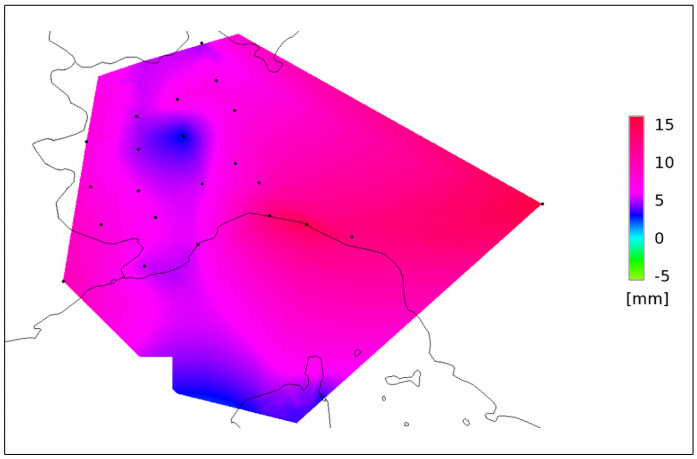

Figure 6.25. ΔPWV map of 9th October 2014 20 UTC on Genoa.

6.2.2. Discussion

As in the case of 4th November 2011 severe meteorological event, the two-hourly PVW maps have been obtained thanks to the previously described procedure, from 00 UTC of 8th October 2014 to 22 UTC of 10th October 2014. Again, the ΔPWV maps have been computed in order to remove the orographic effect. The time chosen to differentiate was the 00 UTC of 6th October 2014, because for the days near the severe event, the PWV values remained quite high and constant through time, this leading to the impossibility of showing the evolution of PWV. For this reason, a day and time "far" from the event were chosen as reference moment, to be used as starting time for differentiation. The obtained ΔPWV maps, from 9th October 2014 00 UTC to 9th October 2014 22 UTC are depicted in Figure 6.26.

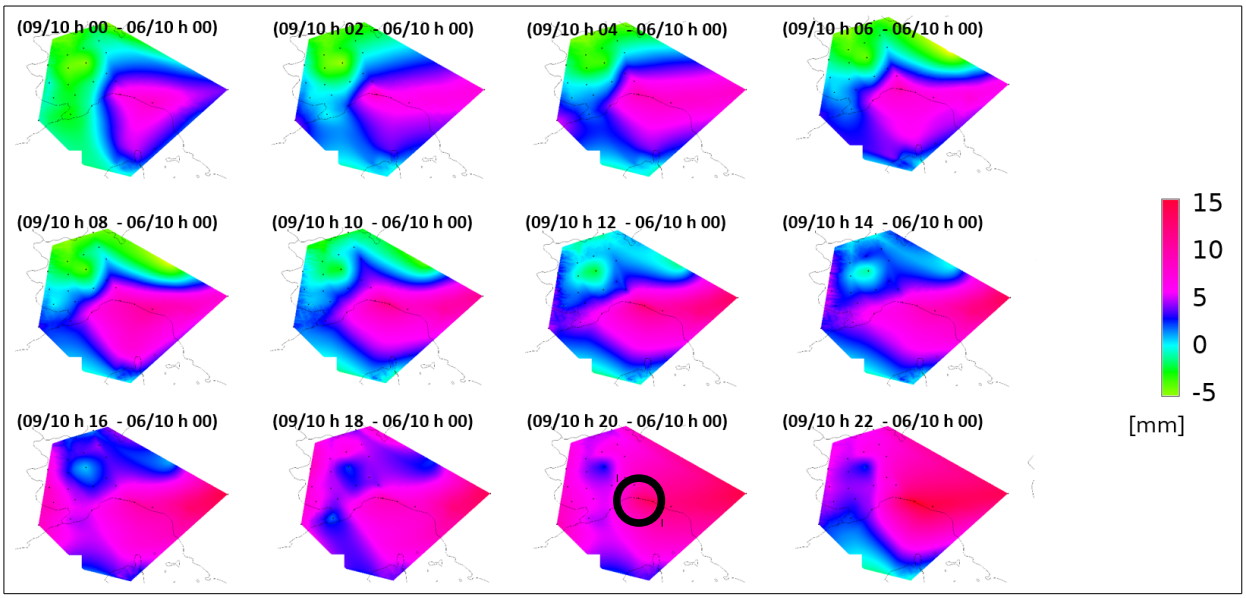

Figure 6.26. Two-hourly ΔPWV maps from 09/10/2014 00 UTC to 22 UTC.

The amount of water vapour increases in time over the study area, with a peak at 20 UTC on Genoa (black circle in Figure 6.26), corresponding to the time of the heaviest rainfall. The quantity of water

vapour remains higher than the one of 6th October 2014 00 UTC for the entire analysed time span on Genoa, as the pink/red colour indicates. Additionally, the ΔPWV maps show the persistence and localization of the meteorological phenomenon. The ΔPWV maps monitored the event in agreement with the time of most intense rainfall, occurred on the 9th October 2014 20 UTC (depicted in Figure 6.25), confirming the good agreement between the obtained results of the procedure and the real behaviour of the phenomena.

7. PWV NEAR REAL-TIME MONITORING

The G4M procedure, described in Chapter 5 and used for the a posteriori analysis of severe meteorological events in Chapter 6, is here employed to interpret meteorological events in simulated near-real time. Indeed, the proposed near real-time analysis is an a posteriori analysis, but it is considered a useful test to evaluate the feasibility of the procedure and its application in near real-time, mainly concerning needed data, computational time, and additional information provided with respect to the a posteriori analysis.

After a brief introduction on motivations of near real-time analysis, the data and the elaboration criteria will be discussed in section 7.1. Section 7.2 is dedicated to the simulated near real-time analysis of 2011 severe event on Genoa. This analysis has been carried out in order to show the contribute of the procedure to interpret this kind of phenomena, in the future perspective of organising an early warning system based on GNSS Meteorology.

7.1. DATA AND ELABORATION CRITERIA

Considering the limited time and space scales of severe meteorological events, which are typically characterised by short duration (15-30 minutes) and extreme localization (in the order of few km), it could be appropriate to perform a near real-time analysis, to evaluate the contribute of GNSS Meteorology and G4M procedure in the interpretation of such phenomena. For this reason, the idea is to produce 2D PWV maps with a shorter time span with respect to the two-hourly which has been used for the a posteriori analysis (see Chapter 6). In particular, a time span of six minutes has been chosen because it was considered compatible with the temporal scales involved in the meteorological phenomena development. Additionally, such a time span is also in accordance with the computational time of the whole elaboration.

7.1.1. GNSS data

As in the case of a posteriori analysis, a network consisting of 181 PSs has been considered to retrieve the ZTD estimations used to obtain PWV. Due to limitations in GAMIT software, which do not allow to elaborate the complete network described in section 3.1 with such a short time span, a different PSs network has been considered. In particular, the network is constituted by the 15 common PSs to the three sub-networks (the so called Core stations[106]), to fix the reference frame and to obtain absolute ZTD

106 BRST, CAGL, GRAS, GRAZ, HERS, MATE, MEDI, POTS, SFER, SJDV, TORI, VILL, WSRT, WTZR, ZIMM.

estimations, by the 14 Regione Piemonte[107] and the 6 Regione Liguria[108] PSs, and GENO and AJAC as additional stations. AJAC has been primarily introduced to have data available towards the south of computational region, whereas GENO has been introduced for further comparison between the two Genoa PSs.

Figure 7.1 reports the computational region and the PSs falling on it. The Core stations are represented in red dots, Regione Piemonte and Regione Liguria PSs are represented in green and blue dots respectively, finally, GENO and AJAC are represented in black dots.

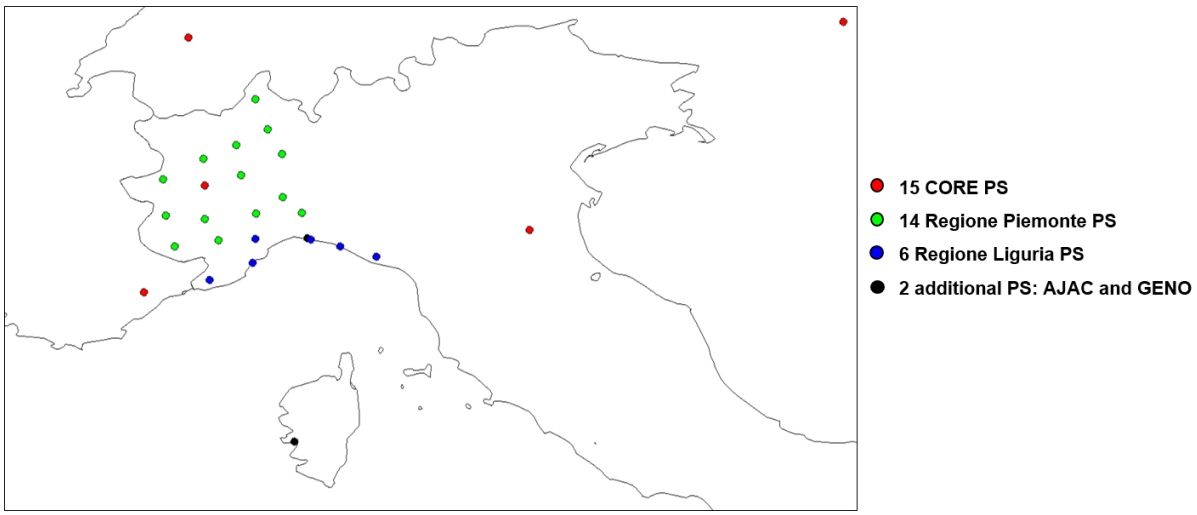

Figure 7.1. PSs network for near real-time elaboration.

Moreover, due to GAMIT limitations, it is not possible to obtain a daily solution with such a short time span (6 minutes), even if the number of PSs has been reduced (from about 70 PSs in each subnetwork, suitable to obtain daily solutions with a two-hourly time span, to 37 PSs for the 6 minutes elaboration). For this reason, a 4 hours elaboration period has been considered. Thanks to the smaller PSs network and the shorter elaboration period, it was possible to retrieve ZTD estimation every 6 minutes.

Concerning the possible biases introduced by these settings, a test was performed on the accordance of 6 minutes and 2 hours ZTD estimations and rms. Figure 7.2 and Table 7.1 report the comparison between 4th November 2011 ZTD 6 minutes and 2 hours estimations, in the four hours from 8 UTC to 12 UTC, while Figure 7.3 reports the same comparison for rms.

107 ALSN, BIEL BUSL CANL CRSN CUOR, DEMN, DOMS, GOZZ, MONV, NOVR, OSTA,SAVI,SERR.

108 BAJA. BEVE, CAMN, CHIV, GENU, LOAN.

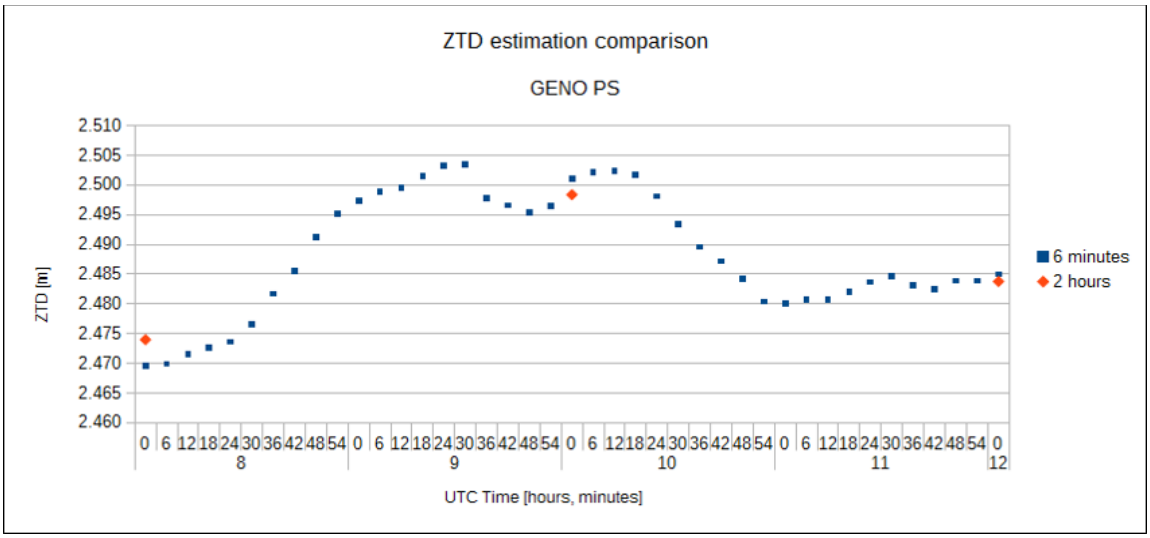

Figure 7.2. Comparison between 6 minutes (blue dots) and 2 hours (red dots) ZTDs.

UTC Time	$ZTD_{6min} - ZTD_{2h}$ [mm]
8	-4
10	-3
12	-1

Table 7.1. Differences between 6 minutes and 2 hours ZTDs.

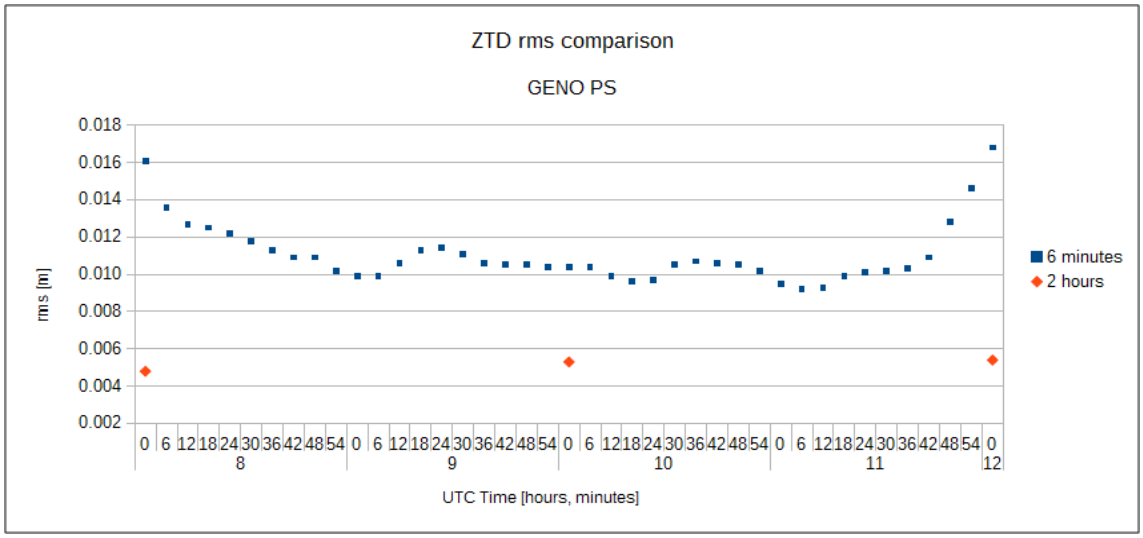

Figure 7.3. Comparison between 6 minutes (blue dots) and 2 hours (red dots) ZTD rms.

As reported in Figure 7.3 and Table 7.1, slightly different ZTD estimations between 2 hours and 6 minutes elaborations, in the order of few mm. Differently, concerning the ZTD rms comparison, higher differences can be appreciated, as noticeable in Figure 7.3. The highest differences in rms values are

mainly located near the start and the end of session; for this reason, only the three central hours of session have been taken into account, removing the first and the last half hours of the 4 hours session.

In general, high rms values could be related to the higher correlation between ZTD estimation in short time span elaborations. Nevertheless, on spite of the observed ZTD and rms differences between 6 minutes and 2 hours elaborations, it seems that higher rms values do not influence the interpretation of the time evolution of the investigated meteorological phenomenon. Thus, 6 minutes PWV maps have been obtained starting from 6 minutes ZTD estimations, as will be shown in section 7.2 for the severe event occurred on Genoa on 4th November 2011.

A final test was performed to evaluate the influence of the presence of both Genoa PSs in the GAMIT ZTD elaboration. To verify the robustness of 6 minutes GAMIT elaboration with respect to the network configuration, three different solutions were computed: the first one including both Genoa PSs (called GENOGENU in the following Figures 7.4 and 7.5), and two solutions including just one of the two PSs (called GENO when only GENO is included and GENU when only GENU is included, respectively). The results of this comparison are shown in Figures 7.4 and 7.5.

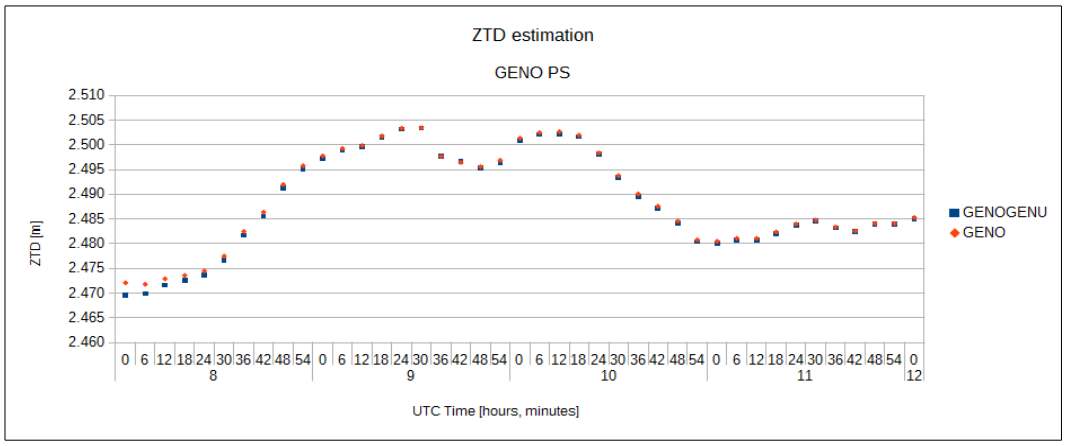

Figure 7.4. ZTD estimations including/excluding GENU PS.

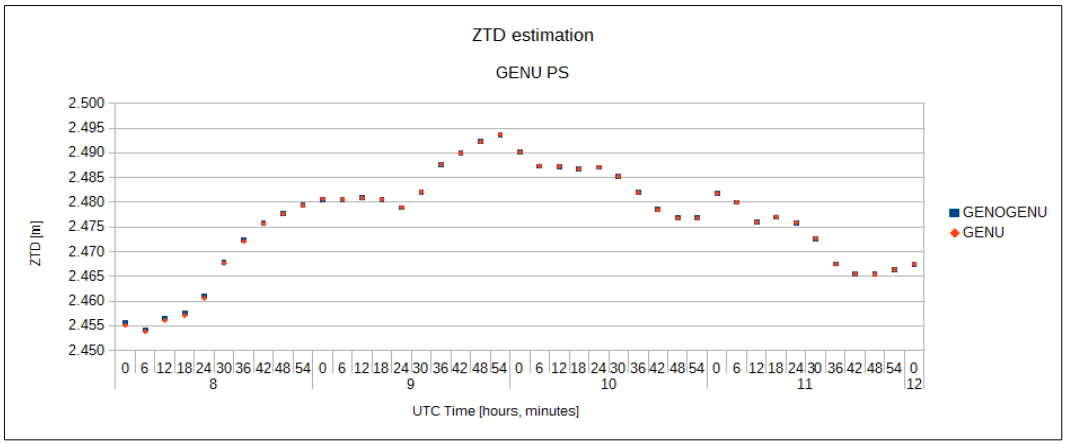

Figure 7.5. ZTD estimations including/excluding GENO PS.

As Figures 7.4 and 7.5 show, the differences encountered in ZTD estimations if GENO or GENU is removed are in the order of less than 1 mm, so that it can be concluded that the presence of both PSs instead of just one of them does not influence the ZTD estimation on the single PS. Regarding the ZTD differences encountered in the whole PS network, Table 7.2 summarises the maximum, minimum and mean difference in the entire network, to evaluate the global effect if one between GENO or GENU is removed.

	GENOGENU-GENO [mm]	GENOGENU-GENU [mm]	GENO-GENU [mm]
Maximum	1.3	0.8	3
Minimum	-2.7	-0.6	-1.9
Mean	0.1	0	0
rms	0.3	0.2	0.3

Table 7.2. ZTD differences in the whole PSs network including/excluding GENO or GENU.

Apart from few PSs for limited instants in the session, the values of ZTD differences are in the order of less than 1 mm. The higher values, in the order of few mm, are typically located in the start of the session, thus they can be considered irrelevant, because the first and the last half hour of the session are removed in the following steps of the procedure.

7.1.2. Pressure and Temperature data

The Pressure and Temperature data needed to retrieve PWV have been obtained by interpolation of NOAA data, supposing a linear behaviour of Pressure and Temperature between two sampled data.
The P and T stations networks are shown in Figure 7.6, on the left and on the right respectively.

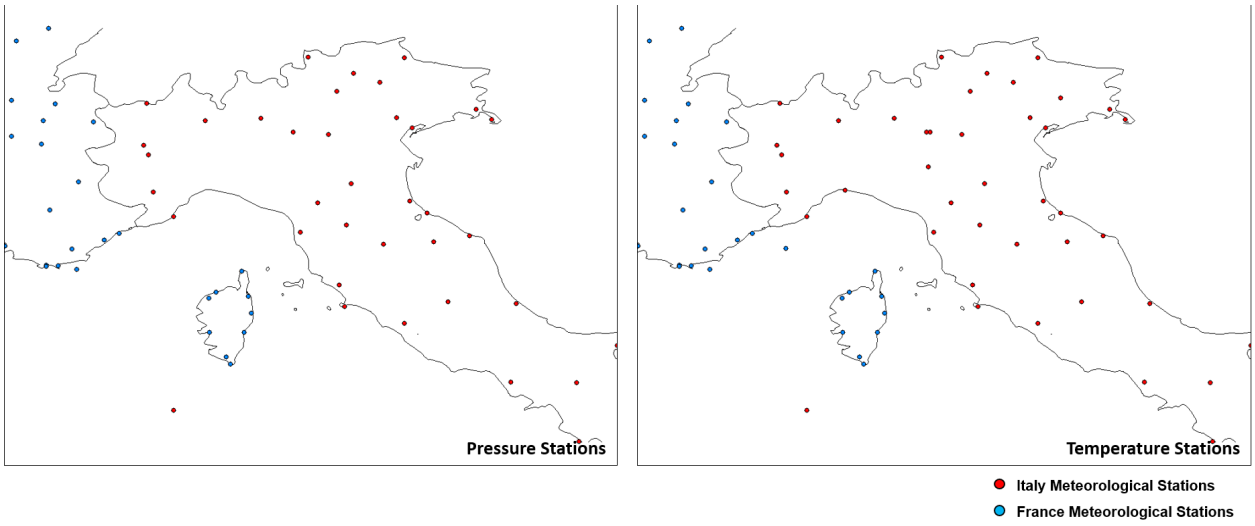

Figure 7.6. P and T meteorological stations.
The Italy MS are represented in red dots, the France MS are represented in blue dots.

P and T data have been downloaded from NOAA archives for Italy and France, using the procedure already described in section 3.5.1. The data have been downloaded for the entire day considered, even if the analysed period is shorter, in order to fill in the eventual gaps of data in the start or in the end of the considered session. The downloaded half-hourly, hourly, two-hourly data have been interpolated to obtain a time step of 6 minutes. The meteorological stations providing less than 80% of data in the chosen period and with more than three-hourly time step have been excluded. All these operations have been carried out simply using a spreadsheet. Once the data had been sampled in a 6 minutes time span, they have been formatted in columns to be used as vector data for the GIS procedure. In particular, two files, one for P and one for T data, have been created. The P and T files are formatted with the first two columns representing the station ID and name, the following three columns containing the stations coordinates (latitude, longitude and elevation), and the other columns containing a P or T data each, referred to a certain time.

7.2. 4TH NOVEMBER 2011 EVENT

The 4th November 2011 severe event on Genoa, already described in section 6.1, has been analysed using a simulated near real-time strategy. The 2D PWV maps have been obtained starting from the previously described data (see section 7.1) for the central three hours of the 4 hours session, using the G4M procedure. The resolution of the realised maps (both for meteorological parameters and for GNSS-derived data) is 8', corresponding to about 250 m.

7.2.1. 2D maps

In the following Figure 7.7, a 30-minutes extraction of the 6 min ΔPWV maps is presented, for the following UTC times: 9.00, 9.30, 10.00, 10.30, 11.00 and 11.30. The ΔPWV maps have been obtained by differentiating in time with respect to 8.30 UTC of 4th November 2011.

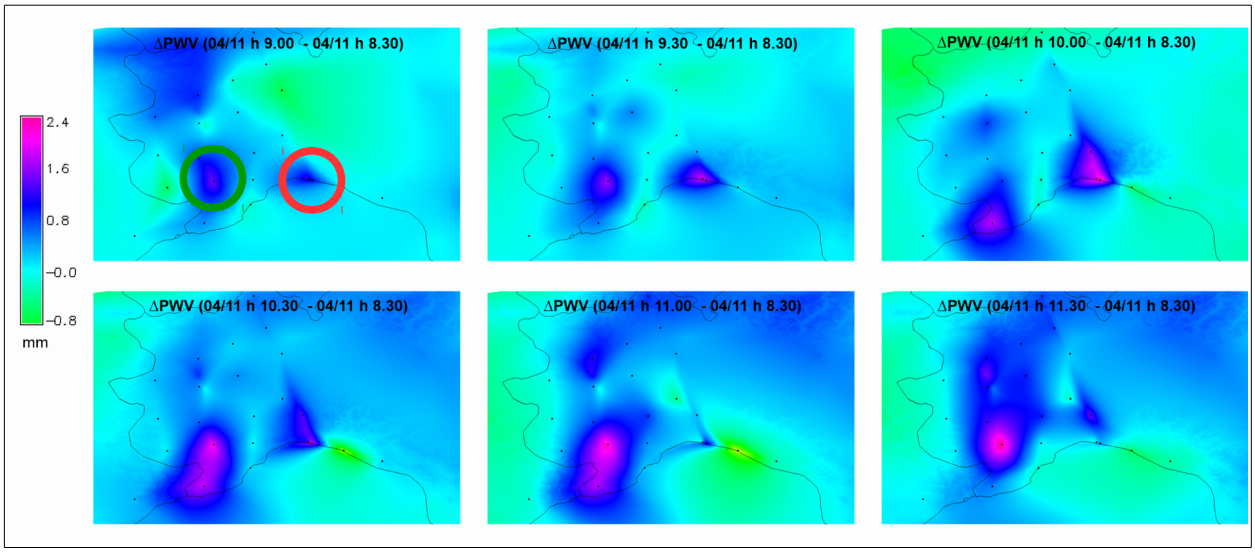

Figure 7.7. Extraction of 6 minutes ΔPWV maps for 4th November 2011 severe events.

As Figure 7.7 suggests, the ΔPWV maps, representing the differences in time of PWV, are capable to highlight both positive and negative differences, corresponding to increasing and decreasing amount of water vapour in atmosphere, and can help to interpret the evolution of PWV. Focusing on Genoa (red circle in Figure 7.7), the time evolution of PWV suggests a low increase (less than 1 mm) at 9 UTC with respect to 8.30 UTC, followed by a rapid and heavy increase (up to about 2.4 mm for GENU PS) between 9.30 and 10 UTC, and then a decrease. This behaviour can be related to the reduction of water vapour in atmosphere due to intense rain, which typically has the effect of making the water vapour content decreasing.

The evolution of ΔPWV is depicted in Figure 7.8 for the two Genoa PSs. It is also interesting to notice that there is a temporal shift between the two peaks of ΔPWV over Genoa PSs, in accordance to the typical propagation of atmospheric perturbations, which usually move from West to East.

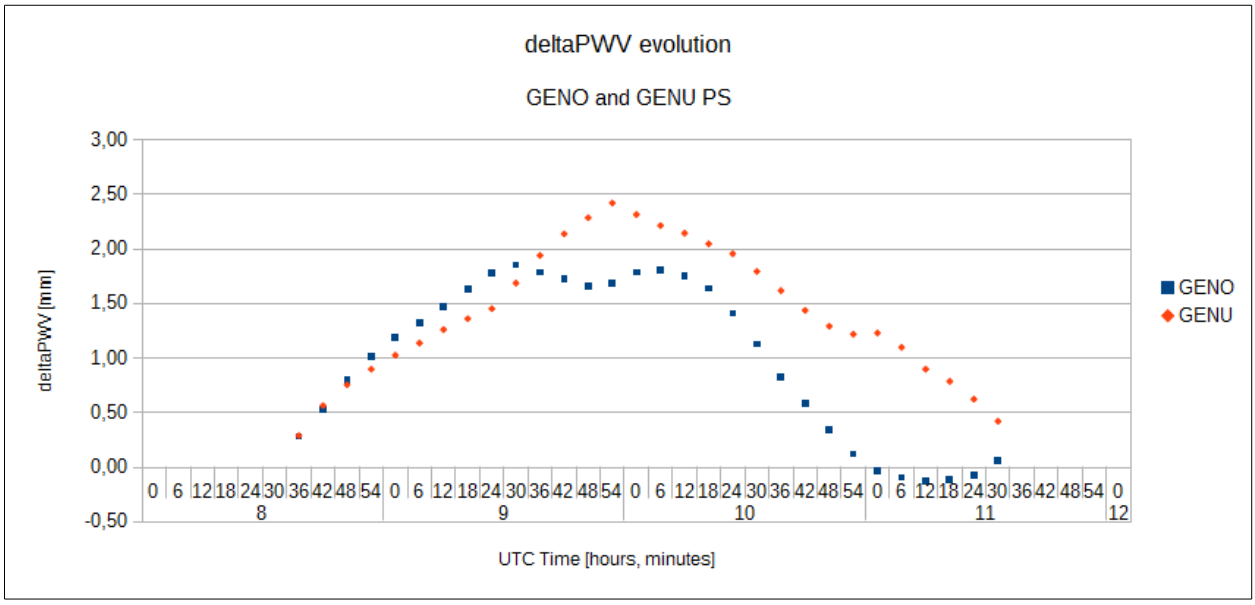

Figure 7.8. ΔPWV evolution over Genoa PSs.

As noticeable in Figure 7.7, apart from the one on Genoa, another ΔPWV peak is visible, in correspondence of MONV PS (green circle in Figure 7.7). Theoretically, only looking at ΔPWV maps without having any additional information, an intense meteorological event should not be excluded over MONV PS. For this reason, to better detect and interpret heavy rain, the analysis of HI (Heterogeneity Index) in combination with ΔPWV can be useful.

7.2.2. HI

As already stated, the role of HI (Heterogeneity Index) is to highlight ΔPWV spatial variability, which seems to be related with the occurrence of intense rains. For this reason, 6 minutes HI maps have been produced from 8.30 UTC to 11.30 UTC. In Figure 7.9, a 30-minutes extraction of the 6 min HI maps is presented, for the following UTC times: 9.00, 9.30, 10.00, 10.30, 11.00 and 11.30. As expected, HI is able to localize in time and space the severe meteorological events. In fact, HI assumes values near zero in the whole area, whereas on Genoa it reaches higher values, this meaning that a higher spatial variability is detected in that area.

Additionally, HI showed another interesting feature: it seems to be related to rain peaks, as Figure 7.10 shows. In the left part of Figure 7.10, the 6 minutes evolution of HI in Genoa is depicted, in the right part the 30 minutes cumulated rain is reported, measured in DICCA meteorological station. It is interesting to notice the correspondence between HI peaks and positive/negative peaks of rain. Just correlating HI and PWV trend it is possible to understand if the rain peak will be positive or negative. In the next future, this approach will be systematically applied to other case studies (significant events, lacked/false meteorological alerts) to validate the reliability of HI, which can be useful in order to prepare an early-

warning system based on near real-time PWV maps, as an independent contribute to meteorological alerts.

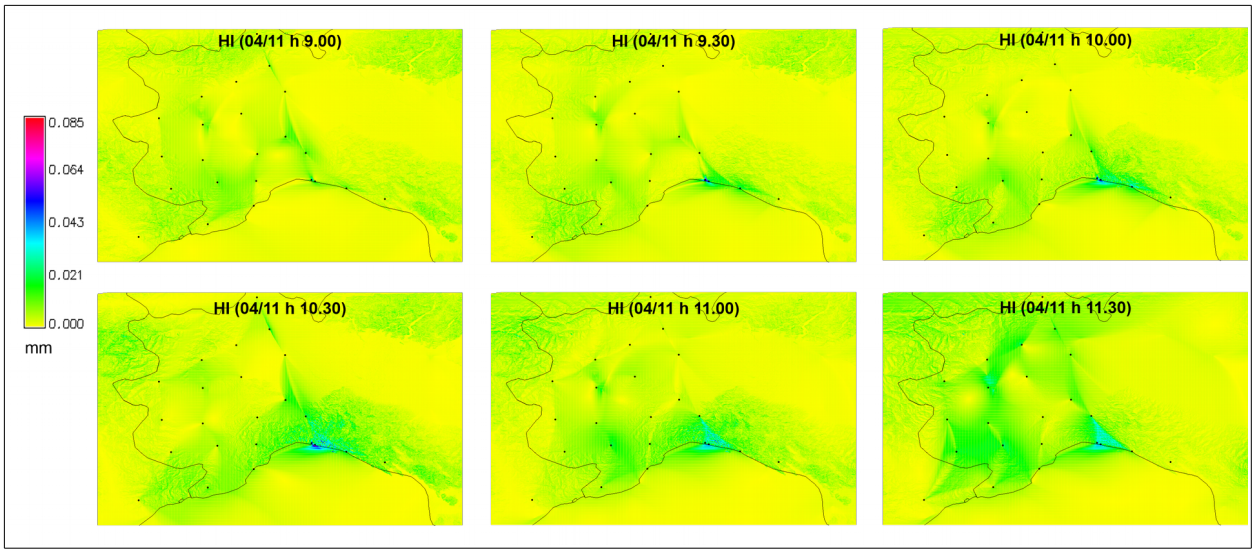

Figure 7.9. Extraction of 6 minutes HI maps for 4th November 2011 severe events.

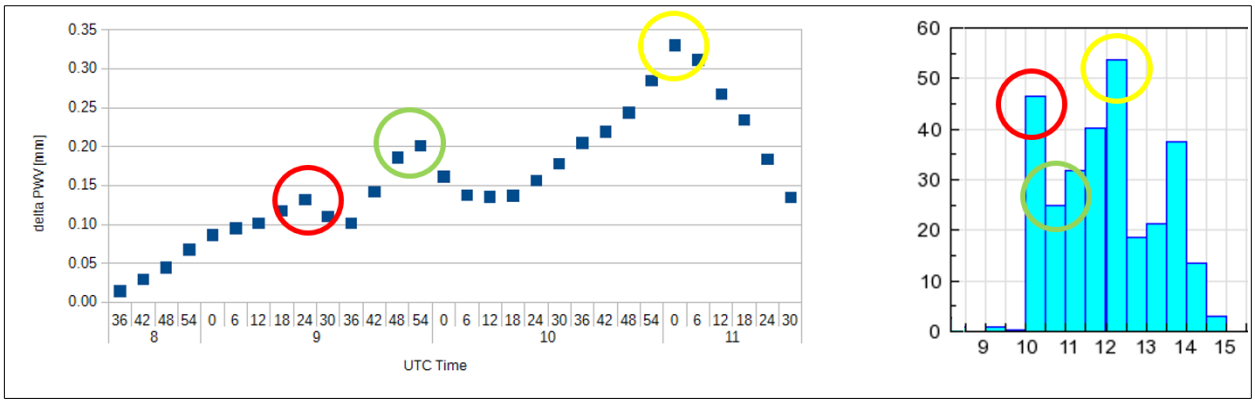

Figure 7.10. Correspondence between HI and rain peaks.

CONCLUSIONS AND PERSPECTIVES

The present work focuses on the possibility to obtain 2D Precipitable Water Vapour (PWV) maps starting from GNSS, Pressure (P) and Temperature (T) data coming from existing infrastructures, as a contribute to GNSS Meteorology. Starting from Bevis' assumptions, a procedure called G4M (GNSS for Meteorology) has been conceived by the Laboratory of Geodesy, Geomatics and GIS to produce 2D PWV maps with high spatial and temporal resolution (1 km and 6 minutes respectively), for both a posteriori and near real-time applications.

The procedure has been applied to two severe meteorological events occurred on Genoa, on 4th November 2011 and 9th October 2014 respectively, on a wide and orographically complex area, covering about the north-west of Italy. The input data of the procedure are Zenith Total Delay (ZTD) estimations, and P and T observations from international stations in different discrete points.

The ZTD values are estimated using GAMIT/GLOBK software for a "regional network" composed by 181 Permanent Stations (PSs) belonging to different international, national and regional networks on the French-Italian border region. The RENAG Database hosts the two-hourly ZTD estimations for the 181 PSs from 1998 to 2012 and, thanks to a recent update, the data until December 2015 will be soon available for climatological and meteorological applications. The ZTD estimations have been validated by means of two different strategies (inter-comparison and comparison with IGS official estimations). The ZTD estimations of the two Genoa's PSs, GENO and GENU, have been used to compute a ZTD climatological average (obtained by averaging the corresponding two-hourly estimations of each year over the all years of measurements) to be compared with ZTD single year evolution; this comparison may be useful to study the possibility of correlate high ZTD values with the occurrence of severe meteorological events. Moreover, the same ZTD time series, together with the environmental data coming from two University of Genoa's Meteorological Stations have been used to retrieve PWV time series for the two PSs and to compute the PWV climatological average. What emerged from the time series analysis is that the overcoming of a certain value of PWV, i.e. the σ, is not a sufficient parameter to identify the occurrence of heavy rainfalls.

Then, to deepen the analysis and the understanding of the meteorological phenomena, the 2D procedure to produce PWV maps has been introduced.

The strength and originality of the procedure lie into the employment of existing infrastructures, the independence from meteorological models, the possibility of automation, the high adaptability to different networks configurations, and the ability to produce high-resolution 2D PWV maps even from sparse input data. In fact, despite the difficulties due to the sparse distribution of P, T and ZTD data, combined with high resolution and wide computational region, the GIS procedure is able to produce 2D PWV maps,

thanks to a simplified physical model to interpolate P and T environmental data. A comparison was performed between P and T 2D maps generated by the simplified physical model and the ones coming from meteorological re-analysis (where P and T fields are modelled using the entire set of existing observations). On spite of the encountered differences, the simplified model is still considered valid for the purpose of interpret the atmosphere and to produce ΔPWV maps. In fact, the differences between PWV from the procedure with the interpolated and the re-analysis P and T don't influence the interpretation of the phenomenon evolution in time, showing a good 1D agreement. A good contribution to obtain a better agreement could be the introduction of new P and T stations (for example, regional meteorological stations could be used) to increase the number of stations involved in the interpolation, thus reducing the spacing between them.

A deep analysis of the different interpolation techniques was carried out, in order to find the most appropriate interpolator which should be suitable, in the future, for near real-time applications too, to produce PWV and ΔPWV maps, representing the differentiation in time of PWV.

The final aim of the 2D procedure was to individuate an indicator to localise in time and space the severe meteorological events. Thanks to the introduction of the Heterogeneity Index (HI), accounting the spatial variability of ΔPWV, it seems possible to individuate the correct timing and location of severe events. Moreover, HI showed a strong correlation to rain peaks, which can be an interesting feature for a future preparation of an early-warning system based on GNSS Meteorology.

The procedure has been applied to two severe meteorological events occurred in Genoa, on 4th November 2011 and on 9th October 2014 respectively. Both of them have been analysed with an a posteriori strategy, using two hourly ZTD, P and T data to obtain 2D PWV maps. Considering the extreme localization and the short duration of heavy rainfall, a simulated near real-time analysis was performed for the 2011 event, to evaluate the contribute of GNSS Meteorology and G4M procedure in the interpretation of such phenomena. For this reason, the 2D PWV maps have been produced with a shorter time span of 6 minutes, which was considered compatible with the temporal scales involved in the meteorological phenomena development. Additionally, such a time span is also in accordance with the computational time of the whole elaboration. The application of the simulated near real-time strategy and the analysis of the event with the HI seem to be promising for future application of the procedure in near real-time.

It is important to underline that the entire procedure is independent from meteorological models and that it could be an innovative integration to them. In the future, the procedure could be applied in near-real time in order to support decisions for now-casting and for an early warning system.

Further applications of the innovative procedure to different test cases (intense or moderate events, false alerts of the civil protection) are planned for the future, to statistically evaluate the performances of the procedure.

ACKNOWLEDGMENTS

First and foremost I wish to express my sincere gratitude to my supervisor, Prof. Bianca Federici: she encouraged me in pursuing the PhD course, and she carefully guided me during these three years, transmitting me her enthusiasm and passion towards scientific research.
Besides, I am especially grateful to Prof. Domenico Sguerso for his inspiration and contribution to this work.
I wish to thank Prof. Toshitaka Tsuda and Prof. Giovanna Venuti for their availability and interest in being the external reviewers of this PhD thesis: it was a pleasure and an honour for me to have such experts to evaluate my work.
I wish to acknowledge all the persons which contributed to this work, directly or indirectly: prof. Andrea Walpersdorf, for hosting me at ISTerre to work with her on RENAG Database update; prof. Andrea Mazzino and Dr. Federico Cassola, for sharing the meteorological re-analysis data; Dr. Laurent Labbouz and Daniele Passoni, for allowing me to use their codes and scripts.

To my family and friends: you know.

REFERENCES

Adams J. C., Brainerd W., Martin J., Smith B., Wagener J., 1992. Fortran 90 Handbook. vol. 32, McGraw-Hill

Adler R. K., 1995. Positioning and mapping international land boundaries. International Boundaries Research Unit, 2(1), pp. 26

Ahlberg, J. H., Nilson, E. N. Walsh, J. L., 1967. The theory of splines and their applications. Academic Press, New York

Altamimi Z., Collilieux X., Métivier L., 2011. ITRF2008: an improved solution of the international terrestrial reference frame. Journal of Geodesy, 85(8), pp. 457-473

Askne J., Nordius H., 1987. Estimation of tropospheric delay for microwaves from surface weather data. Radio Science, 22, pp. 379-386

Bartels R. H., Beatty J. C. Barsky B. A., 1987. An Introduction to Splines for Use in Computer Graphics and Geometric Modeling. Morgan Kaufmann Publishers

Barzaghi R., Sansò F., 1983. Sulla stima empirica della funzione di covarianza. Bollettino di geodesia e scienze affini, anno XLII, n. 4

Basili P., Bonafoni S., Ferrara R., Ciotti P., Fionda E., Betti B., Prini R., Tornatore V., Crespi M., Di Paola S., Baiocchi V., Radicioni F., 2003. Assessment of precipitable water vapour by use of a local GPS network and microwave ground-based radiometer. 11th International Conference on Antennas and Propagation, vol. 2001, pp. 72-76

Belikov V. V., Ivanov V. D., Kontorovich V. K., Korytnik S. A., Semenov A. Y., 1997. The non-Sibsonian interpolation: a new method of interpolation of the values of a function on an arbitrary set of points. Computational Mathematics and Mathematical Physics, 37(1), 9-15

Benciolini B., 1992. Il metodo degli elementi finiti e le sue applicazioni ai modelli digitali delle altezze. I Sistemi Informativi Territoriali, L. Mussio e F. Crosilla Eds. CISM Udine, 153-184

Bennitt G. V., Jupp A., 2012. Operational Assimilation of GPS Zenith Total Delay Observations into the Met Office Numerical Weather Prediction Models. Monthly Weather Review, 140, pp. 2706-2719

Bevis M., Businger S., Herring T., Rocken C., Anthes R., Ware R., 1992. GPS meteorology - Remote sensing of atmospheric water vapor using the Global Positioning System. Journal of Geophysical Research, 97, pp. 15787-15801

Bevis M., Businger S., Chiswell S., Herring T., Anthes R., Rocken C., Ware R., 1994. GPS meteorology: Mapping zenith wet delays onto precipitable water. Journal of applied meteorology, 33, pp. 379-386

Bock O., Bouin M. N., Doerflinger E., Collard P., Masson F., Meynadier R., Nahmani S., Koité M., Balawan K. G. L., Didé, F., Ouedraogo D., Pokperlaar S., Ngamini J. B., Lafore J. P., Janicot S.,

Guichard F., Nuret M., 2008. West African Monsoon observed with ground-based GPS receivers during African Monsoon Multidisciplinary Analysis (AMMA). Journal of Geophysical Research, 113

Boehm J., Schuh H., 2004. Vienna mapping functions in VLBI analyses. Geophysical Research Letters, 31, L01603

Boehm J., Niell A. E., Tregoning P., Schuh H., 2006. Global Mapping Function (GMF): A new empirical mapping function based on numerical weather model data. Geophysical Research Letters, 33, L07304

Boehm J., Werl B., Schuh H., 2006a. Troposphere mapping functions for GPS and very long baseline interferometry from European Centre for Medium-Range Weather Forecasts operational analysis data. Journal of Geophysical Research, 111, B02406

Boehm J., Heinkelmann R., Schuh H., 2007. Short Note: A global model of pressure and temperature for geodetic applications. Journal of Geodesy, 81(6–8), pp. 679-683

Boniface K., Ducrocq V., Jaubert G., Yan X., Brousseau P., Masson F., Champollion C., Chéry J., Doerflinger E., 2009. Impact of high-resolution data assimilation of GPS zenith delay on Mediterranean heavy rainfall forecasting. Annales Geophysicae, 27(7), pp. 2739-2753

Bouma H. R., Stoew B., 2001. GPS observations of daily variations in the atmospheric water vapor content. Physics and Chemistry of the Earth, Part A: Solid Earth and Geodesy, 26, pp. 389-392

Brenot H., Ducrocq V., Walpersdorf A., Champollion C., Caumont O., 2006. GPS zenith delay sensitivity evaluated from high resolution NWP simulations of the 8-9th September 2002 flash-flood over southeastern France. Journal of Geophysical Research, 111, D15105

Brovelli M. A., Reguzzoni M., Sansò F., Venuti, G., 2001. Modelli matematici del terreno per mezzo di interpolatori a spline. Bollettino SIFET, supplemento speciale al n. 2/2001: 55-79

Brunner F. K., Gu M., 1991. An Improved Model for the Dual Frequency Ionospheric Correction of GPS Observations. Manuscripta Geodaetica, 16, pp. 205-214

Burrough P.A., McDonnell R.A., 1998. Principles of Geographical Information Systems. Oxford University Press, New York

Cina A., 2014. Dal GPS al GNSS per la geomatica. Celid

Cosso T., 2009. Contribution of a "pseudo-dynamic" station to the GNSS network solution for real time. PhD Thesis, Politecnico di Milano, Doctorate Course in Geodesy and Geomatics, XXI cycle

Crespi M., Luzietti L., Frattale Mascioli F. M., Rizzi A., 2004. Impiego meteorologico del GPS per la previsione di precipitazioni critiche. Atti 8ª Conferenza Nazionale ASITA, Roma, 14-17 dicembre 2004

Davis P. J., 1975. Interpolation and approximation. Dover, New York.

Davis J. L., Herring T. A., Shapiro I. I., Rogers A. E. E., Elgered G., 1985. Geodesy by interferometry: effects of atmospheric modeling errors on estimates of baseline lengths. Radio Science 20, pp. 1593-1607

Dawoud S., GNSS principles and comparison. Potsdam University

De Pondeca M. S. F. V., Zou X., 2001. A Case Study of the Variational Assimilation of GPS Zenith Delay Observations into a Mesoscale Model. Journal of Applied Meteorology, 40, pp. 1559-1576

De Haan S., 2013. Assimilation of GNSS ZTD and radar radial velocity for the benefit of very-short-range regional weather forecasts. Q. J. R. Meteorol. Soc.

Elgered G., Davis J. L., Herring T. A., Shapiro I. I., 1991. Geodesy by radio interferometry: Water vapor radiometry for estimation of the wet delay, J. Geophys. Res., 96, pp. 6541-6555

Eriksson M., Siska P. P., 2000. Understanding anisotropy computations. Mathematical Geology, 32 (6), 683-700

Ferrando I., Federici B., Sguerso D., 2016. Interpolazione di dati ambientali in GRASS a supporto del monitoraggio GNSS di potenziali precipitazioni intense, Geomatics Workbooks 13 (accepted for publication)

Ferrando I., De Rosa P., Federici B., Sguerso D., 2016a. Spatial interpolation techniques for a near real-time mapping of Pressure and Temperature data, PeerJ Preprints, DOI: 10.7287/peerj.preprints.2223v2

Ferrando I., Federici B., Sguerso D., 2016b. Monitoraggio di eventi meteorici intensi a partire da dati GNSS a supporto di allerte meteo, Atti 20° Conferenza Nazionale ASITA

Fujibe, F., 1988. Diurnal variations of precipitation and thunderstorm frequency in Japan in the warm season. Pap. Meteor. Geophys., 39, pp. 79–94

GRASS Development Team, 2010. Geographic Resources Analysis Support System (GRASS) Software, Version 6.4.0. Open Source Geospatial Foundation http://grass.osgeo.org

Greville T. N. E., 1969. Theory and applications of spline functions, Proceedings of an advanced seminar at University of Winsconsin, Madison, october 7-9, 1968, Academic press- New York

Haas R., Ning T., Elgered G., 2011. Long-Term Trends in the Amount of Atmospheric Water Vapour Derived From Space Geodetic and Remote Sensing Techniques. ESA Proceedings WPP 326: Proc. 3rd Int. Colloquium–Scientific and Fundamental Aspects of the Galileo Programme

Hengl T., Heuvelink G. B., Rossiter D. G., (2007). About regression-kriging: from equations to case studies. Computers & Geosciences, 33(10):1301–1315

Herring T. A., King R. W., McClusky S. C., 2010. GAMIT Reference Manual–Release 10.4. Department of Earth, Atmospheric, and Planetary Sciences, Massachusetts Institute of Technology. ed. USA

Herring T. A., King R. W., McClusky S. C., 2015. GAMIT Reference Manual–Release 10.6. Department of Earth, Atmospheric, and Planetary Sciences, Massachusetts Institute of Technology. ed. USA

Herring T. A., King R. W., Floyd M. A., McClusky S. C., 2015. Introduction to GAMIT/GLOBK. Department of Earth, Atmospheric, and Planetary Sciences, Massachusetts Institute of Technology. ed. USA

Hofierka J., Parajka J., Mitasova H., Mitas L., 2002. Multivariate Interpolation of Precipitation Using Regularized Spline with Tension. Transactions in GIS, 6 (2), 135-150

Hofmann-Wellenhof B., Lichtenegger H., Collins J., 2001. Global Positioning System: theory and practice. Fifth Edition, Springer-Verlag, Wien

Imakiire T., Nakahori Y., 2001. GPS Earth Observation Network (GEONET) Japan. International Conference New Technology for a New Century, FIG Working Week 2001 in Seoul, Republic of Korea, 6-11 May 2001

Imhof E., 2007. Cartographic Relief Presentation. ESRI Inc., pp. 31

Inoue H. Y., Inoue T., 2007. Characteristics of the water-vapor field over the Kanto district associated with summer thunderstorm activities. SOLA, 3, pp. 101-104

Isaaks E. H., Srivastava R. M., 1989. An introduction to applied statistics, Oxford University Press, New York, p. 561

Iwasaki H., Miki T., 2001. Observational study on the diurnal variation in precipitable water associated with the thermally induced local circulation over the "semi-basin" around Maebashi using GPS data. J. Meteor. Soc. Japan, 79, pp. 1077-1091

Iwasaki H., Miki T., 2002. Diurnal variation of convective activity and precipitable water over the "semi-basin" – Preliminary study on the mechanism responsible for the evening convective activity maximum. J. Meteor. Soc. Japan, 80, pp. 439-450

Jin S., Luo O. F., Gleason S., 2009. Characterization of diurnal cycles in ZTD from a decade of global GPS observations. Journal of Geodesy, 83(6), pp. 537-545

Kanda M., Ishida T., Kashima M., Oishi S., 2000. Analysis of temporal and spatial change of a convective thunderstorm in Tokyo metropolitan using GPS precipitable water: case study on 23rd August in 1997. Tenki, 47, pp. 7-15

Kato T., Yoshizaki M., Bessho K., Inoue T., Sato Y., X-BAIU-01 observation group, 2003. Reason for the failure of the simulation of heavy rainfall during X-BAIU-01 - Importance of a vertical profile of water vapor for numerical simulations. J. Meteor. Soc. Japan, 81, pp. 993-1013

Kato T., 2006. Structure of the Band-shaped precipitation system inducing the heavy rainfall observed over northern Kyushu, Japan on 29 June 1999. J. Meteor. Soc. Japan, 84, pp. 129-153

Kato T., Aranami K., 2006. Formation factors of 2004 Niigata-Fukushima and Fukui heavy rainfalls and problems in the predictions using a cloud-resolving model. SOLA, 1, pp. 1-4

Kawabata T., Seko H., Saito K., Kuroda T., Tamiya K., Tsuyuki T., Honda Y., Wakazuki Y., 2007. An assimilation and forecasting experiment for Nerima heavy rainfall case with a cloud resolving non-hydrostatic 4 dimensional variational data assimilation system. J. Meteor. Soc. Japan, 85, pp. 255-276

Kimura F., Kuwagata T., 1995. Horizontal heat fluxes overcomplex terrain computed using a simple mixed layer model and a numerical model. J. Appl. Meteor., 34, pp. 549-558

Koizumi K., Sato Y., 2004. Impact of GPS and TMI precipitable water data on mesoscale numerical weather prediction model forecasts. J. Meteor. Soc. Japan, 82(1B), pp. 453-457

Koizumi K., Ishikawa Y., Tsuyuki T., 2005. Assimilation of precipitation data to the JMA mesoscale model with a four-dimensional variational method and its impact on precipitation forecasts. SOLA, 1, pp. 45-48

Kondo H., 1990. A numerical experiment of the "extended seabreeze" over the Kanto Plain. J. Meteor. Soc. Japan, 68, pp. 419-434

Krige D. G., 1984. Geostatistics and the definition of uncertainty. Inst. Min. Met. Trans., Vol. 93, Sect. A, pp. A41-47

Lachapelle G., 1991. Capabilities of GPS for airborne remote sensing. Canadian Journal of Remote Sensing, 17(4), pp. 305-312

Lagler K., Schindelegger M., Böhm J., Krásná H., Nilsson T., 2013. GPT2: Empirical slant delay model for radio space geodetic techniques. GRL, 40, pp. 1069-1073

Li Z., Fielding E., Cross P., Muller J. P., 2006. Interferometric synthetic aperture radar atmospheric correction: GPS topography-dependent turbulence model. Journal of Geophysical Research, 111, B02404

Lyard F., Lefevre F., Letellier T., Francis O., 2006. Modelling the global ocean tides: A modern insight from FES2004. Ocean Dynamics, 56(5-6), pp. 394-415

Maling D. H., 1989. Measurements from Maps: Principles and Methods of Cartometry. Pergamon Press, pp. 165

Matheron G., 1963. Principles of geostatistics, Economic Geology, 58 (8), 1246-1266

Misra P., Enge P., 2001. Global Positioning System: signals, measurements and performances. Ganga-Jamuna Press, Lincoln, Massachussets

Mitas L., Mitasova H., 1999. Spatial Interpolation, Geographical Information Systems: Principles, Techniques, Management and Applications, GeoInformation International, P.Longley, M.F. Goodchild, D.J. Maguire, D.W.Rhind Eds., Wiley, 481-492

Mitasova H., Mitas, L., 1993. Interpolation by Regularized Spline with Tension: 1. Theory and Implementation. Mathematical Geology, 25 (6), 641-655

Miyazaki S., Saito T., Sasaki M., Hatanaka S., Iimura Y., 1997. Expansion of GSI's Nationwide GPS Array. Bull. Geographical Survey Institute, 43, pp. 23-34

Miyazaki S., Hatanaka Y., Sagiya T., Tada T., 1998. The Nationwide GPS Array as an Earth Observation System. Bull. Geographical Survey Institute, 44, pp. 11-22

Moritz H., 1978. Introduction to interpolation and Approximation, Approximation Methods in Geodesy, H. Moritz e H. Sunkel Eds, Herbert Wichmann Verlag Karlsruhe, 1-46

Morland J., Collaud Coen M., Hocke K., Jeannet P., Mätzler C., 2009. Tropospheric water vapour above Switzerland over the last 12 years. Atmospheric Chemistry and Physics, 9(16), pp. 5975-5988

Nakamura H., Koizumi K., Mannoji N., 2004. Data assimilation of GPS precipitable water vapor into the JMA mesoscale numerical weather prediction model and its impact on rain fall forecast. J. Meteor. Soc. Japan, 82(1B), pp. 441-452

Neteler M., Mitasova, H., 2008. Open source GIS: a GRASS GIS Approach. Third Edition. The International Series in Engineering and Computer Science: Volume 773. pp. 406. Springer, New York, ISBN-10: 038735767X ISBN-13: 978-0-387-35767-6 e-ISBN-13: 978-0-387-68574-8

Niell A. E., 1996. Global mapping functions for the atmosphere delay at radio wavelengths. Journal of Geophysical Research, 101, pp. 3227-3246

Niell A. E., Coster A. J., Solheim F. S., Mendes V. B., Toor P. C., Langley R. B., Upham C. A., 2001. Comparison of measurements of atmospheric wet delay by radiosonde, water vapor radiometer, GPS, and VLBI. J. Atmos. Oceanic Technol., 18, pp. 830–850

Nilsson T., Elgered G., 2008. Long-term trends in the atmospheric water vapor content estimated from ground-based GPS data. Journal of Geophysical Research: Atmospheres, 113(D19)

Ohtani R., 2001. Detection of water vapor variations driven by thermally-induced local circulations using the Japanese continuous GPS array. Geophys. Res. Lett., 28, pp. 151-154

Oigawa M., Realini E., Tsuda T., 2015. Study of water vapor variations associated with meso-γ scale convection: comparison between GNSS and non-hydrostatic model data. SOLA, 2, pp. 27-30

Pebesma E. J., 2004. Multivariable geostatistics in s: the gstat package. Computers & Geosciences, 30:683–691

Pebesma E., Cornford D., Dubois G., Heuvelink G., Hristopoulos D., Pilz J., Stoehlker U., Morin G., Skoien J., 2010. Intamap: the design and implementation of an interoperable automated interpolation web service. Computers & Geosciences, 37:343–352

Piccardo D., Sguerso D., 2007. Il contributo del GPS nelle previsioni di eventi meteorologici significativi. Atti della 11° Conferenza Nazionale ASITA, Torino, 6-9 novembre 2007, vol. 2, pp. 1775-1780

R Development Core Team, 2008. R: A language and environment for statistical computing. R Foundation for Statistical Computing, Vienna, Austria

Realini E., Tsuda T., Sato K., Oigawa M., Iwaki Y., 2012. Analysis of the Temporal and Spatial Variability of the Wet Troposphere at a Local Scale by High-rate PPP Using a Dense GNSS Network. Proceedings of the 25th International Technical Meeting of The Satellite Division of the Institute of Navigation (ION GNSS 2012), Nashville, TN, pp. 3406-3412

Remondi B. W., 1984. Using the Global Positioning System (GPS) phase observation for relative geodesy: modeling, processing and results. Center of Sapace Research, University of Texas at Austin

Resch G. M., 1984. Water vapor radiometry in geodetic applications, Geodetic Refraction, pp. 53-84

Saastamoinen J., 1972. Introduction to practical computation of astronomical refraction. Bulletin Géodésique, 106, pp. 383-397

Saito K., Kato T., Eito H., Muroi C., 2001. Documentation of the meteorological research institute/numerical prediction division unified non hydrostatic model. Tech. Rep. of the MRI, 42, pp. 133

Sakov P., Natural Neighbour interpolation library. CSIRO Marine Research, Hobart, Tasmania; http://www.marine.csiro.au/~sak007

Santerre R., 1991. Impact of GPS satellite sky distribution. Manuscripta Geodaetica, 16, pp. 28-53

Sato T., Kimura F., 2005. Diurnal cycle of convective instability around the central mountains in Japan during the warm season. J. Atmos. Sci., 62, pp. 1626-1636

Sato K., Realini E., Tsuda T., Oigawa M., Iwaki Y., Shoji Y., Seko H., 2013. A High-Resolution, Precipitable Water Vapor Monitoring System Using a Dense Network of GNSS Receivers. Journal of Disaster Research, 8(1), pp. 37-47

Schmid R., Steigenberger P., Gendt G., Ge M., Rothacher M. 2007. Generation of a consistent absolute phase center correction model for GPS receiver and satellite antennas. Journal of Geodesy, 81, pp. 781-798

Seeber C., 1993. Satellite Geodesy: foundations, methods, and applications. Walter de Gruyter, Berlin New York

Seko H., 1998. Variation of PWV derived from GPS data. Kishou, 493, pp. 15463-15467

Seko H., Nakamura H., Shoji Y., Iwabuchi T., 2004. The meso-γ scale water vapor distribution associated with a thunderstorm calculated from a dense network of GPS receivers. J. Meteor. Soc. Japan, 82, pp. 569-586

Seko H., Kawabata T., Tsuyuki T., Nakamura H., Koizumi K., Iwabuchi T., 2004a. Impacts of GPS-derived water vapor and radial wind measured by Doppler Radar on numerical prediction of precipitation. J. Meteor. Soc. Japan, 82, pp. 473-489

Seko H., Shoji Y., Fujibe F., 2007. Evolution and air flow structure of a Kanto thunderstorm on 21 July, 1999 (the Nerima Heavy Rainfall Event). J. Meteor. Soc. Japan, 85, pp. 455-477

Sguerso D., Labbouz L., Walpersdorf A., 2013. 14 years of GPS tropospheric delays in the French-Italian border region: a data base for meteorological and climatological analyses. The International Archives of the Photogrammetry, Remote Sensing and Spatial Information Sciences, XL-5/W3, pp. 7-14

Sguerso D., Federici B., Agrillo G., Ferrando I., 2014. Il contributo della geomatica alla valutazione delle allerte meteorologiche. Newton's Bulletin, Volume: Il prof. Sansò e l'evoluzione della geodesia in Italia, CD-ROM, pp. 1-11

Sguerso D., Labbouz L., Walpersdorf A., 2015. 14 years of GPS tropospheric delays in the French–Italian border region: comparisons and first application in a case study. Applied Geomatics, ed. Springer Verlag, pp. 1-13

Shewchuk J. R., Triangle, a two-dimensional quality mesh generator and Delaunay triangulation, University of California at Berkeley, USA; http://www.cs.cmu.edu/~quake/triangle.html

Shoji Y., Nakamura H., Aonashi K., Ichiki A., Seko H., 2000. Semi-diurnal and diurnal variation of errors in GPS precipitable water vapor at Tsukuba, Japan caused by site displacement due to ocean tidal loading. Earth Planets and Space, 52, pp. 685-690

Shoji Y., Seko H. Iwabuchi T. Nakamura H., 2002. A case study of water vapor variation in a severe thunderstorm in Tokyo by using dense network of GPS. Proceedings of International Conference on Mesoscale Convective Systems and Heavy Rain in East Asia

Shoji Y., Nakamura H., Iwabuchi T, Aonashi K., Seko H., Mishima K., Itagaki A., Ichikawa R., Ohtani R., 2004. Tsukuba GPS dense net campaign observation: Improvement in GPS analysis of slant path delay by stacking one-way postfit phase residuals. J. Meteor. Soc. Japan, 82, pp. 301-314

Shoji Y., 2009. A study of near real-time water vapor analysis using a nationwide dense GPS network of Japan. J. Meteor. Soc. Japan, 87, pp. 1-18

Sibson R., 1981. A brief description of natural neighbour interpolation. In: V. Barnett eds. Interpreting Multivariate Data, Chichester, 21-36, John Wiley.

Sieczka M. and GRASS Development Team, 2006. r.surf.nnbathy GRASS Software, Version 6.4.. Open Source Geospatial Foundation

Skamarock W. C., Klemp J. B., Dudhia J., Gill D. O., Barker D. M., Huang X. Z., Wang W., Powers J. G., 2008. A Description of the Advanced Research WRF Version 3. Technical report, Mesoscale and Microscale Meteorology Division, NCAR, Boulder, Colorado

Sohn D. H., Cho J., 2010. Trend analysis of GPS precipitable water vapor above South Korea over the last 10 years. J. Astron. Space Sci., 27(3), pp. 231-238

Solheim F. S., Vivekanandan J., Ware R. H., Rocken C., 1999. Propagation delays induced in GPS signals by dry air, water vapor, hydrometeors, and other particulates. Journal of Geophysical Research, 104, pp. 9663-9670

Spilker J. J. (1980). Signal structure and performance characteristics, Navigation, 1, Institute of Navigation, pp. 29-54

Steigenberger P., Tesmer V., Krügel M., Thaller D., Schmid R., Vey S., Rothacher M., 2007. Comparisons of homogeneously reprocessed GPS and VLBI long time-series of troposphere zenith delays and gradients. Journal of Geodesy, 81(6-8), pp. 503-514

Tralli D. M., Dixon T. H., Stephens S., 1988. The effect of wet tropospheric path delays on estimation of geodetic baselines in the Gulf of California using the Global Positioning System, J. Geophys. Res., 93, pp. 6545-6557

Tregoning P., Boers R., O'Brien D., 1998. Accuracy of absolute precipitable water vapor estimates from GPS observations. Journal of Geophysical Research: Atmospheres, 103(D22), pp. 28701-28710

Tregoning P., Van Dam T., 2005. Atmospheric pressure loading corrections applied to GPS data at the observation level. Geophysical Research Letters, 32, L22310

Tsuda T., Sato K., Realini E., Oigawa M., Iwaki Y., Shoji Y., Seko H., 2013. A real-time monitoring system of Precipitable Water Vapor (PWV) using a dense GNSS receiver network. Journal of Disaster Research, 8(1), pp. 155-156

Vey S., Calais E., Llubes M., Florsch N., Woppelmann G., Hinderer J., Amalvict M., Lalancette M. F., Simon B., Duquenne F., Haase J. S., 2002. GPS measurements of ocean loading and its impact on zenith tropospheric delay estimates: a case study in Brittany, France. Journal of Geodesy, 76(8), pp. 419-427

Vey S., Dietrich R., Fritsche M., Rülke A., Steigenberger P., Rothacher M., 2009. On the homogeneity and interpretation of precipitable water time series derived from global GPS observations. Journal of Geophysical Research: Atmospheres, 114(D10)

Wackernagel H., 2003. Multivariate geostatistics. An introduction with applications. Springer-Verlag, Berlin

Walpersdorf A., Bouin M. N., Bock O., Doerflinger E., 2007. Assessment of GPS data for meteorological applications over Africa: Study of error sources and analysis of positioning accuracy. Journal of Atmospheric and Solar-Terrestrial Physic, 69(12), pp. 1312-1330

Weston S., 2002. An introduction to the mathematical and construction of splines. http://www.addix.com/products/spline/SplineMathsOverview.pdf

Williams E. R., Weber M. E., Orville R. E., 1989. The relationship between lightning type and convective state of thunderclouds. J. Geophys. Res., 94, pp. 13213-13220

Yan X., Ducrocq V., Poli P., Hakam M., Jaubert G., Walpersdorf A., 2009. Impact of GPS zenith delay assimilation on convective-scale prediction of Mediterranean heavy rainfall. Journal of Geophysical Research: Atmospheres, 114(D3)

Zhang C., Kuo Y., Dai L., Chu Y., Braun J., Zhang J., Li Q., Chen M., 2008. The design and application of network of ground-based GPS water vapor monitoring stations to improve precipitation prediction in the Greater Beijing metropolitan area. The International Archives of the Photogrammetry, Remote Sensing and Spatial Information Sciences, Beijing, China, 37, pp. 517-522

Zimmerman D., Pavlik C., Ruggles A., Armstrong, M., 1999. An experimantal comparison of ordinary and universal kriging and inverse distance weighting. Mathematical Geology, 31, 375-390

APPENDIX

I. THE IONOSPHERE EFFECT ON GNSS SIGNAL

The Ionosphere is a dispersive medium with respect to GNSS signals due to the free electrons and ions present in the layer, which are responsible of the refraction of radio waves in the frequency range from 3 Hz to 30 MHz. In GNSS signal transmission, the biases induced by ionospheric refraction are frequency dependent, thus different carriers experience different ionospheric effects. The ionospheric has the effect of altering the satellite-receiver distance.

I.a. Ionospheric refraction

The *phase velocity* of an electromagnetic wave is the velocity of propagation of the wave itself, given by

$$v_{phase} = \lambda \cdot f \tag{I.1}$$

L1 and L2 carrier waves propagate with phase velocity.
The *group velocity* is the propagation velocity of a group of waves with slightly different frequencies, given by

$$v_{group} = -\frac{df}{d\lambda} \cdot \lambda^2 \tag{I.2}$$

The group velocity has to be taken into account in code measurements.
The relation between phase and group velocity can be expressed by Rayleigh equation

$$v_{group} = v_{phase} - \lambda \cdot \frac{dv_{phase}}{d\lambda} \tag{I.3}$$

Remembering that the propagation velocity is usually obtained as a function of the speed of light and the refractive index n as

$$v = \frac{c}{n} \tag{I.4}$$

the refractive indexes n_{phase} and n_{group} can be written

$$n_{phase} = \frac{c}{v_{phase}}$$
$$n_{group} = \frac{c}{v_{group}} \tag{I.5}$$

The relation between the refractive indexes can be expressed by[109]

$$n_{group} = n_{phase} - \lambda \cdot \frac{dn_{phase}}{d\lambda} \tag{I.6}$$

or, similarly

$$n_{group} = n_{phase} + f \cdot \frac{dn_{phase}}{df} \tag{I.7}$$

According to Seeber (1993), the phase refractive index is approximated by the series

$$n_{phase} = 1 + \frac{c_2}{f^2} + \frac{c_3}{f^3} + \frac{c_4}{f^4} + \ldots \tag{I.8}$$

where the coefficients c_2, c_3 and c_4 are frequency independent and depend only on the electron density N_e along the propagation path. Cutting off the series expansion after the quadratic term, differentiating the obtained equation and substituting in (I.7) yelds

$$n_{group} = 1 - \frac{c_2}{f^2} + f \cdot \frac{2 \cdot c_2}{f^3} = 1 - \frac{c_2}{f^2} \tag{I.9}$$

Observing equations (I.8) and (I.9), and having the following estimate for c_2 (Seeber, 1993)

$$c_2 = -40.3 \cdot N_e \quad [Hz^2] \tag{I.10}$$

where N_e is positive, it's evident that

$$n_{group} > n_{phase}$$
$$v_{group} < v_{phase} \tag{I.11}$$

As a consequence, a group delay and a phase advance can be observed; in other words, the code pseudo-ranges over-estimate while the phase pseudo-ranges are under-estimate the geometric satellite-receiver range.

109 For the mathematical passages, see Hoffmann-Wellenhof et al., 2001, page 98.

I.b. Iono-free combination

The ionospheric bias is usually eliminated by means of a proper carriers combination, called *iono-free combination*.
In the following, the L1 and L2 GPS carriers are taken as example.

I.b.i. Phase pseudo-range

Adding the frequency dependent ionospheric refraction Δ_{ion}, depending on the zenith angle of the satellite (z'), the frequency of the signal (f) and the TVEC[110] and expressed by the relation (see Hofmann-Wellenhof et al., 2001, page 101)

$$\Delta_{ion} = \frac{1}{\cos(z')} \cdot \frac{40.3}{f^2} \cdot \mathrm{TVEC} \tag{I.12}$$

to the phase pseudo-range (1.10), it yields:

$$\begin{aligned} \phi_{L1} &= \frac{1}{\lambda_{L1}} \cdot \rho + \frac{c}{\lambda_{L1}} \cdot \Delta\delta + N_{L1} - \frac{1}{\lambda_{L1}} \cdot \Delta_{ion}(f_{L1}) \\ \phi_{L2} &= \frac{1}{\lambda_{L2}} \cdot \rho + \frac{c}{\lambda_{L2}} \cdot \Delta\delta + N_{L2} - \frac{1}{\lambda_{L2}} \cdot \Delta_{ion}(f_{L2}) \end{aligned} \tag{I.13}$$

Introducing the relation $c = f \cdot \lambda$, the previous equation (I.13) turns in:

$$\begin{aligned} \phi_{L1} &= \frac{f_{L1}}{c} \cdot \rho + f_{L1} \cdot \Delta\delta + N_{L1} - \frac{f_{L1}}{c} \cdot \Delta_{ion}(f_{L1}) \\ \phi_{L2} &= \frac{f_{L2}}{c} \cdot \rho + f_{L2} \cdot \Delta\delta + N_{L2} - \frac{f_{L2}}{c} \cdot \Delta_{ion}(f_{L2}) \end{aligned} \tag{I.14}$$

By collecting the common factors, equation (I.14) can be written in the simplified form

$$\begin{aligned} \phi_{L1} &= f_{L1} \cdot a + N_{L1} - b \cdot \frac{1}{f_{L1}} \\ \phi_{L2} &= f_{L2} \cdot a + N_{L2} - b \cdot \frac{1}{f_{L2}} \end{aligned} \tag{I.15}$$

where

110 Total Vertical Electron Content.

$$a = \frac{\rho}{c} + \Delta\delta$$
$$b = \frac{f^2}{c} \cdot \Delta_{ion} \tag{I.16}$$

In equation (I.16), a represents the geometry term and b represents the ionosphere term.

The ionosphere term can be eliminated by means of a linear combination multiplying by f_{L1} the first equation in (I.15), multiplying by f_{L2} the second equation in (I.15) and performing the difference, as (I.17) shows

$$\phi_{L1} \cdot f_{L1} - \phi_{L2} \cdot f_{L2} = \left(\frac{\rho}{c} + \Delta\delta\right) \cdot \left(f_{L1}^2 - f_{L2}^2\right) + N_{L1} \cdot f_{L1} - N_{L2} \cdot f_{L2} \tag{I.17}$$

Multiplying (I.17) by $\frac{f_{L1}}{\left(f_{L1}^2 - f_{L2}^2\right)}$ and re-arranging the terms, the *iono-free combination* is obtained

$$\phi_{L1} - \frac{f_{L2}}{f_{L1}} \cdot \phi_{L2} = a \cdot f_{L1} + \left(N_{L1} - \frac{f_{L2}}{f_{L1}} \cdot N_{L2}\right) \cdot \frac{f_{L1}^2}{\left(f_{L1}^2 - f_{L2}^2\right)} \tag{I.18}$$

I.b.ii. Code pseudo-range

An analogous operation can be carried out for code pseudo-range (1.7),adding the ionospheric refraction Δ_{ion}

$$L_{L1} = \rho + c \cdot \Delta\delta + \Delta_{ion}(f_{L1})$$
$$L_{L2} = \rho + c \cdot \Delta\delta + \Delta_{ion}(f_{L2}) \tag{I.19}$$

Multiplying by f_{L1}^2 the first equation of (I.19), multiplying by f_{L2}^2 the second equation of (I.19) and computing the difference, equation (I.20) is obtained

$$L_{L1} \cdot f_{L1}^2 - L_{L2} \cdot f_{L2}^2 = \left(f_{L1}^2 - f_{L2}^2\right) \cdot \left(\rho + c \cdot \Delta\delta\right) \tag{I.20}$$

Multiplying (I.20) by $\left(f_{L1}^2 - f_{L2}^2\right)$ and re-arranging the terms, the *iono-free combination* is obtained

$$\left(L_{L1} \cdot \frac{f_{L2}^2}{f_{L1}^2} \cdot L_{L2}\right) \cdot \frac{f_{L1}^2}{\left(f_{L1}^2 - f_{L2}^2\right)} = \rho + c \cdot \Delta\delta \tag{I.21}$$

II. GNSS NETWORK

Station names, coordinates (latitude and longitude) in WGS84, elevations (in meters) and corresponding sub-network are reported in the following Table II.1.

The red colour indicates the stations that were no more available[111] for the updating of GNSS network carried out until 31 December 2015; the green colour indicates the new stations, introduced with the updating.

The stations used to guarantee a common reference frame for the three networks, called Core stations, are indicated in bold character.

Site	Lat [°N]	Lon [°E]	Elev [m]	Net	Start Year	Start DOY[112]	End Year	End DOY
ACCE	44.476	6.988	1321.7	3	2009	278		
ACOR	43.364	-8.399	66.9	1	1998	340		
AGDE	43.296	3.466	65.8	2	2006	247		
AGNE	45.468	7.140	2354.6	2	2005	242		
AIGE	46.248	6.128	473.7	3	2009	138		
AIGL	44.121	3.581	1618.8	1	2002	232		
AJAC	41.927	8.763	98.8	1	2000	22		
ALAC	38.339	-0.481	60.3	1	1998	65		
ALPE	45.087	6.084	1892.2	2	2006	303		
ALSN	44.923	8.616	146.7	3	2010	328		
AMB2	45.541	3.750	617.6	2	2007	142		
ANCY	45.901	6.123	528.8	3	2010	301	2015	76
ARAN	45.715	5.425	289.2	3	2009	46		
ARGR	45.947	7.005	2834.8	2	2007	180		
AUBU	48.217	7.197	1151.8	3	2008	187		
AXPV	43.491	5.333	229.4	1	2002	260		
BACT	44.388	6.650	1205.2	2	2007	143		
BAJA	43.904	7.719	921.8	3	2009	346		
BANN	44.369	4.156	357.6	1	2003	184		
BAST	42.001	9.049	855.1	3	2011	18	2013	351
BAUB	43.877	3.967	211.0	2	2006	247		
BEA2	42.515	3.137	108.2	3	2009	310		
BEVE	44.194	9.769	144.7	3	2009	337		
BIEL	45.561	8.048	480.5	1	2002	247		
BLGN	46.172	5.574	544.7	3	2009	98		
BLIX	43.874	6.367	1077.1	3	2009	114		
BOUS	46.288	2.236	558.5	3	2008	357		
BRET	48.610	2.315	140.3	1	2004	162		
BRST	48.380	-4.497	65.8	1/2/3	1998	304		

111 The motivations of unavailability of the stations can be different: if the end year and doy are indicated in the table, the station was out of order or dismissed. In the other cases, the unavailability is due to the lacked permission to use the station by the GNSS network providers.

112 Day Of Year.

BSCN	47.247	5.989	359.6	1	2001	289		
BUAN	48.486	5.354	416.3	2	2007	317		
BURE	44.633	5.911	2614.6	1	2002	297		
BUSL	45.137	7.152	496.2	3	2010	314		
CAGL[113]	39.136	8.973	238.4	1/2/3	1995	97	2013	263
CAG1	39.230	9.110	135.0	3	2013	254		
CAMN	44.405	8.281	390.1	3	2009	346		
CANL	44.722	8.293	205.5	3	2010	250		
CARZ	46.042	8.680	1165.3	2	2005	237		
CBRY	45.581	5.909	324.7	2	2006	286		
CERN	46.257	6.061	525.9	3	2010	351		
CHAM	45.111	5.881	1874.6	1	2003	353		
CHIV	44.320	9.324	70.7	3	2009	347		
CHIZ	46.133	-0.408	113.2	1	2000	293		
CHMX	45.926	6.873	1120.8	2	2007	180		
CHRN	43.881	4.862	103.0	1	2000	299		
CHTL	45.304	6.359	850.3	1	1999	104		
CLAP	44.248	6.927	1369.9	1	2003	95		
CLFD	45.761	3.111	473.6	2	2006	290		
COMO	45.802	9.096	292.3	1	2001	105		
CORT	42.299	9.153	499.4	3	2011	174		
CRAL	43.128	0.367	658.3	3	2010	40		
CRSN	45.192	8.106	211.7	3	2010	250		
CUOR	45.388	7.648	483.1	3	2010	253		
DEMN	44.316	7.293	862.7	3	2010	251		
DEVE	46.314	8.261	1679.4	2	2005	244		
DOMS	46.119	8.286	365.6	3	2010	287		
EBRE	40.821	0.492	107.8	1	1994	143		
EGLT	45.403	2.052	667.0	1	2001	278		
EOST	48.580	7.763	213.3	2	2007	102		
ERCK	48.873	7.364	296.1	3	2009	77		
ESAB	45.307	4.798	207.7	2	2005	24		
ESCO	42.694	0.976	2508.4	1	1999	111		
EZEV	43.774	7.497	76.7	3	2009	41		
FCLZ	45.643	5.986	1358.3	1	1998	155		
FERR	45.867	7.028	2400.3	2	2007	165		
FJCP	43.048	2.795	322.7	1	2002	103		
FLRC	44.325	3.595	607.9	3	2008	311		
FOND	45.820	6.964	1505.3	3	2010	197		
GENO	44.419	8.921	155.5	1	1998	204		
GENU	44.403	8.959	127.4	3	2009	346		
GINA	43.676	5.787	382.0	1	1998	36		
GLRA	44.839	4.524	814.0	2	2008	10		
GOPE	49.914	14.786	592.6	1	1995	133		
GOZZ	45.747	8.433	416.6	3	2010	287		
GRAS	43.755	6.921	1319.3	1/2/3	1995	53		
GRAZ	47.067	15.493	538.3	1/2/3	1992	164		

113 CAGL has been dismissed since 20/09/2013. Differently from other stations, because it is a Core station, it has been substituted by UCAG.

GRJF	45.303	1.514	458.6	3	2010	244		
GUIL	44.662	6.662	1171.1	2	2007	316		
HERS	50.867	0.336	76.5	1/2/3	1991	244		
JANU	44.910	6.710	2583.9	2	2005	287		
JOUX	46.529	5.796	845.5	1	2000	109		
LACA	43.681	2.728	1315.5	2	2006	122		
LAMP	35.500	12.606	57.8	1	1999	24		
LEBE	45.916	5.625	940.6	2	2005	141		
LFAZ	45.117	5.399	1071.2	2	2005	10		
LOAN	44.119	8.250	70.8	3	2009	346		
LROC	46.159	-1.219	57.9	1	2001	327		
LUCE	47.438	7.268	741.6	2	2007	304		
LUCI	42.386	9.531	63.7	3	2010	46		
LUMI	42.603	8.827	57.0	3	2010	46		
LURI	42.888	9.476	54.2	3	2010	46		
MAKS	47.923	7.032	1237.2	2	2007	121		
MANS	48.019	0.155	168.1	1	1998	100		
MAR2	46.122	7.071	644.1	2	2008	154		
MARG	46.084	6.511	524.2	2	2007	96		
MARS	43.279	5.354	61.8	1	1998	197		
MART	46.122	7.071	644.7	1	2002	37		
MATE	40.649	16.704	535.7	1/2/3	1991	106		
MDOR	45.799	4.809	330.6	1	2002	266		
MEDI	44.520	11.647	50.0	1/2/3	1995	209		
MICH	43.924	5.717	628.2	1	1998	196		
MLVL	48.841	2.587	160.5	1	2000	22		
MODA	45.214	6.710	1182.3	1	1998	289		
MOGN	46.148	4.803	233.0	2	2004	336		
MONC	45.074	7.927	464.5	2	2005	133		
MONV	44.390	7.829	637.7	3	2010	284		
MRGE	45.770	7.061	1722.8	2	2005	251		
MTPL	43.637	3.865	120.3	1	1999	110		
NARB	43.198	2.973	72.8	3	2010	337		
NICA	43.703	7.227	256.5	1	2002	335		
NICE	43.725	7.300	427.3	1	2000	349		
NIME	43.829	4.357	106.2	2	2006	66		
NOT1	36.876	14.990	126.3	1	2000	250		
NOVA	45.447	8.614	218.6	1	1998	121		
NOVR	45.447	8.614	218.6	3	2010	286		
OATO	45.042	7.765	658.8	2	2005	158		
OGAG	44.788	6.540	1356.5	3	2011	200		
OPME	45.713	3.090	708.0	3	2011	173		
OPMT	48.836	2.335	122.6	1	2001	182		
OSTA	44.692	7.188	1309.4	3	2010	252		
PALI	43.376	4.811	60.4	2	2007	100		
PANA	48.855	2.394	120.6	2	2004	162		
PARD	43.431	2.824	622.8	2	2007	184		
PARO	44.446	8.081	849.8	2	2007	284		
PAVI	45.203	9.136	143.7	1	2001	274		
PDOM	45.772	2.948	1466.8	3	2011	193		
PERP	42.689	2.882	96.0	2	2006	181		
PIAA	42.235	8.629	543.4	3	2010	293		

PIAN	41.495	9.056	153.1	3	2010	46		
PIMI	42.936	0.143	2923.4	3	2010	110		
PLOE	47.746	-3.427	73.9	2	2006	338		
POTS	52.379	13.066	144.4	1/2/3	1994	274		
PQRL	42.983	6.206	112.3	1	2003	259		
PRNY	46.905	6.338	883.6	2	2007	249		
PUYA	44.858	6.479	1690.3	2	2005	334		
PUYV	45.044	3.879	710.3	2	2004	239		
RABT	33.998	-6.854	90.1	1	2000	138		
RABU	44.268	6.977	2551.9	1	2003	283		
RG00	41.559	8.794	89.6	1	2000	63		
RIXH	47.733	7.378	366.8	3	2011	70		
ROSD	45.691	6.628	1694.5	2	2005	349		
ROSI	45.625	6.856	1880.0	3	2011	286		
ROTG	48.718	-3.966	56.1	3	2009	238		
RSTL	43.941	5.484	1069.8	1	2002	207		
SAA2	46.306	7.185	1419.6	3	2009	228		
SAAN	46.516	7.301	1419.5	1	2001	330		
SARI	41.858	9.403	57.2	3	2010	46		
SAUV	44.255	4.467	367.4	1	1999	321		
SAVI	44.648	7.661	380.4	3	2010	285		
SCDA	44.795	3.268	1115.4	2	2007	93		
SCLP	45.750	4.426	703.8	2	2004	336	2013	162
SCOP	41.754	9.101	928.0	3	2011	84		
SERR	44.731	8.853	251.2	3	2010	249		
SETE	43.398	3.699	53.9	2	2007	299		
SFER	36.464	-6.206	84.2	1/2/3	1995	352		
SIRT	48.712	2.209	217.5	2	2006	61		
SJDV	45.879	4.677	432.4	1/2/3	1997	287		
SLVT	43.920	3.268	811.8	2	2006	9		
SMNE	48.844	2.425	126.3	1	2000	321		
SMTG	48.641	-2.028	57.8	3	2010	48		
SOPH	43.611	7.054	178.8	1	2001	12		
SOUS	44.875	2.027	597.7	2	2006	346		
STBX	44.259	4.197	219.3	3	2012	54		
STEY	45.235	5.762	1394.9	1	2003	147		
STJ9	48.622	7.684	237.2	1	1999	310		
STMR	43.449	4.422	56.1	2	2008	99		
STPS	46.308	3.294	299.7	2	2006	340		
STV2	44.567	6.106	814.7	2	2007	115		
TENC	45.125	4.288	936.5	1	2004	95		
TETN	35.562	-5.363	63.7	1	2000	142		
TLSE	43.561	1.481	207.2	1	2001	4		
TORI	45.063	7.661	310.8	1/2/3	1996	167		
TRMO	44.285	2.725	810.9	3	2008	190		
TROP	43.219	6.601	369.3	2	2005	249		
TUDA	42.604	9.362	457.7	3	2011	91		
UCAG	39.230	9.111	132.5	1/2/3	2014	106		
VAUD	46.981	5.627	271.5	2	2007	333		
VILL	40.444	-3.952	647.4	1/2/3	1994	316		
VILR	45.073	5.552	1076.7	2	2006	340		
VISN	44.320	4.949	245.7	2	2007	94		

VSFR	48.815	1.870	124.1	2	2004	162		
WELS/WLBH[114]	48.415	7.351	819.1	1	2000	289		
WSRT	52.915	6.605	82.3	1/2/3	1997	152		
WTZR	49.144	12.879	666.0	1/2/3	1995	40		
ZERM	46.001	7.732	1931.2	2	2005	242		
ZIMM	46.877	7.465	956.3	1/2/3	1993	1		

Table II.1. List of GNSS Permanent Stations.

114 WELS changed name in WLBH.

III. P AND T STATIONS

Station names, coordinates (latitude and longitude) in WGS84, elevations (in meters) and observed data (P, T or both) are reported in the following Table III.1.

ID	Site	Country	Lat [°N]	Lon [°E]	Elev [m]	Observed data
72880	BESANCON THISE	France	47.250	5.983	309	P/T
73860	DOLE-TAVAUX	France	47.033	5.417	195	P/T
74820	AMBERIEU	France	45.987	5.328	250.9	P/T
74860	SAINT GEOIRS	France	45.363	5.329	396.8	P/T
74870	GRENONBLE LVD	France	45.220	5.850	220	P/T
74900	MEYTHET	France	45.929	6.099	463.6	P/T
74910	AIX LES BAINS	France	45.638	5.880	237.4	P/T
74970	BOURG ST-MAURICE	France	45.617	6.767	868	P/T
75880	ST-AUBAN-SUR-DURANC	France	44.067	6.000	461	P/T
75910	EMBRUN	France	44.567	6.500	876	P/T
76500	PROVENCE	France	43.436	5.214	22.6	P/T
76600	TOULON	France	43.100	5.933	25	P/T
76610	CAP CEPET	France	43.083	5.933	134	P/T
76670	LE PALYVESTRE	France	43.097	6.146	2.1	P/T
76750	LE CANNET	France	43.385	6.387	80.8	P/T
76780	TOULON/ILE DU LEVAN	France	43.033	6.467	131	P/T
76840	MANDELIEU	France	43.542	6.953	4	P/T
76900	COTE D'AZUR	France	43.658	7.216	3.7	P/T
77530	ILE ROUSSE	France	42.633	8.917	153	P/T
77540	SAINT CATHERINE	France	42.531	8.793	63.7	P/T
77610	CAMPO DELL'ORO	France	41.924	8.803	5.5	P/T
77650	SOLENZARA	France	41.924	9.406	8.5	P/T
77700	CAP PERTUSATO	France	41.367	9.167	116	P/T
77750	ALISTRO	France	42.267	9.533	74	P/T
77800	SUD CORSE	France	41.501	9.098	26.5	P/T
77850	CAP CORSE	France	43.000	9.367	113	P/T
77900	PORETTA	France	42.553	9.484	7.9	P/T
996068	NICE BUOY 61001	France	43.400	7.800	7.9	T
160080	S. VALENTINO ALLA MUTA	Italy	46.750	10.533	1461	P/T
160200	BOLZANO	Italy	46.460	11.326	240.5	P/T
160210	ROLLE PASS	Italy	46.300	11.783	26	P/T
160220	PAGANELLA MOUNTAIN	Italy	46.150	11.033	2129	P/T
160330	DOBBIACO	Italy	46.733	12.217	1226	P/T
160370	AVIANO (USAF)	Italy	46.033	12.617	125	T
160520	PIAN ROSA (MTN TOP)	Italy	45.933	7.700	3488	P/T
160590	TORINO CASELLE	Italy	45.201	7.650	301.4	P/T
160610	TORINO/BRIC CROCE	Italy	45.033	7.733	710	P/T
160660	MALPENSA	Italy	45.631	8.728	233.8	P/T
160760	BERGAMO ORIO AL SERIO	Italy	45.674	9.704	238.4	P/T
160880	GHEDI	Italy	45.432	10.268	101.5	P/T
160900	VILLAFRANCA	Italy	45.396	10.889	72.8	P/T
160980	ISTRANA	Italy	45.685	12.083	41.8	P/T
161050	VENEZIA TESSERA	Italy	45.505	12.352	2.1	P/T

161080	RONCHI DEI LEGIONARI	Italy	45.828	13.472	11.30	P/T
161100	TRIESTE	Italy	45.650	13.750	20	P/T
161140	MONDOVI	Italy	44.383	7.817	560	P/T
161200	GENOVA SESTRI	Italy	44.412	8.842	4	T
161340	CIMONE MOUNTAIN	Italy	44.200	10.700	2173	P/T
161400	BOLOGNA	Italy	44.535	11.289	37.5	P/T
161480	CERVIA	Italy	44.224	12.307	5.5	P/T
161490	RIMINI	Italy	44.020	12.612	12.5	P/T
161530	CAPE MELE	Italy	43.950	8.167	221	P/T
161580	PISA	Italy	43.684	10.393	1.8	P/T
161680	MOUNT ARGENTARIO	Italy	42.383	11.167	632	P/T
161700	FIRENZE	Italy	43.810	11.205	43.9	P/T
161720	AREZZO	Italy	43.467	11.850	249	P/T
161790	FRONTONE	Italy	43.517	12.733	574	P/T
161910	FALCONARA	Italy	43.616	13.362	14.9	P/T
162060	GROSSETO	Italy	42.760	11.072	4.6	P/T
162190	TERMINILLO MOUNTAIN	Italy	42.467	12.983	1875	P/T
162240	VIGNA DI VALLE	Italy	42.083	12.217	270	P/T
162300	PESCARA	Italy	42.432	14.181	14.6	P/T
162530	GRAZZANISE	Italy	41.061	14.082	8.8	P/T
162580	MONTE S. ANGELO	Italy	41.700	15.950	848	P/T
162591	PARMA	Italy	44.824	10.296	49.1	T
162593	MONTICHIARI	Italy	45.429	10.331	108.5	T
162630	TREVICO	Italy	41.050	15.233	1093	P/T
163100	CAPE PALINURO	Italy	40.017	15.283	185	P/T
165220	CAPE CACCIA	Italy	40.567	8.167	205	P/T

Table III.1. List of P and T NOAA stations.

IV. P AND T DATA

In the following sections, some extractions of dat.txt, inv.txt, stn.txt and doc.txt output files are reported to show their structures and the organization of data.

IV.a. doc.txt file

The doc.txt file contains the description of the different columns of the dat.txt file and the numeric symbols used to quantify the various observables in an abbreviated format.
The wind, temperature, dewpoint, pressure and precipitation columns are filled with the corresponding observed quantities; the clouds, precipitation types and weather observables are coded with different symbols, reported in the second part of the file.

```
                    SURFACE HOURLY ABBREVIATED FORMAT

ONE HEADER RECORD FOLLOWED BY DATA RECORDS:
COLUMN DATA DESCRIPTION
01-06 USAF = AIR FORCE CATALOG STATION NUMBER
08-12 WBAN = NCDC WBAN NUMBER
14-25 YR--MODAHRMN = YEAR-MONTH-DAY-HOUR-MINUTE IN GREENWICH MEAN TIME
27-29 DIR = WIND DIRECTION IN COMPASS DEGREES, 990 = VARIABLE, REPORTED AS
   '***' WHEN AIR IS CALM (SPD WILL THEN BE 000)
31-37 SPD & GUS = WIND SPEED & GUST IN MILES PER HOUR
39-41 CLG = CLOUD CEILING--LOWEST OPAQUE LAYER WITH 5/8 OR GREATER COVERAGE,
   IN HUNDREDS OF FEET, 722 = UNLIMITED
43-45 SKC = SKY COVER -- CLR-CLEAR, SCT-SCATTERED-1/8 TO 4/8, BKN-BROKEN-5/8
   TO 7/8, OVC-OVERCAST, OBS-OBSCURED, POB-PARTIAL OBSCURATION
47-47 L = LOW CLOUD TYPE, SEE BELOW
49-49 M = MIDDLE CLOUD TYPE, SEE BELOW
51-51 H = HIGH CLOUD TYPE, SEE BELOW
53-56 VSB = VISIBILITY IN STATUTE MILES TO NEAREST TENTH
58-68 MW MW MW MW = MANUALLY OBSERVED PRESENT WEATHER--LISTED BELOW IN
   PRESENT WEATHER TABLE
70-80 AW AW AW AW = AUTO-OBSERVED PRESENT WEATHER--LISTED BELOW IN PRESENT
   WEATHER TABLE
82-82 W = PAST WEATHER INDICATOR, SEE BELOW
84-92 TEMP & DEWP = TEMPERATURE & DEW POINT IN FAHRENHEIT
94-99 SLP = SEA LEVEL PRESSURE IN MILLIBARS TO NEAREST TENTH
101-105 ALT = ALTIMETER SETTING IN INCHES TO NEAREST HUNDREDTH
```

107-112 STP = STATION PRESSURE IN MILLIBARS TO NEAREST TENTH
114-116 MAX = MAXIMUM TEMPERATURE IN FAHRENHEIT (TIME PERIOD VARIES)
118-120 MIN = MINIMUM TEMPERATURE IN FAHRENHEIT (TIME PERIOD VARIES)
122-126 PCP01 = 1-HOUR LIQUID PRECIP REPORT IN INCHES AND HUNDREDTHS -- THAT IS, THE PRECIP FOR THE PRECEDING 1 HOUR PERIOD
128-132 PCP06 = 6-HOUR LIQUID PRECIP REPORT IN INCHES AND HUNDREDTHS -- THAT IS, THE PRECIP FOR THE PRECEDING 6 HOUR PERIOD
134-138 PCP24 = 24-HOUR LIQUID PRECIP REPORT IN INCHES AND HUNDREDTHS THAT IS, THE PRECIP FOR THE PRECEDING 24 HOUR PERIOD
140-144 PCPXX = LIQUID PRECIP REPORT IN INCHES AND HUNDREDTHS, FOR A PERIOD OTHER THAN 1, 6, OR 24 HOURS (USUALLY FOR 12 HOUR PERIOD FOR STATIONS OUTSIDE THE U.S., AND FOR 3 HOUR PERIOD FOR THE U.S.)
T = TRACE FOR ANY PRECIP FIELD
146-147 SD = SNOW DEPTH IN INCHES

NOTES:
- *'s IN FIELD INDICATES ELEMENT NOT REPORTED.
- SOME VALUES WERE CONVERTED FROM METRIC TO ENGLISH UNITS. THIS WILL OCCASIONALLY RESULT IN MINOR DIFFERENCES VS ORIGINAL DATA DUE TO ROUNDING.
- COLUMN POSITION REFERS TO ASCII TEXT DATA.
- THIS FORMAT CAN BE EASILY IMPORTED INTO A SPREADSHEET OR A DATABASE MANAGEMENT SYSTEM SINCE FIELDS ARE SPACE-DELIMITED.
- THIS FORMAT DOES NOT INCLUDE QUALITY CONTROL FLAGS, WHICH ARE AVAILABLE IN THE ADVANCED FORMAT THROUGH THE CLIMATE DATA ONLINE SYSTEM.

PRESENT WEATHER CODE TABLE

The code that denotes a specific type of weather observed.

00-49 No precipitation at the station at the time of observation

---

00-19 No precipitation, fog, ice fog (except for 11 and 12), duststorm, sandstorm, drifting or blowing snow at the station at the time of observation or, except for 09 and 17, during the preceding hour

---

00: Cloud development not observed or not observable
01: Clouds generally dissolving or becoming less developed
02: State of sky on the whole unchanged
03: Clouds generally forming or developing

04: Visibility reduced by smoke, e.g. veldt or forest fires, industrial smoke or volcanic ashes
05: Haze
06: Widespread dust in suspension in the air, not raised by wind at or near the station at the time of observation
07: Dust or sand raised by wind at or near the station at the time of observation, but no well-developed dust whirl(s) or sand whirl(s), and no duststorm or sandstorm seen or, in the case of ships, blowing spray at the station
08: Well developed dust whirl(s) or sand whirl(s) seen at or near the station during the preceding hour or at the time of observation, but no duststorm or sandstorm
09: Duststorm or sandstorm within sight at the time of observation, or at the station during the preceding hour
10: Mist
11: Patches of shallow fog or ice fog at the station, whether on land or sea, not deeper than about 2 meters on land or 10 meters at sea
12: More or less continuous shallow fog or ice fog at the station, whether on land or sea, not deeper than about 2 meters on land or 10 meters at sea
13: Lightning visible, no thunder heard
14: Precipitation within sight, not reaching the ground or the surface of the sea
15: Precipitation within sight, reaching the ground or the surface of the sea, but distant, i.e., estimated to be more than 5 km from the station
16: Precipitation within sight, reaching the ground or the surface of the sea, near to, but not at the station
17: Thunderstorm, but no precipitation at the time of observation
18: Squalls at or within sight of the station during the preceding hour or at the time of observation
19: Funnel cloud(s) (Tornado cloud or waterspout) at or within sight of the station during the preceding hour or at the time of observation
---
20-29 Precipitation, fog, ice fog or thunderstorm at the station during the preceding hour, but not at the time of observation
---
20: Drizzle (not freezing) or snow grains not falling as shower(s)
21: Rain (not freezing) not falling as shower(s)
22: Snow not falling as shower(s)
23: Rain and snow or ice pellets not falling as shower(s)

24: Freezing drizzle or freezing rain not falling as shower(s)
25: Shower(s) of rain
26: Shower(s) of snow or of rain and snow
27: Shower(s) of hail (Hail, small hail, snow pellets), or rain and hail
28: Fog or ice fog
29: Thunderstorm (with or without precipitation)

30-39 Duststorm, sandstorm, or blowing snow

30: Slight or moderate duststorm or sandstorm has decreased during the preceding hour
31: Slight or moderate duststorm or sandstorm no appreciable change during the preceding hour
32: Slight or moderate duststorm or sandstorm has begun or has increased during the preceding hour
33: Severe duststorm or sandstorm has decreased during the preceding hour
34: Severe duststorm or sandstorm no appreciable change during preceding hour
35: Severe duststorm or sandstorm has begun or has increased during the preceding hour
36: Slight or moderate drifting snow generally low (below eye level)
37: Heavy drifting snow generally low (below eye level)
38: Slight or moderate blowing snow generally high (above eye level)
39: Heavy blowing snow generally high (above eye level)

40-49 Fog or ice fog at the time of observation

40: Fog or ice fog at a distance at the time of observation, but not at the station during the preceding hour, the fog or ice fog extending to a level above that of the observer
41: Fog or ice fog in patches
42: Fog or ice fog, sky visible, has become thinner during the preceding hour
43: Fog or ice fog, sky invisible, has become thinner during preceding hour
44: Fog or ice fog, sky visible, no appreciable change during the preceding hour
45: Fog or ice fog, sky invisible, no appreciable change during preceding hour
46: Fog or ice fog, sky invisible, has begun or has become thicker during the preceding hour

47: Fog or ice fog, sky invisible, has begun or has become thicker during the preceding hour
48: Fog, depositing rime, sky visible
49: Fog, depositing rime, sky invisible

50-99 Precipitation at the station at the time of observation

---

50-59 Drizzle

50: Drizzle, not freezing, intermittent, slight at time of observation
51: Drizzle, not freezing, continuous, slight at time of observation
52: Drizzle, not freezing, intermittent, moderate at time of observation
53: Drizzle, not freezing, continuous, moderate at time of observation
54: Drizzle, not freezing, intermittent, heavy (dense) at time of observation
55: Drizzle, not freezing, continuous, heavy (dense) at time of observation
56: Drizzle, freezing, slight
57: Drizzle, freezing, moderate or heavy (dense)
58: Drizzle and rain, slight
59: Drizzle and rain, moderate or heavy

60-69 Rain

60: Rain, not freezing, intermittent, slight at time of observation
61: Rain, not freezing, continuous, slight at time of observation
62: Rain, not freezing, intermittent, moderate at time of observation
63: Rain, not freezing, continuous, moderate at time of observation
64: Rain, not freezing, intermittent, heavy at time of observation
65: Rain, not freezing, continuous, heavy at time of observation
66: Rain, freezing, slight
67: Rain, freezing, moderate or heavy
68: Rain or drizzle and snow, slight
69: Rain or drizzle and snow, moderate or heavy

70-79 Solid precipitation not in showers

70: Intermittent fall of snowflakes, slight at time of observation
71: Continuous fall of snowflakes, slight at time of observation
72: Intermittent fall of snowflakes, moderate at time of observation
73: Continuous fall of snowflakes, moderate at time of observation

74: Intermittent fall of snowflakes, heavy at time of observation
75: Continuous fall of snowflakes, heavy at time of observation
76: Diamond dust (with or without fog)
77: Snow grains (with or without fog)
78: Isolated star-like snow crystals (with or without fog)
79: Ice pellets

80-99 Showery precipitation, or precipitation with current or recent thunderstorm

---

80: Rain shower(s), slight
81: Rain shower(s), moderate or heavy
82: Rain shower(s), violent
83: Shower(s) of rain and snow mixed, slight
84: Shower(s) of rain and snow mixed, moderate or heavy
85: Show shower(s), slight
86: Snow shower(s), moderate or heavy
87: Shower(s) of snow pellets or small hail, with or without rain or rain and snow mixed, slight
88: Shower(s) of snow pellets or small hail, with or without rain or rain and snow mixed, moderate or heavy
89: Shower(s) of hail (hail, small hail, snow pellets), with or without rain or rain and snow mixed, not associated with thunder, slight
90: Shower(s) of hail (hail, small hail, snow pellets), with or without rain or rain and snow mixed, not associated with thunder, moderate or heavy
91: Slight rain at time of observation, thunderstorm during the preceding hour but not at time of observation
92: Moderate or heavy rain at time of observation, thunderstorm during the preceding hour but not at time of observation
93: Slight snow, or rain and snow mixed or hail (Hail, small hail, snow pellets), at time of observation, thunderstorm during the preceding hour but not at time of observation
94: Moderate or heavy snow, or rain and snow mixed or hail (Hail, small hail, snow pellets) at time of observation, thunderstorm during the preceding hour but not at time of observation
95: Thunderstorm, slight or moderate, without hail (Hail, small hail, snow pellets), but with rain and/or snow at time of observation, thunderstorm at time of observation

96: Thunderstorm, slight or moderate, with hail (hail, small hail, snow pellets) at time of observation, thunderstorm at time of observation
97: Thunderstorm, heavy, without hail (Hail, small hail, snow pellets), but with rain and/or snow at time of observation, thunderstorm at time of observation
98: Thunderstorm combined with duststorm or sandstorm at time of observation, thunderstorm at time of observation
99: Thunderstorm, heavy, with hail (Hail, small hail, snow pellets) at time of observation, thunderstorm at time of observation

PAST WEATHER CODE TABLE

The code that denotes a specific type of past weather observed.
0: Cloud covering 1/2 or less of the sky throughout the appropriate period
1: Cloud covering more than 1/2 of the sky during part of the appropriate period and covering 1/2 or less during part of the period
2: Cloud covering more than 1/2 of the sky throughout the appropriate period
3: Sandstorm, duststorm or blowing snow
4: Fog or ice fog or thick haze
5: Drizzle
6: Rain
7: Snow, or rain and snow mixed
8: Shower(s)
9: Thunderstorm(s) with or without precipitation

LOW CLOUD TYPE

0: No low clouds
1: Cumulus humulis or Cumulus fractus other than of bad weather or both
2: Cumulus mediocris or congestus, with or without Cumulus of species fractus or humulis or Stratocumulus all having bases at the same level
3: Cumulonimbus calvus, with or without Cumulus, Stratocumulus or Stratus
4: Stratocumulus cumulogenitus
5: Stratocumulus other than Stratocumulus cumulogenitus
6: Stratus nebulosus or Stratus fractus other than of bad weather, or both
7: Stratus fractus or Cumulus fractus of bad weather, or both (pannus) usually below Altostratus or Nimbostratus
8: Cumulus and Stratocumulus other than Stratocumulus cumulogenitus, with bases at different levels
9: Cumulonimbus capillatus (often with an anvil), with or without Cumulonimbus calvus, Cumulus, Stratocumulus, Stratus or pannus

MIDDLE CLOUD TYPE

0: No middle clouds
1: Altostratus translucidus
2: Altostratus opacus or Nimbostratus
3: Altocumulus translucidus at a single level
4: Patches (often lenticular) of Altocumulus translucidus, continually changing and occurring at one or more levels
5: Altocumulus translucidus in bands, or one or more layers of Altocumulus translucidus or opacus, progressively invading the sky; these Altocumulus clouds generally thicken as a whole
6: Altocumulus cumulogentis (or cumulonimbogentus)
7: Altocumulus translucidus or opacus in two or more layers, or Altocumulus opacus in a single layer, not progressively invading the sky, or Altocumulus with Altostratus or Nimbostratus
8: Altocumulus castellanus or floccus
9: Altocumulus of a chaotic sky; generally at several levels

HIGH CLOUD TYPE

0: No High Clouds
1: Cirrus fibratus, sometimes uncinus, not progressively invading the sky
2: Cirrus spissatus, in patches or entangled sheaves, which usually do not increase and sometimes seem to be the remains of the upper part of a Cumulonimbus; or Cirrus castellanus or floccus
3: Cirrus spissatus cumulonimbogenitus
4: Cirrus unicinus or fibratus, or both, progressively invading the sky; they generally thicken as a whole
5: Cirrus (often in bands) and Cirrostratus, or Cirrostratus alone, progressively invading the sky; they generally thicken as a whole, but the continuous veil does not reach 45 degrees above the horizon
6: Cirrus (often in bands) and Cirrostratus, or Cirrostratus alone, progressively invading the sky; they generally thicken as a whole; the continuous veil extends more than 45 degrees above the horizon, without the sky being totally covered
7: Cirrostratus covering the whole sky
8: Cirrostratus not progressively invading the sky and not entirely covering it
9: Cirrocumulus alone, or Cirrocumulus predominant among the High clouds

IV.b. dat.txt.file

A sample dat.txt file for 24 hours of observations in S. Valentino alla Muta (Italy) station is presented, split in three tables for improved readability.

The first row indicates the column number, the first column indicates the line number. The terms comparing in the header of the file (row 0) have been explained in the previous section (see IV.a, page 162). Each row (1-24) corresponds to a different hour.

Table IV.1 is relative to wind (columns 4-6) and sky cover (columns 7-12) data; Table IV.2 is relative to observed weather (columns 13-21), temperature (columns 22-23) and pressure data (24-26); Table IV.3 is relative to temperature extreme values (columns 27-28) and precipitation data (columns 29-33).

The symbol "*" means that the corresponding data is not observed in the considered time.

	1	2	3	4	5	6	7	8	9	10	11	12
0	USAF	WBAN	YR--MODAHRMN	DIR	SPD	GUS	CLG	SKC	L	M	H	VSB
1	160080	99999	201410060000	180	2	***	4	OVC	*	*	*	0.4
2	160080	99999	201410060100	190	5	***	4	OVC	*	*	*	0.4
3	160080	99999	201410060200	190	6	***	4	OVC	*	*	*	0.4
4	160080	99999	201410060300	180	2	***	4	OVC	*	*	*	0.4
5	160080	99999	201410060400	180	2	***	6	OVC	*	*	*	0.5
6	160080	99999	201410060500	180	7	***	6	OVC	*	*	*	0.5
7	160080	99999	201410060600	190	7	***	6	OVC	*	*	*	0.5
8	160080	99999	201410060700	180	6	***	4	OVC	*	*	*	0.2
9	160080	99999	201410060800	140	6	***	12	OVC	*	*	*	0.5
10	160080	99999	201410060900	160	5	***	15	BKN	*	*	*	1.9
11	160080	99999	201410061000	160	6	***	20	BKN	*	*	*	3.1
12	160080	99999	201410061100	180	8	***	30	BKN	*	*	*	5.0
13	160080	99999	201410061200	160	9	***	30	BKN	*	*	*	5.0
14	160080	99999	201410061300	170	8	***	30	BKN	*	*	*	5.0
15	160080	99999	201410061400	160	9	***	39	BKN	*	*	*	6.2
16	160080	99999	201410061500	130	7	***	30	BKN	*	*	*	6.2
17	160080	99999	201410061600	130	8	***	30	BKN	*	*	*	6.2
18	160080	99999	201410061700	120	5	***	***	SCT	*	*	*	6.2
19	160080	99999	201410061800	180	3	***	***	SCT	*	*	*	6.2
20	160080	99999	201410061900	150	5	***	***	SCT	*	*	*	6.2
21	160080	99999	201410062000	150	5	***	39	BKN	*	*	*	6.2
22	160080	99999	201410062100	150	7	***	39	BKN	*	*	*	6.2
23	160080	99999	201410062200	140	6	***	39	BKN	*	*	*	6.2
24	160080	99999	201410062300	160	5	***	39	BKN	*	*	*	6.2

Table IV.1. Wind and sky cover data.

	13	14	15	16	17	18	19	20	21	22	23	24	25	26
0	MW	MW	MW	MW	AW	AW	AW	AW	W	TEMP	DEWP	SLP	ALT	STP
1	46	**	**	**	**	**	**	**	4	49	46	******	*****	854.8
2	44	**	**	**	**	**	**	**	4	48	45	******	*****	854.8
3	44	**	**	**	**	**	**	**	4	47	46	******	*****	854.8
4	44	**	**	**	**	**	**	**	4	47	44	******	*****	854.2
5	44	**	**	**	**	**	**	**	4	47	44	******	*****	854.0
6	44	**	**	**	**	**	**	**	4	47	45	******	*****	854.0
7	44	**	**	**	**	**	**	**	4	46	44	******	*****	854.1
8	46	**	**	**	**	**	**	**	4	46	44	******	*****	854.0
9	42	**	**	**	**	**	**	**	4	46	44	******	*****	854.1
10	10	**	**	**	**	**	**	**	4	48	46	******	*****	854.2
11	10	**	**	**	**	**	**	**	2	50	47	******	*****	854.0
12	10	**	**	**	**	**	**	**	2	52	45	******	*****	853.6
13	10	**	**	**	**	**	**	**	2	54	44	******	*****	853.7
14	10	**	**	**	**	**	**	**	2	55	42	******	*****	853.0
15	**	**	**	**	**	**	**	**	*	56	44	******	*****	852.5
16	**	**	**	**	**	**	**	**	*	54	43	******	*****	852.2
17	**	**	**	**	**	**	**	**	*	52	43	******	*****	852.0
18	**	**	**	**	**	**	**	**	*	51	42	******	*****	852.0
19	**	**	**	**	**	**	**	**	*	50	42	******	*****	851.9
20	**	**	**	**	**	**	**	**	*	50	44	******	*****	852.2
21	**	**	**	**	**	**	**	**	*	50	45	******	*****	852.5
22	**	**	**	**	**	**	**	**	*	49	44	******	*****	852.0
23	**	**	**	**	**	**	**	**	*	49	44	******	*****	852.8
24	**	**	**	**	**	**	**	**	*	48	45	******	*****	853.2

Table IV.2. Observed weather, temperature and pressure data.

	27	28	29	30	31	32	33
0	MAX	MIN	PCP01	PCP06	PCP24	PCPXX	SD
1	***	***	*****	0.00	*****	*****	**
2	***	***	*****	*****	*****	*****	**
3	***	***	*****	*****	*****	*****	**
4	***	***	*****	*****	*****	*****	**
5	***	***	*****	*****	*****	*****	**
6	***	***	*****	*****	*****	*****	**
7	***	46	*****	*****	*****	0.00	**
8	***	***	*****	*****	*****	*****	**
9	***	***	*****	*****	*****	*****	**
10	***	***	*****	*****	*****	*****	**
11	***	***	*****	*****	*****	*****	**
12	***	***	*****	*****	*****	*****	**
13	***	***	*****	0.00	*****	*****	**
14	***	***	*****	*****	*****	*****	**
15	***	***	*****	*****	*****	*****	**
16	***	***	*****	*****	*****	*****	**
17	***	***	*****	*****	*****	*****	**
18	***	***	*****	*****	*****	*****	**
19	56	***	*****	*****	*****	0.00	**
20	***	***	*****	*****	*****	*****	**
21	***	***	*****	*****	*****	*****	**
22	***	***	*****	*****	*****	*****	**
23	***	***	*****	*****	*****	*****	**
24	***	***	*****	*****	*****	*****	**

Table IV.3. Extreme temperature values and precipitation data.

IV.c. stn.txt file

The stn.txt file is a formatted file intended to identify and locate the NOAA stations.

Here a sample of stn.txt file for a selected number of Italian NOAA stations is reported.

USAF-WBAN_ID	STATION NAME	COUNTRY	STATE	LAT	LONG	ELEV
160080 99999	S. VALENTINO ALLA MUTA	ITALY		46.750	10.533	1461.0
160200 99999	BOLZANO	ITALY		46.460	11.326	240.5
160210 99999	ROLLE PASS	ITALY		46.300	11.783	2006.0
160220 99999	PAGANELLA MOUNTAIN	ITALY		46.150	11.033	2129.0

V. READ-WRITE NOAA DATA

In the following sections, the *read_NOAA.f90* automatic Fortran code for read-write P and T data from NOAA dat.txt file and the output file are reported.

Due to compatibility issue with Fortran's variable declaration, the symbol "*" appearing in dat.txt file has preventively been substituted with "99999".

V.a. read_NOAA.f90

The *read_NOAA.f90* Fortran code for automatically read and format the P and T data from NOAA stations is here reported.

The sentences coloured in blue are comments, written in order to make the code more understandable.

```
program read_NOAA

implicit none

! Variable declaration
integer :: i, istaz, j, idati, jstaz, kstaz, ora_prec, gg_prec, conta_T,
conta_P, k, ii, kk
integer :: id(50000), numid(50000), jd(50000), numjd(50000), ymdh(50000),
dir(50000), spd(50000), gus(50000), clg(50000), lc(50000), mc(50000),
hc(50000), mw1(50000), mw2(50000), mw3(50000), mw4(50000), aw1(50000),
aw2(50000), aw3(50000), aw4(50000), w(50000), maxt(50000), mint(50000),
y(50000), m(50000), d(50000), h(50000), minu(50000)
real:: lat(50000), lon(50000), elev(50000), vsb(50000), temp(50000),
dew(50000), slp(50000), alt(50000), stp(50000), prec1(50000), prec6(50000),
prec24(50000), precX(50000), sd(50000), stph(50000), temph(50000)
character(25) :: stn_name(500), country(500), state(500), skc(50000)

open(3,file='NOAA_temp.txt')
open(5,file='NOAA_pres.txt')
open(1,file='stn.txt')

! Read the stations info on stn.txt file
i=0
do i=i+1
  read(1,end=100) id(i), num(i), stn_name(i), country(i), state(i), lat(i),
  lon(i), elev(i)
end do
```

```
100 continue
! The number of stations equals the number of lines read on stn.txt file
istaz=i

open(2,file='dat.txt')
! Read the data on dat.txt file
j=0
do j=j+1
   read(2,end=200) jd(j), numjd(j), ymdh(j), dir(j), spd(j), gus(j), clg(j),
   skc(j), lc(j), mc(j), hc(j), vsb(j), mw1(j), mw2(j), mw3(j), mw4(j),
   aw1(j), aw2(j), aw3(j), aw4(j), w(j), temp(j), dew(j), slp(j), alt(j),
   stp(j), maxt(j), mint(j), prec1(j), prec6(j), prec24(j), precX(j), sd(j)
! Convert T from Fahrenheit to Kelvin
   if (temp(j).ne.99999) temp(j)=(temp(j)+459.67)/1.8
end do
200 continue
! The number of data equals the number of lines read on dat.txt file
idati=j

j=0
i=0
do i=i+1,istaz
   if (id(i).eq.jd(1)) go to 20
end do
20 jstaz=1
! Date conversion
do j=j+1,idati
   y(j)=ymdh(j)/100000000
   m(j)=(ymdh(j)-y(j)*100000000)
   m(j)=m(j)/1000000
   d(j)=(ymdh(j)-y(j)*100000000-m(j)*1000000)
   d(j)=d(j)/10000
   h(j)=(ymdh(j)-y(j)*100000000-m(j)*1000000-d(j)*10000)
   h(j)=h(j)/100
   minu(j)=(ymdh(j)-y(j)*100000000-m(j)*1000000-d(j)*10000-h(j)*100)
!  Round the minutes which differ from 0: minutes from 50 to 59 are
   approximated to 0 of the following hour (h=h+1), minutes from 1 to 10 are
   approximated to 0 of the present hour (h=h)
   if (minu(j).ge.50.and.minu(j).le.59) then
```

```
      minu(j)=0
      h(j)=h(j)+1
    end if
    if (minu(j).ge.1.and.minu(j).le.10) then
      minu(j)=0
      h(j)=h(j)
    end if
end do

!!!! PROCEDURE TO FILL IN THE GAPS AND SELECT TWO-HOURLY DATA !!!!
j=0
do j=j+1,idati
! Definition of previous hour (ora_prec) and previous day (gg_prec), to be
    compared with the actually read hour and day
    kstaz=0
    ora_prec=0
    gg_prec=d(1)
! conta_P and conta_T are counters used to automatically exclude the stations
    with a small amount of data (less than 80%) in the writing phase
    conta_P=0
    conta_T=0
! Writing instructions, to be applied if the actually read station differs
    from the previous
    if (jd(j+1).ne.jd(j)) then
      do k=jstaz,j
! Select only even hours
if (minu(k).eq.0.and.(mod(h(k),2).eq.0)) then
if (h(k).eq.h(k+1).and.d(k).eq.d(k+1).and.stp(k).gt.5000) go to 50
! Fill in the hour(s) gap if the currently read day is the last read
          if(d(k).eq.gg_prec) then
            do ii=ora_prec+2,h(k)-2,2
              kstaz=kstaz+1
              stph(kstaz)=99999
              temph(kstaz)=99999
              conta_P=conta_P+1
              conta_T=conta_T+1
            end do
            ora_prec=h(k)
            gg_prec=d(k)
```

```
            kstaz=kstaz+1
            stph(kstaz)=stp(k)
            temph(kstaz)=temp(k)
            if(stp(k).gt.5000) conta_P=conta_P+1
            if(temp(k).eq.99999) conta_T=conta_T+1
          else
! Fill in the hour(s) gap if the currently read day is NOT the last read
! Fill in the final hour(s) gap of the last read day (if present)
            do ii=ora_prec+2,22,2
              kstaz=kstaz+1
              stph(kstaz)=99999
              temph(kstaz)=99999
              conta_P=conta_P+1
              conta_T=conta_T+1
            end do
! Fill in the day(s) gap from the last read day to the actual (if present)
            do ii=gg_prec+1,d(k)-1,1
              do kk=0,22,2
                kstaz=kstaz+1
                stph(kstaz)=99999
                temph(kstaz)=99999
                conta_P=conta_P+1
                conta_T=conta_T+1
              end do
            end do
! Fill in the initial hour(s) gap of the actual day (if present)
            do ii=0,h(k)-2,2
              kstaz=kstaz+1
              stph(kstaz)=99999
              temph(kstaz)=99999
              conta_P=conta_P+1
              conta_T=conta_T+1
            end do
            ora_prec=h(k)
            gg_prec=d(k)
            kstaz=kstaz+1
            if(stp(k).gt.5000) conta_P=conta_P+1
            if(temp(k).eq.99999) conta_T=conta_T+1
            stph(kstaz)=stp(k)
```

```
            temph(kstaz)=temp(k)
          end if
end if
     50 end do
! Fill in the hour(s) gap between the last read hour and the final hour (22)
   for the final day
     if (h(j).lt.22) then
do ii=ora_prec+2,22,2
          kstaz=kstaz+1
          stph(kstaz)=99999
          temph(kstaz)=99999
          conta_P=conta_P+1
          conta_T=conta_T+1
end do
     end if
! Write on P and T files
     i=0
     do i=i+1,istaz
if (id(i).eq.jd(j)) go to 30
     end do
     30 if (conta_P.le.0.2*kstaz) then
write(5,3000) jd(j), stn_name(i), lat(i), lon(i), elev(i), stph(1:kstaz)
     end if
     if (conta_T.le.0.2*kstaz) then
write(3,3000) jd(j), stn_name(i), lat(i), lon(i), elev(i), temph(1:kstaz)
     end if
     jstaz=j+1
   end if
end do
close(2)
close(1)
close(5)
close(4)
close(3)

3000 format(i6,1x,a25,1x,f6.3,1x,f6.3,1x,f8.3,510(1x,f10.3))
end program
```

V.b. P and T output files

Pressure (Table V.1) and Temperature (Table V.2) output files for the first 5 P and T stations.
The columns correspond to station ID (column 1), station name (column 2), coordinates (columns 3-5), and data (columns 6-…).

ID	Name	Lat	Lon	Elev	00	02	04	...
160080	S. Valentino a Muta	46.75	10.53	1461	854.8	854.8	854.0	
160220	Paganella Mountain	46.15	11.03	2129	785.8	99999	785.2	
160520	Pian Rosa	45.93	7.70	3488	663.6	663.1	663.4	
160610	Torino	45.03	7.73	710	934.6	934.0	934.0	
160880	Ghedi	45.43	10.26	101.5	99999	99999	99999	

Table V.1. Pressure output file.

ID	Name	Lat	Lon	Elev	00	02	04	...
160080	S. Valentino a Muta	46.75	10.53	1461	282.6	281.5	281.5	
160083	Resia Pass	46.83	10.50	1800	99999	282.0	280.9	
160220	Paganella Mountain	46.15	11.03	2129	276.5	99999	275.9	
160520	Pian Rosa	45.93	7.70	3488	269.3	269.3	268.1	
160610	Torino	45.03	7.73	710	285.9	284.3	284.3	

Table V.2. Temperature output file.

VI. A SAMPLE OF RINEX FILE

A sample of the GENO2250.16d RINEX file is reported in the following. The RINEX file refers to GENO Permanent Station (Genova, Italy) on 12th August 2016. As the suffix "16d" suggests, it is a Hatanaka compressed file.

```
1.0                 COMPACT RINEX FORMAT                    CRINEX VERS   /
  TYPE
  RNX2CRX ver.4.0.7                       13-Aug-16 01:10     CRINEX PROG /
  DATE
   2.11           OBSERVATION DATA    G (GPS)             RINEX VERSION /
  TYPE
  teqc  2013Mar15                         20160813 01:03:26UTCPGM / RUN BY /
  DATE
  Linux2.4.20-8|i386|gcc|Win32-MinGW32|=                      COMMENT
  teqc  2016Apr1                          20160813 01:01:03UTCCOMMENT
  Linux 2.4.20-8|Pentium IV|gcc -static|Linux|486/DX+         COMMENT
  BIT 2 OF LLI FLAGS DATA COLLECTED UNDER A/S CONDITION       COMMENT
  GENO                                                        MARKER NAME
  12712M002                                                   MARKER NUMBER
  Automatic           ASI_e-geos                              OBSERVER /
  AGENCY
  220203888           TRIMBLE 4700        1.20                REC # / TYPE /
  VERS
  11730               TRM29659.00     NONE                    ANT # / TYPE
   4507893.6351   707622.0357  4441604.8112                 APPROX POSITION
  XYZ
   0.0000        0.0000        0.0000                  ANTENNA: DELTA H/E/N
   1     1                                              WAVELENGTH FACT
  L1/2
   7    L1    L2    C1    P1    P2    S1    S2            # / TYPES OF OBSERV
   17                                                     LEAP SECONDS
   SNR is mapped to RINEX snr flag value [0-9]               COMMENT
   L1 & L2: min(max(int(snr_dBHz/6). 0). 9)                  COMMENT
   2016     8    12     0     0    0.0000000     GPS         TIME OF FIRST
  OBS
   END OF HEADER
  &16  8 12  0  0  0.0000000  0  8G07G30G06G28G05G02G13G09
```

```
3&-67387176473 3&-52834048694 3&20822084391  3&20822078688 3&53000 3&45000
48474   4 4 4
3&-61362046711 3&-47792822009 3&20087392025  3&20087388548 3&53000 3&50000
48484   4 4 4
3&-51735494117 3&-40245284305 3&24886377765  3&24886379079 3&37000 3&18000
46434   4 4 4
3&-18429435402 3&-14614003529 3&23276710295  3&23276705016 3&44000 3&28000
47444   4 4 4
3&-33798074551 3&-26276561237 3&21084359671  3&21084354264 3&52000 3&44000
48474   4 4 4
3&-47515444793 3&-36998598898 3&22939007458  3&22939000433 3&45000 3&32000
47454   4 4 4
3&-10778207000 3&-8862852712 3&23096348763  3&23096342662 3&47000 3&29000
47444   4 4 4
3&-71649392187 3&-55792564153 3&23072270811  3&23072268448 3&45000 3&31000
47454   4 4 4
               3

-44004441 -34289182 -8373728  -8373727 0 0
-93305668 -72705704 -17755482  -17754983 -1000 0
12275722 9565471 2335963  2335217 -1000 2000
-186179004 -145074523 -35428769  -35428847 -1000 -1000
-143247254 -111621223 -27259023  -27258773 0 0
-20692781 -16124285 -3937677  -3937977 0 -2000
-176108684 -137227484 -33512441  -33510373 -1000 1000    5
-9439840 -7355742 -1796357  -1795977 0 -1000
             1 &
```

VII. A SAMPLE OF SITE LOG SHEET

The log sheet of GENO PS is reported in the following.

The file, compiled under the IGS's specifications, contains the site identification, documentation on monument and on eventual changes through time of receiver, antenna and other PS components. If the PS undergoes some modification, they have to be specified in the log sheet, which should be kept updated.

```
     GENO Site Information Form (site log)
     International GNSS Service
     See Instructions at:
       ftp://igscb.jpl.nasa.gov/pub/station/general/sitelog_instr.txt

0.   Form
     Prepared by (full name)  : Giuseppe Colucci
     Date Prepared            : 2016-03-01
     Report Type              : UPDATE
     If Update:
      Previous Site Log       : geno_20150803.log
      Modified/Added Sections : 3.5

1.   Site Identification of the GNSS Monument
     Site Name                : Genova - Istituto Idrografico della Marina
     Four Character ID        : GENO
     Monument Inscription     : Stable pillar on the roof
     IERS DOMES Number        : 12712M002
     CDP Number               :
     Monument Description     : PILLAR
       Height of the Monument : 1.2 m
       Monument Foundation    : CONCRETE BLOCK
       Foundation Depth       :
     Marker Description       : CHISELLED CROSS
     Date Installed           : 2001-08-22T00:00Z
     Geologic Characteristic  : BEDROCK
       Bedrock Type           : SEDIMENTARY
       Bedrock Condition      :
       Fracture Spacing       :
       Fault zones nearby     :
         Distance/activity    :
     Additional Information   :
```

```
2.   Site Location Information
     City or Town             : Genova
     State or Province        : LIGURIA
     Country                  : Italy
     Tectonic Plate           : EURASIAN
     Approximate Position (ITRF)
       X coordinate (m)       : 4507890.2717
       Y coordinate (m)       : 707618.9744
       Z coordinate (m)       : 4441603.0081
       Latitude (N is +)      : +442509.84
       Longitude (E is +)     : +0085515.96
       Elevation (m,ellips.)  : 137.0
     Additional Information   :

3.   GNSS Receiver Information
3.1  Receiver Type            : TRIMBLE 4000SSI
     Satellite System         : GPS
     Serial Number            : 21512
     Firmware Version         : 7.29
     Elevation Cutoff Setting : 15 deg
     Date Installed           : 1998-07-23T00:00Z
     Date Removed             : 2001-08-22T00:00Z
     Temperature Stabiliz.    : 20.0 +/-
     Additional Information   :
3.2  Receiver Type            : TRIMBLE 4000SSI
     Satellite System         : GPS
     Serial Number            : 32811
     Firmware Version         : Nav 7.19 Sig 3.04
     Elevation Cutoff Setting : 5 deg
     Date Installed           : 2001-08-22T00:00Z
     Date Removed             : 2002-08-12T00:00Z
     Temperature Stabiliz.    : 20.0 +/-
     Additional Information   :
3.3  Receiver Type            : TRIMBLE 4000SSI
     Satellite System         : GPS
     Serial Number            : 32257
     Firmware Version         : Nav 7.19 Sig 3.04
     Elevation Cutoff Setting : 5 deg
```

```
     Date Installed           : 2002-08-13T00:00Z
     Date Removed             : 2013-05-21T10:00Z
     Temperature Stabiliz.    : 20.0 +/-
     Additional Information   :
3.4  Receiver Type            : TRIMBLE 4700
     Satellite System         : GPS
     Serial Number            : 220203888
     Firmware Version         : Nav 1.20 Sig 0.00
     Elevation Cutoff Setting : 5 deg
     Date Installed           : 2013-05-21T14:00Z
     Date Removed             : 2015-08-03T12:35Z
     Temperature Stabiliz.    :
     Additional Information   :
3.5  Receiver Type            : TRIMBLE 4700
     Satellite System         : GPS
     Serial Number            : 220203888
     Firmware Version         : Nav 1.20
     Elevation Cutoff Setting : 0 deg
     Date Installed           : 2015-08-03T12:35Z
     Date Removed             : CCYY-MM-DDThh:mmZ
     Temperature Stabiliz.    :
     Additional Information   :
3.x  Receiver Type            : (A20, from rcvr_ant.tab; see instructions)
     Satellite System         : (GPS+GLO+GAL+BDS+QZSS+SBAS)
     Serial Number            : (A20, but note the first A5 is used in SINEX)
     Firmware Version         : (A11)
     Elevation Cutoff Setting : (deg)
     Date Installed           : (CCYY-MM-DDThh:mmZ)
     Date Removed             : (CCYY-MM-DDThh:mmZ)
     Temperature Stabiliz.    : (none or tolerance in degrees C)
     Additional Information   : (multiple lines)

4.   GNSS Antenna Information
4.1  Antenna Type             : TRM29659.00     NONE
     Serial Number            : 11730
     Antenna Reference Point  : BPA
     Marker->ARP Up Ecc. (m)  : 0.0000
     Marker->ARP North Ecc(m) : 0.0000
     Marker->ARP East Ecc(m)  : 0.0000
```

```
     Alignment from True N    : 0 deg
     Antenna Radome Type      : NONE
     Radome Serial Number     :
     Antenna Cable Type       : RG214
     Antenna Cable Length     : 30 m
     Date Installed           : 1998-07-23T00:00Z
     Date Removed             : CCYY-MM-DDThh:mmZ
     Additional Information   : On Feb 27, 2014 cable connector was replaced
                              : by a new one
4.x  Antenna Type             : (A20, from rcvr_ant.tab; see instructions)
     Serial Number            : (A*, but note the first A5 is used in SINEX)
     Antenna Reference Point  : (BPA/BCR/XXX from "antenna.gra"; see instr.)
     Marker->ARP Up Ecc. (m)  : (F8.4)
     Marker->ARP North Ecc(m) : (F8.4)
     Marker->ARP East Ecc(m)  : (F8.4)
     Alignment from True N    : (deg; + is clockwise/east)
     Antenna Radome Type      : (A4 from rcvr_ant.tab; see instructions)
     Radome Serial Number     :
     Antenna Cable Type       : (vendor & type number)
     Antenna Cable Length     : (m)
     Date Installed           : (CCYY-MM-DDThh:mmZ)
     Date Removed             : (CCYY-MM-DDThh:mmZ)
     Additional Information   : (multiple lines)

5.   Surveyed Local Ties
5.x  Tied Marker Name         :
     Tied Marker Usage        : (SLR/VLBI/LOCAL CONTROL/FOOTPRINT/etc)
     Tied Marker CDP Number   : (A4)
     Tied Marker DOMES Number : (A9)
     Differential Components from GNSS Marker to the tied monument (ITRS)
       dx (m)                 : (m)
       dy (m)                 : (m)
       dz (m)                 : (m)
     Accuracy (mm)            : (mm)
     Survey method            : (GPS
   CAMPAIGN/TRILATERATION/TRIANGULATION/etc)
     Date Measured            : (CCYY-MM-DDThh:mmZ)
     Additional Information   : (multiple lines)
```

```
6.   Frequency Standard
6.1  Standard Type            : INTERNAL
       Input Frequency        :
       Effective Dates        : 1998-07-23/CCYY-MM-DD
       Notes                  :
6.x  Standard Type            : (INTERNAL or EXTERNAL H-MASER/CESIUM/etc)
       Input Frequency        : (if external)
       Effective Dates        : (CCYY-MM-DD/CCYY-MM-DD)
       Notes                  : (multiple lines)

7.   Collocation Information
7.x  Instrumentation Type     : (GPS/GLONASS/DORIS/PRARE/SLR/VLBI/TIME/etc)
       Status                 : (PERMANENT/MOBILE)
       Effective Dates        : (CCYY-MM-DD/CCYY-MM-DD)
       Notes                  : (multiple lines)

8.   Meteorological Instrumentation
8.1.x  Humidity Sensor Model  :
       Manufacturer           :
       Serial Number          :
       Data Sampling Interval : (sec)
       Accuracy (% rel h)     : (% rel h)
       Aspiration             : (UNASPIRATED/NATURAL/FAN/etc)
       Height Diff to Ant     : (m)
       Calibration date       : (CCYY-MM-DD)
       Effective Dates        : (CCYY-MM-DD/CCYY-MM-DD)
       Notes                  : (multiple lines)
8.2.x  Pressure Sensor Model  :
       Manufacturer           :
       Serial Number          :
       Data Sampling Interval : (sec)
       Accuracy               : (hPa)
       Height Diff to Ant     : (m)
       Calibration date       : (CCYY-MM-DD)
       Effective Dates        : (CCYY-MM-DD/CCYY-MM-DD)
       Notes                  : (multiple lines)
8.3.x  Temp. Sensor Model     :
       Manufacturer           :
       Serial Number          :
```

```
       Data Sampling Interval : (sec)
       Accuracy               : (deg C)
       Aspiration             : (UNASPIRATED/NATURAL/FAN/etc)
       Height Diff to Ant     : (m)
       Calibration date       : (CCYY-MM-DD)
       Effective Dates        : (CCYY-MM-DD/CCYY-MM-DD)
       Notes                  : (multiple lines)
8.4.x  Water Vapor Radiometer :
       Manufacturer           :
       Serial Number          :
       Distance to Antenna    : (m)
       Height Diff to Ant     : (m)
       Calibration date       : (CCYY-MM-DD)
       Effective Dates        : (CCYY-MM-DD/CCYY-MM-DD)
       Notes                  : (multiple lines)
8.5.x  Other Instrumentation  : (multiple lines)

9.   Local Ongoing Conditions Possibly Affecting Computed Position
9.1.x  Radio Interferences    : (TV/CELL PHONE ANTENNA/RADAR/etc)
       Observed Degradations  : (SN RATIO/DATA GAPS/etc)
       Effective Dates        : (CCYY-MM-DD/CCYY-MM-DD)
       Additional Information : (multiple lines)
9.2.x  Multipath Sources      : (METAL ROOF/DOME/VLBI ANTENNA/etc)
       Effective Dates        : (CCYY-MM-DD/CCYY-MM-DD)
       Additional Information : (multiple lines)
9.3.x  Signal Obstructions    : (TREES/BUILDINGS/etc)
       Effective Dates        : (CCYY-MM-DD/CCYY-MM-DD)
       Additional Information : (multiple lines)

10.  Local Episodic Effects Possibly Affecting Data Quality
10.x Date                     : (CCYY-MM-DD/CCYY-MM-DD)
     Event                    : (TREE CLEARING/CONSTRUCTION/etc)

11.  On-Site, Point of Contact Agency Information
     Agency                   : e-geos S.p.A. - una societÃ  ASI/Telespazio
     Preferred Abbreviation   : TPZ
     Mailing Address          : P.O.BOX OPEN - 75100 Matera, ITALY
     Primary Contact
       Contact Name           : G. Colucci
```

```
      Telephone (primary)    : ++39.0835.377574
      Telephone (secondary)  :
      Fax                    :
      E-mail                 : giuseppe.colucci@e-geos.it
    Secondary Contact
      Contact Name           : R. Faccia, F. Ambrico
      Telephone (primary)    : ++39.0835.377540
      Telephone (secondary)  :
      Fax                    :
      E-mail                 : gpsgeo@hp835.mt.asi.it
    Additional Information   :

12. Responsible Agency (if different from 11.)
    Agency                   : Agenzia Spaziale Italiana
    Preferred Abbreviation   : ASI
    Mailing Address          : P.O.BOX OPEN - 75100 Matera, ITALY
    Primary Contact
      Contact Name           : Dott. Giuseppe Bianco
      Telephone (primary)    : ++39.0835.377509
      Telephone (secondary)  :
      Fax                    :
      E-mail                 : giuseppe.bianco@asi.it
    Secondary Contact
      Contact Name           :
      Telephone (primary)    :
      Telephone (secondary)  :
      Fax                    :
      E-mail                 :
    Additional Information   :

13. More Information
    Primary Data Center      : ASI
    Secondary Data Center    : BKG
    URL for More Information : http://geodaf.mt.asi.it/html/gps/info.html
    Hardcopy on File
      Site Map               :
      Site Diagram           :
      Horizon Mask           :
      Monument Description   :
```

Site Pictures :
Additional Information :
Antenna Graphics with Dimensions

TRM29659.00
Trimble L1/L2 Dorne Margolin element with chokerings
Model 29659.00

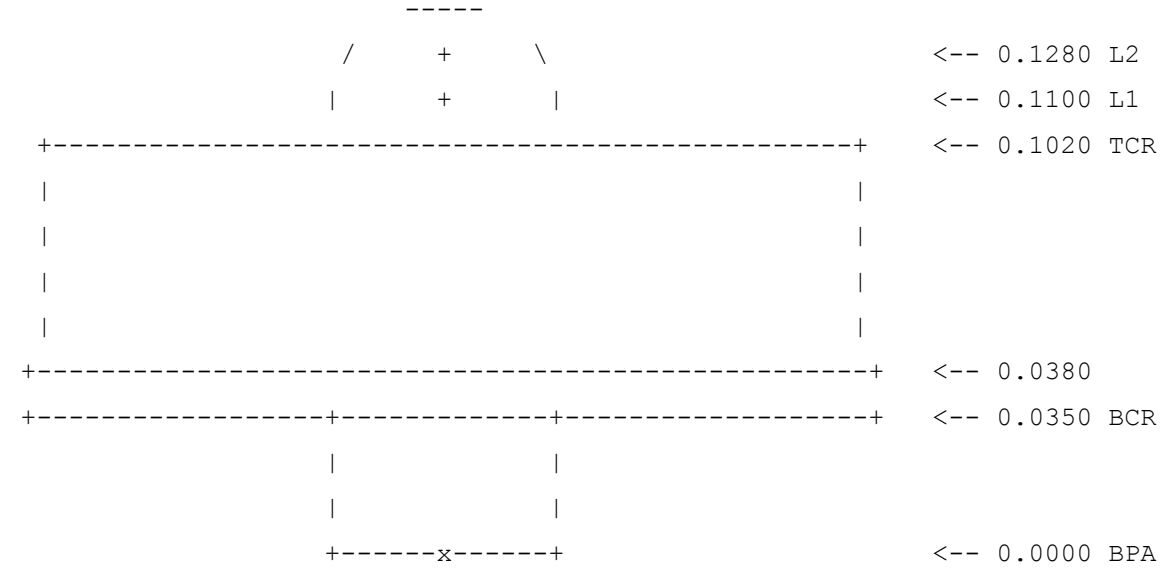

ARP: Antenna Reference Point

VIII. GAMIT CONTROL AND DATA FILES

In the following sections, the GAMIT control and data files will be reported and briefly commented and explained in their most important features. For further deepening, it is recommended to refer to GAMIT manual.

All the following are the files used in the updating of the ZTD DataBase and refer to 2015 for net1.

The symbol "#" indicates a comment.

VIII.a. process.defaults

The first section of the process.defaults file names the directories to be used for the processing.

```
# process.defaults
  #
  #  Do not remove any of these entries. To by-pass a function, set the value
  to null: ""
  ## LOCAL DIRECTORIES
  # Directory for translation of raw data
   set rawpth = "$procdir/raw"
  # Directory path for raw archives (search all levels)
   set rawfnd = ""
  # Input files for RINEX translators
   set mpth = "$procdir/mkrinex"
  # RINEX files directory
   set rpth = "$procdir/rinex"
  # Directory path for RINEX archives (search all levels)
   set rnxfnd = ""
  # Broadcast orbit directory
   set bpth = "$procdir/nav"
  # IGS files directory
   set ipth = "$procdir/igs"
  # G-files directory
   set gpth = "$procdir/gfiles"
  # GAMIT and GLOBK tables directory
   set tpth = "$procdir/tables"
  # Output gifs directory
   set gifpth = "$procdir/gifs"
  # Globk solution directory
   set glbpth = "$procdir/gsoln"
  # Globk binary h-file directory
```

```
 set glfpth = "$procdir/glbf"
# Directory path for other h-files (search all levels)
 set hfnd = ""
# Template files
 set templatepth = "$procdir/templates"
# Place to store temporary control files
 set cpth = "$procdir/control"
# Archive root directory (cannot be null)
 set archivepth = "$procdir/archive"
```

The session variables specify the sampling interval, number of epochs and the start time.

The next four entries allow to control how station.info and the lfile. are updated.

The rinex_ftpsites option specifies what remote archives are to be searched for RINEX files[115].

The minimum x-file size option allows to exclude from processing data from short sessions (the 300-block, i.e. 300 Kb on most machines, default limit corresponds to about 3 hours of tracking).

The search window options is helpful to look for RINEX files named with different doy from the one being processed, this assuring that no local data are missing. Setting these parameters to 0 helps in save time, if all data are within the expected 0-24h span.

```
##GAMIT
  # Set sampling interval, number of epochs, and start time for processing
   set sint = '30'
   set nepc = '2880'
   set stime = '0 0'
  # Variables for updating tables
   set stinf_unique = "-u"
   set stinf_nosort = "-nosort"
   set stinf_slthgt = "2.00"
  # Set "Y" to use RINEX header coordinates not in lfile or apr file
   set use_rxc = "N"
  # Broadcast orbits
   set brdc = 'brdc'
  # Minimum x-file size to be processed (Def. 300 blocks; most OS use 1 Kb
  blocks)
   set minxf = '300'
  # Set search window for RINEX files which might contain data for day -
  default check the previous day
   set rx_doy_plus = 0
```

115 Different archives can be added by editing gg/tables/ftp_info with the ftp specifications.

```
 set rx_doy_minus = 0
# Default globk .apr file
 set aprf = itrf08.apr
# Set compress (copts), delete (dopts) and archive (aopts) options.
# Possible d-, c-, and a- opts: D, H, ao, ac, as, b, c, d, e, g, h, i, j,
k, l, m, o, p, q, t, x, ps, all"
 set dopts = ( c x k p ao )
 set copts = ( D h )
 set aopts = ( h o q as D )
# Set the rinex ftp archives (defined in ftp_info) you would like to look
for data in.
# (Default archives searched are: sopac, cddis and unavco).
set rinex_ftpsites = (sopac cddis unavco kreiz igne bkge igni geodaf)
```

The resource settings prevent processing from starting if there is inadequate disk space to complete it.

```
## RESOURCES
# Minimum raw disk space in Kbytes
set minraw = '30000'
# Minimum RINEX disk space in Kbytes
set minrinex = '30000'
# Minimum archive disk space in Kbytes
set minarchive = '20000'
# Minimum working disk space in Kbytes
set minwork = '200000'
```

The only system-dependent setting likely to need changing is the path for the convert program, used to convert the sky plots from postscript to gif. It is also possible to indicate an email address to which to send the summary of elaboration.

```
## SYSTEM-DEPENDENT SETTINGS
# UNIX df command must be set to return the correct form set udf = 'df -k'
# UNIX mail command
#  Most machines
 set umail = 'mail -s'
#  HP
# set umail = 'mailx -s'
# Mail address for the processing report
 set mailto = 'ilaria.ferrando@edu.unige.it'
# Host name for email and anonymous ftp password use
 set machine = 'ujf-grenoble.fr'
# Ghostscript path
```

```
set gspath = '/usr/bin'
# ImageMagick path fir gif conversion
set impath = '/usr/bin/X11'
## Web interface .html file.
 set htmlinfo = 'mitnet.html'
```

VIII.b. sites.defaults

The header of the file explains the structure of the file and the options for getting the RINEX (ftp or local).

The blue comments are personal comment in the file, to be more exhaustive.

```
# File to control the use of stations in the processing
  # Format: site expt keyword1 keyword2 ...
  # where the first token is the 4- or 8-character site name (GAMIT uses
  # only 4 characters, GLOBK allows only 4 unless there are earthquakes or
  # renames), the second token is the 4-character experiment name, and the
  # remaining tokens, read free-format, indicate how the site is to be used #
  in the processing.
  # All sites for which there are RINEX files in the local directory will  #
  be used automatically and do not need to be listed.
  #
  # GAMIT:
  # ftprnx = sites to ftp from rinex data archives.
  # ftpraw = sites to ftp from raw data archives.
  # localrx = sites names used to search for rinex files on your local
  system.
  # required in conjunction with rnxfnd path variable set in
  process.defaults.
  # xstinfo = sites to exclude from automatic station.info updating.
  # xsite = sites to exclude from processing, all days or specified days
  # GLOBK:
  #  glrepu = sites used in the GLRED repeatability solution (default use
  all)
  #  glreps = sites used for reference frame definition (stabilization) in
  GLORG for the GLRED repeatabilitiy solution (default is IGS list)
  #  glts = sites to plot as time series from GLRED repeatability solution
  (default all)
  #
  # may use the following
```

```
# all_sites tubixstinfo
# individual station commands will override all_sites if they follow it
# 15 stations common for the 3 networks (6 IGS "CORE" stations + 7 IGS with
ITRF solution + 2 EUREF without ITRF sol (SJDV and TORI)
 brst_gps  net1 ftprnx xstinfo
 cagl_gps  net1 ftprnx xstinfo
 cag1_gps  net1 ftprnx xstinfo
 gras_gps  net1 ftprnx xstinfo
 graz_gps  net1 ftprnx xstinfo
 hers_gps  net1 ftprnx xstinfo
 mate_gps  net1 ftprnx xstinfo
 medi_gps  net1 ftprnx xstinfo
 pots_gps  net1 ftprnx xstinfo
 sfer_gps  net1 ftprnx xstinfo
 sjdv_gps  net1 ftprnx xstinfo
 tori_gps  net1 ftprnx xstinfo
 ucag_gps  net1 ftprnx xstinfo
 vill_gps  net1 ftprnx xstinfo
 wsrt_gps  net1 ftprnx xstinfo
 wtzr_gps  net1 ftprnx xstinfo
 zimm_gps  net1 ftprnx xstinfo
# 55 other stations (installed before day 162, 2004)
 acor_gps  net1 ftprnx  xstinfo
 aigl_gps  net1 ftprnx  xstinfo
 ajac_gps  net1 ftprnx  xstinfo
 alac_gps  net1 ftprnx  xstinfo
 axpv_gps  net1 ftprnx  xstinfo
 bann_gps  net1 ftprnx  xstinfo
 biel_gps  net1 ftprnx  xstinfo
 bret_gps  net1 ftprnx  xstinfo
 bscn_gps  net1 ftprnx  xstinfo
 bure_gps  net1 ftprnx  xstinfo
 cham_gps  net1 ftprnx  xstinfo
 chiz_gps  net1 ftprnx  xstinfo
 chrn_gps  net1 ftprnx  xstinfo
 chtl_gps  net1 ftprnx  xstinfo
 clap_gps  net1 ftprnx  xstinfo
 como_gps  net1 ftprnx  xstinfo
 ebre_gps  net1 ftprnx  xstinfo
```

```
eglt_gps  net1 ftprnx  xstinfo
esco_gps  net1 ftprnx  xstinfo
fclz_gps  net1 ftprnx  xstinfo
fjcp_gps  net1 ftprnx  xstinfo
geno_gps  net1 ftprnx  xstinfo
gina_gps  net1 ftprnx  xstinfo
gope_gps  net1 ftprnx  xstinfo
joux_gps  net1 ftprnx  xstinfo
lamp_gps  net1 ftprnx  xstinfo
lroc_gps  net1 ftprnx  xstinfo
mans_gps  net1 ftprnx  xstinfo
mars_gps  net1 ftprnx  xstinfo
mart_gps  net1 ftprnx  xstinfo
mdor_gps  net1 ftprnx  xstinfo
mich_gps  net1 localrx xstinfo
mlvl_gps  net1 ftprnx  xstinfo
moda_gps  net1 ftprnx  xstinfo
mtpl_gps  net1 ftprnx  xstinfo
nica_gps  net1 ftprnx  xstinfo
nice_gps  net1 ftprnx  xstinfo
not1_gps  net1 ftprnx  xstinfo
nova_gps  net1 ftprnx  xstinfo
opmt_gps  net1 ftprnx  xstinfo
pavi_gps  net1 ftprnx  xstinfo
pqrl_gps  net1 ftprnx  xstinfo
rabt_gps  net1 ftprnx  xstinfo
rabu_gps  net1 ftprnx  xstinfo
rg00_gps  net1 ftprnx  xstinfo
rstl_gps  net1 ftprnx  xstinfo
saan_gps  net1 ftprnx  xstinfo
sauv_gps  net1 ftprnx  xstinfo
smne_gps  net1 ftprnx  xstinfo
soph_gps  net1 ftprnx  xstinfo
stey_gps  net1 ftprnx  xstinfo
stj9_gps  net1 ftprnx  xstinfo
tenc_gps  net1 ftprnx  xstinfo
tetn_gps  net1 ftprnx  xstinfo
tlse_gps  net1 ftprnx  xstinfo
wlbh_gps  net1 ftprnx  xstinfo
```

Among all the stations in net1, only MICH needs the RINEX to be downloaded manually (as `localrx` token suggests), while all the other stations have publicly available ftp sites containing their RINEX.

VIII.c. station.info

All of the receiver and antenna information specific to a particular site occupation is recorded in station.info. The values entered correspond to a single occupation, of either one day or a series of days. Each of the data columns must be exactly the width shown and be separated by two spaces.
Due to the hgh number of column, the station.info has been split into three files; for improved readability, the first column containing the line number has been inserted (it is not present in station.info).
The first six entries are almost always included as shown: `SITE` is the 4-character code for the observing site, `Station Name` is a 16-character description, `Session Start` and `Session Stop` are the start/stop times for the entries, `Ant Ht` is the antenna height above the monument, and `HtCod` indicates what physical point on the antenna structure the height refers to and whether it is a direct or slant height.
The code `9999 999 0 0` in `Session Stop` means that means that since the date in `Session Start` no further modification occurred.

```
  # Station.info written by MSTINF user ilaria          on 2015-10-29  18:10
  * Reference file : station.info
  * Merged station.info file : all.station.info
  *
  *SITE  Station Name    Session Start      Session Stop       Ant Ht   HtCod
 1 ACCE  Acceglio        2009 278 16  0  0  9999 999  0  0  0   0.0000  DHARP
 2 ACOR  A Coruna        1998 340 10 10  0  2001 353  0  0  0   3.0420  DHARP
 3 ACOR  A Coruna        2001 353  0  0  0  2004 106  0  0  0   3.0420  DHARP
 4 ACOR  A Coruna        2004 106  0  0  0  2007  76 23 59  0   3.0420  DHARP
 5 ACOR  A Coruna        2007  77  0  0  0  2008 112  9  0  0   3.0460  DHARP
 6 ACOR  A Coruna        2008 112  9 30  0  2008 340 12 30  0   3.0460  DHARP
 7 ACOR  A Coruna        2008 340 12 30  0  2010  33  9 30  0   3.0460  DHARP
 8 ACOR  A Coruna        2010  34  0  0  0  2010  42  9  0  0   3.0460  DHARP
 9 ACOR  A Coruna        2010  43  0  0  0  2010 165  8 59  0   3.0460  DHARP
10 ACOR  A Coruna        2010 165  9  0  0  2010 179 12  0  0   3.0460  DHARP
11 ACOR  A Coruna        2010 180  0  0  0  2010 202  9  0  0   3.0460  DHARP
12 ACOR  A Coruna        2010 202  9  0  0  2011 140 10 11  0   3.0460  DHARP
13 ACOR  A Coruna        2011 140 10 20  0  2011 144 11 15  0   3.0460  DHARP
14 ACOR  A Coruna        2011 144 11 32  0  2011 298  8  0  0   3.0460  DHARP
15 ACOR  A Coruna        2011 298  8  0  0  2012 347 13 28  0   3.0460  DHARP
16 ACOR  A Coruna        2012 347 13 41  0  9999 999  0  0  0   3.0460  DHARP
17 AGDE  Cap d'Agde pur  2006 247 12  0  0  9999 999  0  0  0   0.0000  DHARP
```

18	AGNE	Lago Agnel	2005	242	12	0	0	9999	999	0	0	0	0.0000	DHARP
19	AIGE	INTERNAT AI	2009	138	0	0	0	2009	154	10	12	0	0.0000	DHARP
20	AIGE	INTERNAT AI	2009	154	10	12	0	2010	190	7	55	0	0.0000	DHARP
21	AIGE	INTERNAT AI	2010	190	7	55	0	2011	7	7	45	0	0.0000	DHARP
22	AIGE	INTERNAT AI	2011	7	7	45	0	2011	318	9	0	0	0.0000	DHARP
23	AIGE	INTERNAT AI	2011	318	9	0	0	2012	117	18	15	0	0.0000	DHARP
24	AIGE	INTERNAT AI	2012	117	18	15	0	2014	121	14	15	0	0.0000	DHARP
25	AIGE	INTERNAT AI	2014	121	14	15	0	2015	107	8	0	0	0.0000	DHARP
26	AIGE	INTERNAT AI	2015	107	8	0	0	2015	173	7	15	0	0.0000	DHARP
27	AIGE	INTERNAT AI	2015	173	7	15	0	2015	236	5	40	0	0.0000	DHARP
28	AIGE	INTERNAT AI	2015	236	5	40	0	9999	999	0	0	0	0.0000	DHARP

The following entries refer to the antenna coordinates (if provided) and specify the receiver type and version, the software version, which is used for filtering sample time, and the receiver serial number, as indicated on the station log sheet.

	Ant N	Ant E	Receiver Type	Vers	SwVer	Receiver SN
1	0.0000	0.0000	LEICA GRX1200PRO	7.53	7.53	355247
2	0.0000	0.0000	ASHTECH UZ-12	UE00-0A12	9.73	00224
3	0.0000	0.0000	ASHTECH UZ-12	ZC00	9.92	12109
4	0.0000	0.0000	ASHTECH UZ-12	ZC00	9.92	12110
5	0.0000	0.0000	LEICA GRX1200PRO	5.00	5.00	459187
6	0.0000	0.0000	LEICA GRX1200PRO	5.62	5.62	459187
7	0.0000	0.0000	LEICA GRX1200PRO	6.02	6.02	459187
8	0.0000	0.0000	LEICA GRX1200PRO	7.53	7.53	459187
9	0.0000	0.0000	LEICA GRX1200PRO	7.80	7.80	459187
10	0.0000	0.0000	LEICA GRX1200PRO	7.80/2.125	7.80	459187
11	0.0000	0.0000	LEICA GRX1200PRO	8.00/2.125	8.00	459187
12	0.0000	0.0000	LEICA GRX1200PRO	8.00/2.125	8.00	459187
13	0.0000	0.0000	LEICA GRX1200PRO	8.10/2.125	8.10	459187
14	0.0000	0.0000	LEICA GRX1200PRO	8.20/2.125	8.20	459187
15	0.0000	0.0000	LEICA GRX1200PRO	8.20/2.125	8.20	459187
16	0.0000	0.0000	LEICA GRX1200PRO	8.20/2.127	8.20	459187
17	0.0000	0.0000	TRIMBLE NETRS	1.1-3	1.13	4603204324
18	0.0000	0.0000	LEICA GRX1200PRO	7.53	7.53	453323
19	0.0000	0.0000	TRIMBLE NETR5	Nav 3.64	3.64	4649K03417
20	0.0000	0.0000	TRIMBLE NETR5	Nav 4.03	4.03	4649K03417
21	0.0000	0.0000	TRIMBLE NETR5	4.15	4.15	4649K03417
22	0.0000	0.0000	TRIMBLE NETR5	4.19	4.19	4649K03417
23	0.0000	0.0000	TRIMBLE NETR5	4.43	4.43	4649K03417

```
24 0.0000  0.0000  TRIMBLE NETR5     4.48                    4.48  4649K03417
25 0.0000  0.0000  TRIMBLE NETR5     4.85                    4.85  4649K03417
26 0.0000  0.0000  TRIMBLE NETR9     4.85                    4.85  5448R50073
27 0.0000  0.0000  TRIMBLE NETR9     5.01                    5.01  5448R50073
28 0.0000  0.0000  TRIMBLE NETR9     5.03                    5.03  5448R50073
```

Finally, the antenna and dome type are defined, together with the antenna serial number, as reported in the station log sheet.

```
 Antenna Type     Dome   Antenna SN
 1 LEIAT504         LEIS   104072
 2 ASH700936D_M     SNOW   16122
 3 ASH700936D_M     SNOW   16122
 4 ASH700936D_M     SNOW   16122
 5 LEIAT504         LEIS   103033
 6 LEIAT504         LEIS   103033
 7 LEIAT504         LEIS   103033
 8 LEIAT504         LEIS   103033
 9 LEIAT504         LEIS   103033
10 LEIAT504         LEIS   103033
11 LEIAT504         LEIS   103033
12 LEIAT504         LEIS   103033
13 LEIAT504         LEIS   103033
14 LEIAT504         LEIS   103033
15 LEIAT504         LEIS   103033
16 LEIAT504         LEIS   103033
17 TRM41249.00      TZGD   CRN 19995007
18 LEIAT504         LEIS   102721
19 TRM55971.00      NONE   30318081
20 TRM55971.00      NONE   30318081
21 TRM55971.00      NONE   30318081
22 TRM55971.00      NONE   30318081
23 TRM55971.00      NONE   30318081
24 TRM55971.00      NONE   30318081
25 TRM55971.00      NONE   30318081
26 TRM59800.00      NONE   5347354897
27 TRM59800.00      NONE   5347354897
28 TRM59800.00      NONE   5347354897
```

VIII.d. .apr

A sample of .apr file is here reported. The columns correspond to: name of the stations (column 1), coordinates (columns 2-4) and velocities (columns 5-8) at a specified epoch (column 9).

```
 OPMT_GPS  4202777.36946   171368.00214  4778660.20474   -0.01250
0.01783    0.01075 2005.149
 TLSE_GPS  4627851.83091   119640.01650  4372993.55345   -0.01136
0.01925    0.01207 2005.000
 TLSE_2PS  4627851.82824   119640.02010  4372993.55185   -0.01136
0.01925    0.01207 2005.000
 TOUL_GPS  4627846.02934   119629.33310  4372999.81790   -0.01136
0.01925    0.01207 2005.000
 BELL_GPS  4775849.44184   116814.28467  4213018.91380   -0.01017
0.01883    0.01266 2000.599
 SHEE_GPS  3983074.30919    51683.15905  4964639.78355   -0.01239
0.01688    0.01060 2003.976
 EBRE_GPS  4833520.20277    41537.01134  4147461.49520   -0.01081
0.01952    0.01236 2000.423
 EBRE_2PS  4833520.18487    41537.04945  4147461.51248   -0.01081
0.01952    0.01236 2002.006
 HERS_GPS  4033470.11053    23672.88716  4924301.31367   -0.01296
0.01673    0.01044 2005.000
 HERS_2PS  4033470.10935    23672.89232  4924301.31500   -0.01296
0.01673    0.01044 2005.000
 HERS_3PS  4033470.10841    23672.89106  4924301.30980   -0.01296
0.01673    0.01044 2005.000
 HERS_4PS  4033470.11463    23672.90952  4924301.32542   -0.01296
0.01673    0.01044 2005.000
 HERS_5PS  4033470.10727    23672.88987  4924301.31277   -0.01296
0.01673    0.01044 2005.000
 HERT_GPS  4033460.92389    23537.79811  4924318.25560   -0.01296
0.01673    0.01044 2005.000
 HERT_2PS  4033460.91994    23537.80024  4924318.25515   -0.01296
0.01673    0.01044 2005.000
```

VIII.e. lfile.

A sample of lfile. is here reported. The columns correspond to: name of the stations (column 1), coordinates (columns 2-4) and velocities (columns 5-8) at a specified epoch (column 9).

```
 OPMT_GPS  4202777.36946   171368.00214  4778660.20474   -0.01250
0.01783    0.01075 2005.149
 TLSE_GPS  4627851.83091   119640.01650  4372993.55345   -0.01136
0.01925    0.01207 2005.000
 TLSE_2PS  4627851.82824   119640.02010  4372993.55185   -0.01136
0.01925    0.01207 2005.000
 TOUL_GPS  4627846.02934   119629.33310  4372999.81790   -0.01136
0.01925    0.01207 2005.000
 BELL_GPS  4775849.44184   116814.28467  4213018.91380   -0.01017
0.01883    0.01266 2000.599
 SHEE_GPS  3983074.30919    51683.15905  4964639.78355   -0.01239
0.01688    0.01060 2003.976
 EBRE_GPS  4833520.20277    41537.01134  4147461.49520   -0.01081
0.01952    0.01236 2000.423
 EBRE_2PS  4833520.18487    41537.04945  4147461.51248   -0.01081
0.01952    0.01236 2002.006
 HERS_GPS  4033470.11053    23672.88716  4924301.31367   -0.01296
0.01673    0.01044 2005.000
 HERS_2PS  4033470.10935    23672.89232  4924301.31500   -0.01296
0.01673    0.01044 2005.000
 HERS_3PS  4033470.10841    23672.89106  4924301.30980   -0.01296
0.01673    0.01044 2005.000
 HERS_4PS  4033470.11463    23672.90952  4924301.32542   -0.01296
0.01673    0.01044 2005.000
 HERS_5PS  4033470.10727    23672.88987  4924301.31277   -0.01296
0.01673    0.01044 2005.000
```

VIII.f. sestbl.

In the sestbl. the parameters to be used for elaboration are set. For extended explanation, refer to GAMIT manual. A space starting a line means that the line is a comment and it is not used for elaboration. All the lines of advanced options (optional controls) are commented.

```
Session Table

  Processing Agency = LGI

  Satellite Constraint = Y         ; Y/N  (next two lines are free-format but
                                          'all' must be present)
                 all       a      e      i     n       w       M     rad1
```

```
rad2  rad3  rad4  rad5  rad6  rad7  rad8  rad9;
                          0.01  0.01   0.01   0.01    0.01    0.01   0.01
0.01  0.01  0.01  0.01  0.01  0.01  0.01  0.01

Choice of Experiment = RELAX.    ; BASELINE/RELAX./ORBIT
Type of Analysis = 1-ITER        ; 1-ITER/0-ITER (no postfit autcln)/PREFIT

   This now redundant AUTCLN Postfit = R             ; R causes repeat run.
Choice of Observable = LC_AUTCLN ; L1_SINGLE/L1&L2/L1_ONLY/L2_ONLY/LC_ONLY/
                                 ; L1,L2_INDEPEND./LC_HELP/LC_AUTCLN
Station Error = ELEVATION 10 5   ; 1-way L1, a**2 + (b**2)(L**2) in mm,
ppm,                                        default = 10. 0.
Use N-file = Y                   ; Y/N (default no): automatic procedure to
                                       reweight by station
AUTCLN Command File = autcln.cmd ; Filename; default none (use default
options)
Decimation Factor = 1            ; FOR SOLVE, default = 1
Quick-pre decimation factor = 1  ; 1st iter or autcln pre, default same as
                                       Decimation Factor
Quick-pre observable = LC_ONLY   ; for 1st soln, default same as Choice of
                                       observable

Ionospheric Constraints =  0.0 mm + 8.00 ppm
Ambiguity resolution WL = 0.15 0.15 1000. 99. 500.   ; used for LC_HELP
only
Ambiguity resolution NL = 0.15 0.15 1000. 99. 15000. ; Allow long baselines
with                                                              LC_AUTCLN

Zenith Delay Estimation = Y     ; Yes/No  (default No)
Interval zen = 2                ; 2 hrs = 13 knots/day
Zenith Constraints = 0.50       ; zenith-delay a priori constraint in
meters
Zenith Variation = 0.03 100.    ; zenith-delay variation, tau in
                                            meters/sqrt(hr), hrs (default
.02 100.)
Elevation Cutoff = 0            ; default 0 to use value in autcln.cmd
Atmospheric gradients = Y       ; Yes/Np  (default No)
Number gradients = 8            ; number of gradient parameters per day (NS
or                               ES); default 1
```

```
Gradient Constraints = 0.03     ; gradient at 10 deg elevation in meters;
                                        default 0.03 m
     Gradient Variation = .03 100    ; gradient variation

Update T/L files = L_ONLY       ; T_AND_L (default), T_ONLY, L_ONLY, NONE
Update tolerance = .3           ; minimum adjustment for updating L-file
                                        coordinates, default .3 m

Met obs source = GPT 50  ufile        ; hierarchical list:  RNX ufile
GPT/STP                                       [humid value]; default GTP 50

Output met = N                  ; write the a priori met values to a z-file
Use met.list = N
Use met.grid = N
DMap = GMF                      ; GMF(default)/NMFH/VMF1
WMap = GMF                      ; GMF(default)/NMFW/VMF1
Use map.list = N
Use map.grid = N
Yaw Model = Y                   ; Y/N  default = Y
Radiation Model for ARC = BERNE
Inertial frame = J2000
Tides applied = 31              ;  Binary coded: 1 earth  2 freq-dep  4
pole  8                                ocean  16 remove mean for pole tide

                                ;  32 atmosphere ;  default = 31
Use otl.list = N
Use otl.grid = Y
Use atl.list = N
Use atl.grid = N
Etide model = IERS03            ; IERS96/IERS03
Apply atm loading = Y           ; Y/N for atmospheric loading
Use atml.list = N
Use atml.grid = Y
Antenna Model = AZEL            ; NONE/ELEV/AZEL  default = ELEV
SV antenna model = ELEV         ; NONE/ELEV       default = NONE
SV antenna off = N              ; Y/N to estimate satellite antenna offsets

Delete AUTCLN input C-files = Y ; Y/N ; default Y to force rerun of MODEL
                                 Scratch directory = /tmp
```

```
Optional controls:

  Inertial frame = B1950          ; B1950/J2000 (default = J2000)

  Initial ARC                     ; Y/N  default = Yes
  Final ARC                       ; Y/N  default = No
  Radiation Model for ARC         ; SPHRC/BERNE/SRDYB/SVBDY  default =
SPHRC
  Reference System for ARC        ; WGS72/WGS84/MERIT/IGS92 (default =
IGS92)
  Tabular interval for ARC        ; 900. seconds (new default), 1350.
seconds
  Stepsize for ARC                ; 75. seconds (new default), 168.75
seconds

  Earth Rotation                  ; Diurnal/Semidirunal terms: Binary
coded:                                      1=pole 2=UT1 4=Ray model;
default=7
  Estimate EOP                    ; Binary coded: 1 wob  2 ut1 4 wob rate
8                                 ut1 rate
  Wobble Constraint = 3. 0.3      ; Default 3. (arcsec) 0.3 (arcsec/day)
  UT1 Constraint = 0.00002 0.02   ; Default .00002 (sec) 0.02 (sec/day)

  Number Zen = 4                  ; number of zenith-delay parameters
  Zenith Constraints = 0.50       ; zenith-delay a priori constraint in m
  Zenith Model = PWL              ; PWL (piecewise linear)/CON (step)
  Zenith Variation = 0.02 100.    ; zenith-delay variation, tau in
                                        meters/sqrt(hr), hrs
  Gradient Constraints = 0.03     ; gradient at 10 deg elevation in meters

  Gradient Variation = .01 100    ; gradient variation
  Tropospheric Constraints = NO   ; YES/NO   (spatial constraint)

  Antenna Model                   ; NONE/ELEV/AZEL  default = NONE
  Tide Model                      ; Binary coded: 1 earth 2 freq-dep 4 pole
8                                 ocean   default = 15
  Yaw Model                       ; YES/NO  default = YES
  I-file = N                      ; Use I-file (Y/N)  (default Y)
```

```
  AUTCLN Postfit = Y              ; Assume 'Y' if 'Type of analysis = 1-
ITER'                                 (autcln.cmd.postfit file also)
  Delete AUTCLN input C-files = Y ; YES/NO/Intermediate (default no)
  Quick-pre observable = LC       ; For 1st iter or autcln pre
  AUTCLN Command File             ; Filename; default none
  Delete eclipse data = POST      ; ALL/NO/POST (Default = NO)
  SCANDD control                  ; BOTH (default) /NONE/FIRST/FULL/IFBAD
see                                   manual sec. 5.2
  Iteration                       ; CFILES / XFILES (default)
  Edit AUTCLN Command File        ; YES/NO; default = NO (no longer needed)

  Ambiguity resolution WL         ; default = 0.15 0.15 1000.  10. 500.
  Ambiguity resolution NL         ; default = 0.15 0.15 1000.  10. 500.
  Type of Biases                  : IMPLICIT (default for quick), EXPLICIT
                                        (default for full)
  H-file solutions                ; ALL ; LOOSE-ONLY
  Station Error = BASELINE 10. 0.  ; 1-way L1, a**2 + (b**2)(L**2) in mm,
                                        ppm, default = 10. 0.
  Station Error = UNIFORM 10.       ; 1-way L1 in mm, default = 10.
  Station Error = ELEVATION 4.3 7.0 ; 1-way L1 , a**2 + b**2/sin(elev)**2
in                                      mm, default = 4.3 7.0
  Satellite Error = UNIFORM 0.      ; 1-way L1 in mm (added quadratically
to                                      station error) default = 0.
  Select Epochs                   ; Enter start and stop epoch number
                                              (applies only to SOLVE)
  Decimation Factor               ; FOR SOLVE, default = 1
  Quick-pre decimation factor = 10 ; 1st iter or autcln pre, default same
as                                      Decimation Factor
  Elevation Cutoff = 15.          ; For SOLVE, overrides the MODEL or
AUTCLN                                      values if they are lower
  Correlation print               ; Threshhold for printing correlations
                                        (default 0.9999)

  Export Orbits                   ; YES/NO  default = NO
  Orbit id                        ; 4-char code read only if Export Orbits
=                                       YES
  Orbit Format                    ; SP1/SP3 (NGS Standard Products)
  Orbit organization              ; 3-char code read only if Export Orbits
```

```
=                                        YES
  Reference System for Orbit = ITR93 ; ITR92/ITR91/ITR90/WGS84/MERIT
  Lunar eclipses = Y               ; Set = N to turn off lunar eclipses in
                                        ARC to match model of GAMIT < 10.2

  Delete all input C-files        ; YES/NO  default = NO
  Delete MODEL input C-files      ; YES/NO  default = NO
  Delete AUTCLN input C-files     ; YES/NO  default = NO
  Update T/L files                ; T_AND_L (default), T_ONLY, L_ONLY, NONE

  Update tolerance                ; minimum adjustment for updating L-file
                                        coordinates, default .3 m
  SOLVE-only = YES                ; YES/NO  default = NO
  X-compress = YES                ; Uncompress/compress X-files  default N

  SCANDD control                  ; FULL (default), FIRST, BOTH, IFBAD,
NONE
  Run CTOX = YES                  ; Make clean X-files from C-files default
N
  Bias apriori = 100.             ; Optional constraint on biases for
                                              LC_AUTCLN
  SOLVE print  = Y                ; Turn on SOLVE output to screen
```

VIII.g. sittbl.

The sittbl. contains options that can be set on a station-by-station basis. The following extract contains the a priori station constraints to be applied in GAMIT to enhance ambiguity resolution.

```
SITE              FIX    --COORD.CONSTR.--
        << default for regional stations >>
  ALL               NNN    100.  100.   100.
        << IGS core stations >>
  VILL VILL_GPS     NNN    0.005 0.005  0.01
  MATE MATE_GPS     NNN    0.005 0.005  0.01
  GRAZ GRAZ_GPS     NNN    0.005 0.005  0.01
  POTS POTS_GPS     NNN    0.005 0.005  0.01
  WTZR WTZR_GPS     NNN    0.005 0.005  0.01
  WSRT WSRT_GPS     NNN    0.005 0.005  0.01
```

VIII.h. autcln.cmd

The final control file for GAMIT is autcln.cmd. It is complicated but can almost always be left unchanged. Cases for which the default settings have to be modified include data from codeless receivers, stations with poorly precise a priori coordinates (not better than 10 m), or short sessions (< ~3 hours).

```
* This group must be first
eq_file ../tables/itrf08_com.eq
make_svs ../tables/sat1.apr
com_file comb.com
srt_file comb.srt
sol_file comb.sol
* File(s) for a priori coordinates
apr_file ../tables/itrf08_comb.apr
* Earth-rotation values (not needed if pmu free in final combination)
x in_pmu ../tables/pmu.usno
* Sites to include in the solution (default is all)
use_site clear
use_site mate ankr_gps kit3 nico sofi zwen kant
use_site -zwen
* (1) Max chi**2,(2) Max prefit diff,(3) Max rotation;defaults are 100 10000
10000
max_chi 30 50 2000.0
* Apply the pole tide whenever not applied in GAMIT
app_ptid ALL
* Invoke glorg for stabilization
org_cmd glorg_comb.cmd
org_opt PSUM GDLF CMDS
* Set minimal globk print options since using glorg output
prt_opt NOPR
* Allow the network to be loose since using glorg for stabilization
apr_neu all 10 10 10 0 0 0
* Satellites are loose if using global data - ignored if GAMIT BASELINE mode
x apr_svs all 100 100 100 10 10 10 1R
* but tight if GAMIT RELAX mode and not combining with global data
x apr_svs all .05 .05 .05 .005 .005 .005 .01 .01 FR
* EOP loose if estimating rotation in glorg
apr_ut1 100 10
apr_wob 100 100 10 10
* but tight if estimating only translation in glorg
```

```
x apr_ut1 .25 .1
x apr_wob .25 .25 .1 .1
* UT1 loose if orbits fixed
apr_ut1
* Write out an h-file if needed for future combinations
x out_glb H------.GLX
```

IX. GAMIT BASH SCRIPTS

In the following paragraphs, several bash scripts to control GAMIT elaboration are presented.
The bash script to automatically download RINEX data (*prepare_rinex*) is reported in section IX.a; the bash script to prepare GAMIT command files (*prepare_gamit*) is reported in section IX.b, whereas one of its output files can be found in IX.c.
The section IX.d is dedicated to the script (*extract_atm*) to extract the atmospheric parameters, ZTDs and gradients. The three output files are reported in sections IX.e, IX.f and IX.g.

IX.a. *prepare_rinex*

The prepare_rinex bash script is intended to download local RINEX files from archives. It has originally been written by Laurent Labbouz and slightly modified.
The code reported as example allows to download the RINEX data of year 2012 for MICH PS (Saint Michel l'Observatoire, France), which is the only PS in net1 with local RINEX data.

```
#!/bin/bash
for i in {1..365}
do
sh_get_rinex -archive kreiz -yr 2012 -doy $i -sites mich
done
```

IX.b. *prepare_gamit*

The *prepare_gamit* bash script is intended to produce multiple output files which can be run in parallel with the aim to optimize time. The code simply divides each year (2015, in this example) in 30 doys[116] slots; the *sh_gamit* commands related to these doys will be written as separated lines in the corresponding output file (named run.XX, with XX from 1 to 12).

```
#!/bin/bash
  for dd in {1..29}
  do
  echo "sh_gamit -orbit IGSF -expt net1 -eops usno -d 2015 $dd > test$dd.out
  " >> run.1
  done

for dd in {30..59}
  do
```

116 Apart from the first output file, which is made of 29 doys, and the last output file, which is made of 36 doys or 37 doys for leap years.

```
  echo "sh_gamit -orbit IGSF -expt net1 -eops usno -d 2015 $dd > test$dd.out
  " >> run.2
  done
...
for dd in {330..365}
  do
  echo "sh_gamit -orbit IGSF -expt net1 -eops usno -d 2015 $dd > test$dd.out
  " >> run.12
  done
```

IX.c. *prepare_gamit* output file

The following is a sample of one of the run.XX files produced by *prepare_gamit*. The file is a simple list of *sh_gamit* commands, one for each line of the file.

```
sh_gamit -orbit IGSF -expt net1 -eops usno -d 2015 90 > test090.out
sh_gamit -orbit IGSF -expt net1 -eops usno -d 2015 91 > test091.out
sh_gamit -orbit IGSF -expt net1 -eops usno -d 2015 92 > test092.out
sh_gamit -orbit IGSF -expt net1 -eops usno -d 2015 93 > test093.out
sh_gamit -orbit IGSF -expt net1 -eops usno -d 2015 94 > test094.out
sh_gamit -orbit IGSF -expt net1 -eops usno -d 2015 95 > test095.out
sh_gamit -orbit IGSF -expt net1 -eops usno -d 2015 96 > test096.out
sh_gamit -orbit IGSF -expt net1 -eops usno -d 2015 97 > test097.out
sh_gamit -orbit IGSF -expt net1 -eops usno -d 2015 98 > test098.out
sh_gamit -orbit IGSF -expt net1 -eops usno -d 2015 99 > test099.out
sh_gamit -orbit IGSF -expt net1 -eops usno -d 2015 100 > test100.out
```

IX.d. *extract_atm*

The *extract_atm* bash script is intended to extract ZTDs and gradients from GAMIT O-file. It has originally been written by Laurent Labbouz. It firstly creates a folder (net1_atm, in the example) where to store the data, then reads the PS names from an ancillary file (st_liste_net1.txt) containing the names of the PS, extracts ZTDs and gradients from the O-file for every day of every year, and produces three output files (.az, .ns, .ew).

```
#!/bin/bash
  mkdir net1_atm

  while read st ; do
  echo $st
```

```
  for i in {1998..2015}

do
for j in {1..366} ; do
  b=`printf %03d $j`

  if [ -f /data/gps/gamit/hymex/net1/$i/$b/onet1a.$b ] ; then

  grep 'ATM_ZEN R' /data/gps/gamit/hymex/net1/$i/$b/onet1a.$b | grep -i $st |
  cut -c19-34,46-65  >> net1_atm/$st.$i.net1.az
  grep 'NS_GRAD R' /data/gps/gamit/hymex/net1/$i/$b/onet1a.$b | grep -i $st |
  cut -c19-36,46-65  >> net1_atm/$st.$i.net1.ns
  grep 'EW_GRAD R' /data/gps/gamit/hymex/net1/$i/$b/onet1a.$b | grep -i $st |
  cut -c19-36,46-65  >> net1_atm/$st.$i.net1.ew

  else
  echo /data/gps/gamit/hymex/net1/$i/$b/onet1a.$b missing
  fi
  done
  done
  echo station $st completed
  done < <( cat net1/st_liste_net1.txt )
```

IX.e. *extract_atm* .az output

The following file is an extraction of .az file for ACOR PS (Acoruna, Spain) in 2012 (the complete name of the output file is ACOR.2012.net1.az), from 25th to 26th April. The ZTD are estimated every two hours, so that there are 13 estimates for each day.

The different columns correspond to: year, month, day, hour, minute, rms and ZTD estimation.

```
2012  4 25  0  0   0.0063    2.4210
2012  4 25  2  0   0.0038    2.4217
2012  4 25  4  0   0.0039    2.4287
2012  4 25  6  0   0.0040    2.3416
2012  4 25  8  0   0.0036    2.3331
2012  4 25 10  0   0.0040    2.3539
2012  4 25 12  0   0.0037    2.3554
2012  4 25 14  0   0.0036    2.3612
2012  4 25 16  0   0.0038    2.3573
2012  4 25 18  0   0.0037    2.3504
2012  4 25 20  0   0.0037    2.3559
```

```
2012  4 25 22  0   0.0043    2.3573
2012  4 26  0  0   0.0078    2.3531
2012  4 26  0  0   0.0052    2.3664
2012  4 26  2  0   0.0030    2.3475
2012  4 26  4  0   0.0030    2.3536
2012  4 26  6  0   0.0031    2.3514
2012  4 26  8  0   0.0029    2.3604
2012  4 26 10  0   0.0032    2.3767
2012  4 26 12  0   0.0029    2.3835
2012  4 26 14  0   0.0029    2.3870
2012  4 26 16  0   0.0029    2.3795
2012  4 26 18  0   0.0032    2.3874
2012  4 26 20  0   0.0030    2.3936
2012  4 26 22  0   0.0036    2.3955
```

IX.f. *extract_atm* .ns output

The following file is an extraction of .ns file for ACOR PS (Acoruna, Spain) in 2012 (the complete name of the output file is ACOR.2012.net1.ns), from 25th to 26th April.

The gradients are estimated seven times a day.

The different columns correspond to: year, month, day, hour, minute, rms and N-S gradient.

```
2012  4 25  0  0 -   0.0191   -0.0245
2012  4 25  3 26 -   0.0131   -0.0323
2012  4 25  6 52 -   0.0132   -0.0309
2012  4 25 10 18 -   0.0136   -0.0244
2012  4 25 13 44 -   0.0130   -0.0151
2012  4 25 17 10 -   0.0131   -0.0146
2012  4 25 20 36 -   0.0150   -0.0157
2012  4 26  0  2 -   0.0203   -0.0088
2012  4 26  0  0 -   0.0160   -0.0302
2012  4 26  3 26 -   0.0102   -0.0344
2012  4 26  6 52 -   0.0111   -0.0146
2012  4 26 10 18 -   0.0114   -0.0070
2012  4 26 13 44 -   0.0105   -0.0048
2012  4 26 17 10 -   0.0109   -0.0142
2012  4 26 20 36 -   0.0127   -0.0175
```

IX.g. *extract_atm* .ew output

The following file is an extraction of .ew file for ACOR PS (Acoruna, Spain) in 2012 (the complete name of the output file is ACOR.2012.net1.ew), from 25th to 26th April.

The different columns correspond to: year, month, day, hour, minute, rms and E-W gradient.

```
2012  4 25  0  0 -   0.0197    0.0117
2012  4 25  3 26 -   0.0156    0.0179
2012  4 25  6 52 -   0.0138    0.0238
2012  4 25 10 18 -   0.0135    0.0269
2012  4 25 13 44 -   0.0139    0.0255
2012  4 25 17 10 -   0.0139    0.0248
2012  4 25 20 36 -   0.0137    0.0313
2012  4 26  0  2 -   0.0195    0.0334
2012  4 26  0  0 -   0.0168    0.0181
2012  4 26  3 26 -   0.0128    0.0196
2012  4 26  6 52 -   0.0113   -0.0071
2012  4 26 10 18 -   0.0112    0.0075
2012  4 26 13 44 -   0.0117    0.0022
2012  4 26 17 10 -   0.0120   -0.0071
2012  4 26 20 36 -   0.0117    0.0037
```

X. FORTRAN CODES TO FORMAT AND COMPARE ZTD ESTIMATIONS

The following sections X.a and X.b are dedicated to the description of the codes implemented to automatically read, write and formatting the ZTDs coming from GAMIT processing and the ZTD from IGS official estimations, respectively.

X.a. GAMIT ZTD estimations

In this section, the *read_GAMIT_ZTD.f90* Fortran code to read, write and formatting the GAMIT ZTD output files (NAME.year.netX.az) is presented, together with the ancillary file (*input_GAMIT.txt*) containing the PS to be elaborated and a sample of the output file.

X.a.i. *input_GAMIT.txt* ancillary file

The *input_GAMIT.txt* file is a simple file containing a number of rows equal to the number of PS to be included in the formatting operations performed by *read_GAMIT_ZTD.f90* Fortran code. Each row contains the PS name, the year, the starting month and day and the ending month and day to be elaborated. In the example, the whole year 2011 is considered for the Core stations. Logically, each station can have a different year and starting/ending dates.

```
BRST  2011  1     1     12    31
CAGL  2011  1     1     12    31
GRAS  2011  1     1     12    31
GRAZ  2011  1     1     12    31
HERS  2011  1     1     12    31
MATE  2011  1     1     12    31
MEDI  2011  1     1     12    31
POTS  2011  1     1     12    31
SFER  2011  1     1     12    31
SJDV  2011  1     1     12    31
TORI  2011  1     1     12    31
VILL  2011  1     1     12    31
WSRT  2011  1     1     12    31
WTZR  2011  1     1     12    31
ZIMM  2011  1     1     12    31
```

X.a.ii. *read_GAMIT_ZTD.f90* Fortran code

The *read_GAMIT_ZTD.f90* Fortran code for automatically reading and formatting the ZTD and corresponding rms from GAMIT output is here reported.

The sentences coloured in blue are comments, written in order to make the code more understandable.

```
Program read_GAMIT_ZTD

implicit none

! Variable declaration
integer :: nh, nrighe, iriga
integer :: nora(12), annomese(12)
integer :: anno, anno_dopo, mese, giorno, ora, minuti
integer :: mesei, giornoi, mesef, giornof
integer :: idoi, fdoi, doi, doi_1
integer :: i, j, k, ii, nyear, nmonth, nday, nhour, nminute
real :: rms, ZTD
integer :: endoffile
integer :: ora_prec, giorno_1
character(4) :: nomeSP
character(32) :: nomefileinp, nomefileout, stringa
character(4) :: canno, canno_dopo

do nh=1,12
nora(nh)=nh*2
end do

annomese(1)=31
annomese(2)=28
annomese(3)=31
annomese(4)=30
annomese(5)=31
annomese(6)=30
annomese(7)=31
annomese(8)=31
annomese(9)=30
annomese(10)=31
annomese(11)=30
annomese(12)=31
! Open the file containing PS names, start year and day, end year and day
open(3,file='./input_GAMIT.txt')

do
 read(3,*,end=20)nomeSP,anno,mesei,giornoi,mesef,giornof
```

```
! Write year (anno) and following year (anno_dopo) as character
 write(canno,'(i4)') anno
 anno_dopo=anno+1
 write(canno_dopo,'(i4)') anno_dopo

! If a leap year is read from the input file (3), a day is added to February
 if (((anno-2000)/4.0)-int((anno-2000)/4.0).eq.0) annomese(2)=29

! Date conversion: from start month (mesei) and day (giornoi) to initial doy
   (idoi); from end month (mesef) and day (giornof) to final doy (fdoi)
 idoi=0
 if (mesei.ge.2) then
  do i=2,mesei
   idoi=idoi+annomese(i-1)
  end do
  idoi=idoi+giornoi
 else
  idoi=giornoi
 end if
 fdoi=0
 if (mesef.ge.2) then
  do i=2,mesef
   fdoi=fdoi+annomese(i-1)
  end do
  fdoi=fdoi+giornof
 else
  fdoi=giornof
 end if

! Output file definition
 nomefileout=('./'//nomeSP//'_net1.'//canno)
 open(2,file=nomefileout)

! Input file definition
 nomefileinp=('./net1_2011/'//nomeSP//'.'//canno//'.net1.az')
 open(1,file=nomefileinp)
 iriga=1
 nrighe=1
```

```
! Count the rows in input file
 do
  read(1,*,end=30)stringa
  if (stringa.eq.canno_dopo) go to 30
  nrighe=nrighe+1
 end do
 30 close(1)

 endoffile=nrighe
 open(4,file=nomefileinp)

! Empty input file
 if (endoffile.eq.1) then
  do i=idoi,fdoi
   do j=0,22,2
    write(2,*)i,j,99999,99999
   end do
  end do
 else
! Not empty input file, definition of previous doy (doi_1) and hour
   (ora_prec), to be compared with the actually read hour and day
  doi_1=idoi-1
  ora_prec=-2
! Read the input file
  do i=1,endoffile-1
   read(4,1500,end=10)anno,mese,giorno,ora,minuti,rms,ZTD
   doi=0
! Date conversion: from month (mese) and day (giorno) to doy (doi)
   if (mese.ge.2) then
    do j=2,mese
     doi=doi+annomese(j-1)
    end do
    doi=doi+giorno
   else
    doi=giorno
   end if

! Test to check that the read doy belongs to the interval to be processed
   if(doi.ge.idoi.and.doi.le.fdoi) then
```

```
    if(ora.ne.0) iriga=2
    if(ora.eq.0) iriga=iriga+1
! Counter to skip the fist 0
    if (iriga.eq.3) go to 40

!!!! PROCEDURE TO FILL IN THE GAPS !!!!
    if(doi.eq.doi_1+1) then
     if(ora.eq.ora_prec+2) then
! No day(s), no hour(s) gaps
      write(2,200)doi,ora,rms*1000,ZTD*1000
      ora_prec=ora_prec+2
     else
! Fill in the hour(s) gap if the currently read day is the last read
      do ii=ora_prec+2,ora-2,2
       write(2,100)doi,ii,99999,99999
       ora_prec=ora
      end do
      write(2,200)doi,ora,rms*1000,ZTD*1000
     end if
    else
! Fill in the hour(s) gap if the currently read day is NOT the last read
! Fill in the final hour(s) gap of the last read day (if present)
     do ii=ora_prec+2,22,2
      write(2,100)doi_1+1,ii,99999,99999
     end do
! Fill in the day(s) gap from the last read day to the actual (if present)
     do ii=doi_1+2,doi-1,1
      do k=0,22,2
       write(2,100)ii,k,99999,99999
      end do
     end do
     doi_1=doi-1
! Fill in the initial hour(s) gap of the actual day (if present)
     do ii=0,ora-2,2
      write(2,100)doi,ii,99999,99999
     end do
     write(2,200)doi,ora,rms*1000,ZTD*1000
     ora_prec=ora
    end if
```

```
   end if
  40 end do
 end if

 10 close(4)
 close(2)
end do
20 close(3)

1500 format(i4,4i3,f9.4,1x,f9.4)
100 format(i3,2x,i2,2x,i5,4x,i5)
200 format(i3,2x,i2,2x,f5.2,2x,f7.2)

end program
```

X.a.iii. *read_GAMIT_ZTD.f90* output

Once processed with *read_GAMIT_ZTD.f90* Fortran code, the GAMIT output (e.g. POTS.2011.net1.az) is formatted in the way shown in the sample below. The example shows an extraction of the entire output file, for 30th June and 1st July 2011 (doy 181 and 182 respectively). The different columns represent: doy, hour, rms (in mm) and ZTD (in mm).

```
      181   0   5.90  2431.70
      181   2   3.80  2437.40
      181   4   3.50  2440.70
      181   6   3.70  2454.00
      181   8   3.50  2476.00
      181  10   3.50  2483.90
      181  12   3.90  2481.80
      181  14   3.50  2473.50
      181  16   3.80  2470.80
      181  18   3.80  2408.00
      181  20   3.70  2349.30
      181  22   4.00  2344.50
      182   0   4.40  2368.10
      182   2   3.00  2380.70
      182   4   2.60  2375.70
      182   6   2.80  2375.80
      182   8   2.70  2381.90
      182  10   2.70  2392.20
      182  12   2.90  2392.20
```

```
182  14   2.70  2391.60
182  16   3.00  2392.90
182  18   2.90  2386.00
182  20   2.90  2397.30
182  22   3.10  2387.20
183   0   4.40  2378.60
```

X.b. IGS ZTD estimations

In this section, the *read_IGS_ZTD.f90* Fortran code to read, write and formatting the IGS official ZTD estimations files (name.0doy.yyzpd) is presented, together with the ancillary file (*input_IGS.txt*) containing the PS to be elaborated, a sample of official IGS ZTD estimation file, and a sample of the output file.

X.b.i. *input_IGS_PS*.txt ancillary file

The *input_IGS.txt* file is a simple file containing a number of rows equal to the number of PS to be included in the formatting operations performed by *read_IGS_ZTD.f90* Fortran code. Each row contains the PS name, the year, the starting and ending doy to be elaborated.
In the example, the whole year 2002 is considered for 16 selected PS. Logically, each station can have a different year and starting/ending doys.

```
ajac  2002  001   365
cagl  2002  001   365
ebre  2002  001   365
gope  2002  001   365
graz  2002  001   365
hers  2002  001   365
mate  2002  001   365
medi  2002  001   365
not1  2002  001   365
pots  2002  001   365
rabt  2002  001   365
sfer  2002  001   365
vill  2002  001   365
wsrt  2002  001   365
wtzr  2002  001   365
zimm  2002  001   365
```

X.b.ii. IGS ZTD estimation file (name.doy0.YYzpd)

The IGS ZTD estimation of 2nd February 2002 for CAGL PS (Cagliari, Italy), is reported, to make the following Fortran code more understandable. The complete name of the file is cagl.0330.02zpd.
The starting lines (until line 30) are headers, to be skipped by *read_IGS_ZTD.f90 code*. The 5-minutes ZTD estimates are reported in the following lines, formatted as: NAME YY:DDD:SSSSS ZTD RMS where YY is the year, DDD the doy, SSSSS the epoch (in seconds).

```
%=TRO 1.00 JPL 05:102:00000 JPL 02:033:00000 02:033:85500 P CAGL
  +FILE/REFERENCE
   DESCRIPTION        Jet Propulsion Laboratory, Pasadena, CA USA
   OUTPUT             Total ZPD Products using IGS gps orbit and clock
   CONTACT            Sung.H.Byun@jpl.nasa.gov, Yoaz.E.Bar-Sever@jpl.nasa.gov
   SOFTWARE           Gipsy-Oasis
   HARDWARE           i686-Linux
   INPUT              IGS gps orbit and clock solutions, site rinex file.
  -FILE/REFERENCE
  +FILE/COMMENT
   This file is generated for all current IGS sites found in
   ftp://igscb.jpl.nasa.gov/igscb/station/log/
  -FILE/COMMENT
  +INPUT/ACKNOWLEDGMENTS
   IGS International GPS Service
  -INPUT/ACKNOWLEDGMENTS
  +TROP/DESCRIPTION
  *KEYWORD_____________________ VALUE(S)_____________
   SAMPLING INTERVAL                          300
   SAMPLING TROP                              300
   ELEVATION CUTOFF ANGLE                     7.0
   TROP MAPPING FUNCTION         NIELL
   SOLUTION_FIELDS_1             TROTOT STDDEV
  -TROP/DESCRIPTION
  +TROP/STA_COORDINATES
  *SITE PT SOLN T STA_X_______ STA_Y_______ STA_Z_______ SYSTEM REMARK
   cagl  A    1 P  4893378.862   772649.726  4004182.124 IGS00  Mean
  -TROP/STA_COORDINATES
  +TROP/SOLUTION
  *SITE EPOCH_______ TROTOT STDEV
   CAGL 02:033:00000 2361.1   2.3
   CAGL 02:033:00300 2361.1   2.2
```

```
 CAGL 02:033:00600 2361.1   2.1
 CAGL 02:033:00900 2361.1   2.0
 CAGL 02:033:01200 2360.8   2.0
 CAGL 02:033:01500 2361.1   1.9
 CAGL 02:033:01800 2361.5   1.9
 CAGL 02:033:02100 2361.6   1.8
 CAGL 02:033:02400 2361.8   1.8
 CAGL 02:033:02700 2362.0   1.8
 CAGL 02:033:03000 2362.1   1.7
 CAGL 02:033:03300 2362.0   1.7
 CAGL 02:033:03600 2362.5   1.7
```

X.b.iii. *read_IGS_ZTD.f90* Fortran code

The *read_IGS_ZTD.f90* Fortran code for automatically reading and formatting the IGS official ZTD estimations and corresponding rms output is here reported.

The sentences coloured in blue are comments, written in order to make the code more understandable.

```
Program read_IGS

  implicit none

! Variable declaration
  integer :: nfol, nfolc, nfold, nfolu
  integer :: nrighe, endoffile
  integer :: nh, i, j, ii
  integer :: giorno, giorno_1, secondi, ora, ora_prec, anno
  integer :: nora(12)
  integer :: idoi, fdoi
  integer :: annom, annoc, annod, annou
  real :: rms, ZTD
  character(3) :: cnfol
  character(1) :: cnfolc, cnfold, cnfolu
  character(4) :: nomeSP, nnSP
  character(30) :: nomefileinp, nomefileout, stringa
  character(4) :: canno
  character(1) :: cannom, cannoc, cannod, cannou

  ! Two-hourly time resolution
  do nh=0,11
   nora(nh)=nh*2
```

```
   end do

! Open the file containing PS names (nomeSP), years (anno), initial and final
   doys (idoi and fdoi)
   open(3,file='./input_IGS.txt')

   do
    read(3,*,end=20)nomeSP,anno,idoi,fdoi

! Decimal notation scomposition for year and doy
    annom=anno/1000
    annoc=(anno-annom*1000)/100
    annod=(anno-annom*1000-annoc*100)/10
    annou=(anno-annom*1000-annoc*100-annod*10)
    write(cannom,'(i1)') annom
    write(cannoc,'(i1)') annoc
    write(cannod,'(i1)') annod
    write(cannou,'(i1)') annou
    write(canno,'(i4)') anno

    giorno_1=idoi-1

   ! Output file definition
    nomefileout=('./'//nomeSP//'_IGS.'//canno)
    open(2,file=nomefileout)

   ! Input file definition (the folders name correspond to doys)
    do nfol=idoi,fdoi                    ! **
     nfolc=nfol/100
     nfold=(nfol-nfolc*100)/10
     nfolu=nfol-nfolc*100-nfold*10
     write(cnfolc,'(i1)') nfolc
     write(cnfold,'(i1)') nfold
     write(cnfolu,'(i1)') nfolu

nomefileinp=('./'//canno//'/'//cnfolc//cnfold//cnfolu//'/'//nomeSP//cnfolc//
cnfold//cnfolu//'0.'//cannod//cannou//'ZTD')

     open(1,file=nomefileinp)
```

```
      nrighe=1

    ! Count input file rows
      do
       read(1,*,end=30)stringa
       if (stringa.eq.('%=ENDTRO')) go to 30
       nrighe=nrighe+1
      end do

      30 close(1)
      endoffile=nrighe

      open(4,file=nomefileinp)
      if (endoffile.eq.1) then
! Empty input file
       do j=0,22,2
        write(2,100)nfol,j,99999,99999
       end do
      else
! Not empty input file
! Skip the headers, definition of start hout (nh) and previous hour
    (ora_prec), to be compared with the actually read hour
       do i=1,30
        read(4,*,end=40)stringa
       end do
       nh=0
       ora_prec=-2

    ! Read input file
       do i=31,endoffile-2
        read(4,1500,end=40)nnSP,giorno,secondi,ZTD,rms
! Trasformation of epochs (secondi) in hour (ora)
        ora=secondi/3600
        if(ora.eq.nora(nh)) then
! No hour(s) gap, two-hourly extraction from 5-minutes ZTD estimations
       write(2,200)giorno,ora,rms,ZTD
         ora_prec=nora(nh)
```

```
        nh=nh+1
       else
! Fill in the hour(s) gap
        if (ora.gt.nora(nh)) then
         if (ora_prec+2.le.nora(nh)) then
          do ii=ora_prec+2,nora(nh),2
           write(2,100)giorno,ii,99999,99999
           ora_prec=nora(nh)
           nh=nh+1
          end do
         end if
        end if
       end if
      end do
     end if
     10 close(1)
     40 close (4)
     giorno_1=giorno
 end do
   close(2)

  end do
  20 close(3)

  1000 format(a32)
  1500 format(1x,a4,4x,i3,1x,i5,1x,f6.1,f6.1)
100 format(3i,2x,2i,2x,5i,4x,5i)
200 format(3i,2x,2i,2x,f5.2,2x,f7.2)

  end program
```

X.b.iv. *read_IGS_ZTD.f90* output

Once processed with *read_IGS_ZTD.f90* Fortran code, the IGS official ZTD estimations (e.g. cagl.0330.02zpd) is formatted in the way shown in the sample below (cagl_IGS.2002). The example shows an extraction of the entire output file, for 2nd and 3rd February 2002 (doy 033 and 034 respectively). The different columns represent: doy, hour, rms (in mm) and ZTD (in mm).

```
      33   0   2.30  2361.10
      33   2   1.60  2360.20
      33   4   1.40  2353.00
```

```
33   6   1.30  2351.60
33   8   1.40  2354.50
33  10   1.60  2358.00
33  12   1.20  2359.10
33  14   1.50  2362.80
33  16   1.50  2367.00
33  18   1.50  2374.90
33  20   1.20  2375.80
33  22   1.80  2366.30
34   0   2.50  2362.00
34   2   1.60  2360.50
34   4   1.40  2354.90
34   6   1.50  2357.80
34   8   1.50  2361.60
34  10   1.90  2365.00
34  12   1.20  2361.30
34  14   1.50  2362.10
34  16   1.60  2357.30
34  18   1.50  2355.30
34  20   1.10  2356.80
34  22   1.80  2358.70
35   0   2.00  2359.10
```

X.c. *compare_GAMIT_IGS_ZTD.f90* Fortran code

In this section, the *compare_GAMIT_IGS_ZTD.f90* Fortran code to compute the differences between GAMIT and IGS ZTD estimations , together with the ancillary file (cfr.*txt*) containing the PS to be elaborated and a sample of the output file.

X.c.i. *cfr.txt* ancillary file

The *cfr.txt* file is a simple file containing a number of rows equal to the number of PS to be included in the omparison operations performed by *compare_GAMIT_IGS_ZTD.f90* Fortran code. Each row contains the PS name in upper-case letters, the PS name in lower-case letters and the year.
In the example, the whole year 2002 is considered for 16 selected PS. Logically, each station can have a different year.

```
AJAC  ajac  2002
CAGL  cagl  2002
EBRE  ebre  2002
GOPE  gope  2002
```

```
GRAZ  graz  2002
HERS  hers  2002
MATE  mate  2002
MEDI  medi  2002
NOT1  not1  2002
POTS  pots  2002
RABT  rabt  2002
SFER  sfer  2002
VILL  vill  2002
WSRT  wsrt  2002
WTZR  wtzr  2002
ZIMM  zimm  2002
```

X.c.ii. *compare_GAMIT_IGS_ZTD.f90*

The *compare_GAMIT_IGS_ZTD.f90* Fortran code for automatically comparing the GAMIT and IGS ZTD estimations is here reported.

The sentences coloured in blue are comments, written in order to make the code more understandable.

```
Program compare_GAMIT_IGS_ZTD

  implicit none

! Variable declaration
  integer :: nrighe, i
  integer :: anno, doiI,doiG, oraI, oraG
  real :: rmsI, rmsH
  real :: ZTDI, ZTDG
  character(4) :: nomeGamit, nomeIGS
  character(30) :: nomefileout, nomefileinpG, nomefileinpI
  character(4) :: canno

! Open input file and read the PS to be processed
  open(4,file='cfr.txt')
  nrighe=1
  do
   read(4,*,end=40)nomeGamit,nomeIGS,anno
   nrighe=nrighe+1
   write(canno,'(i4)') anno

  ! Output file definition
```

```
    nomefileout=('./cfr_GAMIT_IGS_'//nomeIGS//'.'//canno)
    open(3,file=nomefileout)

   ! GAMIT input file definition
    nomefileinpG=('./GAMIT/'//nomeGamit//'_net1.'//canno)
    open(2,file=nomefileinpG)

   ! IGS input file definition
    nomefileinpI=('./IGS/'//nomeIGS//'_IGS.'//canno)
    open(1,file=nomefileinpI)
 i=1

! Read from input files
    do
     read(2,*,end=20)doiG,oraG,rmsG,ZTDG
     read(1,*,end=10)doiI,oraI,rmsI,ZTDI

   ! ZTD values different from 99999 and equal starting date and time
     if (ZTDG.ne.99999.and.ZTDI.ne.99999) then
      if (doiG.eq.doiI.and.oraG.eq.oraI) then
       write(3,*)doiG,oraH,ZTDG,ZTDI,ZTDG-ZTDI
      else
! Starting date and/or hour are not the same
       write(3,*)'Errore!'
      end if
     else
! At least one ZTD estimation is 99999
      write(3,*)doiG,oraH,ZTDG,ZTDI,99999
     end if
     i=i+1
    end do
    10 close(1)
    20 close(2)
    close(3)
   end do
   40 close(4)
   1000 format(a4,a4,i4)
   end program
```

X.c.iii. *compare_GAMIT_IGS_ZTD.f90* output

Once processed with *compare_GAMIT_IGS_ZTD.f90* Fortran code, the GAMIT and IGS official ZTDs are compared and the differences are stored in a file like the following one (cfr_GAMIT_IGS_cagl.2002). The example shows an extraction of the entire output file, for 2nd and 3rd February 2002 (doy 033 and 034 respectively). The different columns represent: doy, hour, GAMIT ZTD, IGS ZTD and differences (GAMIT-IGS). ZTD estimations and ZTD differences are expressed in mm.

```
33           0   2354.20       2361.10      -6.90
33           2   2356.10       2360.20      -4.10
33           4   2347.30       2353.00      -5.70
33           6   2351.10       2351.60      -0.50
33           8   2349.10       2354.50      -5.40
33          10   2355.30       2358.00      -2.70
33          12   2357.20       2359.10      -1.90
33          14   2358.60       2362.80      -4.20
33          16   2365.20       2367.00      -1.80
33          18   2377.30       2374.90       2.40
33          20   2366.30       2375.80      -9.50
33          22   2360.70       2366.30      -5.60
34           0   2355.20       2362.00      -6.80
34           2   2358.10       2360.50      -2.40
34           4   2350.70       2354.90      -4.20
34           6   2355.30       2357.80      -2.50
34           8   2355.50       2361.60      -6.10
34          10   2364.50       2365.00      -0.50
34          12   2359.30       2361.30      -2.00
34          14   2360.10       2362.10      -2.00
34          16   2357.70       2357.30       0.40
34          18   2354.60       2355.30      -0.70
34          20   2350.10       2356.80      -6.70
34          22   2360.40       2358.70       1.70
35           0   2354.70       2359.10      -4.40
```

XI. ZTD AND GRADIENT FILES FROM RENAG DB

ZTD (GENO_net1_ZTD_2000_v1.0.dat) and gradients (GENO_net1_GRD_2000_v1.0.dat) files in ASCII formats will be presented in the following sections XI.a and XI.b respectively. They are relative to GENO PS and year 2000.

XI.a. GENO_net1_ZTD_2000_v1.0.dat

```
GENO
lat     lon     alt
44.419      8.921 110.018
doy_1998        doy     year            month   day     hours   minutes
  RMS_err ZTD
731.0000    1.0000      2000.0000   1.0000      1.0000      0.0000
      0.0000      0.0046      2.3418
731.0833    1.0833      2000.0000   1.0000      1.0000      2.0000
      0.0000      0.0040      2.3435
731.1667    1.1667      2000.0000   1.0000      1.0000      4.0000
      0.0000      0.0035      2.3415
731.2500    1.2500      2000.0000   1.0000      1.0000      6.0000
      0.0000      0.0037      2.3472
731.3333    1.3333      2000.0000   1.0000      1.0000      8.0000
      0.0000      0.0037      2.3590
731.4167    1.4167      2000.0000   1.0000      1.0000      10.0000
      0.0000      0.0034      2.3666
731.5000    1.5000      2000.0000   1.0000      1.0000      12.0000
      0.0000      0.0033      2.3622
731.5833    1.5833      2000.0000   1.0000      1.0000      14.0000
      0.0000      0.0040      2.3629
731.6667    1.6667      2000.0000   1.0000      1.0000      16.0000
      0.0000      0.0035      2.3726
731.7500    1.7500      2000.0000   1.0000      1.0000      18.0000
      0.0000      0.0038      2.3674
731.8333    1.8333      2000.0000   1.0000      1.0000      20.0000
      0.0000      0.0040      2.3798
731.9167    1.9167      2000.0000   1.0000      1.0000      22.0000
      0.0000      0.0042      2.3825
732.0000    2.0000      2000.0000   1.0000      2.0000      0.0000
      0.0000      0.0054      2.3613
```

```
732.0833    2.0833      2000.0000   1.0000      2.0000      2.0000
      0.0000      0.0035      2.3624
732.1667    2.1667      2000.0000   1.0000      2.0000      4.0000
      0.0000      0.0031      2.3605
732.2500    2.2500      2000.0000   1.0000      2.0000      6.0000
      0.0000      0.0033      2.3630
732.3333    2.3333      2000.0000   1.0000      2.0000      8.0000
      0.0000      0.0033      2.3634
732.4167    2.4167      2000.0000   1.0000      2.0000      10.0000
      0.0000      0.0030      2.3642
732.5000    2.5000      2000.0000   1.0000      2.0000      12.0000
      0.0000      0.0029      2.3602
732.5833    2.5833      2000.0000   1.0000      2.0000      14.0000
      0.0000      0.0036      2.3665
732.6667    2.6667      2000.0000   1.0000      2.0000      16.0000
      0.0000      0.0033      2.3707
732.7500    2.7500      2000.0000   1.0000      2.0000      18.0000
      0.0000      0.0034      2.3592
732.8333    2.8333      2000.0000   1.0000      2.0000      20.0000
      0.0000      0.0036      2.3582
732.9167    2.9167      2000.0000   1.0000      2.0000      22.0000
      0.0000      0.0040      2.3570
733.0000    3.0000      2000.0000   1.0000      3.0000      0.0000
      0.0000      0.0050      2.3686
733.0833    3.0833      2000.0000   1.0000      3.0000      2.0000
      0.0000      0.0036      2.3690
733.1667    3.1667      2000.0000   1.0000      3.0000      4.0000
      0.0000      0.0032      2.3625
733.2500    3.2500      2000.0000   1.0000      3.0000      6.0000
      0.0000      0.0034      2.3638
733.3333    3.3333      2000.0000   1.0000      3.0000      8.0000
      0.0000      0.0035      2.3633
733.4167    3.4167      2000.0000   1.0000      3.0000      10.0000
      0.0000      0.0033      2.3629
733.5000    3.5000      2000.0000   1.0000      3.0000      12.0000
      0.0000      0.0030      2.3584
733.5833    3.5833      2000.0000   1.0000      3.0000      14.0000
      0.0000      0.0038      2.3652
```

```
733.6667    3.6667      2000.0000   1.0000      3.0000      16.0000
      0.0000      0.0033      2.3624
733.7500    3.7500      2000.0000   1.0000      3.0000      18.0000
      0.0000      0.0035      2.3609
733.8333    3.8333      2000.0000   1.0000      3.0000      20.0000
      0.0000      0.0036      2.3632
733.9167    3.9167      2000.0000   1.0000      3.0000      22.0000
      0.0000      0.0038      2.3637
734.0000    4.0000      2000.0000   1.0000      4.0000      0.0000
      0.0000      0.0049      2.3673
734.0833    4.0833      2000.0000   1.0000      4.0000      2.0000
      0.0000      0.0038      2.3656
734.1667    4.1667      2000.0000   1.0000      4.0000      4.0000
      0.0000      0.0035      2.3620
734.2500    4.2500      2000.0000   1.0000      4.0000      6.0000
      0.0000      0.0036      2.3612
734.3333    4.3333      2000.0000   1.0000      4.0000      8.0000
      0.0000      0.0039      2.3601
734.4167    4.4167      2000.0000   1.0000      4.0000      10.0000
      0.0000      0.0036      2.3610
734.5000    4.5000      2000.0000   1.0000      4.0000      12.0000
      0.0000      0.0032      2.3578
734.5833    4.5833      2000.0000   1.0000      4.0000      14.0000
      0.0000      0.0040      2.3635
734.6667    4.6667      2000.0000   1.0000      4.0000      16.0000
      0.0000      0.0035      2.3618
734.7500    4.7500      2000.0000   1.0000      4.0000      18.0000
      0.0000      0.0037      2.3689
734.8333    4.8333      2000.0000   1.0000      4.0000      20.0000
      0.0000      0.0039      2.3723
734.9167    4.9167      2000.0000   1.0000      4.0000      22.0000
      0.0000      0.0042      2.3743
```

XI.b. GENO_net1_GRD_2000_v1.0.dat

```
GENO
lat     lon     alt
43.364      -8.399      66.9
doy_1998        doy     year            month   day     hours   minutes
  err_NS  grad_NS err_EW  grad_EW
```

```
731.0000    1.0000      2000.0000   1.0000      1.0000      0.0000
      0.0000      0.0170      -0.0172     0.0191      -0.0172
731.1431    1.1431      2000.0000   1.0000      1.0000      3.0000
      26.0000     0.0136      -0.0124     0.0143      -0.0066
731.2861    1.2861      2000.0000   1.0000      1.0000      6.0000
      52.0000     0.0139      -0.0108     0.0121      0.0046
731.4292    1.4292      2000.0000   1.0000      1.0000      10.0000
      18.0000     0.0137      -0.0136     0.0130      0.0005
731.5722    1.5722      2000.0000   1.0000      1.0000      13.0000
      44.0000     0.0135      0.0000      0.0135      -0.0005
731.7153    1.7153      2000.0000   1.0000      1.0000      17.0000
      10.0000     0.0144      0.0020      0.0136      -0.0066
731.8583    1.8583      2000.0000   1.0000      1.0000      20.0000
      36.0000     0.0149      0.0023      0.0150      -0.0200
732.0000    2.0000      2000.0000   1.0000      2.0000      0.0000
      0.0000      0.0182      -0.0115     0.0222      -0.0169
732.1431    2.1431      2000.0000   1.0000      2.0000      3.0000
      26.0000     0.0120      -0.0101     0.0126      -0.0095
732.2861    2.2861      2000.0000   1.0000      2.0000      6.0000
      52.0000     0.0126      -0.0040     0.0110      -0.0101
732.4292    2.4292      2000.0000   1.0000      2.0000      10.0000
      18.0000     0.0122      -0.0004     0.0117      -0.0137
732.5722    2.5722      2000.0000   1.0000      2.0000      13.0000
      44.0000     0.0122      0.0116      0.0123      -0.0100
732.7153    2.7153      2000.0000   1.0000      2.0000      17.0000
      10.0000     0.0135      -0.0007     0.0122      -0.0079
732.8583    2.8583      2000.0000   1.0000      2.0000      20.0000
      36.0000     0.0134      -0.0090     0.0138      -0.0136
733.0000    3.0000      2000.0000   1.0000      3.0000      0.0000
      0.0000      0.0167      -0.0134     0.0214      -0.0103
733.1431    3.1431      2000.0000   1.0000      3.0000      3.0000
      26.0000     0.0129      -0.0076     0.0134      -0.0043
733.2861    3.2861      2000.0000   1.0000      3.0000      6.0000
      52.0000     0.0134      -0.0072     0.0114      -0.0002
733.4292    3.4292      2000.0000   1.0000      3.0000      10.0000
      18.0000     0.0130      -0.0075     0.0125      0.0009
733.5722    3.5722      2000.0000   1.0000      3.0000      13.0000
      44.0000     0.0128      0.0046      0.0130      0.0085
```

```
733.7153    3.7153      2000.0000   1.0000      3.0000      17.0000
      10.0000     0.0139      0.0031      0.0129      0.0028
733.8583    3.8583      2000.0000   1.0000      3.0000      20.0000
      36.0000     0.0141      -0.0007     0.0140      -0.0014
734.0000    4.0000      2000.0000   1.0000      4.0000      0.0000
      0.0000      0.0174      -0.0112     0.0213      -0.0082
734.1431    4.1431      2000.0000   1.0000      4.0000      3.0000
      26.0000     0.0136      -0.0076     0.0139      -0.0047
734.2861    4.2861      2000.0000   1.0000      4.0000      6.0000
      52.0000     0.0142      -0.0022     0.0120      -0.0007
734.4292    4.4292      2000.0000   1.0000      4.0000      10.0000
      18.0000     0.0138      0.0011      0.0130      0.0077
734.5722    4.5722      2000.0000   1.0000      4.0000      13.0000
      44.0000     0.0136      0.0108      0.0137      0.0148
734.7153    4.7153      2000.0000   1.0000      4.0000      17.0000
      10.0000     0.0145      0.0086      0.0135      0.0120
734.8583    4.8583      2000.0000   1.0000      4.0000      20.0000
      36.0000     0.0149      0.0129      0.0147      0.0069
```

XII. DISTAV METEOROLOGICAL STATION DATA

In the following sections a sample of DISTAV MS data (section XII.a), the Fortran code to extract two hourly observations of Pressure and Temperature (section XII.b) and the code output (section XII.c) are presented.

XII.a. A sample of DISTAV MS data

An extraction of year 2009 meteorological observation file (called "meteo-Balbi-2009.csv") is here presented. The different columns correspond to:

- columns 1-4: date (month, day, year) and hour;
- columns 5-7: mean, minimum and maximum temperature (in °C);
- column 8: pressure (in hPa).

```
Data e ora TMed TMin TMax Pa
  01 01 09 00 4.8 4.5 5.3 1018.0
  01 01 09 01 4.4 4.2 4.9 1017.1
  01 01 09 02 4.7 4.4 5.3 1016.4
  01 01 09 03 4.9 4.5 5.3 1016.2
  01 01 09 04 3.9 3.6 4.5 1016.1
  01 01 09 05 4.0 3.4 4.3 1015.0
  01 01 09 06 3.9 3.5 4.4 1014.4
  01 01 09 07 4.4 3.7 5.3 1014.1
  01 01 09 08 4.0 2.9 5.3 1014.1
  01 01 09 09 2.7 2.3 3.7 1014.4
  01 01 09 10 3.3 2.8 3.9 1015.0
  01 01 09 11 3.6 3.3 4.1 1015.4
  01 01 09 12 3.4 2.9 4.0 1015.6
  01 01 09 13 4.1 3.1 5.8 1015.3
  01 01 09 14 6.4 5.7 6.9 1014.4
  01 01 09 15 7.4 6.8 8.3 1013.8
  01 01 09 16 8.2 7.9 8.6 1014.2
  01 01 09 17 8.0 7.6 8.3 1014.1
  01 01 09 18 7.5 7.3 7.9 1014.4
  01 01 09 19 8.0 7.6 8.8 1014.2
  01 01 09 20 8.2 8.0 8.5 1014.5
  01 01 09 21 7.0 6.3 8.3 1014.4
  01 01 09 22 7.3 6.4 9.1 1013.9
  01 01 09 23 7.7 6.9 9.2 1014.1
  01 02 09 00 7.4 6.9 8.3 1013.8
```

XII.b. *read_DISTAV.f90* Fortran code

The *read_DISTAV.f90* Fortran code for automatically reading and formatting the DISTAV MS P and T data is here reported.

The sentences coloured in blue are comments, written in order to make the code more understandable.

```
Program read_DISTAV

  implicit none

! Varible declaration
  integer :: nline, ym(12), nh, iriga
  integer :: i, j, ii, k, jj
  integer :: idoy, fdoy, doy, doy_1, h_prev
  integer :: m, g, a, h
  character(4) :: cyear
  real :: Tmed, Tmin, Tmax, TmedK, pres
  character(10) :: stringa

  idoy=1

! Number of days in every month
  ym(1)=31
  ym(2)=28
  ym(3)=31
  ym(4)=30
  ym(5)=31
  ym(6)=30
  ym(7)=31
  ym(8)=31
  ym(9)=30
  ym(10)=31
  ym(11)=30
  ym(12)=31

  do jj=2002,2015
   write(cyear,'(i4)')jj
! Definition of input files
   open(1,file='meteo-Balbi-'//cyear//'.csv')
 nline=0
```

```
! Do cycle to count the number of lines in the input file
    do
     read(1,*,end=10)stringa
     nline=nline+1
    end do
    10 close(1)

! Open input and output files
    open(2,file='meteo-Balbi-'//cyear//'.csv')
    open(3,file='meteo-Balbi-'//cyear//'_check.txt')
! Header of output file
    write(3,*)'doy   h   P hPa   T °C    T K'

! Definition of previous doy (doy_1) e previous hour (h_prev)
    doy_1=0
    h_prev=-2

! Do cycle to skip the header of input file
    do i=1,1
     read(2,*)stringa
    end do

   ! Read from input file and transform temperature from °C to K
    do i=2,nline
     read(2,*)m,g,a,h,Tmed,Tmin,Tmax,pres
     TmedK = Tmed + 273.15

! Bisestile year verification
     if ((a/4.0)-int(a/4.0).eq.0) then
      ym(2)=29
      fdoy=366
     else
      ym(2)=28
      fdoy=365
     end if

! Doy computation
     doy=0
     if (m.ge.2) then
```

```
      do j=2,m
       doy=doy+ym(j-1)
      end do
      doy=g+doy
     else
      doy=g
     end if

! Instruction to select only even two-hourly data if no hour(s) and day(s)
   gap(s) is detected
     if (mod(h,2).eq.0) then
      if (pres.ne.0.0) then
       if(doy.eq.doy_1+1) then
        if(h.eq.h_prev+2) then
         write(3,300)doy,h,pres,Tmed,TmedK
         h_prev=h_prev+2
        else
! Gap(s) between the read hour and the last written
         do ii=h_prev+2,h-2,2
          write(3,301)doy,ii,99999,99999,99999
          h_prev=h
         end do
         write(3,300)doy,h,int(pres),Tmed,TmedK
        end if
       else
! Gap(s) between the read doy and the last written
! Fill hour gap(s) of the last written doy
        do ii=h_prev+2,22,2
       write(3,301)doy_1+1,ii,99999,99999,99999
        end do
! Fill day gap(s) between the present doy and the last written doy
        do ii=doy_1+2,doy-1,1
       do k=0,22,2
          write(3,301)ii,k,99999,99999,99999
         end do
      end do
      doy_1=doy-1
! Fill hour gap(s) of the read doy
        do ii=0,h-2,2
```

```
         write(3,301)doy,ii,99999,99999,99999
        end do
        write(3,300)doy,h,int(pres),Tmed,TmedK
        h_prev=h
       end if
      end if
     end if
    end do

    if (doy .ne. fdoy) then
! Fill hour gap(s) of the last written doy
     if (mod(h,2).eq.0) then
      do ii=h+2,22,2
       write(3,301)doy,ii,99999,99999,99999
      end do
     else
      do ii=h+1,22,2
       write(3,301)doy,ii,99999,99999,99999
      end do
     end if
! Fill day gaps(s) between the last written doy and the final doy
     do ii=doy+1,fdoy
    do k=0,22,2
       write(3,301)ii,k,99999,99999,99999
      end do
     end do
    end if
   end do
   close(3)
   20 close(2)
   300 format(1x,i3,2x,i2,3x,f6.1,3x,f4.1,2x,f5.1)
   301 format(1x,i3,2x,i2,4x,i5,2x,i5,2x,i5)
   end program
```

XII.c. *read_DISTAV.f90* output

Once processed with *read_DISTAV.f90* Fortran code, the DISTAV MS P and T data are formatted in the way shown in the sample below. The different columns represent: doy, hour, Pressure (in hPa), Temperature (in °C and in K). Both P and T data are referred to the MS elevation (58.3 m a.s.l.).

doy	h	P hPa	T °C	T K
1	0	1018.0	4.8	277.9
1	2	1016.4	4.7	277.9
1	4	1016.1	3.9	277.0
1	6	1014.4	3.9	277.0
1	8	1014.1	4.0	277.1
1	10	1015.0	3.3	276.4
1	12	1015.6	3.4	276.5
1	14	1014.4	6.4	279.5
1	16	1014.2	8.2	281.4
1	18	1014.4	7.5	280.6
1	20	1014.5	8.2	281.4
1	22	1013.9	7.3	280.4

XIII. DICCA METEOROLOGICAL STATION DATA

In the following sections a sample of DICCA MS data (section XIII.a), the Fortran code to extract two hourly observations of Pressure and Temperature (section XIII.b) and the code output (section XIII.c) are presented.

XIII.a. A sample of DICCA MS data

An extraction of year 2009 meteorological observation file (called "2009.txt") is here presented. The different columns correspond to:

- column 1 and 2: julian day and doy
- column 3: progressive counter to enumerate the data. It goes from 1 to 48, corresponding to half-hourly time step;
- columns 4-8: date (day, mont, year) and time (hour, minute);
- column 9: temperature (in °C);
- column 10: humidity;
- column 11: pressure (in hPa);
- column 12: solar radiation (in W/m^2);
- column 13: wind velocity (in km/h);
- column 14: rain with respect to the preceding half hour (in mm).

julian	ga	N	g	m	a	h	m	temp	umi	pres	rad	vento	pio
								C	%	hPa	W/Mq	Kmh	mm
2454833	1	1	1	1	2009	0	0	3.4	100	1025	0	0.0	0.4
2454833	1	2	1	1	2009	0	30	3.6	100	1025	0	0.0	0.0
2454833	1	3	1	1	2009	1	0	3.9	100	1024	0	0.0	0.0
2454833	1	4	1	1	2009	1	30	4.3	100	1024	0	0.0	0.0
2454833	1	5	1	1	2009	2	0	4.1	100	1023	0	0.0	0.0
2454833	1	6	1	1	2009	2	30	3.6	100	1024	0	6.1	0.0
2454833	1	7	1	1	2009	3	0	3.0	100	1024	0	7.3	0.2
2454833	1	8	1	1	2009	3	30	2.4	100	1024	0	7.7	0.0
2454833	1	9	1	1	2009	4	0	2.5	100	1023	0	9.1	0.0
2454833	1	10	1	1	2009	4	30	2.9	99	1022	0	6.9	0.0
2454833	1	11	1	1	2009	5	0	3.0	96	1022	0	6.6	0.0
2454833	1	12	1	1	2009	5	30	3.0	94	1022	0	3.1	0.0
2454833	1	13	1	1	2009	6	0	3.0	92	1022	0	5.2	0.0
2454833	1	14	1	1	2009	6	30	3.4	89	1021	0	0.0	0.0
2454833	1	15	1	1	2009	7	0	4.0	87	1021	0	0.0	0.0
2454833	1	16	1	1	2009	7	30	3.6	85	1021	0	7.9	0.0

```
2454833   1 17   1   1 2009   8  0   2.7   86  1021    0   11.3  0.0
2454833   1 18   1   1 2009   8 30   2.1   89  1021   22   11.7  0.0
2454833   1 19   1   1 2009   9  0   2.3   88  1023   63   10.9  0.0
2454833   1 20   1   1 2009   9 30   2.8   86  1022   91    6.7  0.0
2454833   1 21   1   1 2009  10  0   3.0   85  1023  114    4.9  0.0
2454833   1 22   1   1 2009  10 30   3.0   83  1023  109    9.9  0.0
2454833   1 23   1   1 2009  11  0   3.1   83  1023  105    9.1  0.0
2454833   1 24   1   1 2009  11 30   3.4   82  1022   98   11.2  0.0
2454833   1 25   1   1 2009  12  0   3.6   81  1022  404    8.3  0.0
```

XIII.b. *read_DICCA.f90* Fortran code

The *read_DICCA.f90* Fortran code for automatically reading and formatting the DICCA MS P and T data is here reported.

The sentences coloured in blue are comments, written in order to make the code more understandable.

```
Program read_DICCA

  implicit none

! Varible declaration
  integer :: nline, ym(12), nh, nhour(12)
  integer :: i, j, ii, k, jj
  integer :: idoy, fdoy, doy_1, h_prev
  integer :: julian, ga, N, g, m, a, h, minu, umi, pres, rad
  character(4) :: cyear
  real :: temp, vento, pio, tempK
  integer :: iriga
  character(10) :: stringa

  idoy=1

! Number of days in every month
  ym(1)=31
  ym(2)=28
  ym(3)=31
  ym(4)=30
  ym(5)=31
  ym(6)=30
  ym(7)=31
  ym(8)=31
```

```
   ym(9)=30
   ym(10)=31
   ym(11)=30
   ym(12)=31

   do jj=1998,2015
    write(cyear,'(i4)')jj
   ! Definition of input files
 open(1,file=cyear//'.txt')
   ! Bisestile year verification
    if (((jj-2000)/4.0)-int((jj-2000)/4.0).eq.0) ym(2)=29
    if (((jj-2000)/4.0)-int((jj-2000)/4.0).eq.0) then
     fdoy=366
    else
     fdoy=365
    end if

    nline=0
! Do cycle to count the number of lines in the input file
    do
     read(1,*,end=10)stringa
      nline=nline+1
    end do
    10 close(1)

! Open input and output files
    open(2,file=cyear//'.txt')
    open(3,file=cyear//'check_new')
! Header of output file
    write(3,*)'doy   h  P hPa   T °C    T K'

! Definition of previous doy (doy_1) e previous hour (h_prev)
    doy_1=0
    h_prev=-2

! Do cycle to skip the header of input file
    do i=1,2
     read(2,*)stringa
    end do
```

```
    do i=2,nline
     read(2,200)julian,ga,N,g,m,a,h,minu,temp,umi,pres,rad,vento,pio
     tempK = temp + 273.15
! Instruction to skip the first blank line after the header
      if (ga.ne.0) then
! Instruction to select only even two-hourly data if no hour(s) and day(s)
  gap(s) is detected
      if (mod(h,2).eq.0 .and. minu.eq.0) then
      if ((pres.ne.0 ) .and. (pres.ne.-1)) then
       if(ga.eq.doy_1+1) then
        if(h.eq.h_prev+2) then
         write(3,300)ga,h,pres,temp,tempK
         h_prev=h_prev+2
        else
! Gap(s) between the read hour and the last written
         do ii=h_prev+2,h-2,2
          write(3,301)ga,ii,99999,99999,99999
          h_prev=h
         end do
         write(3,300)ga,h,pres,temp,tempK
        end if
       else
! Gap(s) between the read doy and the last written
! Fill hour gap(s) of the last written doy
        do ii=h_prev+2,22,2
         write(3,301)doy_1+1,ii,99999,99999,99999
        end do
! Fill day gap(s) between the present doy and the last written doy
        do ii=doy_1+2,ga-1,1
         do k=0,22,2
          write(3,301)ii,k,99999,99999,99999
         end do
        end do
      doy_1=ga-1
! Fill hour gap(s) of the read doy
        do ii=0,h-2,2
         write(3,301)ga,ii,99999,99999,99999
        end do
```

```
        write(3,300)ga,h,pres,temp,tempK
        h_prev=h
       end if
      end if
      end if
     end if
    end do

    if (g .ne. fdoy) then
! Fill hour gap(s) of the last written doy
     if (mod(h,2).eq.0) then
      do ii=h+2,22,2
       write(3,301)ga,ii,99999,99999,99999
      end do
     else
     do ii=h+1,22,2
       write(3,301)ga,ii,99999,99999
      end do
     end if
! Fill day gaps(s) between the last written doy and the final doy
     do ii=ga+1,fdoy
      do k=0,22,2
       write(3,301)ii,k,99999,99999
      end do
     end do
    end if
   end do
   close(3)
   20 close(2)

   200
   format(1x,i7,1x,i3,1x,i2,2x,i2,1x,i2,1x,i4,2x,i2,1x,i2,1x,f5.1,2x,i3,1x,
      i5,2x,i3,2x,f4.1,1x,f4.1)
   300 format(1x,i3,2x,i2,3x,i4,3x,f4.1,2x,f5.1)
   301 format(1x,i3,2x,i2,3x,i5,3x,i5,2x,i5)
   end program
```

XIII.c. *read_DICCA.f90* output

Once processed with *read_DICCA.f90* Fortran code, the DICCA MS P and T data are formatted in the way shown in the sample below. The different columns represent: doy, hour, Pressure (in hPa), Temperature (in °C and in K). Both P and T data are referred to the MS elevation (40 m a.s.l.).

doy	h	P hPa	T °C	T K
1	0	1025	3.4	276.5
1	2	1023	4.1	277.2
1	4	1023	2.5	275.6
1	6	1022	3.0	276.1
1	8	1021	2.7	275.9
1	10	1023	3.0	276.1
1	12	1022	3.6	276.8
1	14	1021	6.6	279.8
1	16	1021	6.7	279.9
1	18	1021	5.9	279.0
1	20	1022	5.7	278.9
1	22	1021	6.3	279.4

XIV. MATLAB CODE FOR PWV SENSITIVITY ANALYSIS

In the following sections, the main program (section XIV.a) and the functions (XIV.b) to make the different parameters vary in the corresponding tolerance intervals, in order to compute the PWV variability and sensitivity to the variation of each variable.

XIV.a. Main program: SIGMA_PWV_sensitivity.m

The main program is here reported. After the definition of the variables and their rms, a *switch* expression is introduced. Depending on the choice on the varying parameter, the corresponding function is called to draw PWV and σ_{PWV} values in the variable tolerance interval.

The sentences coloured in blue are comments, written to make the code more understandable.

```
% Definition of parameters and their rms
xrho=10^3;                % Kg(MASS)/m^3
xRv=461.7;                % J/(kg*K) gas constant
xk2=17;                   % K/mbar
Sk2=10;
vetk2=[7:20/6:27];
xk3=3.777*10^5;           % K^2/mbar
Sk3=0.03*10^5;
vetk3=[xk3-3*Sk3:Sk3:xk3+3*Sk3];
xTs=20+273.15;            % K
STs=1
xTm=70.2+0.72*xTs;        % K
STm=0.72*STs;
vetTm=[xTm-3*STm:STm:xTm+3*STm];
xZTD=2.5;                 % m
SZTD=0.003;
vetZTD=[xZTD-3*SZTD:SZTD:xZTD+3*SZTD];
xP=1013;                  % mbar
SP=1;
vetP=[xP-3*SP:SP:xP+3*SP];
xlat=45;                  % grad
xlat=45;
xz=1;                     % km

caso_n = input('variable: 1->k2 2->k3 3->Tm 4->P 5->ZTD ');
switch caso_n
    case 1
```

```
% Sensitivity function for k2
    [ VPWV, VsigmaPWV ] = PWV_propaga_k2( vetk2, Sk2, xk3, Sk3, xTm, STm, xP,
            SP, xZTD, SZTD, xrho, xRv, xlat, xz);
        figure (1)
        scatter(VPWV(:),vetk2(:));
        title('PWV varying k2');
        xlabel('PWV [m]');
        ylabel('k2 [K/mbar]');
        figure (2)
        scatter(VsigmaPWV(:),vetk2(:));
        title('SigmaPWV varying k2');
        xlabel('SigmaPWV [m]');
        ylabel('k2 [K/mbar]');
    case 2
% Sensitivity function for k3
    [ VPWV, VsigmaPWV ] = PWV_propaga_k3( xk2, Sk2, vetk3, Sk3, xTm, STm, xP,
            SP, xZTD, SZTD, xrho, xRv, xlat, xz);
        figure (1)
        scatter(VPWV(:),vetk3(:));
        title('PWV varying k3');
        xlabel('PWV [m]');
        ylabel('k3 [K^2/mbar]');
        figure (2)
        scatter(VsigmaPWV(:),vetk3(:));
        title('SigmaPWV varying k3');
        xlabel('SigmaPWV [m]');
        ylabel('k3 [K^2/mbar]');
    case 3
% Sensitivity function for Tm
    [ VPWV, VsigmaPWV ] = PWV_propaga_Tm( xk2, Sk2, xk3, Sk3, vetTm, STm, xP,
            SP, xZTD, SZTD, xrho, xRv, xlat, xz);
        figure (1)
        scatter(VPWV(:),vetTm(:));
        title('PWV varying Tm');
        xlabel('PWV [m]');
        ylabel('Tm [K]');
        figure (2)
        scatter(VsigmaPWV(:),vetTm(:));
        title('SigmaPWV varying Tm');
```

```
        xlabel('SigmaPWV [m]');
        ylabel('Tm [K]');
    case 4
% Sensitivity function for P
    [ VPWV, VsigmaPWV ] = PWV_propaga_P( xk2, Sk2, xk3, Sk3, xTm, STm, vetP,
            SP, xZTD, SZTD, xrho, xRv, xlat, xz);
        figure (1)
        scatter(VPWV(:),vetP(:));
        title('PWV varying P');
        xlabel('PWV [m]');
        ylabel('P [mbar]');
        figure (2)
        scatter(VsigmaPWV(:),vetP(:));
        title('SigmaPWV varying P');
        xlabel('SigmaPWV [m]');
        ylabel('P [mbar]');
    case 5
% Sensitivity function for ZTD
    [ VPWV, VsigmaPWV ] = PWV_propaga_ZTD( xk2, Sk2, xk3, Sk3, xTm, STm, xP,
            SP, vetZTD, SZTD, xrho, xRv, xlat, xz);
        figure (1)
        scatter(VPWV(:),vetZTD(:));
        title('PWV varying ZTD');
        xlabel('PWV [m]');
        ylabel('ZTD [m]');
        figure (2)
        scatter(VsigmaPWV(:),vetZTD(:));
        title('SigmaPWV varying ZTD');
        xlabel('SigmaPWV [m]');
        ylabel('ZTD [m]');
end
```

XIV.b. Ancillary functions

The following functions are used in combination with the *switch* expression, to compute the PWV and σ_{PWV} values in the tolerance interval of the chosen variable and to produce the corresponding graphs.
First of all the variance-covariance matrix and PWV are defined. The partial derivatives are computed and used to define the Jacobian matrix. Finally, PWV variance propagation is computed.
The sentences coloured in blue are comments, written to make the code more understandable.

XIV.b.i. PWV_propaga_k2.m

```
function [ VPWV, VsigmaPWV ] = PWV_propaga_k2( vetk2, Sk2, xk3, Sk3, xTm,
  STm, xP, SP, xZTD, SZTD, xrho, xRv, xlat, xz)

for n=1:7;
xk2=vetk2(n);
% Variance-covariance matrix
Cxx(1,1)=Sk2^2;
Cxx(2,2)=Sk3^2;
Cxx(3,3)=STm^2;
Cxx(4,4)=SP^2;
Cxx(5,5)=SZTD^2;
% PWV
PGr=((10^8/(xrho*xRv))*(xk2+(xk3/xTm))^-1);
VPWV(n)=((10^8/(xrho*xRv))*(xk2+(xk3/xTm))^-1)*(xZTD-((2.277*10^-3*xP)/(1-
  0.00266*cos(2*xlat)-0.00028*xz)));
% Partial derivatives
syms rho Rv k2 k3  Tm P lat z ZTD
dPWV=@(rho,Rv,k2,k3,Tm,P,lat,z,ZTD) ((10^8/(rho*Rv))*(k2+(k3/Tm))^-1)*(ZTD-
  ((2.277*10^-3*P)/(1-0.00266*cos(2*lat)-0.00028*z)));

d_k2=diff(dPWV(rho,Rv,k2,k3,Tm,P,lat,z, ZTD),k2);
vd_k2= vpa(subs(d_k2,[rho,Rv,k2,k3,Tm,P,lat,z, ZTD],
  [xrho,xRv,xk2,xk3,xTm,xP,xlat,xz,xZTD]));

d_k3=diff(dPWV(rho,Rv,k2,k3,Tm,P,lat,z, ZTD),k3);
vd_k3= vpa(subs(d_k3,[rho,Rv,k2,k3,Tm,P,lat,z, ZTD],
  [xrho,xRv,xk2,xk3,xTm,xP,xlat,xz,xZTD]));

d_Tm=diff(dPWV(rho,Rv,k2,k3,Tm,P,lat,z, ZTD),Tm);
vd_Tm= vpa(subs(d_Tm,[rho,Rv,k2,k3,Tm,P,lat,z, ZTD],
  [xrho,xRv,xk2,xk3,xTm,xP,xlat,xz,xZTD]));

d_P=diff(dPWV(rho,Rv,k2,k3,Tm,P,lat,z, ZTD),P);
vd_P= vpa(subs(d_P,[rho,Rv,k2,k3,Tm,P,lat,z, ZTD],
  [xrho,xRv,xk2,xk3,xTm,xP,xlat,xz,xZTD]));

d_ZTD=diff(dPWV(rho,Rv,k2,k3,Tm,P,lat,z, ZTD),ZTD);
```

```
vd_ZTD= vpa(subs(d_ZTD,[rho,Rv,k2,k3,Tm,P,lat,z, ZTD],
   [xrho,xRv,xk2,xk3,xTm,xP,xlat,xz,xZTD]));
% Jacobian matrix
J(1)=vd_k2;
J(2)=vd_k3;
J(3)=vd_Tm;
J(4)=vd_P;
J(5)=vd_ZTD;
% Variance propagation
Cpwv=J*Cxx*J';
VsigmaPWV(n)=Cpwv^0.5;
end
end
```

XIV.b.ii. PWV_propaga_k3.m

```
function [ VPWV, VsigmaPWV ] = PWV_propaga_k3( xk2, Sk2, vetk3, Sk3, xTm,
   STm, xP, SP, xZTD, SZTD, xrho, xRv, xlat, xz)
for n=1:7;
xk3=vetk3(n);
% Variance-covariance matrix
Cxx(1,1)=Sk2^2;
Cxx(2,2)=Sk3^2;
Cxx(3,3)=STm^2;
Cxx(4,4)=SP^2;
Cxx(5,5)=SZTD^2;
% PWV
PGr=((10^8/(xrho*xRv))*(xk2+(xk3/xTm))^-1);
VPWV(n)=((10^8/(xrho*xRv))*(xk2+(xk3/xTm))^-1)*(xZTD-((2.277*10^-3*xP)/(1-
   0.00266*cos(2*xlat)-0.00028*xz)));
% Partial derivatives
syms rho Rv k2 k3  Tm P lat z ZTD
dPWV=@(rho,Rv,k2,k3,Tm,P,lat,z,ZTD) ((10^8/(rho*Rv))*(k2+(k3/Tm))^-1)*(ZTD-
   ((2.277*10^-3*P)/(1-0.00266*cos(2*lat)-0.00028*z)));

d_k2=diff(dPWV(rho,Rv,k2,k3,Tm,P,lat,z, ZTD),k2);
vd_k2= vpa(subs(d_k2,[rho,Rv,k2,k3,Tm,P,lat,z, ZTD],
   [xrho,xRv,xk2,xk3,xTm,xP,xlat,xz,xZTD]));

d_k3=diff(dPWV(rho,Rv,k2,k3,Tm,P,lat,z, ZTD),k3);
```

```
vd_k3= vpa(subs(d_k3,[rho,Rv,k2,k3,Tm,P,lat,z, ZTD],
   [xrho,xRv,xk2,xk3,xTm,xP,xlat,xz,xZTD]));

d_Tm=diff(dPWV(rho,Rv,k2,k3,Tm,P,lat,z, ZTD),Tm);
vd_Tm= vpa(subs(d_Tm,[rho,Rv,k2,k3,Tm,P,lat,z, ZTD],
   [xrho,xRv,xk2,xk3,xTm,xP,xlat,xz,xZTD]));

d_P=diff(dPWV(rho,Rv,k2,k3,Tm,P,lat,z, ZTD),P);
vd_P= vpa(subs(d_P,[rho,Rv,k2,k3,Tm,P,lat,z, ZTD],
   [xrho,xRv,xk2,xk3,xTm,xP,xlat,xz,xZTD]));

d_ZTD=diff(dPWV(rho,Rv,k2,k3,Tm,P,lat,z, ZTD),ZTD);
vd_ZTD= vpa(subs(d_ZTD,[rho,Rv,k2,k3,Tm,P,lat,z, ZTD],
   [xrho,xRv,xk2,xk3,xTm,xP,xlat,xz,xZTD]));
% Jacobian matrix
J(1)=vd_k2;
J(2)=vd_k3;
J(3)=vd_Tm;
J(4)=vd_P;
J(5)=vd_ZTD;
% Variance propagation
Cpwv=J*Cxx*J';
VsigmaPWV(n)=Cpwv^0.5;
end
end
```

XIV.b.iii. PWV_propaga_P.m

```
function [ VPWV, VsigmaPWV ] = PWV_propaga_P( xk2, Sk2, xk3, Sk3, xTm, STm,
   vetP, SP, xZTD, SZTD, xrho, xRv, xlat, xz)

for n=1:7;
xP=vetP(n);
% Variance-covariance matrix
Cxx(1,1)=Sk2^2;
Cxx(2,2)=Sk3^2;
Cxx(3,3)=STm^2;
Cxx(4,4)=SP^2;
Cxx(5,5)=SZTD^2;
% PWV
```

```
PGr=((10^8/(xrho*xRv))*(xk2+(xk3/xTm))^-1);
VPWV(n)=((10^8/(xrho*xRv))*(xk2+(xk3/xTm))^-1)*(xZTD-((2.277*10^-3*xP)/(1-
   0.00266*cos(2*xlat)-0.00028*xz)));
% Partial derivatives
syms rho Rv k2 k3  Tm P lat z ZTD
dPWV=@(rho,Rv,k2,k3,Tm,P,lat,z,ZTD) ((10^8/(rho*Rv))*(k2+(k3/Tm))^-1)*(ZTD-
   ((2.277*10^-3*P)/(1-0.00266*cos(2*lat)-0.00028*z)));

d_k2=diff(dPWV(rho,Rv,k2,k3,Tm,P,lat,z, ZTD),k2);
vd_k2= vpa(subs(d_k2,[rho,Rv,k2,k3,Tm,P,lat,z, ZTD],
   [xrho,xRv,xk2,xk3,xTm,xP,xlat,xz,xZTD]));

d_k3=diff(dPWV(rho,Rv,k2,k3,Tm,P,lat,z, ZTD),k3);
vd_k3= vpa(subs(d_k3,[rho,Rv,k2,k3,Tm,P,lat,z, ZTD],
   [xrho,xRv,xk2,xk3,xTm,xP,xlat,xz,xZTD]));

d_Tm=diff(dPWV(rho,Rv,k2,k3,Tm,P,lat,z, ZTD),Tm);
vd_Tm= vpa(subs(d_Tm,[rho,Rv,k2,k3,Tm,P,lat,z, ZTD],
   [xrho,xRv,xk2,xk3,xTm,xP,xlat,xz,xZTD]));

d_P=diff(dPWV(rho,Rv,k2,k3,Tm,P,lat,z, ZTD),P);
vd_P= vpa(subs(d_P,[rho,Rv,k2,k3,Tm,P,lat,z, ZTD],
   [xrho,xRv,xk2,xk3,xTm,xP,xlat,xz,xZTD]));

d_ZTD=diff(dPWV(rho,Rv,k2,k3,Tm,P,lat,z, ZTD),ZTD);
vd_ZTD= vpa(subs(d_ZTD,[rho,Rv,k2,k3,Tm,P,lat,z, ZTD],
   [xrho,xRv,xk2,xk3,xTm,xP,xlat,xz,xZTD]));
% Jacobian matrix
J(1)=vd_k2;
J(2)=vd_k3;
J(3)=vd_Tm;
J(4)=vd_P;
J(5)=vd_ZTD;
% Variance propagation
Cpwv=J*Cxx*J';
VsigmaPWV(n)=Cpwv^0.5;
end
end
```

XIV.b.iv. PWV_propaga_Tm.m

```
function [ VPWV, VsigmaPWV ] = PWV_propaga_Tm( xk2, Sk2, xk3, Sk3, vetTm,
  STm, xP, SP, xZTD, SZTD, xrho, xRv, xlat, xz)

for n=1:7;
xTm=vetTm(n);
% Variance-covariance matrix
Cxx(1,1)=Sk2^2;
Cxx(2,2)=Sk3^2;
Cxx(3,3)=STm^2;
Cxx(4,4)=SP^2;
Cxx(5,5)=SZTD^2;
% PWV
PGr=((10^8/(xrho*xRv))*(xk2+(xk3/xTm))^-1);
VPWV(n)=((10^8/(xrho*xRv))*(xk2+(xk3/xTm))^-1)*(xZTD-((2.277*10^-3*xP)/(1-
  0.00266*cos(2*xlat)-0.00028*xz)));
% Partial derivatives
syms rho Rv k2 k3  Tm P lat z ZTD
dPWV=@(rho,Rv,k2,k3,Tm,P,lat,z,ZTD) ((10^8/(rho*Rv))*(k2+(k3/Tm))^-1)*(ZTD-
  ((2.277*10^-3*P)/(1-0.00266*cos(2*lat)-0.00028*z)));

d_k2=diff(dPWV(rho,Rv,k2,k3,Tm,P,lat,z, ZTD),k2);
vd_k2= vpa(subs(d_k2,[rho,Rv,k2,k3,Tm,P,lat,z, ZTD],
  [xrho,xRv,xk2,xk3,xTm,xP,xlat,xz,xZTD]));

d_k3=diff(dPWV(rho,Rv,k2,k3,Tm,P,lat,z, ZTD),k3);
vd_k3= vpa(subs(d_k3,[rho,Rv,k2,k3,Tm,P,lat,z, ZTD],
  [xrho,xRv,xk2,xk3,xTm,xP,xlat,xz,xZTD]));

d_Tm=diff(dPWV(rho,Rv,k2,k3,Tm,P,lat,z, ZTD),Tm);
vd_Tm= vpa(subs(d_Tm,[rho,Rv,k2,k3,Tm,P,lat,z, ZTD],
  [xrho,xRv,xk2,xk3,xTm,xP,xlat,xz,xZTD]));

d_P=diff(dPWV(rho,Rv,k2,k3,Tm,P,lat,z, ZTD),P);
vd_P= vpa(subs(d_P,[rho,Rv,k2,k3,Tm,P,lat,z, ZTD],
  [xrho,xRv,xk2,xk3,xTm,xP,xlat,xz,xZTD]));

d_ZTD=diff(dPWV(rho,Rv,k2,k3,Tm,P,lat,z, ZTD),ZTD);
```

```
vd_ZTD= vpa(subs(d_ZTD,[rho,Rv,k2,k3,Tm,P,lat,z, ZTD],
   [xrho,xRv,xk2,xk3,xTm,xP,xlat,xz,xZTD]));
% Jacobian matrix
J(1)=vd_k2;
J(2)=vd_k3;
J(3)=vd_Tm;
J(4)=vd_P;
J(5)=vd_ZTD;
% Variance propagation
Cpwv=J*Cxx*J';
VsigmaPWV(n)=Cpwv^0.5;
end
end
```

XIV.b.v. PWV_propaga_ZTD.m

```
function [ VPWV, VsigmaPWV ] = PWV_propaga_ZTD( xk2, Sk2, xk3, Sk3, xTm, STm,
   xP, SP, vetZTD, SZTD, xrho, xRv, xlat, xz)

for n=1:7;
xZTD=vetZTD(n);
% Variance-covariance matrix
Cxx(1,1)=Sk2^2;
Cxx(2,2)=Sk3^2;
Cxx(3,3)=STm^2;
Cxx(4,4)=SP^2;
Cxx(5,5)=SZTD^2;
% PWV
PGr=((10^8/(xrho*xRv))*(xk2+(xk3/xTm))^-1);
VPWV(n)=((10^8/(xrho*xRv))*(xk2+(xk3/xTm))^-1)*(xZTD-((2.277*10^-3*xP)/(1-
   0.00266*cos(2*xlat)-0.00028*xz)));
% Partial derivatives
syms rho Rv k2 k3  Tm P lat z ZTD
dPWV=@(rho,Rv,k2,k3,Tm,P,lat,z,ZTD) ((10^8/(rho*Rv))*(k2+(k3/Tm))^-1)*(ZTD-
   ((2.277*10^-3*P)/(1-0.00266*cos(2*lat)-0.00028*z)));

d_k2=diff(dPWV(rho,Rv,k2,k3,Tm,P,lat,z, ZTD),k2);
vd_k2= vpa(subs(d_k2,[rho,Rv,k2,k3,Tm,P,lat,z, ZTD],
   [xrho,xRv,xk2,xk3,xTm,xP,xlat,xz,xZTD]));
```

```
d_k3=diff(dPWV(rho,Rv,k2,k3,Tm,P,lat,z, ZTD),k3);
vd_k3= vpa(subs(d_k3,[rho,Rv,k2,k3,Tm,P,lat,z, ZTD],
   [xrho,xRv,xk2,xk3,xTm,xP,xlat,xz,xZTD]));

d_Tm=diff(dPWV(rho,Rv,k2,k3,Tm,P,lat,z, ZTD),Tm);
vd_Tm= vpa(subs(d_Tm,[rho,Rv,k2,k3,Tm,P,lat,z, ZTD],
   [xrho,xRv,xk2,xk3,xTm,xP,xlat,xz,xZTD]));

d_P=diff(dPWV(rho,Rv,k2,k3,Tm,P,lat,z, ZTD),P);
vd_P= vpa(subs(d_P,[rho,Rv,k2,k3,Tm,P,lat,z, ZTD],
   [xrho,xRv,xk2,xk3,xTm,xP,xlat,xz,xZTD]));

d_ZTD=diff(dPWV(rho,Rv,k2,k3,Tm,P,lat,z, ZTD),ZTD);
vd_ZTD= vpa(subs(d_ZTD,[rho,Rv,k2,k3,Tm,P,lat,z, ZTD],
   [xrho,xRv,xk2,xk3,xTm,xP,xlat,xz,xZTD]));
% Jacobian matrix
J(1)=vd_k2;
J(2)=vd_k3;
J(3)=vd_Tm;
J(4)=vd_P;
J(5)=vd_ZTD;
% Variance propagation
Cpwv=J*Cxx*J';
VsigmaPWV(n)=Cpwv^0.5;
end
end
```